

Durham E-Theses

Luminescence behaviour of macrocycle metal complexes

Williams, James Anthony Gareth

How to cite:

Williams, James Anthony Gareth (1995) *Luminescence behaviour of macrocycle metal complexes*, Durham theses, Durham University. Available at Durham E-Theses Online:
<http://etheses.dur.ac.uk/5313/>

Use policy

The full-text may be used and/or reproduced, and given to third parties in any format or medium, without prior permission or charge, for personal research or study, educational, or not-for-profit purposes provided that:

- a full bibliographic reference is made to the original source
- a [link](#) is made to the metadata record in Durham E-Theses
- the full-text is not changed in any way

The full-text must not be sold in any format or medium without the formal permission of the copyright holders.

Please consult the [full Durham E-Theses policy](#) for further details.

The copyright of this thesis rests with the author.
No quotation from it should be published without
his prior written consent and information derived
from it should be acknowledged.

LUMINESCENCE BEHAVIOUR OF MACROCYCLE METAL COMPLEXES

James Anthony Gareth Williams

A thesis submitted in part-fulfilment of the degree of Doctor of Philosophy
of the University of Durham

October 1995

Research carried out at the Department of Chemistry

1992 - 1995



11 DEC 1995

LUMINESCENCE BEHAVIOUR OF MACROCYCLE METAL COMPLEXES

James Anthony Gareth Williams

ABSTRACT

Luminescent complexes of lanthanide ions are of growing interest because the long lifetime of emission allows time-resolved detection procedures to be employed. A key step in the development of such systems lies in the preparation of highly luminescent complexes which display high stability in aqueous solution.

A series of ligands based on 1,4,7,10-tetraazacyclododecane have been prepared, in which the nitrogen atoms are appended with coordinating phosphinate or amide groups, or a combination of both. The compounds obtained are octadentate ligands which form water-soluble lanthanide complexes of high stability. Complexes incorporating aryl groups in the pendent arms have been prepared and some display intense metal luminescence following excitation into the organic chromophores. A back energy transfer process occurs in the terbium complexes containing naphthyl or quinolinone groups.

Measurements of the luminescence lifetimes in H_2O and D_2O show that there are no metal-bound water molecules in the tetrabenzylphosphinate complexes. Those incorporating one amide and three phosphinate groups display hydration states between 0 and 1. An attempt has been made to correlate this information with that obtained from an analysis of the nuclear magnetic resonance dispersion profiles of related gadolinium complexes. The complexes incorporating secondary amide groups display an additional deactivation pathway for the metal excited state involving energy transfer into N-H bonds.

The luminescence behaviour of four macrocyclic tetraamide ligands incorporating naphthyl fluorophores has been studied. These compounds exhibit distinctive changes in luminescence in the presence of quenching (eg. Pb^{2+} , Cu^{2+} and Ni^{2+}) and non-quenching ions (eg. Cd^{2+} and Zn^{2+}). This behaviour extends to non-aqueous solution. The protonated tetranaphthyl ligand forms an intramolecular excimer in which the excimer emission displays a sensitive dependence on the polarity of the solvent.

University of Durham
October 1995

DECLARATION

The research described in this thesis was undertaken at the Department of Chemistry of the University of Durham between October 1992 and September 1995. All of the work is my own, except where specifically stated otherwise. No part of it has been submitted previously for a degree at this or any other University.

STATEMENT OF COPYRIGHT

The copyright of this thesis rests with the author. No quotation from it should be published without his prior written consent and information derived from it should be acknowledged.

ACKNOWLEDGEMENTS

It is a pleasure to thank all of the people with whom I have worked whilst at Durham for their help and support.

I am especially grateful to Professor David Parker for his enthusiastic supervision of my work. His sound advice and constant encouragement, together with his patience and good humour, lead to a supervisor with whom it has been a privilege to work. At times, a comparison with a certain Mirandola¹ springs to mind but, when this is not so appropriate and the answers are far from clear, it is always stimulating to discuss with him the puzzles which the chemistry presents.

The experience acquired by Dr. Kanthi Senanayake (née Pulkody) in the field of the phosphinate ligands has been of great benefit. Her advice in this area has been highly valued, as have been her kindness and friendship of the past three years. Dr. Andrew Beeby is the resident oracle as far as practical aspects of luminescence are concerned. His advice on this subject and his assistance with the flash photolysis work are greatly appreciated. Dr. Tony Patti brought his enthusiasm with him from Australia on both of his visits. He proved to be an edifying companion to work alongside in the lab. and one with whom it was almost too easy to while away the hours during our nocturnal columnning sessions.

Professor Silvio Aime and Dr. Mauro Botta are the unknown faces in Italy who have provided a wealth of NMR information on the complexes. Professor Jim Riehl and his group in Michigan have carried out circularly polarised luminescence studies using an inspired new approach to the study of racemic mixtures.

The technical staff at Durham have ably supplied their skills and support throughout the work.

Finally, I should like to express my sincere thanks to all of the postgraduate and postdoctoral workers within the group for their help, interest and support and, above all, for their friendship.

¹ Giovanni Picco della Mirandola was a philosopher of the Italian Renaissance, of whom it was said that "he knew all that there is to know.....and much else besides".

CONTENTS

List of Abbreviations	v
Chapter 1	
Introduction	1
1.1 Introduction	1
1.2 Luminescence	1
1.3 Lanthanide luminescence	3
1.3.1 Electronic configurations and transitions	3
1.3.2 Effect of water on lanthanide luminescence	6
1.3.3 Number of coordinated water molecules from luminescence	9
1.3.4 Methods of photo-excitation of lanthanide ions	11
1.4 Applications of lanthanide luminescence	12
1.5 Complexing agents for lanthanides	18
1.5.1 Some general points	18
1.5.2 Macrocyclic complexing agents	20
1.6 Desirable properties of luminescent lanthanide probes	23
1.6.1 Some general points	23
1.6.2 Absorbance	23
1.6.3 Lifetime of emission	24
1.6.4 Hydration state, q	25
1.6.5 Quantum yields	25
1.7 Some examples of recent work	26
1.7.1 Cryptates and ligands containing 2, 2'-bipyridine	26
1.7.2 Calixarenes	28
1.7.3 Polyaminopolycarboxylate ligands	29
1.8 Lanthanide NMR	31
1.8.1 Paramagnetic shifts	31
1.8.2 NMR line-broadening effects of lanthanide ions	36
1.8.3 The exceptional behaviour of Gd^{3+} : Relaxivity and its application in MRI	37
1.9 Fluorescence detection of metal ions	41
1.9.1 Systems incorporating macrocyclic receptors	42
1.9.2 Examples which make use of acyclic ligands	46
References for Chapter 1	48

Chapter 2

Lanthanide Complexes of Tetraazamacrocyclic Ligands

Bearing Four Pendent Phosphinate Arms

56

2.1	Introduction	56
2.2	Ligand Synthesis	57
2.3	Complex formation	58
2.4	Earlier results concerning the structures of the ligand and its yttrium complex	58
2.5	Solution studies	61
2.6	NMR studies of complexes in solution	61
2.7	Luminescence of terbium and europium complexes	74
2.7.1	UV absorbance spectra	74
2.7.2	Luminescence of [Tb.27] ⁻	75
2.7.3	Luminescence of [Eu.27] ⁻	79
2.7.4	Excited state lifetimes	81
2.8	Other methods for probing the hydration state in solution	85
2.8.1	¹⁷ O Paramagnetic shifts	85
2.8.2	Relaxivity of the gadolinium complexes	87
2.9	Circularly polarised luminescence	90
2.10	Methoxybenzylphosphinate complexes	99
2.11	Accounting for the high luminescence quantum yields	102
	References for Chapter 2	111

Chapter 3

Lanthanide Complexes Of Tetraazamacrocyclic Ligands Incorporating

One Carboxamide and Three Phosphinate Coordinating Arms

115

3.1	Introduction	115
3.2	Synthesis of the amide ligands	116
3.3	Complex formation	118
3.4	Solution NMR studies	118
3.4.1	Introduction	118
3.4.2	Structural possibilities	121
3.4.3	Partial assignment of the europium spectra	126
3.4.4	Determination of Yb-P distances by T_1 measurements	129
3.4.5	Spectral resolution of the enantiomeric complexes	132

3.5	Luminescence of the europium and terbium complexes	134
3.5.1	Terbium spectra	134
3.5.2	Europium spectra	137
3.5.3	Lifetimes and hydration states	144
3.5.4	Hydration states and the correlation of Gd ³⁺ NMRD information with luminescence measurements	146
	Appendix to Chapter 3: Routes to triphosphinate esters and acids of 12N ₄	154
	References for Chapter 3	157

Chapter 4

	Luminescence Properties of Tetraazamacrocyclic Ligands Incorporating Four Pendent Amide Arms and Their Complexes with Lanthanides and Other Ions	159
4.1	Introduction	159
4.2	Ligand syntheses	160
4.3	UV absorbance of 39 - 42	169
4.4	Fluorescence of 39	169
4.5	Fluorescence of 41 and 42	174
4.6	Fluorescence of 40	179
4.7	Effect of metal ions on the fluorescence of 39	182
4.7.1	In solution in acetonitrile	182
4.7.2	In water	185
4.8	Effect of metal ions on the fluorescence of 40	188
4.9	Effect of metal ions on the fluorescence of 41 and 42	193
4.10	Effect of added β -cyclodextrin on naphthyl fluorescence	199
4.11	Preparation, isolation and characterisation of metal complexes of 39 and 40	201
4.12	Luminescence of the europium complexes of 39 - 42	204
4.13	Luminescence properties of the terbium complexes of 39 and 40	209
4.13.1	Introduction	209
4.13.2	Characteristics of the terbium emission spectra	209
4.13.3	A flash photolysis study	211
4.13.4	Effect of β -cyclodextrin on terbium luminescence	217
4.14	Other experiments using flash photolysis	219
4.15	Terbium and europium complexes of 12N ₄ tetraamides incorporating a quinolinone group as sensitiser	220
	References for Chapter 4	228

Chapter 5	
Experimental Procedures	232
5.1 Synthetic procedures and characterisation	232
5.1.1 General points	232
5.1.2 Details for Chapter 2	234
5.1.3 Details for Chapter 3	236
5.2 Experimental details of luminescence measurements	262
5.2.1 Ultra-violet spectroscopy	262
5.2.2 Luminescence spectroscopy: instrumentation	262
5.2.3 Acquisition of fluorescence and phosphorescence spectra	264
5.2.4 Lifetimes of luminescence	266
5.2.5 Quantum yields	267
5.2.6 Effect of metal ions on fluorescence intensities	268
5.2.7 Effect of added β -cyclodextrin	269
5.2.8 Degassing of solutions	270
5.2.9 Variable temperature luminescence spectroscopy	270
5.2.10 Flash photolysis and laser induced emission studies	273
References for Chapter 5	275
Appendix	
Courses, Lectures and Seminars Attended	276

ABBREVIATIONS

Compounds

12N ₄	1,4,7,10-tetraazacyclododecane
14N ₄	1,4,8,11-tetraazacyclotetradecane
BAPTA	1,2-bis(<i>o</i> -aminophenoxy)ethane- <i>N,N,N',N'</i> -tetraacetic acid
BCPDA	4,7-bis(chlorosulfo)phenyl)-1,10-phenanthroline-2,9,-dicarboxylic acid
bipy	2,2'-bipyridine
DOTA	1,4,7,10-tetraazacyclododecane-1,4,7,10-tetraacetic acid
dpa	2,6-dipicolinate
dpm	dipivaloylmethane
DTPA	diethylenetriamine- <i>N,N,N'',N',N'</i> -pentaacetic acid
EDTA	ethylenediamine- <i>N,N,N',N'</i> -tetraacetic acid
EGTA	ethyleneglycolbis(β -aminoethylether)- <i>N,N,N',N'</i> -tetraacetic acid
NOBA	<i>meta</i> -nitrobenzylalcohol
Np	2-naphthyl
pyr	pyrene
TETA	1,4,8,11-tetraazacyclotetradecane-1,4,8,11-tetraacetic acid
THF	tetrahydrofuran
TMT	terpyridine-bis(methylenamine)tetraacetic acid
TTHA	triethylenetetraaminehexaacetic acid
TRITA	1,4,7,10-tetraazacyclotridecane-1,4,7,10-tetraacetic acid

Techniques and Spectroscopy

CD	circular dichroism
CPL	circularly polarised luminescence
PEM	photoelastic modulator
HPLC	high performance liquid chromatography
IR	infra red spectroscopy
br	broad
m	medium
s	strong
str	stretching vibration
w	weak
mp	melting point
MS	mass spectrometry
CI	chemical ionisation
DCI	desorbed chemical ionisation
EI	electron impact ionisation

ESMS	electrospray ionisation mass spectrometry
ES +	electrospray ionisation using positive ion detection mode
ES -	electrospray ionisation using negative ion detection mode
FAB	fast atom bombardment
M	molecular ion
MRI	magnetic resonance imaging
NMR	nuclear magnetic resonance
COSY	correlation spectroscopy
br	broad
d	doublet
m	multiplet
s	singlet
t	triplet
VT	variable temperature
NMRD	nuclear magnetic resonance dispersion
TLC	thin layer chromatography

Photophysical processes

CT	charge transfer
IC	internal conversion
ISC	inter-system crossing
LMCT	ligand-to-metal charge transfer
nr	non-radiative processes
PET	photoinduced electron transfer

Miscellaneous

M	mol dm^{-3}
I	ionic strength (mol dm^{-3})
Ln	generic symbol for a lanthanide ion

Chapter 1

CHAPTER 1

Introduction

1.1 Introduction

The work described in this thesis is concerned with the luminescence properties of metal complexes of macrocyclic ligands. There are three components to this work. The first objective is the quest for highly luminescent complexes of lanthanide ions, of high kinetic and thermodynamic stability. Such complexes are potentially useful as probes or labels in biological applications, for example in fluoroimmunoassay. A second aim has been the attempt to correlate the luminescence and structural information amassed on these complexes with the behaviour of the related gadolinium complexes, which are potential paramagnetic contrast agents for use in magnetic resonance imaging. Finally, the luminescence properties of the free ligands may be strongly influenced by the presence of metal ions of the appropriate size and coordination preferences. This leads to the possibility of sensitive and selective detection methods for certain metal ions.

1.2 Luminescence

The word 'luminescence' refers to the emission of light by materials other than that which occurs through the process of incandescence. (This latter phenomenon relates to the fact that all materials increasingly emit radiation of shorter wavelengths as their temperature is increased: when the temperature is high enough, visible light is emitted). In any light-emitting process, the sample must absorb an appropriate amount of energy from a suitable source prior to emission of light. Luminescence is subdivided into a number of categories according to the origin of this energy. Examples include bioluminescence (emission of light by living animals and plants where an exoenergetic biochemical reaction provides the excitation energy), chemiluminescence (that which may occur during the course of a chemical reaction and consecutive to absorption of energy by the reactant molecules) and electroluminescence (light accompanying an electric discharge, for example in a rarefied gas, or after bombardment by electrons -

sometimes referred to as cathodoluminescence). The work described here is concerned exclusively with photoluminescence, namely the emission of ultra-violet, visible or near-infrared light upon exposure to light having the same energy (resonance) or a higher energy. The phenomenon of photoluminescence may be further subdivided into fluorescence and phosphorescence. Historically, the distinction was made according to the relative timescales of the emission; thus, if the light emission was observed to persist after the excitation was discontinued, the light-emitting process was referred to as phosphorescence. Not surprisingly, this rapidly became an ambiguous distinction and the modern definition of phosphorescence is the emission of light after energy transfer to a state of higher spin (eg. triplet states in organic compounds). Figure 1.1 shows the electronic transitions giving rise to these two processes in the form of a simplified Jablonski diagram, which illustrates some of the processes which may occur when a typical fluorescent organic molecule absorbs a photon of light of appropriate energy.

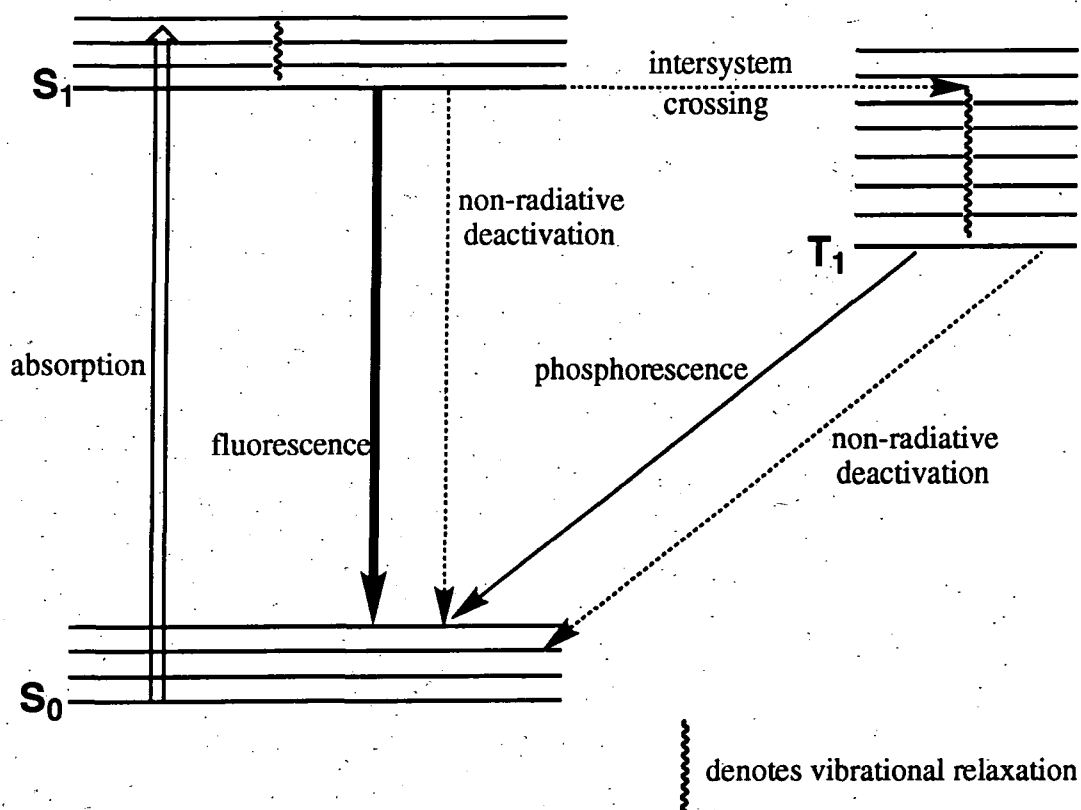


FIGURE 1.1 Simplified Jablonski diagram illustrating some of the processes which may occur following the absorption of light by a typical fluorescent organic molecule and the distinction between fluorescence and phosphorescence.

The spin-forbidden nature of the phosphorescent transition ($T_1 - S_0$) gives rise to the long natural luminescence lifetime which is often a feature of phosphorescence (emission timescales may be of the order of milliseconds to seconds in the absence of other deactivating processes). In contrast, fluorescence is a fully allowed process and decays very rapidly after excitation, typically over nanoseconds to microseconds. In practice, it usually turns out that long-lived phosphorescence is not observable under ambient conditions. This reflects the occurrence of highly competitive radiationless deactivation pathways for the triplet state, including thermally activated processes and quenching by dissolved molecular oxygen or other species. This point will be returned to in later sections.

1.3 Lanthanide Luminescence

1.3.1 Electronic configurations and transitions

The lanthanide elements arise from the progressive filling up of the 4f electron subshell. The $4f^n$ configuration of a lanthanide ion gives rise to a large number of states whose energies are determined by a combination of interelectronic repulsion, spin-orbit coupling and the ligand field. In principle, owing to the relatively large spin-orbit coupling observed for the lanthanides, an intermediate coupling scheme should be invoked to describe the spin-orbit coupling but in practice, the simpler Russell-Saunders coupling scheme proves to be a reasonable approximation.¹ The electrostatic interaction yields terms, $(2S+1)L$, with separations of the order of 10^4 cm^{-1} . Spin-orbit coupling then splits these terms into J states, the separations of which are typically in the region of 10^3 cm^{-1} . The ground states are predicted using Hund's rules. The separation between adjacent J levels, as obtained from the emission spectra for example, follows the Landé interval rule fairly well (i.e. separation between level J and (J-1) is proportional to J), which provides some justification for the use of the Russell-Saunders coupling scheme.

Owing to their relatively small radial extensions, the 4f orbitals are effectively shielded from the environment by the $5s^2 5p^6$ arrangement and are only minimally involved in

bonding. This has two important implications for the spectra of lanthanide ions in solution. Firstly, ligand-field splittings are very small, of the order of 10^2cm^{-1} . Thus, when an f-f transition occurs from one spectroscopic term of a $4f^n$ configuration to another term of the same configuration, the spectral band which arises is extremely sharp (both in absorption and in emission).² The bands are similar to those of free atoms and are quite unlike the broad d-d bands observed in the absorbance spectra of transition metal complexes (where ligand-field splittings are typically several thousand wavenumbers). The second point concerns the probability of such transitions. Electric dipole transitions between states of f^n configuration are parity (Laporte) forbidden. However, the interaction with the ligand field or with its vibrational states mixes electronic states of different parity into the 4f wavefunction, which gives rise to forced (or induced) electric dipole transitions.³ The weak nature of this interaction means that only small contributions are added to the 4f wavefunctions and so the oscillator strength remains low. This leads to very low extinction coefficients in the absorbance spectra: they are rarely greater than $1 \text{ M}^{-1} \text{cm}^{-1}$. Magnetic dipole transitions are allowed by the parity rule, but their oscillator strengths are extremely low and of a similar magnitude to those of the forced electric dipole transitions.

In emission, the low transition probabilities lead to long natural luminescence lifetimes. A theoretical treatment of luminescence allows radiative lifetimes to be estimated using the Einstein coefficient to express the rate of relaxation of an excited state to a particular final state.^{2,4} In addition to the dipole oscillator strength, the rate of relaxation is proportional to $(\Delta E)^3$ where ΔE is the energy gap between the two states. The energy levels of the trivalent lanthanide ions are shown in the energy level diagram in Figure 1.2. It is apparent that Gd^{3+} might be expected to have the shortest natural luminescence lifetime, as it has the largest energy gap between emissive and next-lower state. This is not the case, however, because in the case of Gd^{3+} , this is the only transition which can occur (there are no other low-lying states) whereas for the other metals, there are several other lower states available to which the excited state can relax: it is the total radiative relaxation rate which determines the natural luminescence

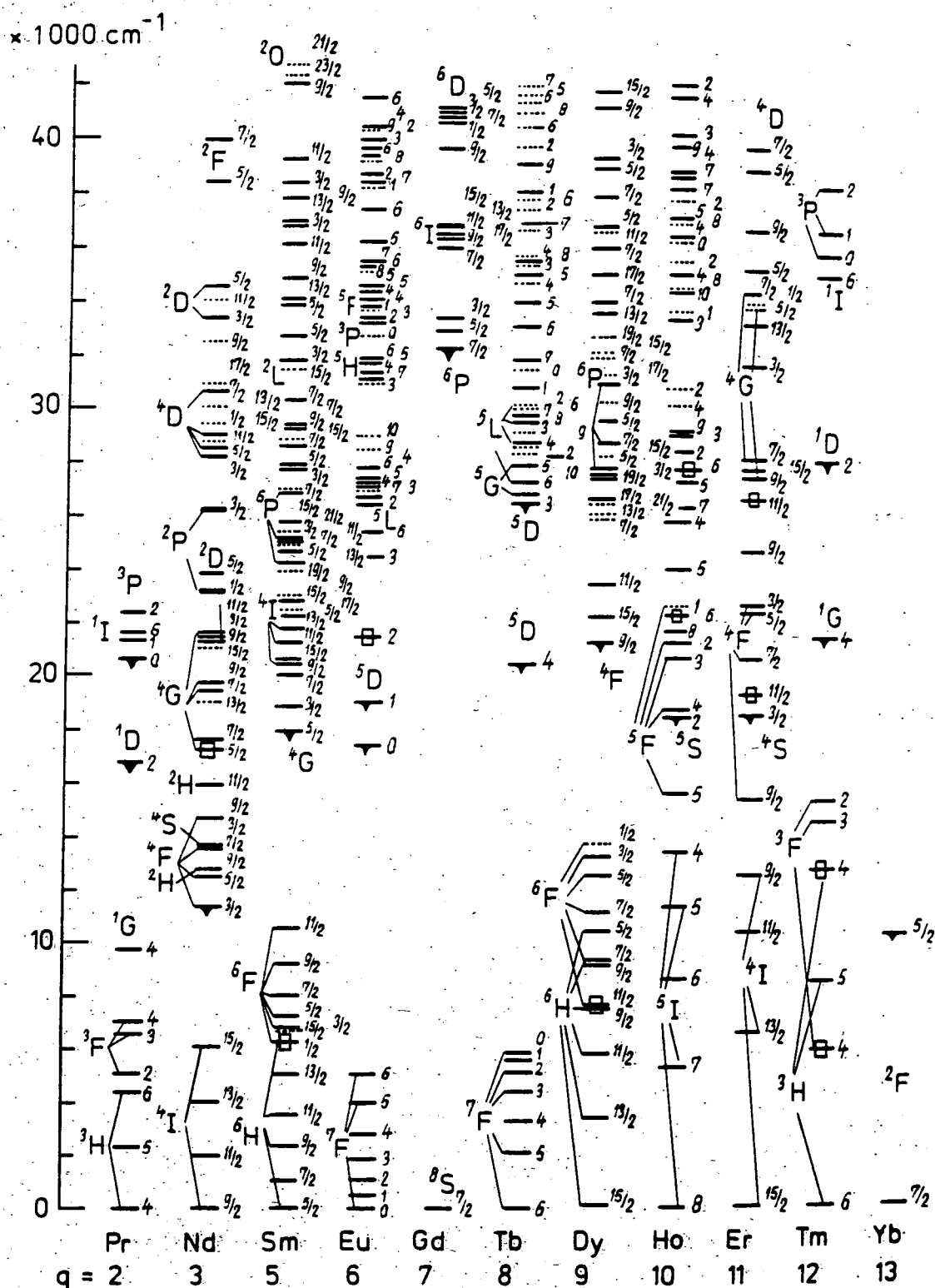


FIGURE 1.2 Energy levels of the trivalent lanthanides (except Ce^{3+} and Pm^{3+}); q is the number of 4f electrons. Excited levels frequently showing luminescence are indicated by a black triangle. Calculated energy levels are shown by dotted lines. The large empty area in the middle of the figure ($q = 5 - 9$) corresponds to a large gap between the highest-level having the same S_{max} as the ground state and the lowest level of the lowest term with $S_{\text{max}} - 1$. From reference 1; copyright Springer Verlag (Berlin Heidelberg). Reproduced with permission.

lifetime; i.e. the sum of the relaxation rates to all states lower in energy than the emissive state. The calculated radiative lifetimes for excited states of the aqueous lanthanide ions are shown in Table 1.1.

TABLE 1.1 *Calculated radiative lifetimes of excited states of the aqueous Ln³⁺ ions.^a*

	Nd	Pm	Sm	Eu	Gd	Tb	Dy	Ho	Er
	⁴ F _{3/2}	⁵ F ₁	⁴ G _{5/2}	⁵ D ₀	⁶ P _{7/2}	⁵ D ₄	⁴ F _{9/2}	⁵ S ₂	⁴ S _{3/2}
E_{ex}^{b} (cm ⁻¹)	11 460	12 400	17 900	17 277	32 200	20 500	21 100	18 500	18 350
$\tau_{\text{R}}(\text{J})^{\text{c}}$ (ms)	0.42	0.65	6.26	9.67	10.9	9.02	1.85	0.37	0.66

(a) Data from reference 2. (b) Energy of the excited state ²S+¹L_J. (c) The values are the total radiative lifetimes including electric and magnetic dipole transitions.

In fact, the experimental decay times for the ions in solution turn out to be one or two orders of magnitude lower than the estimated values.² This indicates that the decay of the emitting state is greatly affected by non-radiative transitions. In the solid state, it has been shown that the non-radiative rate of deactivation has an exponential dependence on the energy gap ΔE between the emissive level and the next lower-lying level.⁵ The relaxation mechanism is interpreted as a 'multiphonon process' which becomes less probable as the number of phonons that must be simultaneously excited to conserve energy increases.^{5,6}

1.3.2 Effect of water on lanthanide luminescence

Evidence for such an interpretation and its applicability to aqueous solutions has been provided by a number of investigations into the effect of substitution of D₂O for H₂O in aqueous solutions of lanthanide ions.⁷⁻¹⁷ The H₂O-D₂O system is particularly convenient for study since the substitution of D₂O for H₂O has been shown to exert no

change in the absorption spectrum of a Ln^{3+} ion⁷⁻⁹ (in contrast to the situation for transition metals¹⁸). Thus, any changes in luminescence intensity will reflect the effect of isotopic substitution on the emissive state. Kropp and Windsor showed in the 1960s that the luminescence of Eu^{3+} and Tb^{3+} was more intense in D_2O than in H_2O .^{7,10} Moreover, the ratio of the intensity of luminescence of a given Ln^{3+} state in D_2O to that of the same state in H_2O bore, at least to some extent, an inverse relation to the energy gap between the emissive state and the next lower level. Similarly, lifetimes were found to be about one order of magnitude higher in D_2O . These results, together with some lifetime data obtained later by others, are summarised in Table 1.2.

TABLE 1.2 *Luminescence intensities and lifetimes of lanthanide excited states in H_2O and D_2O ^a*

	Sm^{3+}	Eu^{3+}	Gd^{3+}	Tb^{3+}	Dy^{3+}
$I_{\text{D}}/I_{\text{H}}^{\text{b}}$	12 ± 6	18.0 ± 1.8	1.0 ± 0.2	7.8 ± 0.8	12 ± 3
ΔE^{c} (cm^{-1})	7 500	12 300	32 100	14 700	7 800
$\tau_{\text{D}_2\text{O}}$ (ms)	0.053 ^d	1.9	---	3.3	0.038 ^d
$\tau_{\text{H}_2\text{O}}$ (ms)	0.0022 ^d	0.10	2.3 ^d	0.39	0.0023 ^d

(a) Results of Kropp and Windsor (reference 7) except where indicated otherwise.

(b) Relative intensities for solutions of the nitrate salts at a concentration of 0.1M.

(c) ΔE is the difference in energy between the excited (resonance) level and the next lower level (eg. $^5\text{D}_0$ -- $^7\text{F}_6$ separation in Eu^{3+}). (d) From reference 14.

Kropp and Windsor concluded that the quenching of luminescence in aqueous solutions occurred via energy transfer into O-H stretching vibrations and that the rate was proportional to the number of O-H oscillators associated with the lanthanide ion. In general terms, the probability of an A-B oscillator becoming excited from the ground vibrational level, v'' , to a higher level, v' , decreases rapidly as v' increases, owing to the poorer Franck-Condon overlap of the two wavefunctions. Thus, energy transfer into

O-D vibrations is less efficient than for O-H as the former has a smaller vibrational stretching frequency: bridging of a given energy gap ΔE will require excitation to a higher vibrational level, v' , for D_2O than for H_2O . This gives rise to the observed enhancement of the luminescence intensity in D_2O . This interpretation also accounts for the observed variation in the magnitude of the effect for the different lanthanide ions: energy transfer into O-H (or O-D) vibrations becomes less probable as the energy gap ΔE between the emissive and next lower level increases, consistent with the observed measurements (Table 1.2). Figure 1.3 is a scaled diagram which illustrates these effects as applied to europium and terbium.

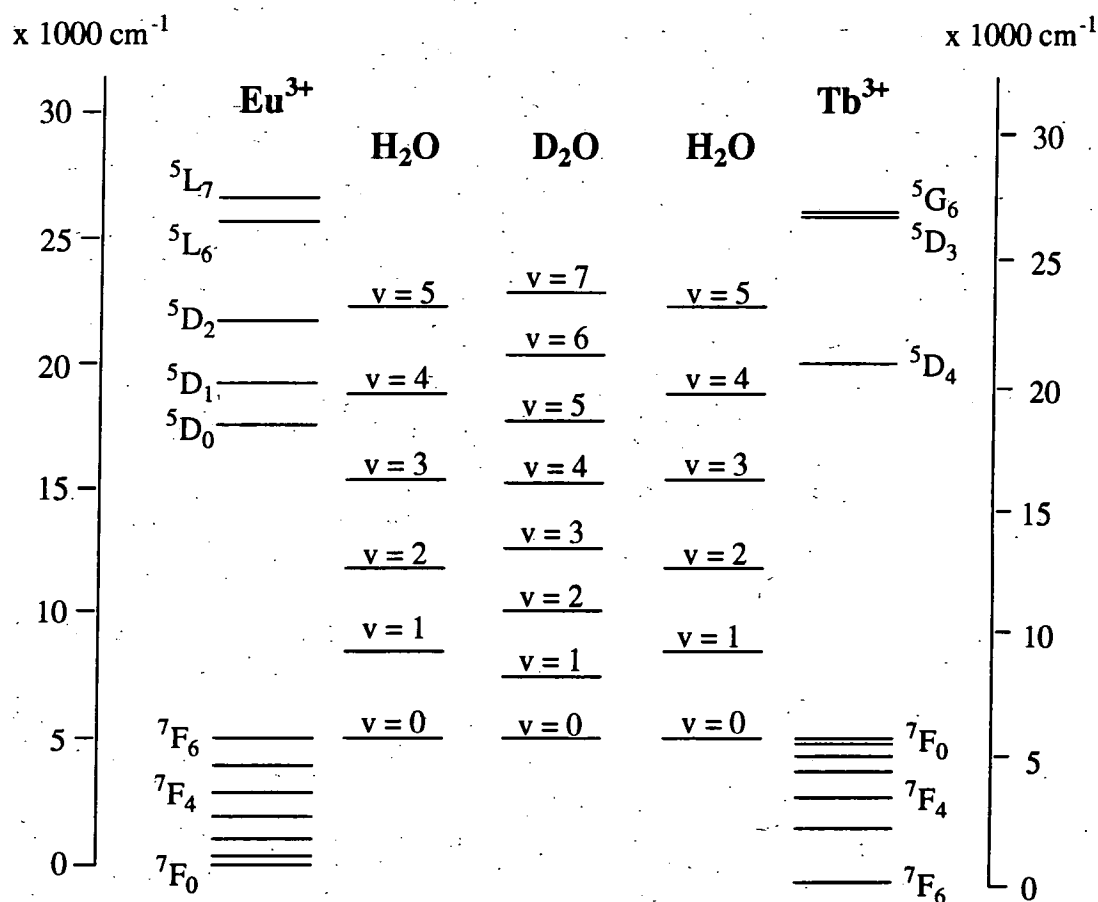


FIGURE 1.3 The deactivating effect of water: relative energy levels of the Ln^{3+} electronic states and the O-H or O-D vibrational levels. An offset has been applied such that the lowest vibrational level of O-H or O-D is shown at the same energy as the highest level of the ground manifold of the Ln^{3+} ion. Ln^{3+} energy levels from reference 1; $\nu_{O-H} = 3405$ and $\nu_{O-D} = 2520 \text{ cm}^{-1}$ (reference 19).

Further evidence in support of the rôle of high energy vibrations was provided by the observation of vibronic satellites in the emission spectrum of Gd^{3+} , due to coupling of O-H or O-D vibrations to the emitting state.¹²

It is clear from these investigations (Table 1.2) that only three of the lanthanide ions, namely europium, gadolinium and terbium, are ever likely to be useful as luminescent probes in aqueous media. Samarium and dysprosium, whilst predicted to have relatively long natural luminescence lifetimes (Table 1.1), suffer from very efficient deactivation by O-H or O-D oscillators,¹⁴ owing to the small energy gaps between their emissive and lower states (Figure 1.2). The remaining ions (Pr^{3+} , Nd^{3+} , Ho^{3+} , Er^{3+}) have energy gaps between the emitting level and the next lower level of less than 6500 cm^{-1} and their luminescence is barely detectable in H_2O or D_2O .

At the other extreme, the gap in Gd^{3+} is so large that multiphonon-like relaxation is already highly improbable when the coordinating group is OH, so that substitution of D_2O has no further detectable effect.^{7,14} On this basis, $\text{Gd}(\text{III})$ would appear to be an ideal candidate for use as a luminescent probe in aqueous solution. This proves not to be the case since the large energy gap gives rise to emission at an inconvenient wavelength in the UV (312 nm) and excitation must be achieved at wavelengths shorter than this which is of little practicable use.

On the basis of these results, it is not surprising that europium and terbium have been the focus of most of the research in this area over the past 25 years and are the subject of the work described here.

1.3.3 Number of coordinated water molecules from luminescence

The work of Kropp and Windsor^{7,10} and subsequently Haas and Stein^{12,13} showed that the deactivating effect of coordinated water molecules could be partitioned from the other modes of depopulation of the emissive state. Thus:

$$k_{\text{obs}}^{\text{H}_2\text{O}} = k^0 + \sum k_i^{\text{nr}} + k_{\text{OH}} \quad (1)$$

where k^0 is the natural luminescence rate constant for emission of photons (in the absence of other deactivating processes), Σk_i^{nr} is the sum of the rate constants for non-radiative pathways of deexcitation not involving O-H oscillators and k_{OH} is the rate constant for non-radiative energy transfer to the O-H oscillators of coordinated water molecules. In D_2O the k_{OH} term may be neglected and so, in pure D_2O , equation (1) reduces to:

$$k_{obs}^{D_2O} = k^0 + \Sigma k_i^{nr} \quad (2)$$

Subtracting (2) from (1) gives:

$$\Delta k_{obs} = k_{obs}^{H_2O} - k_{obs}^{D_2O} = k_{OH} \quad (3)$$

The work of Heller¹¹ and subsequently that of Haas and Stein¹³ showed that OH oscillators act independently in the deexcitation process and so k_{OH} is directly proportional to the number of water molecules, q , associated with the metal ion. Thus:

$$\Delta k_{obs} = k_{OH} = A' \cdot q \quad (4)$$

(where A' is a constant specific to a given metal ion).

Rearranging gives:

$$q = A_{Ln} \cdot (\tau_{H_2O}^{-1} - \tau_{D_2O}^{-1}) \quad (5)$$

where τ is the luminescence lifetime (the reciprocal of the rate constant k) and A_{Ln} is a proportionality constant for the lanthanide Ln.

Empirical proportionality constants (for europium and terbium complexes) have been determined and reported extensively by Horrocks and Sudnick¹⁵⁻¹⁷ from a study of several crystalline solids and solutions where the number of Ln^{III} ion-coordinated water molecules was known from X-ray crystallography. Plots of $\Delta\tau^{-1}$ versus the known number of coordinated water molecules, q , were linear, with high correlation coefficients, thereby validating the theory.¹⁷ The proportionality constants obtained were

$$A_{Eu} = 1.05$$

$$A_{Tb} = 4.2$$

for τ in milliseconds in eq. (5); estimated error in $q = \pm 0.5$.

Thus, lifetime measurements in H₂O and D₂O may be used to provide an estimate of the hydration state of lanthanide complexes. The estimated error of ± 0.5 in q is surprisingly large, especially bearing in mind that the precision of the lifetime measurements is usually high. This probably reflects the fact that the A_{Ln} constants are empirical parameters derived from a study of a very limited number of complexes and a correlation with the number of metal-bound water molecules as obtained from X-ray structural analyses. In fact, it is not always clear that the behaviour in solution will be the same as that in the solid state. The possibility of small changes in the equilibrium metal-water distance from one complex to another (which might affect the efficiency of deactivation by O-H) is not taken into account and neither are processes such as N-H / N-D or C-H / C-D exchange, which may possibly occur in some compounds.

1.3.4 Methods of photo-excitation of lanthanide ions

It was pointed out in section 1.3.1 that the bands observed in Ln^{III} absorbance spectra are always weak, with molar absorption coefficients usually $< 1 \text{ M}^{-1}\text{cm}^{-1}$. One outcome of this is that the excited states are not readily populated by conventional sources of light. This poses a disadvantage for the use of lanthanides as luminescent probes, as it places an unsatisfactory limit on detection levels.

The advent of lasers has provided a means of circumventing this problem. The high selectivity of laser light (with narrow bandwidths typically $< 0.02 \text{ nm}$) and its high intensity, coupled with the high sensitivity of modern photon counting methods, largely compensates for this disadvantage. Europium and terbium may be excited in the visible region by readily available lasers: Eu^{III} is excited at 580 nm, often using Rhodamine 6G as the dye, whilst Tb^{III} may be excited at 488 nm by the use of coumarin 102, for example, or the 488 nm line of an argon laser.

Sensitised emission: the *antenna effect*

Sensitised emission provides another possible solution to the problem. Interest in this phenomenon began in 1942 following the work of Weissman, who undertook a study of

salicylaldehyde and β -diketonate complexes of europium.²⁰ He found that the absorption of UV light by the ligands resulted in emission lines characteristic of the Eu^{III} ion. Balzani has coined the term 'antenna effect' for the observation of sensitised emission.²¹ The 'antenna' is a group (here the ligand) which absorbs strongly and transfers its excitation energy to the metal which, in accepting this energy, becomes excited to the emissive state. If the antenna has a high extinction coefficient and the energy transfer process is efficient, then the 'effective' molar absorption coefficient of the metal is vastly increased and intense luminescence may result following excitation by conventional light sources.

This early work by Weissman foreshadowed a large amount of research in the 1960s and beyond on the photophysics of such complexes, using direct laser excitation of both the ligand and the metal emissive state.²²⁻²⁶ In most cases, a ligand-localised triplet state was implicated in donating energy to the emissive levels of the metal, following ligand singlet excitation. No firm evidence was found to support the alternative view proposed in one case of energy transfer from the excited ligand singlet state.²⁷ In some cases and especially for terbium, an efficient deexcitation mechanism of the emissive level via the ligand T_1 state was postulated in order to account for temperature-dependent quantum yields and lifetimes.^{28,29} Sato and Wada attempted to establish a relationship between the energy of the emissive Ln^{III} state and the lowest triplet state of the β -diketone ligands.²⁵ For Eu^{III} , the efficiency of energy transfer was found to be a maximum when the $^5\text{D}_0$ -ligand T_1 separation was of the order of 800 - 1200 cm^{-1} . No conclusions could be reached for the Tb^{III} systems.

1.4 Applications of lanthanide luminescence

The luminescence of europium and terbium has found a number of applications in diverse areas of the chemical and biological sciences over the past 25 years. Research in the solid state has focused primarily on the way in which the luminescence can provide information on the local site symmetry of the lanthanide ion, from a group theoretical analysis of the observed splittings of the f-f transitions.^{3,30} Eu^{III} is

particularly suited to this work as the low J values restrict the number of transitions that can be observed. Systems as diverse as crown ether complexes and zeolites have been studied.³ In solution, analogous studies have included attempts to elucidate the structural features of lanthanide shift reagents³¹ and the nature of adduct formation with a variety of substrates.^{32,33}

The lanthanides have found use as luminescent chromophores for liquid chromatographic detection of aromatic aldehydes and ketones,³⁴ owing to the sensitised emission which may be induced by such compounds (section 1.3.4). Liquid chromatographic detection of nucleotides and nucleic acids has also been proposed.³⁵ All of the common bases of nucleic acids are able to sensitise Tb(III) emission, guanine being the most efficient. Curiously, sensitisation is not observed in the double-stranded polymer.

The application of lanthanide ion luminescence to problems in protein chemistry has received a good deal of attention.²² This arose following the observation of emission from protein-bound Tb^{III} ions, sensitised by the fluorescent aromatic amino acid residues, phenylalanine, tryptophan and tyrosine.³⁶ Most of this work has been carried out using calcium-binding proteins, where the lanthanide ion occupies the calcium binding site.^{37,16} The use of luminescence excitation spectra provides a means of determining which aromatic amino acid residues of the protein are responsible for energy transfer to the bound terbium and hence may provide information on the metal binding site.³⁸

Estimates of the distance between the energy donor and the acceptor ion have also been made.^{37,39} Such measurements assume a Förster dipole-dipole resonance mechanism of energy transfer, the efficiency of which depends on the inverse 6th power of the distance between donor and acceptor.⁴⁰ Both terbium(III) and europium(III) may act as donors to other metal ions (for example, iron(III) and cobalt(II) respectively) and this has been used to estimate intermetal distances.^{41,42}

The potential use of lanthanide complexes as luminescent labels for analyses in biological media has attracted a great deal of attention.^{3,43,50} Figure 1.4 provides a simplified, schematic illustration of the general principle. Many commercially available assays for important biological molecules are based on such a procedure. In the majority of these, the reporter group (shaded circle in Figure 1.4) is a radioisotope, as this permits detection at extremely low levels.⁴⁴ Drawbacks of such systems include the problems and possible health hazards associated with the handling and disposal of radiolabelled substances and the fact that the lifetime of the assay kits may be limited by the half-life of the radioisotope. It has long been recognised that luminescence can potentially provide an equally sensitive detection method, where such drawbacks do not arise. A number of systems are indeed available which make use of fluorescent reporter groups.⁴³

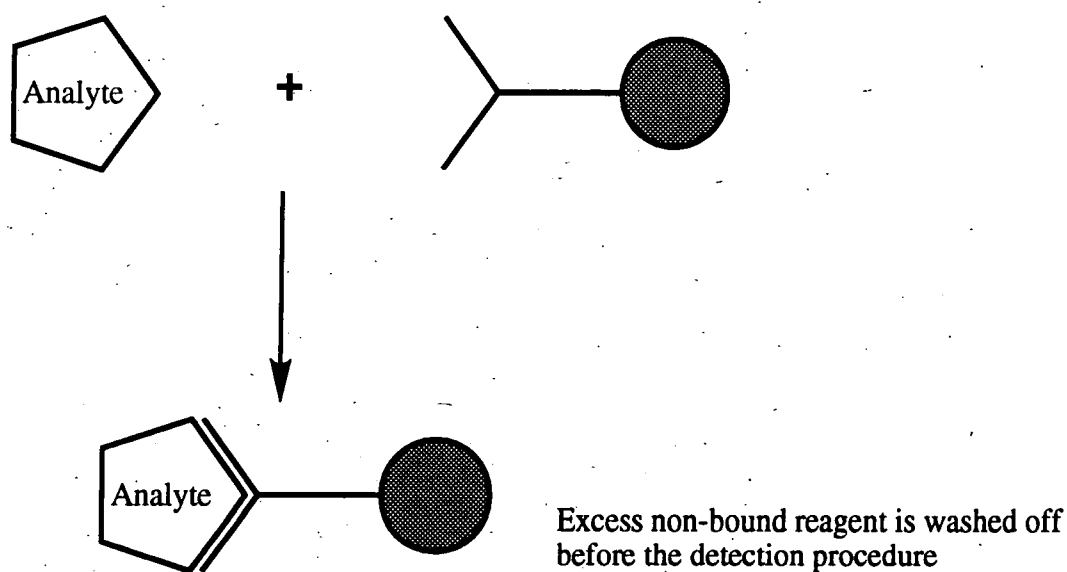


FIGURE 1.4 *Schematic diagram of the general principle of an assay making use of a luminescent or radiolabelled reporter group*

The targeting part of the system (shown as > in Figure 1.4) may be a protein or antibody fragment, raised by immunological methods to recognise selectively and bind strongly to the target biomolecule of interest, in which case the technique is referred to as fluoroimmunoassay. In terms of both sensitivity and selectivity, immunological

methods are far superior to any other analytical methods for the determination of biological materials in very low concentration.⁴⁴

The concept is by no means limited to immunological assays, however. Systems based on simpler, reversible targeting species for detecting smaller molecules may be envisaged, for example the use of small peptides,⁴⁵ nucleic acid strands⁴⁶ or cyclodextrins.⁴⁷ In such cases, the use of a luminescent label may provide further advantages over radioisotopes as the binding of the analyte may cause a direct effect on the luminescence, for example a triggering or quenching of the emission or a shift in the emission or excitation wavelength maxima. In addition to detection systems of this sort, such luminescent compounds may also be used as 'tags' to monitor the fate of molecules within cells.

In any application intended for use in biological media, however, the use of fluorescent labels faces a disadvantage, namely the problem of background fluorescence leading to decreased sensitivity. Any biological sample, including serum, is likely to contain a large number of fluorescent compounds (compounds as simple as the aromatic amino acids, for example, along with substances such as NADH or bilirubin) and will therefore exhibit substantial and variable levels of background fluorescence. This interferes with the signal from the fluorescent label and cannot be corrected for properly. Scattered light and Raman bands are further potential problems, especially where the Stokes' shift is small.

The use of luminescent lanthanides as labels potentially provides an elegant solution to this problem.⁴³ The background fluorescence of biological materials is almost invariably short-lived compared to the long luminescence lifetimes of europium(III) and terbium(III). This allows a time-resolved detection method to be used, the basis of which is shown in Figure 1.5.

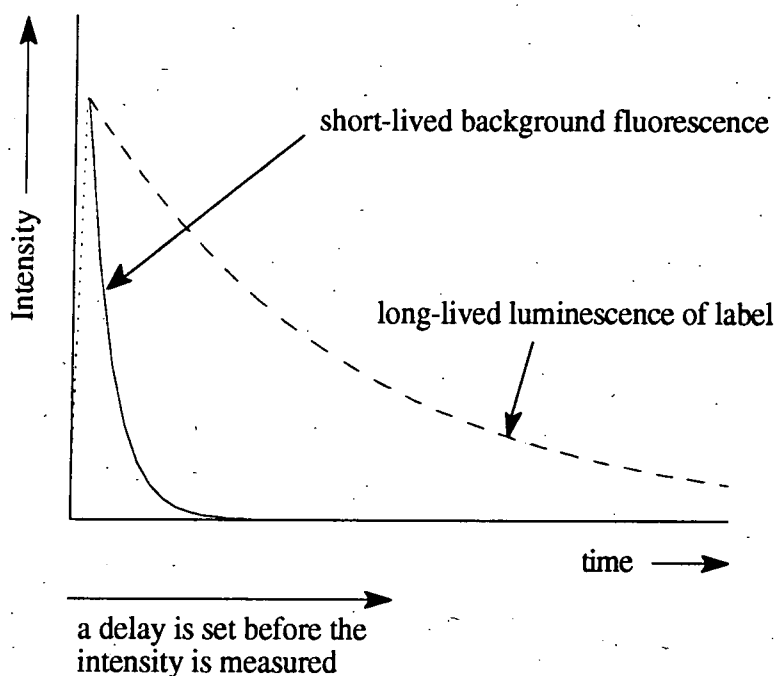


FIGURE 1.5 *Illustrating the principle of time-resolved detection to eliminate background fluorescence.*

Pulsed excitation is used, whereby the sample is excited by a brief pulse of light, perhaps of $10\mu\text{s}$ or less. The intensity of the background fluorescence rises rapidly over the duration of the flash but decays almost immediately (typically on the nanosecond-to-microsecond timescale). In contrast, the luminescence of the lanthanide ion also grows rapidly during the flash but then decays over a much longer timescale, potentially over several milliseconds (depending on the lifetime of the emissive state under the conditions used). This allows a delay to be set between the excitation pulse and the measurement of the lanthanide luminescence, during which time the background fluorescence and scattered light decay to negligible levels. In this way, interference from the luminescence of the biological material is minimised. Provided that the luminescence decay is highly reproducible (i.e. lifetime is constant) then the measured luminescence over the integration time will be directly proportional to the concentration of the analyte.

In principle, any phosphorescent molecule with a sufficiently long phosphorescence lifetime could be used in this way. However, in most cases, the observation of long-lived phosphorescence requires the use of deoxygenated solutions and, in many cases, low temperatures, in order to reduce competitive deactivation processes. The attraction of the lanthanides lies in the fact that long-lived luminescence may be observed under ambient conditions. Two other advantages of lanthanide luminescence may be cited. Firstly their emission spectra show bands which are very narrow and remarkably insensitive to environmental changes: the wavelengths barely shift more than ± 2 nm on changing conditions such as temperature or indeed the coordination site. Secondly, the use of sensitised emission gives rise to a large Stokes' shift (often > 200 nm) such that there is unlikely to be any overlap of the emission bands with strong absorbance bands: concentration-dependent self-absorption problems therefore do not arise.

Commercial kits are currently available which make use of two europium complexes in a two-step procedure.^{3,48} In order to use Eu^{III} as a label, the ion has to be bound strongly to the immunoreactive component and this has been achieved using the polycarboxylic acid ligand EDTA. Excitation of the metal through this ligand is inefficient and the ligand provides poor protection of the metal from the deactivating effect of solvent water molecules, with the result that the luminescence is too weak to be used directly for analytical purposes. Instead, following reaction with the target molecule, the europium is dissociated from the EDTA complex by reducing the pH to 2-3 and is re-complexed by a second ligand, normally a β -diketone, which provides a strongly luminescent complex for detection.⁴⁹ Owing to the very low solubility of β -diketones in water, this second step has to be carried out in the presence of a non-ionic detergent which dissolves the organic component in a micellar phase and also helps to exclude water molecules from the europium ion; excess trioctylphosphine oxide is also added to aid in this second effect. β -Diketone complexes of the lanthanides do not have sufficient stability in aqueous solution to be linked directly to the immunoreactive component.

Whilst such systems have enjoyed considerable success in the detection of low concentrations of molecules such as hormones,³ and as labelling methods for cloned DNA probes used in hybridisation assays,⁴⁶ it has been recognised that a preferable and more widely applicable assay configuration would involve a strongly luminescent complex directly bound to the immunoreactants, allowing direct quantitation to be performed. In addition, analytical procedures based on a direct modulation of the luminescence on binding of the analyte, as discussed earlier, may then be achieved. Such systems become realistic if lanthanide complexes can be prepared which are simultaneously strongly luminescent and stable under aqueous conditions.

1.5 Complexing Agents for Lanthanides

1.5.1 Some general points

In their complexation chemistry, the lanthanide ions resemble the alkaline earth ions much more closely than the transition metals.⁵¹ The variety of coordination numbers and geometric structures of lanthanide complexes indicates that the constraints of metal-ligand orbital interactions, as observed in transition metal complexes, do not apply.⁵² High coordination numbers are favoured (typically 8 - 12) apparently limited largely by steric effects. The cations behave as hard acids (proton-like behaviour) showing a preference for ligands containing hard oxygen or nitrogen donors rather than soft bases such as sulfur or phosphorus.⁵³ The effect of charge is particularly important: the high charge density of the Ln^{3+} cations favours complexation by poly-anionic ligands. Indeed, the neutral R-OH group⁵⁴ is significantly inferior to charged oxygen donors such as carboxylates, for example.⁷⁷ The polarisability of the donor is also a factor. Thus, nitrogen donors are favoured and amide groups are able to bind efficiently to the metal via the oxygen atom. Complex stability in aqueous solution is sought but water is in fact the most difficult environment to achieve high stabilities, owing to the high affinity of the metal ions for water molecules as ligands.

The use of chelating ligands is a widely-used means of enhancing complex stabilities, by virtue of the chelate effect.^{55,56} The size of the chelate ring is an important

dissociation is acid or cation catalysed and the complex is sufficiently flexible to permit protonation of one of the binding nitrogen atoms. This effect is exacerbated by the net negative charge of the complex (2-), which favours protonation.

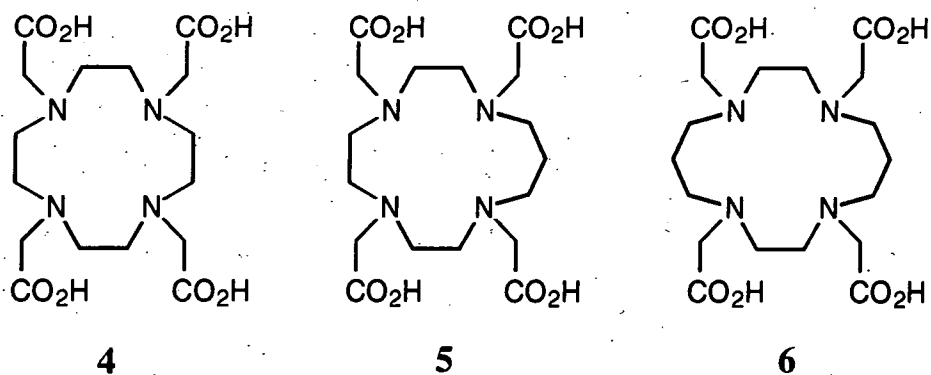
1.5.2 Macrocyclic Complexing Agents

Macrocyclic ligands are those which contain at least 9 atoms in a ring with at least three potential donor groups. They form complexes which almost invariably display higher thermodynamic and kinetic stability than their open-chain analogues. The enhanced stability exceeds that which can be attributed to the extra chelate effect associated with an additional chelate ring.⁶⁵ This has been termed the 'macrocyclic effect',⁶⁶ the origins of which have been the subject of a good deal of research effort. The consensus is that the enhanced thermodynamic stabilities are not derived from an enthalpic or entropic effect alone but from a combination, their relative importance varying according to the cation and macrocycle involved. The kinetic inertness towards metal ion dissociation displayed by many macrocyclic complexes has been ascribed to the relatively rigid conformations of the macrocycles in their complexes. The conformational restrictions of the macrocycle make the transition states in the stepwise dissociation energetically unfavourable. In contrast, the greater flexibility of acyclic ligands leads to a much larger range of energetically accessible conformations and thus more labile complexes.

A large variety of macrocyclic ligands with pendent donor groups have been prepared.⁶⁵ Such pendent arms often serve to increase the stability of a macrocyclic complex and may lead to greater selectivity and hence metal ion discrimination. The use of neutral oxygen donors has been popular; for example, hydroxyethyl pendent groups generally produce a marked decrease in complex stability for small metal ions but a moderate increase in stability for larger ions such as Pb^{2+} .^{67,68} Other groups commonly used include pyridyl,⁶⁹ phenolate,⁷⁰ 2-aminoethyl,⁷¹ amide⁷² and carboxylate⁷³ groups. The use of carboxylate groups has been found to impart enhanced stability at low pH: this arises from their ability to aid resistance to

protonation on the heteroatoms of the macrocyclic ring.⁷⁴ In contrast, the use of phenolate groups gives improved stability in basic media.⁷⁰

As discussed earlier, the lanthanides display high coordination numbers, typically 8 or higher, and a preference for hard nitrogen and oxygen donors and for ligands which are negatively charged. Thus, it might be expected that the ligands which are most likely to form strong complexes with lanthanides will be octadentate, anionic and will contain at least some oxygen and nitrogen donors (as is the case for DTPA mentioned earlier). With this in mind, a number of tetraaza macrocycles bearing 4 oxygen-containing pendent arms have been prepared⁷⁵ and the thermodynamic and, in some cases, kinetic stabilities of their complexes have been investigated. Most of these contain carboxylate donors⁷⁶⁻⁸² and three are shown in Figure 1.7, with 12, 13 and 14 membered macrocyclic rings.



M ³⁺	DOTA	TRITA	TETA
Eu ³⁺	28.2 ^a	---	15.5 ^a
Y ³⁺	24.9 ^b	19.6 ^b	16.3 ^b

(a) reference 80. (b) reference 74.

FIGURE 1.7. Some macrocyclic tetraazacarboxylate ligands. Thermodynamic stabilities ($\log K_{ML}$) of their Eu³⁺ and Y³⁺ complexes are shown, determined by potentiometric titration in aqueous solution at 298K, $I = 0.1$, except for [Eu.DOTA]⁻, where the value was obtained through a gravimetric analysis. The values are therefore not directly comparable but the important point is the trend in each case.

The stability constants for the formation of 1:1 complexes with Eu^{3+} and the related rare-earth ion Y^{3+} are shown; the stability constants show the following trend:



In contrast to the behaviour of crown ethers, for example, this variation in stability constants does not reflect a matching of ring size with the metal ion radius. This is due to the fact that the metal does not lie in the plane of the 4 ring nitrogen donors, as the cavity is not sufficiently large to accommodate a lanthanide ion. This is clearly apparent in the X-ray structure of NaEuDOTA , for example, which shows that the 8 donor atoms in DOTA form a square antiprism about the europium cation with the tetraaza ring as one square face.⁸² (The ninth coordination site in the monocapped square-antiprismatic structure is occupied by a water molecule). Stabilities, therefore, would not be expected to arise from a simple situation of a fit between the aza ring and the cation but must also include the position of the acetate arms which bind to the cation. A further point relates to the preference of large ions, such as the lanthanides, for 5-ring over 6-ring chelates mentioned earlier.^{59,60} Whereas DOTA complexes contain solely 5-ring chelates, 6-membered propylenediamine chelates occur in the complexes of TRITA and TETA.

Greatly enhanced kinetic inertness is also a feature of DOTA complexes compared to those of larger ring systems or related acyclic ligands (such as DTPA).⁷⁴ This probably reflects the greater conformational rigidity of the former, disfavours the pathway that leads to protonation of the ring nitrogens and a more efficient shielding of the metal ion from attack by an oxonium ion (H_3O^+).

1.6 Desirable properties of luminescent lanthanide probes

1.6.1 Some general points

Some recent examples of attempts to obtain stable, luminescent complexes of the lanthanides are described in section 1.7. It is useful first, however, to provide some indication as to the criteria by which such compounds may be assessed and a summary of some of the luminescence properties which need to be examined.

Applications of luminescent lanthanide complexes almost invariably involve their use in aqueous solution, normally at physiological pH (= 7.4). Thus, solubility in water is essential, as is complex stability under such conditions. Moreover, water molecules are able to deactivate the lanthanide emissive states (section 1.3.2) thereby decreasing the intensity and lifetime of emission. Results which are quoted only for solvents such as acetonitrile therefore need to be treated with some caution: good results in such solvents may not necessarily extend to the behaviour in aqueous solution.

The ligand must be capable of being modified readily to allow covalent linkage to the targeting vehicle by means of a water-stable functionality, without affecting the luminescence properties of the complex. A more difficult point to predict is the effect of the complex on the targeting part of the molecule: the complex should not inhibit binding of the analyte, be it through steric, electrostatic or other effects. In the case of immunoassay, it is important that the complex does not denature its binding protein. Interaction with other components of the biological sample should be minimal.

1.6.2 Absorbance

It must be possible to excite the complex at a suitable wavelength. Biological samples absorb strongly below about 330 nm; excitation wavelengths below this value are therefore undesirable as only a small proportion of the incident light will be absorbed by the complex, with a resulting loss of sensitivity. Detection limits will be at their lowest if the absorbance of the antenna is strong; hence a high extinction coefficient at the excitation wavelength is required.

1.6.3 Lifetime of emission

If a single light-emitting species is present and there is no quenching of the emissive state by other excited state molecules, then monoexponential decay of the luminescence is expected. That is, the intensity at time t after an excitation pulse will be given by:

$$I_t = I_0 \exp(-k_{\text{obs}}t) \quad (6)$$

where I_0 is the intensity at time $t = 0$. The decay curve is characterised by k_{obs} , the observed rate constant for deactivation of the emissive state, which is given by the sum of the radiative rate constant (k^0) and the first order rate constants for competing non-radiative processes (k^{nr}):

$$k_{\text{obs}} = k^0 + \sum k_i^{\text{nr}} \quad (7)$$

The lifetime of the emission is then the reciprocal of the observed rate constant and as such is the time taken for the intensity of emission to fall to $1/e$ of its initial value.

$$\tau_{\text{obs}} = (k_{\text{obs}})^{-1} \quad (8)$$

The half-life ($t_{1/2}$) of emission is sometimes quoted instead; this is related to the lifetime through:

$$t_{1/2} = \log_e 2 \cdot \tau \quad (9)$$

A long luminescence lifetime is clearly a requirement for time-resolved assays. Lifetime measurements also provide an indication of the efficiency of the light-emitting process (cf. quantum yields below): a long lifetime (approaching the calculated natural luminescence lifetime, τ^0 [$=1/k^0$]) indicates that non-radiative processes are not competing efficiently with luminescence. Conversely, short lifetimes are indicative of highly competitive, non-radiative deactivating processes which will be reflected in a reduced quantum yield.

Aside from these points, the lifetime is a useful probe of sample homogeneity. If more than one light-emitting species is present, then multi-exponential decay of the luminescence is likely to arise.

1.6.4 Hydration state, q .

As discussed in section 1.3.3, measurements of lifetimes in H_2O and D_2O can provide an indication of the extent to which the emissive state may be deactivated by energy transfer into O-H vibrations. Clearly it is desirable to minimise deactivation *via* this pathway to obtain optimum luminescence. Thus, a low value of the hydration state, q , is sought; i.e. the ligand should ideally provide an efficient shielding of the metal from the solvent water molecules.

1.6.5 Quantum Yield

The quantum yield of emission is perhaps the most useful piece of information as it provides a measure of the efficiency of the emission process. In cases where the emitting state is also the absorbing state (eg. for fluorescence or direct laser excitation of the emissive state of a lanthanide ion), the quantum yield of emission (ϕ_{em}) is the ratio of the radiative rate constant k^0 to the sum of all rate constants for processes that deactivate the emitting state (eq. 10) and as such is the fraction of molecules that are deactivated by emission of light.

$$\phi_{\text{em}} = \frac{k^0}{k^0 + \sum k_i^{\text{nr}}} \quad (10)$$

{Here, $\sum k_i^{\text{nr}}$ is the sum of the rate constants for non-radiative deactivation processes, unimolecular or pseudo-unimolecular; this expression does not apply in the presence of dynamic bimolecular quenching}.

The quantity $(k^0 + \sum k_i^{\text{nr}})^{-1}$ is the observed luminescence lifetime, τ_{obs} , as discussed above. Hence:

$$\phi_{\text{em}} = k^0 \cdot \tau_{\text{obs}} \quad (11)$$

which indicates that there is a direct dependence of the quantum yield on the luminescence lifetime. Of course, this reflects the fact that a high quantum yield is more likely to be obtained when the non-radiative pathways of deactivation are not able to compete efficiently with luminescence.

For systems in which the emitting state is not the one which is initially populated by absorption of light (eg. for phosphorescence and for sensitised emission), the quantum yield will also depend on the efficiency of formation of the emissive state from the initially-populated state (usually the first excited singlet state). Thus, for ligand-sensitised lanthanide luminescence, the emissive quantum yield will also be dependent both on the efficiency of formation of the state from which energy transfer occurs (in most cases this is thought to be the T_1 state of the antenna) *and* on the efficiency of the energy transfer process itself (η_{et}). Thus:

$$\phi_{em} = \phi_T \cdot \eta_{et} \cdot k^0 \cdot \tau_{obs} \quad (12)$$

where ϕ_T is the quantum yield of formation of the triplet state.

The quantum yield of emission is in fact the ratio of the number of photons emitted to the number of photons absorbed. Clearly all three quantities (ϕ_T , η_{et} and τ_{obs}) must be optimised in order to obtain a high value and hence low detection limits.

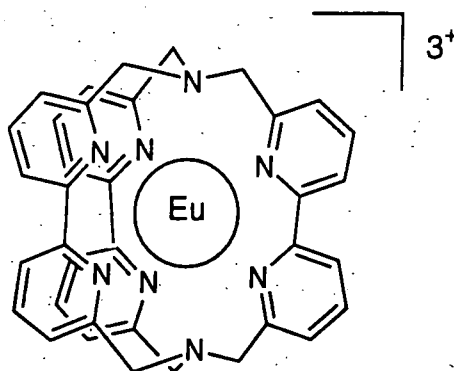
1.7 Some examples of recent work

1.7.1 Cryptates and ligands containing 2, 2'-bipyridine⁸³

Cryptands are tricyclic ligands which generally resemble the crown ethers in their complexation chemistry.⁸⁴ Their complexes with alkali and alkaline-earth cations are usually rather more stable than those of crown ethers of similar cavity size, however, and they are expected to form complexes with the lanthanide ions with a reasonably high degree of shielding of the metal from the solvent.

With this in mind, lanthanide complexes of the bipy.bipy.bipy cryptand **7**, which contains three 2, 2'-bipyridine units, have been prepared.^{85,86} The bipyridine groups absorb strongly in the UV (ca. 300 nm). Excitation in this region results in an energy transfer process from the ligand to the metal ion.⁸⁷ The rather low values of the emission quantum yields (ϕ_{H_2O} for Eu = 0.02; for Tb = 0.03) indicate that the light

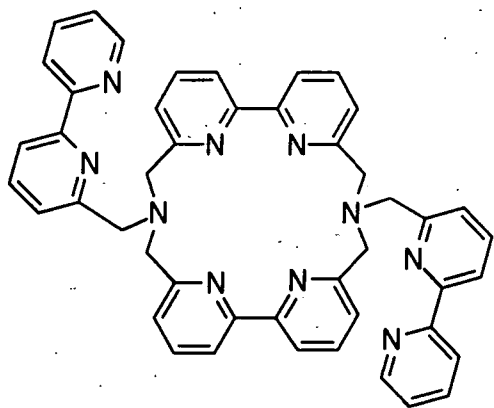
absorbed by the ligand is not converted efficiently into light emitted by the metal ion. In the europium complex, the efficiency of energy transfer from the ligand to the metal 5D_0 state was estimated to be 10%. This low conversion efficiency was attributed to the presence of LMCT levels, which provide the bipy singlet state, and possibly also the triplet, with a direct deactivation pathway to the ground state. A further factor contributing to the low quantum yield is the poor shielding of the metal ion from the solvent water molecules, as reflected in the short lifetime of emission ($\tau_{H_2O}^{300K} = 0.34$ ms). Comparison with the lifetime in D_2O indicates that about 2.5 water molecules are coordinated to the metal ion. In the terbium complex, a strong temperature-dependence of the lifetime and intensity was observed, which was attributed to a thermally activated depopulation pathway for the emissive state by back-energy transfer to the ligand T_1 .



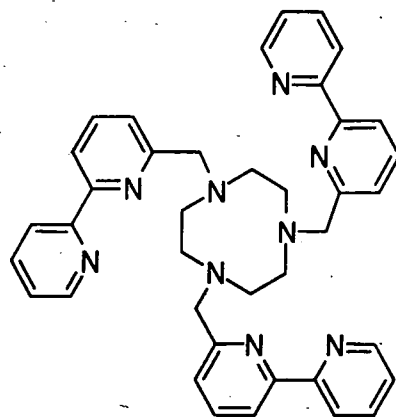
7

The use of 2, 2'-bipyridine as an antenna has been extended to branched macrocyclic ligands such as **8**⁸⁸ and **9**⁶⁹. The lanthanide complexes of both of these ligands show a greatly improved shielding from the solvent water: lifetimes are not substantially shorter in H_2O than in D_2O . The europium complex of **8** shows enhanced luminescence ($\phi_{H_2O}^{300K} = 0.1$) compared to that of ligand **7** ($\phi_{H_2O}^{300K} = 0.02$).⁸⁸ The terbium complex is reported to be unstable in aqueous solution. This is a strange observation, especially bearing in mind that the stability of the europium complex was not commented upon. Such behaviour is, of course, particularly undesirable in any potential application and casts some doubt on the suitability of these systems for further

development. The terbium complex of ligand **9**, on the other hand, shows a remarkably high quantum yield on ligand excitation, $\phi_{\text{H}_2\text{O}}^{300\text{K}} = 0.37$. Curiously, no temperature dependence is observed in this case, implying that the thermally-activated back energy transfer does not occur in this compound.⁶⁹



8



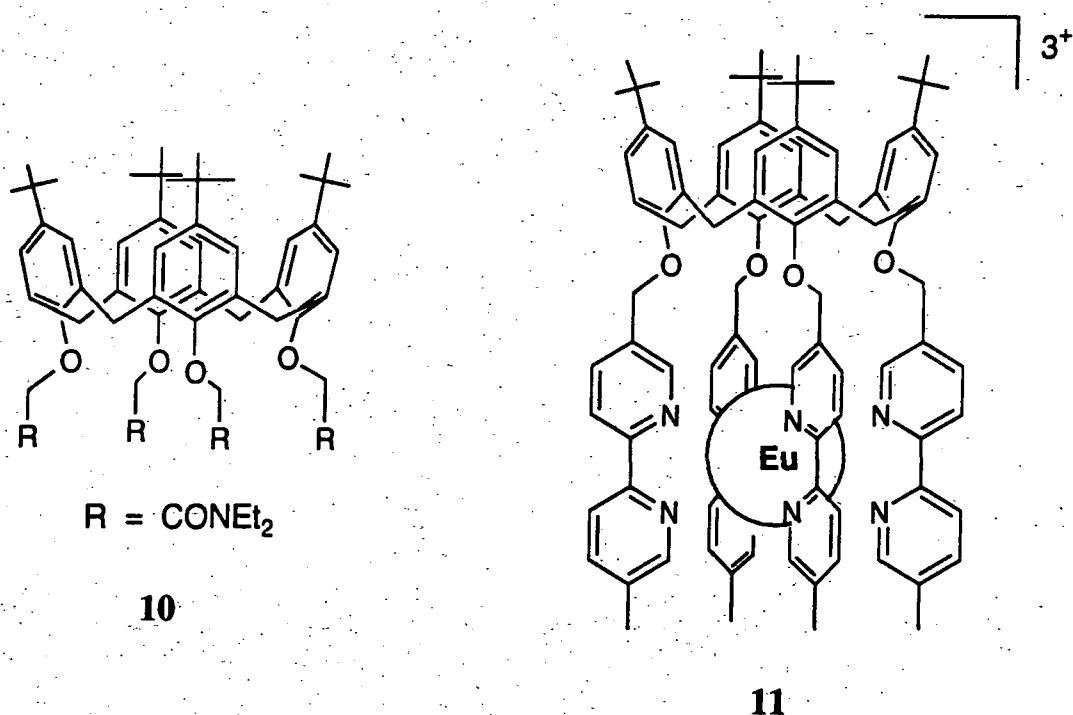
9

1.7.2 Calixarenes

Europium(III) and terbium(III) ions have been encapsulated in the *para*-*t*-butylcalix[4]arene-tetraacetamide ligand **10**; the complexes are relatively stable and are water-soluble.⁸⁹ Lifetime measurements in H₂O and D₂O have shown that there is one water molecule coordinated to the metal ion. Energy transfer from the phenyl groups to the metal ions is observed. The luminescence quantum yield is very low for the europium complex, again ascribed to deactivation via a LMCT state, whilst that of the terbium complex is quite high, $\phi_{\text{H}_2\text{O}}^{300\text{K}} = 0.2$.

In an attempt to increase the absorbance of systems of this type and to extend the excitation wavelength to a longer, more practicable value, Ungaro and co-workers have prepared related calixarenes in which 2 or 4 of the amide groups are replaced by bipyridine groups.⁹⁰ The use of 6-substituted bipyridine groups gave complexes of rather poor stability (formation constants were estimated to be of the order of 10^5 M^{-1} in acetonitrile) and solid samples could not be isolated. The use of the less sterically demanding 5,5'-disubstituted 2,2'-bipyridines in compound **11** gave more stable

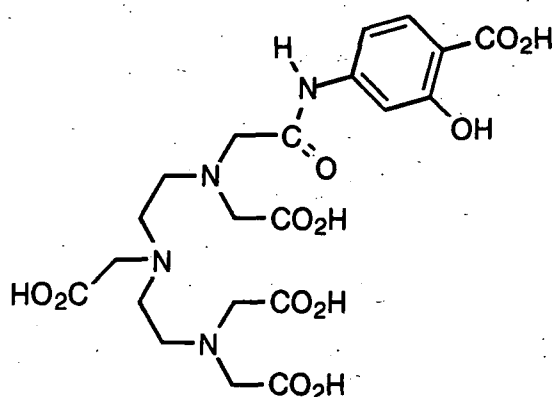
complexes and with high extinction coefficients ($\epsilon = 3.9 \times 10^4 \text{ M}^{-1}\text{cm}^{-1}$). The europium complex of this ligand displayed a particularly high quantum yield of 0.15, although it should be noted that all of the reported measurements were carried out in acetonitrile. The luminescence efficiency in water would be expected to be substantially lower, owing to the O-H deactivating effect; it is unclear from the work published so far whether the complexes are indeed stable in aqueous solution - it is likely that they are not. Similarly, the work of Shinkai on analogous aryl ketone appended calixarenes shows that, whilst good results are obtained in acetonitrile, the quantum yields fall drastically in methanol.⁹¹



1.7.3 Polyaminopolycarboxylate ligands

As mentioned in section 1.5.1, the acyclic ligand DTPA (3) (Figure 1.6) forms complexes of high thermodynamic stability with lanthanide ions (stability constants of the order of 10^{22}). Attempts have been made to append the DTPA molecule with a strong chromophore in the hope that this would act as an antenna and give rise to strongly luminescent, stable lanthanide complexes. The reaction of DTPA anhydride with p-aminosalicylic acid (pAS) gave a suitable ligand 12 which formed a highly luminescent Tb^{III} complex.⁹² It was claimed in the original report that the OH and

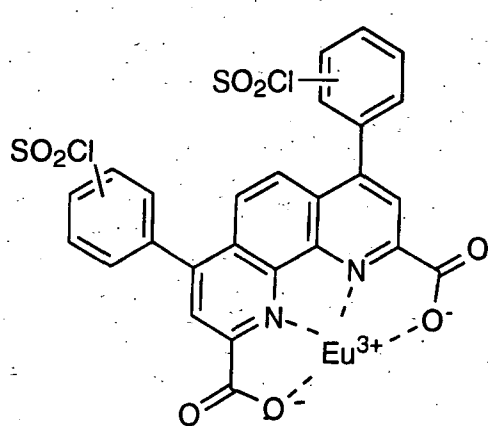
CO_2^- groups of the aryl ring may bind to the metal, enhancing both the complex stability and energy transfer efficiency. However, it is clear from the structure (12) that if the amide carbonyl binds to the metal, then there is no way in which these groups will also be able to bind. In fact, this ligand was not purified or characterised and must therefore have consisted of at least a mixture of DTPA, DTPA-pAS and DTPA-(pAS)₂. Nevertheless, the reagent has been linked to proteins by reaction with the $-\text{NH}_2$ group of a suitable amino acid and a study with human serum albumin was carried out in this way which showed a detection limit of 5 pmol on excitation at 312 nm, (using conventional instrumentation). The lifetime of emission was found to be 1.58 ms; subsequent work by another group gave a value of 0.1 for the quantum yield in aqueous solution.⁹³ This same reagent (again it was not purified) has been used in a number of more recent studies for labelling of proteins,^{94,95} hormones,⁹⁵ human IgG⁹⁵ and oligonucleotides.^{93, 96} One of these studies clearly demonstrates one of the important advantages of lanthanide luminescence mentioned in section 1.4, namely the fact that the large Stokes' shift ensures that concentration-dependent self-absorption problems do not arise. It was found that an exceptionally large amount of the terbium label, over 200 moles of complex per mole of analyte, could be conjugated to the compounds tested without self-quenching becoming a problem.⁹⁵



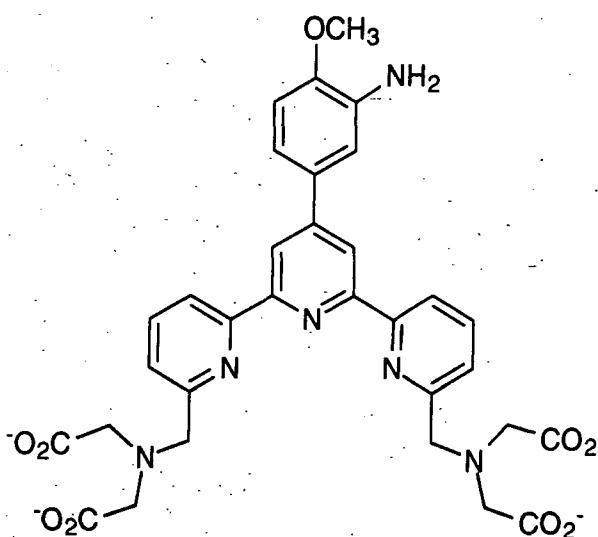
12

Two other noteworthy ligands of the polyaminopolycarboxylate type are 13 and 14. The europium complex of BCPDA has been the subject of thorough investigation in a

number of bioassay applications,^{50,97,98} it is commercially available under the name FIAgen™. Covalent linkage to proteins or nucleic acids is accomplished through the sulfonyl chloride groups but one drawback of this system is that multiple labelling is essential in order to achieve sufficient sensitivity for most applications. A preliminary report on EuTMT has demonstrated excellent detection limits for a labelled oligonucleotide.⁹⁹ The long luminescence lifetime of 1.4 ms in aqueous solution is consistent with formation of a 9-coordinate complex with the metal and hence efficient shielding from water molecules.



13

BCPDA: Eu³⁺ complex

14

TMT

1.8 Lanthanide NMR

1.8.1 Paramagnetic Shifts

When a molecule interacts with a lanthanide cation (for example, through a Lewis basic atom in a ligand) any NMR active nucleus within the molecule may experience a magnetic moment arising from the unpaired f electrons, which can lead to a shift in the NMR resonance frequency. This is the basis of the use of lanthanide complexes as NMR shift reagents.¹⁰⁰ For a purely electrostatic interaction between the metal cation and the Lewis base, a shift will arise only for those cations which have an anisotropic distribution of f electrons (i.e. all the lanthanide (III) cations except Gd³⁺). Such a shift is known as a dipolar or pseudocontact shift. If however there is some covalent

character to the interaction, then a small amount of unpaired electron spin density can reach atoms in the ligand molecule (especially for those atoms directly bonded to the metal or within one or two bond lengths) and this may result in a second type of shift called the contact shift. The extent to which the electron spin density interacts with the nucleus under observation is determined by the nuclear hyperfine coupling interaction, often given the symbol A .

The pseudocontact shift might be expected to predominate for lanthanide complexes as the unpaired electrons occupy 4f orbitals which are well-shielded from the 'valence orbitals' involved in bonding between the metal and a ligand. However, this does not always prove to be the case, as exemplified below, and the contact contribution may be dominant. The observed shift is additive:

$$\delta_{\text{obs}} = \delta_{\text{dia}} + \delta_{\text{dip}} + \delta_{\text{con}} \quad (13)$$

where δ_{dip} and δ_{con} are the chemical shift changes arising from the pseudocontact and contact contributions respectively and δ_{dia} is the shift which may arise on binding of an analogous, diamagnetic ion (the diamagnetic ions La^{3+} , Lu^{3+} or Y^{3+} are often used to determine this quantity).

Contact shift

As discussed in section 1.3.1, the Russell-Saunders coupling scheme provides a satisfactory approximation for the lanthanides, J being a good quantum number. The temperature-independent magnetic moment μ_{eff} of a free f^n ion in a single J state is given by:

$$\mu_{\text{eff}} = g_J [J(J+1)]^{1/2} \quad (14)$$

in units of the Bohr magneton and where the Landé g -factor is

$$g_J = 1 + \frac{J(J+1) - L(L+1) + S(S+1)}{2J(J+1)} \quad (15)$$

This expression accurately predicts the observed magnetic moments of all the Ln^{3+} ions, with the exception of Eu^{3+} and Sm^{2+} (where low-lying excited states which are significantly populated at room temperature need to be taken into account).⁵²

There are $(2J+1)$ components to each J level; the spin moment of each of these components is given by:¹⁰¹

$$\langle S_z \rangle_{J_z} = (g_J - 1) \cdot J_z$$

It has been shown that, when an external magnetic field B is applied at a temperature T , then the resulting thermal average $\langle S \rangle_{\text{av}}$ of the spin moment for the total J manifold is given by:^{101,102}

$$\langle S \rangle_{\text{av}} = \frac{-\beta B}{3kT} g_J (g_J - 1) \cdot J(J + 1) \quad (17)$$

where β is the Bohr magneton.

For a nucleus located on a ligand bound to a lanthanide ion, the change in the effective magnetic field, ΔB , at the NMR nucleus due to the contact interaction with the unpaired f electrons is related to this averaged spin moment through:¹⁰³

$$\Delta B = K_{\text{con}} \cdot A \cdot \langle S \rangle_{\text{av}} \quad (18)$$

where A is the hyperfine interaction constant between the two nuclei and K_{con} is a numerical factor which includes the gyromagnetic ratio of the nucleus being observed and accounts for the dimensions in which A is expressed.

Clearly, the contact contribution, δ_{con} , to the paramagnetic shift is directly dependent on ΔB ; hence, from equations 18 and 17:

$$\delta_{\text{con}} \propto \langle S \rangle_{\text{av}} \quad (19)$$

and therefore:

$$\delta_{\text{con}} \propto (g_J - 1) \quad (20)$$

Values of $(g_J - 1)$ are tabulated in Table 1.3. The paramagnetic ^{17}O shifts observed for aqueous solutions of the lanthanides (column 7 of the table) exhibit the same sign variation as this quantity $(g_J - 1)$ although the magnitude of the changes from one ion to the next are not completely rationalised and the value for europium is clearly incorrect,

TABLE 1.3 Some NMR parameters for the paramagnetic lanthanide ions

Ln^{3+}	f^n	$2S+1L_J$ for ground state	$(g_J - 1)$	$\langle S \rangle_{av}^a$	C_J^b	^{17}O shift in aquo ion ^{c,d}	^{1}H shift in $\text{Ln}(\text{dpa})_3$ ^{c,e}	^{1}H shift in aquo ion ^{c,f}	$\Delta V_{1/2}^g$
Ce	f^1	$2F_{5/2}$	-1/7	-0.98	-6.3	-28	---	---	---
Pr	f^2	$3H_4$	-1/5	-2.97	-11.0	-58	-13	0.27	5.6
Nd	f^3	$4I_{9/2}$	-3/11	-4.49	-4.2	-77	-7.6	0.32	4.0
Pm	f^4	$5I_4$	-2/5	4.01	2.0	---	---	---	---
Sm	f^5	$6H_{5/2}$	-5/7	0.06	-0.7	-2	-1.3	---	4.4
Eu	f^6	$7F_0$	-1	10.68	4.0	144	12	---	5.0
Gd	f^7	$8S_{7/2}$	1	31.50	0.0	424	---	3.01	---
Tb	f^8	$7F_6$	1/2	31.82	-86	411	-92	-10.53	96
Dy	f^9	$6H_{15/2}$	1/3	28.55	-100	363	-100	-6.95	200
Ho	f^{10}	$5I_8$	1/4	22.63	-39	300	-51	-4.88	50
Er	f^{11}	$4I_{15/2}$	1/5	15.37	33	244	31	3.83	50
Tm	f^{12}	$3H_6$	1/6	8.21	53	123	64	9.29	65
Yb	f^{13}	$2F_{7/2}$	1/7	2.59	22	33	23	2.52	12

(a). Calculated $\langle S \rangle_{av}$ values for prediction of contact shifts (104). (b) Bleaney's C_J values for predicting dipolar shifts, normalised to 100 for Dy^{3+} (107). (c) A negative sign indicates a shift to high frequency. (d) Values in ppm (102). (e) dpa is 2,6-dipicolinate; shifts are normalised to 100 for Dy^{3+} (108). (f) Values in ppm (109). (g). Half-height widths of the methyl resonance of 2-picoline in the presence of the tris(dipivaloylmethane) complex of the lanthanide (III) ion; values in Hz (111).

perhaps not surprisingly bearing in mind the presence of the low-lying excited states mentioned earlier. The use of a more sophisticated 2nd order treatment, which includes the effects of mixing with higher energy states, gives the values of $\langle S \rangle_{av}$ shown in the 5th column of the table;¹⁰⁴ these values accurately account for the observed ^{17}O shifts and also account for analogous ^{14}N trends. This confirms the hypothesis that it is the contact shift which dominates when nuclei such as ^{14}N or ^{17}O , which possess a lone pair of electrons, bond directly to the metal ion, with a direct interaction of the nucleus with the metal electron spin vector. Further evidence in support of a dominant contact contribution in such cases is provided by observations of Gd^{3+} complexes where no dipolar contribution is expected (see above); eg. the ^{14}N resonance in a pyridine adduct of $\text{Gd}(\text{dpm})_3$ shows an upfield shift of 1450 ppm.¹⁰⁵ A further point is apparent from equation 17, namely that the contact shifts are expected to show an inverse dependence on temperature.

Pseudocontact or dipolar shifts

A theoretical treatment of pseudocontact shifts has been carried out by Bleaney.¹⁰⁶ For an axially symmetric complex, the dipolar shift of a nucleus of a bound ligand, whose position relative to the metal is represented by the polar coordinates r and θ , is given by equation (21):

$$\delta_{\text{dip}} = C_J \cdot \frac{\beta^2}{60 (kT)^2} \cdot \left\{ \frac{(3\cos^2\theta - 1)}{r^3} \right\} \cdot P' \quad (21)$$

and $C_J = g^2 J (J + 1) (2J - 1) (2J + 3) \langle J_{||} J \rangle$

where $\langle J_{||} J \rangle$ is a numerical coefficient derived from certain matrix elements of J .

The parameter P' is a crystal-field splitting coefficient; for an isostructural series of Ln^{3+} complexes, its value is expected to remain constant. Under such conditions, the sign and relative magnitudes of the pseudocontact shifts at a given nucleus are expected to be determined by the value of C_J .¹⁰⁷ The values of C_J calculated by Bleaney are shown in Table 1.3 (normalised to 100 for Dy^{3+}). Comparison with the observed ^1H

shifts of the complexes of the 2,6-dipicolinate (dpa) ligand¹⁰⁸ shows that these values accurately account for both the sign and magnitude of the shifts in such a system, indicating that the dipolar contribution must be predominant in this case. It is apparent from equation 21 that, unlike the T^{-1} dependence of contact shifts, the dipolar shifts are expected to display a T^{-2} dependence. Also shown in Table 1.3 are the ^1H shifts for the aquo complexes; it is clear that these values are not properly accounted for by either theory alone, indicating that both types of shift are contributing significantly here. The relative contributions were assessed and shown to vary substantially from one metal to the next. The dependence of the dipolar shifts on the quantity $(3 \cos^2\theta - 1)/r^3$ often allows a good deal of structural information to be obtained from an analysis of the observed shifts.

1.8.2 NMR line-broadening effects of lanthanide ions

In addition to their shifting effects, the unpaired electrons on the lanthanide ions are also expected to give rise to broadened NMR lines, by catalysing the relaxation of the observed nucleus.¹¹⁰ An important quantity determining the NMR line width is the longitudinal electron-spin relaxation time T_{1e} . A qualitatively useful picture in describing the effect of T_{1e} is to consider the effect of a single unpaired electron on the NMR resonance of a proton. In the limit of a very long electronic relaxation time, a doublet would be expected for the proton NMR resonance, owing to coupling to the electron's magnetic moment. Neglecting the dipolar contribution, the separation of the two lines of the doublet would be proportional to the nuclear hyperfine coupling constant, A , between proton and electron. (This would resemble the situation observed in EPR).

The effect of electron spin relaxation corresponds to exchange of the proton between the two environments (with chemical shifts $A/2h$ and $-A/2h$) and the rate of this exchange process is determined by the electron-spin relaxation time T_{1e} . The usual limiting conditions of chemical exchange may then be applied. Thus, if the rate of exchange (i.e. T_{1e}^{-1}) is much less than the separation of the two lines (in Hz) then a

doublet is expected. On the other hand, if T_{1e}^{-1} is much larger than the separation then a single line is predicted (at a position determined by the relative populations of the two components of the doublet). For intermediate values of T_{1e} , a broad line is expected.

Such a picture is an oversimplified view of the effect and it ignores the dipolar contribution which normally dominates. However, use of the Solomon equation to describe the dipolar effect shows that T_{1e} has a similar effect in this case too.¹¹⁰ In practice, it turns out that for all the lanthanide ions, with the exception of Gd^{3+} , the values of T_{1e} are sufficiently short (ca. 10^{-13} s) as to give rise to quite sharp lines. This is especially true of the early lanthanides, which accounts for their popularity as shift reagents: they are able to shift resonances without giving rise to excessive line-broadening. Table 1.3 (10th column) provides an indication of the relative broadening abilities of the lanthanide(III) ions. One noteworthy feature which arises from the theory is that line-broadening is expected to be more severe in the presence of stronger applied magnetic fields; an important implication is that NMR spectra of lanthanide complexes are often best acquired using low-field instruments.

1.8.3 The exceptional behaviour of Gd^{3+} : Relaxivity and its application in MRI

As stated at the end of the previous section, Gd^{3+} differs from the other Ln^{3+} ions in that it typically has a much longer electron spin relaxation time (ca. 10^{-10} - 10^{-9} s depending on the structure and symmetry of the complex). This is also reflected in the fact that only in Gd^{3+} salts is an electron resonance observable at room temperature. This property of long electronic relaxation, together with the high magnetic moment of Gd^{3+} ($S = 7/2$) means that the relaxation rates of nuclei in the vicinity of the metal are increased to such an extent that their NMR resonances become extremely broad and indeed are rarely observable. Although this poses a problem in terms of acquiring NMR spectra of gadolinium complexes, the ability of Gd^{3+} to catalyse the relaxation of nearby nuclei to such an extent has been put to good use in the application of Gd^{3+} complexes as contrast agents in magnetic resonance imaging.

Magnetic resonance imaging (MRI) is a diagnostic imaging technique which relies on the detection of NMR signals of water protons in the body.^{112,113} The fundamental difference from a laboratory NMR spectrometer is the use of a gradient magnetic field. This causes water protons to resonate at slightly different frequencies depending on their position in the field. The detected signals thereby incorporate spatial information which is decoded by a computer to provide the image.

Paramagnetic compounds (such as those of Gd^{3+}) increase the proton relaxation rate of the water in which they are dissolved. The relaxation time of a proton of a water molecule coordinated to Gd^{3+} is reduced typically by a factor of about $10^5 - 10^6$. This effect can be used to enhance the observed signal intensity in the MRI experiment and may allow the image to be acquired more quickly: the patient is administered with a suitable highly stable complex of the metal prior to the scan. Moreover, such complexes may localise in certain tissues more than others and this gives rise to increased contrast in the image and potentially more useful information. The MRI pulse sequence is usually chosen such that the effect of the paramagnetic centre on the longitudinal relaxation rate, T_1 , is dominant.

Relaxivity

The longitudinal relaxivity, R_1 , of a paramagnetic compound M is defined through:

$$(1/T_1)_{obs} - (1/T_1)_{dia} = R_1 [M] \quad (22)$$

where the term on the left is the difference in the solvent relaxation rates in the presence and absence of M. Thus, the relaxivity of a paramagnetic species is the slope of a plot of $(1/T_1)_{obs}$ against the concentration of the paramagnetic compound, normally in units of $mM^{-1}s^{-1}$.

There are two limiting cases for the mechanism of paramagnetic relaxation of water protons in the presence of a Gd^{3+} ion, namely inner-sphere and outer-sphere. The two contributions are additive:

$$R_1 = R_1^{os} + R_1^{is} \quad (23)$$

(where R_1^{os} and R_1^{is} are the outer and inner sphere contributions respectively).

The outer-sphere relaxation process involves the electron-nuclear magnetic dipolar coupling which occurs when solvent water molecules approach the metal complex during their translational diffusion. A quantitative description has been provided by Freed¹¹⁴ (albeit from a rather different context). The parameters determining the magnitude of R_1^{os} are the distance of closest approach, a , between the metal complex and the outer-sphere water protons, the electronic relaxation time T_{1e} of the metal ion, and the relative diffusion coefficients D for solvent and solute.

The inner-sphere contribution involves dipolar coupling between the metal ion and the protons of a water molecule which is held in a fixed position near the metal (usually directly coordinated) for a time τ_M longer than that necessary for the complex and the solvent water molecule to diffuse apart. Efficient catalysis of the relaxation of bulk water protons requires that the residence time τ_M of the water molecule at the metal is short,¹¹⁵ this is clear from the following relationship:

$$R_1^{\text{is}} \propto \frac{q}{T_{1M} + \tau_M} \quad (24)$$

(where q is the number of inner-sphere water molecules).

Thus, the relaxivity is a maximum when τ_M is much shorter than T_{1M} (T_{1M} is the relaxation time of protons of inner-sphere water molecules, typically 10^{-6} - 10^{-5} s for small Gd^{3+} complexes). This is known as the fast-exchange condition. The lability of gadolinium-bound water molecules (leading to short τ_M values) is one feature which makes Gd^{3+} complexes so attractive in this application.

The value of T_{1M} may be predicted using the Solomon-Bloembergen-Morgan equations given below.¹¹³

$$\frac{1}{T_{1M}} = \frac{2}{15} \frac{\gamma_H^2 g^2 \beta^2 S(S+1)}{r^6} \left\{ \frac{7\tau_C}{1 + \omega_S^2 \tau_C^2} + \frac{3\tau_C}{1 + \omega_H^2 \tau_C^2} \right\} \quad (25)$$

$$\frac{1}{\tau_C} = \frac{1}{\tau_R} + \frac{1}{\tau_S} + \frac{1}{\tau_M} \quad (26)$$

$$\frac{1}{\tau_S} = \frac{1}{5\tau_{SO}} \left\{ \frac{1}{1 + \omega_S^2 \tau_V^2} + \frac{4}{1 + 4\omega_S^2 \tau_V^2} \right\} \quad (27)$$

where γ_H is the gyromagnetic ratio of the proton; g is the electronic Landé factor; β is the Bohr magneton; S is the electronic spin quantum number; r is the distance of the inner sphere water protons from the paramagnetic ion; τ_R is the molecular reorientational correlation time and ω_S and ω_H are the Larmor frequencies for electron and proton respectively. The frequency dependence of the electronic relaxation time τ_S is expressed in equation 27, being dependent on its value at zero magnetic field (τ_{SO}) and on a field-independent correlation time τ_V related to the modulation of the ligand field by collision with solvent molecules.

Clearly, a large amount of structural and dynamic information is potentially available if the observed relaxivity can be correlated with these theoretical relationships. Such information may be extracted from the magnetic-field dependence of the relaxivity by fitting this to the calculated dependence, commencing with an appropriate choice of parameters. A plot of the relaxivity versus applied magnetic field (or more usually the corresponding proton Larmor frequency) is known as a nuclear magnetic resonance dispersion (NMRD) profile. Such profiles are obtained experimentally by means of a field-cycling relaxometer, which allows the relaxation rate to be determined over a large range of magnetic fields. The values of the parameters obtained by such a fitting procedure may be subjected to a further check by comparing the temperature-dependence of the observed NMRD profile with that predicted on the basis of the known temperature-dependence of several of the parameters.¹¹⁶

Some representative NMRD profiles are shown in Chapters 2 and 3. Although the preparation of Gd^{3+} complexes has not been the focus of the work described in subsequent chapters, the luminescence results for Eu^{3+} and Tb^{3+} complexes are to some extent complementary to the information which may be obtained from the NMRD profiles of related Gd^{3+} complexes. This is particularly true of the parameter q (the hydration state or number of bound water molecules); luminescence lifetimes provide an independent assessment of this quantity which may be useful in interpreting the NMRD profiles (eg. with reference to the parameters r and a discussed earlier and to the partitioning of the observed relaxivity between outer and inner sphere contributions¹¹²). Conclusions drawn for Eu^{3+} and Tb^{3+} complexes are likely to be applicable to Gd^{3+} as well owing to the similarity of the three ions, Gd lying as it does between Eu and Tb and all three having very similar ionic radii. These concepts are developed further in Chapter 3.

1.9 Fluorescence Detection of Metal Ions

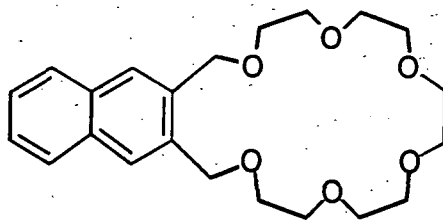
The detection of metal ions through their effect on the fluorescence of suitable organic molecules is a further example of the general detection scheme shown in Figure 1.4. Of course, here the analyte is a discrete metal ion rather than a complex biological molecule and the targeting part of the system is normally a relatively small, abiotic entity. A further distinction is that, in this case, a direct perturbation of the fluorescence on binding of the analyte is sought (eg. a change in fluorescence intensity or the relative intensities of two or more bands, or a shift in the emission or excitation wavelengths). The inherent Lewis basicity of synthetic hosts for metal ions means that, in many cases, the proton H^+ is able to exert a similar effect to that of metal ions. Thus, many systems (for example, those which incorporate nitrogen donors such as the aza crowns) are often highly pH sensitive.¹¹⁷ This has led to some interesting pH sensors although, in the field of metal ion detection, it may pose some disadvantages such as a requirement for buffered solutions.

That metal ions may have a profound influence on fluorescence has been known for over a century but only over the past 20 years has a rational approach to the design of fluorescent chemosensors been pursued. The recent systems differ from their predecessors in that the receptor is not an intrinsic part of the fluorophore: the two may be separated by several atoms and the resulting molecule may have properties characteristic of both of the isolated entities. The field is an increasingly active area of research and is the subject of a number of recent reviews.¹¹⁷⁻¹²¹ It is appropriate here to cite only a few examples which are of rather more relevance to the work described in Chapter 4. It is perhaps first worth noting two general caveats concerning these results. The first is that, as for the lanthanide complexes discussed earlier, most practical applications that are envisaged are for use in aqueous solution: this often proves to be a more difficult medium than organic solvents, due in large part to the unfavourable thermodynamics and kinetics of desolvation which often accompany ion-binding in water. A second noteworthy point is that a "positive response", for example an increase rather than a decrease in emission intensity, is preferable as this will normally allow greater detection sensitivity.

1.9.1 Systems incorporating macrocyclic receptors

The first study of metal binding to a macrocycle appended with a fluorophore appears to be that of Sousa in 1977, who examined the effect of alkali metals on the naphthyl fluorescence in systems such as **15**.¹²² The study was carried out in a 95% ethanol glass at 77K, allowing phosphorescence quantum yields and lifetimes to be measured in addition to fluorescence intensities. For compound **15**, addition of alkali metal ions resulted in a decrease in fluorescence intensity (eg. in the presence of 1 mol Cs⁺, ϕ_f was reduced to 1/6 of its value in the free ligand). In light of the corresponding increase in phosphorescent quantum yields which were observed, these changes were attributed to perturbations of the triplet naphthyl energy on metal binding. A heavy atom effect (enhanced spin-orbit coupling) was also invoked in the case of Cs⁺. Small increases in fluorescence intensity were observed in the case of the related 1,8-naphtho-21-crown-6

system, ascribed to an increase in the S_1 - T_1 separation and hence a decreased rate of ISC.

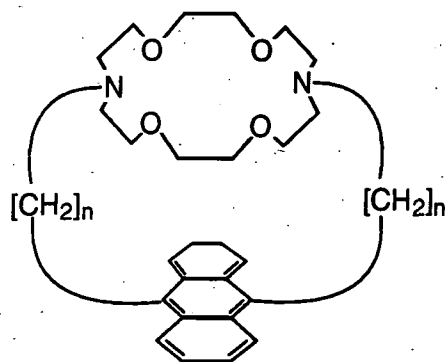


15

Many systems prepared to date rely on the effect of the metal ion on the rate of photoinduced electron transfer (PET) as a non-radiative deexcitation pathway competitive with fluorescence. Such an approach is possible if the receptor contains functional groups with oxidation potentials sufficiently low for electron transfer to occur to the first excited singlet state of the fluorophore. Quenching of fluorescence by such an electron transfer process, sometimes giving rise to exciplex emission, is well-known. A quantitative description of the thermodynamics of such processes has been put forward by Weller.¹²³ The application of PET to detection of metal ions (or other species) requires that, on binding of the guest, the oxidation potentials of these receptor groups are perturbed to such an extent that the electron transfer process becomes energetically less favourable and hence less competitive with fluorescence as a deactivation pathway: under such circumstances, metal binding will lead to a fluorescence enhancement. This approach has been the subject of a recent review.¹¹⁷ It is useful to note that in many cases, and especially where the redox active groups in the receptor are amines, proton binding will give rise to a similar effect.

The application of this principle to the detection of metal ions using macrocycles was reported in 1985 by Desvergne *et al.*, who prepared some macrobicyclic anthraceno-cryptands **16** and **17**.^{124,125} The cryptand **16** displayed only weak fluorescence in degassed methanol (compared to 9,10-dipropyl anthracene as a standard); weak exciplex emission was observed centred at about 520 nm in addition to the usual anthryl

fluorescence. These observations were attributed to efficient deactivation of the anthryl singlet state through photoinduced electron transfer from the amine groups of the cryptand. Addition of an excess of trifluoroacetic acid led to an 18-fold increase in the emission intensity and loss of the long-wavelength band, indicating that N-protonation inhibits the PET process. Complexation of alkali metal ions (along with Ag^+ and Tl^+) gave rise to a similar, albeit less pronounced, effect: the maximum enhancement was observed for K^+ which gave rise to a 7-fold increase in emission intensity.



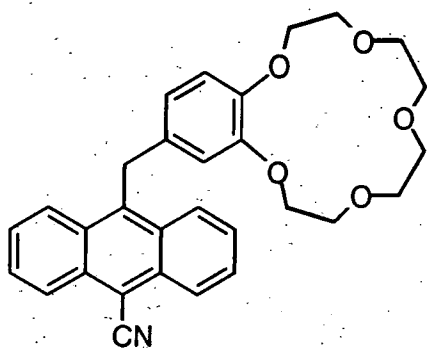
16 $n = 3$

17 $n = 2$

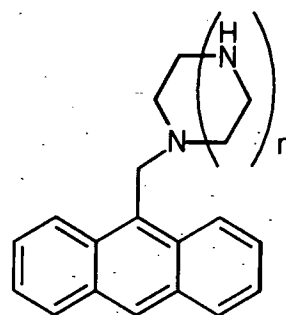
The smaller cryptand **17** exhibited very different behaviour. The unprotonated ligand displayed intense anthryl fluorescence, indicating that PET deactivation was not competitive in this case. This was thought to arise from a conformational difference (compared to **16**) whereby the nitrogen lone pairs are oriented such that they may hydrogen-bond to solvent methanol molecules. Alkali metals showed little effect on the fluorescence intensity but addition of Ag^+ or Tl^+ resulted in substantial quenching and a shift in the position of the anthryl fluorescence.

Systems such as those mentioned above prove to be highly sensitive to protons in addition to metal ions which, as mentioned earlier, imposes limitations on their use. An attempt to overcome the competitive effect of protons in sensors of this general type has been made by de Silva,^{117, 126} who has employed the all-oxygen crown in ligand **18**. The oxidation potentials associated with alkoxybenzenes are sufficiently low for a PET

mechanism of deactivation of the anthryl fluorescence to occur here, the efficiency of which is reduced on binding of alkali metal cations. The highest fluorescence enhancement factor was observed for sodium, for which the maximum value was 15 in methanol. The other alkali metal ions displayed substantially weaker effects and, most notably, there was virtually no sensitivity to protons. It was noted that, at high salt concentrations, the fluorescence intensities were observed to fall off after passing through a maximum; this was attributed to axial anion pairing to the macrocycle-bound cation which has the effect of decreasing the charge density on the metal cation.



18



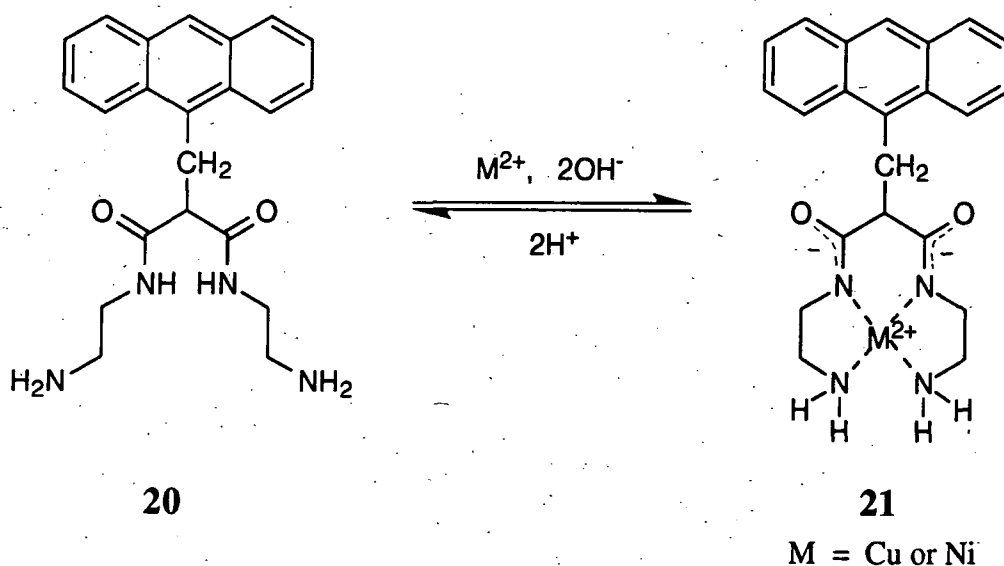
n = 1 - 5

19

The studies discussed above were carried out in methanol: metal ion complexation is likely to be too weak in aqueous solution to allow detection to be achieved in this medium. Czarnik has prepared polyazamacrocycles of the type **19** which are able to form strong complexes with certain transition metal ions in water.^{127,128} Again, protonation may give rise to the same effect but, at pH 12, complexation by Zn^{2+} or Cd^{2+} ions affords good fluorescence enhancements. In contrast, binding of inherently quenching metal ions such as Cu^{2+} or Hg^{2+} under non-basic conditions leads to decreases in fluorescence intensity. In both cases, no interference was observed from sodium ions, even when present in large excess, reflecting the low affinity of azamacrocycles for the alkali metals. An interesting feature of this system is the distortion of the shape of the anthryl fluorescence band which occurs on binding of Cd^{II} to the ligand **19** where $n = 4$: a new emission band with $\lambda_{\text{max}} = 446 \text{ nm}$ is observed. It was postulated that this might be due to Cd^{II} π -complexation by the anthracene.

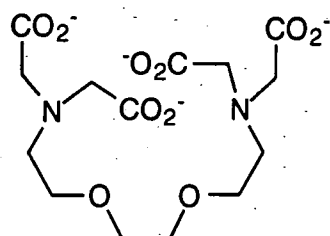
1.9.2 Examples which make use of acyclic ligands

The ligand **20** has been reported recently by Fabbrizzi.¹²⁹ Here the anthryl fluorescence is not affected by changes in pH but the ligand is able to bind the quenching metal ions Cu^{II} and Ni^{II} (in 4:1 $\text{CH}_3\text{CN} / \text{H}_2\text{O}$) giving rise to a large decrease in the fluorescence intensity. This metal binding is dependent on pH: binding of Cu^{II} occurs at pH 6 or higher, whilst Ni^{II} does not bind until the pH has reached about 8. Thus, discrimination between these 2 ions is possible; other related metals such as Mn^{II} , Co^{II} and Zn^{II} are not able to undergo coordination by the dioxotetraaza unit¹³⁰ and therefore show no interference. Fluorescence quenching by transition metal ions such as Cu^{II} and Ni^{II} is well-known, although the mechanism by which it occurs is not always clear; here it may involve either an energy transfer mechanism or a M^{II} -to-anthracene electron transfer process with transient formation of ligand-stabilised M^{III} .



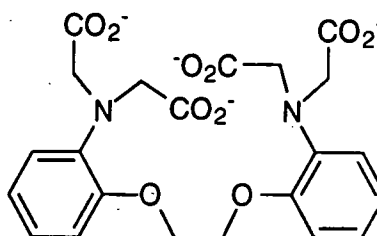
One final group of metal ion fluorescent indicators is worthy of mention, owing to the success they have enjoyed in living cells. These are the EGTA-based systems for Ca^{2+} detection pioneered largely by Tsien^{121,131} {EGTA = ethyleneglycolbis(β -aminoethylether)-N,N,N',N'-tetraacetic acid **22**}. EGTA shows a high selectivity ($> 10^5$) for Ca^{2+} over Mg^{2+} . The related ligand BAPTA **23** was prepared which preserves the Ca^{2+} to Mg^{2+} specificity. Moreover, the UV absorbance and fluorescence spectra of the aromatic rings are strongly perturbed by Ca^{2+} binding: this arises because the

nitrogen lone pairs conjugate with the aromatic π orbitals in the absence of Ca^{2+} but are not available to do so when Ca^{2+} binds. Incorporation of the nitrogen donors into aromatic rings provides the additional benefit of reduced H^+ interference, owing to the lower pK_a of anilines compared to aliphatic amines.



EGTA

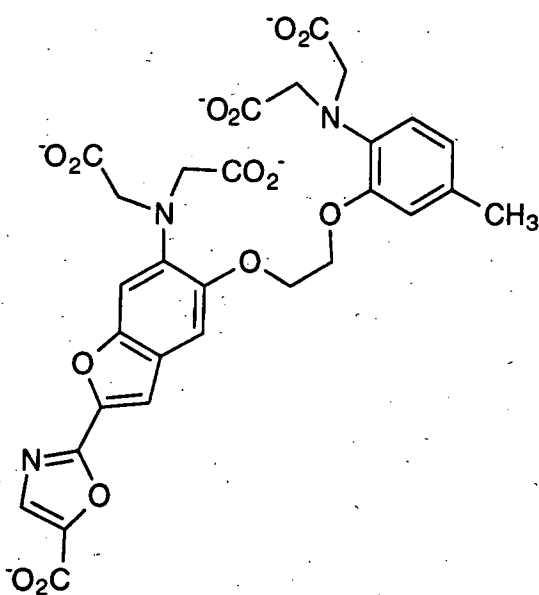
22



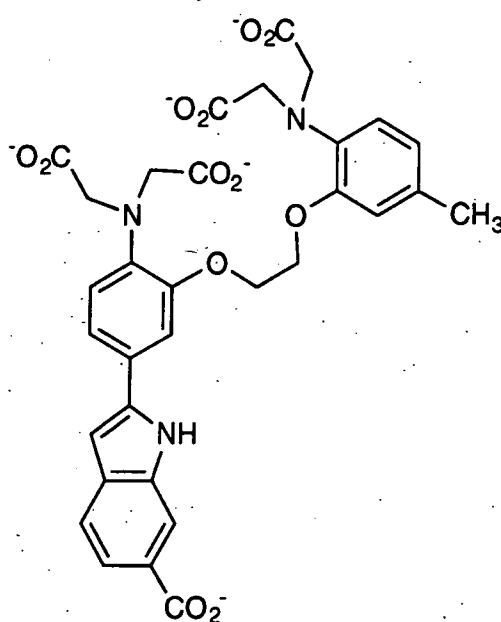
BAPTA

23

Clearly, the fluorescence emission of BAPTA itself occurs at wavelengths which are too short to be of practical use and a good deal of work has been directed at appending this ligand with strongly fluorescent chromophores. The compounds 'fura-2' and 'indo-1' (24 and 25) have been successfully applied to the monitoring of Ca^{2+} in cells; these show large shifts in the near-UV excitation spectra and in the visible emission spectrum (for indo-1) on binding of Ca^{2+} .



24



25

References for Chapter 1

1. R. Reisfeld and C.K. Jørgensen, 'Lasers and Excited States of Rare Earths', Springer Verlag: Berlin, 1977.
2. W.T. Carnall, 'The Absorption and Fluorescence Spectra of Rare Earth Ions in Solution' in 'Handbook on the Physics and Chemistry of Rare Earths', eds. K.A. Gschneider, Jr. and L. Eyring, North Holland Publishing Company: Amsterdam, 1979. Chapter 24.
3. J.-C.G. Bünzli in 'Lanthanide Probes in Life, Chemical and Earth Sciences', eds. J.-C.G. Bünzli and G.R. Choppin, Elsevier: Amsterdam, 1989. Chapter 7.
4. N.J. Turro, 'Modern Molecular Photochemistry', University Science Books: Mill Valley, California, 1991. Chapter 5.
5. L.A. Risberg and H.W. Moss, *Phys. Rev.*, 1968, **174**, 429.
6. G.E. Barasch and G.E. Dieke, *J. Chem. Phys.*, 1965, **43**, 988.
7. J.L. Kropp and M.W. Windsor, *J. Chem. Phys.*, 1965, **42**, 1599.
8. P.K. Gallagher, *J. Chem. Phys.*, 1965, **43**, 1742.
9. R. Borkowski, H. Forest and D. Grafstein, *J. Chem. Phys.*, 1965, **42**, 2974.
10. J.L. Kropp and M.W. Windsor, *J. Chem. Phys.*, 1963, **39**, 2769; *idem, ibid*, 1966, **45**, 761.
11. A. Heller, *J. Am. Chem. Soc.*, 1966, **88**, 2058.
12. Y. Haas and G. Stein, *Chem. Phys. Lett.*, 1971, **11**, 143.
13. Y. Haas and G. Stein, *J. Phys. Chem.*, 1971, **75**, 3677.
14. G. Stein and E. Wurzburg, *J. Chem. Phys.*, 1975, **62**, 208.
15. W. DeW. Horrocks, Jr. and D.R. Sudnick, *Science*, 1979, **206**, 1194.
16. W. DeW. Horrocks, Jr., G.R. Schmidt, D.R. Sudnick, C. Kittrell and R.A. Bernheim, *J. Am. Chem. Soc.*, 1977, **99**, 2378.
17. W. DeW. Horrocks, Jr. and D.R. Sudnick, *Acc. Chem. Res.*, 1981, **14**, 384.
18. J. Halpern and A.C. Harkness, *J. Chem. Phys.*, 1959, **31**, 1147.
J. Bigeleisen, *J. Chem. Phys.*, 1960, **32**, 1583.
19. D.F. Hornig, H.F. White and F.P. Redding, *Spectrochim. Acta*, 1958, **12**, 338.

20. S.I. Weissman, *J. Chem. Phys.*, 1942, **10**, 214.
21. V. Balzani and F. Scandola, 'Supramolecular Photochemistry', Ellis Horwood: Chichester, 1991. Chapter 12.
22. A comprehensive review is provided by: W. DeW. Horrocks, Jr. and M. Albin, 'Lanthanide Ion Luminescence in Coordination Chemistry and Biochemistry', *Prog. Inorg. Chem.*, 1984, **31**, 1-106.
23. W.R. Dawson, J.L. Kropp and M.W. Windsor, *J. Chem. Phys.*, 1966, **45**, 2410.
24. M. Tanaka, G. Yamaguchi, J. Shiokawa and C. Yamanaka, *Bull. Chem. Soc. Jpn.*, 1970, **43**, 549.
25. S. Sato and W. Wada, *Bull. Chem. Soc. Jpn.*, 1970, **43**, 1955.
26. W.M. Watson, R.P. Zerger, J.T. Yardley and G.D. Stucky, *Inorg. Chem.*, 1975, **14**, 2675.
27. M. Kleinerman, *J. Chem. Phys.*, 1969, **51**, 2370.
28. M. Kleinerman and S. Choi, *J. Chem. Phys.*, 1968, **49**, 3901.
29. R.W. Harrigan and G.A. Crosby, *J. Chem. Phys.*, 1970, **52**, 4912.
30. M.C.F. Cunha, H.F. Brito, L.B. Zinner, G. Vicenti and A.B. Nascimento, *Coord. Chem. Rev.*, 1992, **119**, 1-28.
31. C.C. Bryden and C.N. Reilley, *Anal. Chem.*, 1982, **54**, 610.
32. H.G. Brittain and F.S. Richardson, *J. Chem. Soc. Dalton Trans.*, 1976, 2253.
33. H.G. Brittain, *J. Am. Chem. Soc.*, 1979, **101**, 1733. *Idem*; *J. Chem. Soc. Dalton Trans.*, 1979, 1187. *Idem*, *Inorg. Chem.*, 1980, **19**, 640.
34. D.S. Gross and H. Simpkins, *J. Biol. Chem.*, 1981, **256**, 9593.
35. T.J. Wenzel and L.M. Collette, *J. Chromatogr.*, 1988, **436**, 299.
36. C.K. Luk, *Biochemistry*, 1971, **10**, 2838.
37. J. Bruno, W.DeW. Horrocks, Jr. and R.J. Zauhar, *Biochemistry*, 1992, **31**, 7016.
38. H.G. Brittain, F.S. Richardson and R.B. Martin, *J. Am. Chem. Soc.*, 1976, **98**, 8255.
39. W.DeW. Horrocks and W.E. Collier, *J. Am. Chem. Soc.*, 1981, **103**, 2856.

40. C.R. Cantor and P.R. Schimmel, 'Biophysical Chemistry', W.H. Freeman: San Francisco, 1980. Volume 2.
41. C.F. Meares and J.E. Ledbetter, *Biochemistry*, 1977, **16**, 5178.
42. E.T. O'Keeffe, R.L. Hill and J.E. Bell, *Biochemistry*, 1980, **19**, 4954.
43. I. Hemmilä, *Clin. Chem.*, 1985, **31**, 359, (review). *Idem, ibid*, 1979, **25**, 353, (review).
44. J.Klein, 'Immunology', Blackwell Scientific: Boston, Mass., 1990.
45. P. Gottlieb, E. Hazum, E. Tzechoval, M. Feldman, S. Segal and M. Fridkin, *Biochem. Biophys. Res. Comm.*, 1984, **119**, 203.
46. A. Oser, W.K. Roth and G. Valet, *Nucleic Acids Res.*, 1988, **16**, 1181.
J. Coates, P.G. Sammes, G. Yahioğlu, R.M. West and A.J. Garman, *J. Chem. Soc. Chem. Commun.*, 1994, 2311.
47. D.M. Gravett and J.E. Guillet, *J. Am. Chem. Soc.*, 1993, **115**, 5970.
A. Ueno, 'Fluorescent Cyclodextrins for Detecting Organic Compounds with Molecular Recognition', in 'Fluorescent Chemosensors for Ion and Molecule Recognition', ed: A.W. Czarnik, ACS Symposium Series, 1993, Volume 538, pp 74 - 84; American Chemical Society: Washington, DC, 1993.
48. J.U. Eskola, T.J. Nevalainen and T.N.-E. Lövgren, *Clin. Chem.*, 1983, **29**, 1777.
49. E. Soini and H. Kojola, *Clin. Chem.*, 1983, **29**, 65. I. Hemmilä, V.-M. Mikkala and S. Dakubu, *Anal. Biochem.*, 1984, **137**, 375.
50. E.F.G. Dickson, A. Pollak and E.P. Diamandis, *Photochem. Photobiol.*, 1995, **27**, 3 (review).
51. S.A. Cotton and F.A. Hart, 'The Heavy Transition Elements', Macmillan: London, 1975. Chapter 10.
52. A.G. Sharpe, 'Inorganic Chemistry', 2nd edition, Longman: Harlow, 1985.
53. G.R. Choppin in 'Lanthanide Probes in Life, Chemical and Earth Sciences', eds. J.-C.G. Bünzli and G.R. Choppin; Elsevier: Amsterdam, 1989. Chapter 1.

-
54. K.O.A. Chin, J.R. Morrow, C.H. Lake and M.R. Churchill, *Inorg. Chem.*, 1994, **33**, 656.
 55. G. Schwarzenbach, *Helv. Chim. Acta*, 1952, **35**, 2344.
 56. C.-S. Chung, *J. Chem. Educ.*, 1984, **61**, 1062. J.J.R. Frausto da Silva, *J. Chem. Educ.*, 1983, **60**, 390.
 57. C.A.M. Vijverberg, J.A. Peters, A.P.G. Kieboom and H. van Bekkum, *Tetrahedron*, 1986, **42**, 167.
 58. R.S. Reid and B. Podaniye, *Can. J. Chem.*, 1987, **65**, 1508.
 59. R.D. Hancock and A.E. Martell, *Chem. Rev.*, 1989, **89**, 1875.
 60. R.D. Hancock, *J. Chem. Educ.*, 1992, **69**, 615.
 61. E.R. Birnbaum in 'Gmelin Handbook of Inorganic Chemistry', 8th edition; Springer Verlag: Berlin, 1984; Vol. D5, p136.
 62. A.E. Martell and R.M. Smith, 'Critical Stability Constants', Plenum: New York, 1989. Volume 6.
 63. M. Kodama, T. Koike, A.B. Mahatma and E. Kimura, *Inorg. Chem.*, 1991, **30**, 1270.
 64. M.K. Moi, C.F. Meares and S.J. DeNardo, *J. Am. Chem. Soc.*, 1988, **110**, 6266.
 65. L.F. Lindoy; 'The Chemistry of Macrocyclic Ligand Complexes'; Cambridge University Press: Cambridge, 1989.
 66. D.K. Cabbiness and D.W. Margerum, *J. Am. Chem. Soc.*, 1969, **91**, 6540.
 67. R.D. Hancock, *Pure Appl. Chem.*, 1986, **58**, 1445.
 68. R.D. Hancock, R. Bhavan, P.W. Wade, J.C.A. Boeyens, S.M. Dobson, *Inorg. Chem.*, 1989, **28**, 187.
 69. L. Prodi, M. Maestri, R. Ziessel and V. Balzani, *Inorg. Chem.*, 1991, **30**, 3798.
 70. E. Kimura, M. Yamaoka, M. Morioka and T. Koike, *Inorg. Chem.*, 1986, **25**, 3883. E. Kimura, T. Koike and K. Toriumi, *Inorg. Chem.*, 1988, **27**, 3687.

-
71. I. Murase, M. Mikuriya, H. Sonoda and S. Kida, *J. Chem. Soc., Chem. Commun.*, 1984, 692; I. Murase, M. Mikuriya, H. Sonoda, Y. Fukuda and S. Kida, *J. Chem. Soc., Dalton Trans.*, 1986, 953.
72. R. Katakya, K.E. Matthes, P.E. Nicholson, D. Parker and H.-J. Buschmann; *J. Chem. Soc., Perkin Trans. 2*; 1990, 1425; R. Katakya, D. Parker, A. Teasdale, J.P. Hutchinson and H.-J. Buschmann; *J. Chem. Soc., Perkin Trans. 2*; 1992, 1347.
73. H. Stetter and W. Frank, *Angew. Chem. Int. Ed. Engl.*, 1976, **15**, 686.
74. J.P.L. Cox, K.J. Jankowski, R. Katakya, D. Parker, N.R.A. Beeley, B.A. Boyce, M.A.W. Eaton, K. Millar, A.T. Millican, A. Harrison and C. Walker, *J. Chem. Soc., Chem. Commun.*, 1989, 797.
75. V. Alexander, *Chem. Rev.*, 1995, **95**, 273.
76. H. Stetter, W. Franka and R. Mertens, *Tetrahedron*, 1981, **37**, 767.
77. J.F. Desreux, *Inorg. Chem.*, 1980, **19**, 1319.
78. J.F. Desreux, E. Merciny and M.-F. Loncin, *Inorg. Chem.*, 1981, **20**, 987.
79. M.-R. Spirlet, J. Rebizant, M.-F. Loncin and J.F. Desreux, *Inorg. Chem.*, 1984, **23**, 4278.
80. M.F. Loncin, J.F. Desreux and E. Merciny, *Inorg. Chem.*, 1986, **25**, 2646.
81. K. Takenouchi, K. Watanabe, Y. Kato, T. Koike and E. Kimura, *J. Org. Chem.*, 1993, **58**, 1955.
82. M.-R. Spirlet, J. Rebizant, J.F. Desreux and M.-F. Loncin, *Inorg. Chem.*, 1984, **23**, 359.
83. These studies have been the subject of a recent review: N. Sabbatini, M. Guardigli and J.-M. Lehn, *Coord. Chem. Rev.*, 1993, **123**, 201.
84. B. Dietrich, J.-M. Lehn, J.-P. Sauvage and J. Blanzat, *Tetrahedron*, 1973, **29**, 1629. B. Dietrich, J.-M. Lehn and J.-P. Sauvage, *ibid*, 1973, **29**, 1647. J.-M. Lehn and J.-P. Sauvage, *J. Am. Chem. Soc.*, 1975, **97**, 6700.
85. B. Alpha, J.-M. Lehn and G. Mathis, *Angew. Chem. Int. Ed. Engl.*, 1987, **26**, 266.

-
86. I. Bkouche-Waksman, J. Guilhem, C. Pascard, B. Alpha, R. Deschenaux and J.-M. Lehn, *Helv. Chim. Acta.*, 1991, **74**, 1163.
 87. B. Alpha, R. Ballardini, V. Balzani, J.-M. Lehn, S. Perathoner and N. Sabbatini, *Photochem. Photobiol.*, 1990, **52**, 299.
 88. V. Balzani, J.-M. Lehn, J. van de Loosdrecht, A. Mecati, N. Sabbatini and R. Ziessel, *Angew. Chem. Int. Ed. Engl.*, 1991, **30**, 190.
 89. N. Sabbatini, M. Guardigli, A. Mecati, V. Balzani, R. Ungaro, E. Ghidini, A. Casnati, A. Pochini, *J. Chem. Soc. Chem. Commun.*, 1990, 878.
 90. N. Sabbatini, M. Guardigli, I. Manet, R. Ungaro, A. Casnati, C. Fischer, R. Ziessel and G. Ulrich, *New J. Chem.*, 1995, **19**, 137.
 91. N. Sato and S. Shinkai, *J. Chem. Soc. Perkin. Trans. 2*, 1993, 621.
 92. M.P. Bailey, B.F. Rocks and C. Riley, *Analyst*, 1984, **109**, 1449.
 93. S.S. Saavedra and E.G. Picozza, *Analyst*, 1989, **114**, 835.
 94. J. Siepak, *Analyst*, 1989, **114**, 529.
 95. A. Canfi, M.P. Bailey and B.F. Rocks, *Analyst*, 1989, **114**, 1407.
 96. A. Oser, M. Collasius and G. Valet, *Anal. Biochem.*, 1990, **191**, 295.
 97. E.P. Diamandis and T.K. Christopoulos, *Anal. Chem.*, 1990, **62**, 1149.
 98. R.A. Evangelista, A. Pollak, B. Allore, E.F. Templeton, R.C. Morton and E.P. Diamandis, *Clin. Biochem.*, 1988, **21**, 173.
 99. A.K. Saha, K. Kross, E.D. Kloszewski, D.A. Upson, J.L. Toner, R.A. Snow, C.D.V. Black and V.C. Desai, *J. Am. Chem. Soc.*, 1993, **115**, 11032.
 100. A.D. Sherry and C.F.G.C. Geraldès in 'Lanthanide Probes in Life, Chemical and Earth Sciences', Eds: J.-C.G. Bunzli and G.R. Choppin, Elsevier: Amsterdam, 1989. Chapter 4.
 101. R.D. Fischer in 'NMR of Paramagnetic Molecules: Principles and Applications', Eds: G.N. LaMar, W. DeW. Horrocks Jr. and R.H. Holm, Academic Press: London, 1973. Chapter 13.
 102. W.B. Lewis, J.A. Jackson, J.F. Lemons and H. Taube, *J. Chem. Phys.*, 1962, **36**, 694.

-
103. J.P. Jesson, *J. Chem. Phys.*, 1967, **47**, 579.
 104. R.M. Golding and M.P. Halton, *Aust. J. Chem.*, 1972, **25**, 2577.
 105. M. Witanowski, L. Stefaniak, H. Januszewski and Z.W. Wolkowski, *J. Chem. Soc. Chem. Commun.*, 1971, 573.
 106. B. Bleaney, *J. Magn. Resonance*, 1972, **8**, 91.
 107. B. Bleaney, C.M. Dobson, B.A. Levine, R.B. Martin, R.J.P. Williams and A.V. Xavier, *J. Chem. Soc. Chem. Commun.*, 1972, 791.
 108. H. Donato, Jr. and R.B. Martin, *J. Am. Chem. Soc.*, 1972, **94**, 4129.
 109. J. Reuben and D. Fiat, *J. Chem. Phys.*, 1969, **51**, 4909.
 110. T.J. Swift in 'NMR of Paramagnetic Molecules: Principles and Applications', Eds: G.N. LaMar, W. DeW. Horrocks Jr. and R.H. Holm, Academic Press: London, 1973. Chapter 2.
 111. W. DeW. Horrocks, Jr. and J.P. Sipe III, *Science*, 1972, **177**, 994.
 112. M.F. Tweedle in 'Lanthanide Probes in Life, Chemical and Earth Sciences', Eds: J.-C.G. Bunzli and G.R. Choppin, Elsevier: Amsterdam, 1989. Chapter 5.
 113. R.B. Lauffer, *Chem. Rev.*, 1987, **87**, 901.
 114. J.H. Freed, *J. Chem. Phys.*, 1978, **68**, 4034.
 115. S. Aime, M. Botta, M. Fasano, S. Paoletti, P.C. Anelli, F. Uggeri and M. Virtuani, *Inorg. Chem.*, 1994, **33**, 4707.
 116. S. Aime, M. Botta, G. Ermondi, F. Fedeli, F. Uggeri, *Inorg. Chem.*, 1992, **31**, 1100.
 117. R.A. Bissell, A.P. de Silva, H.Q.N. Gunaratne, P.L.M. Lynch, G.E.M. Maguire, C.P. McCoy and K.R.A.S. Sandanayake, *Top. Curr. Chem.*, 1993, **168**, 223.
 118. R.A. Bissell, A.P. de Silva, H.Q.N. Gunaratne, P.M. Lynch, G.E.M. Maguire and K.R.A.S. Sandanayake, *Chem. Soc. Rev.*, 1992, **21**, 187.
 119. A.W. Czarnik, *Acc. Chem. Res.*, 1994, **27**, 302.

-
120. A collection of reviews by a number of the leading research groups in the field is provided in: 'Fluorescent Chemosensors for Ion and Molecule Recognition', Ed: A.W. Czarnik, American Chemical Society: Washington, DC, 1993.
 121. R.Y. Tsien, *Chem. Eng. News*, 1994, (Issue July 18th, 1994), 34.
 122. L.R. Sousa and J.M. Larson, *J. Am. Chem. Soc.*, 1977, **99**, 307.
 123. A. Weller, *Pure Appl. Chem.*, 1968, **16**, 115.
D. Rehm and A. Weller, *Isr. J. Chem.*, 1970, **8**, 259.
 124. J.P. Konopelski, F. Kotzyba-Hibert, J.-M. Lehn, J.-P. Desvergne, F. Fagès, A. Castellan, H. Bouas-Laurent, *J. Chem. Soc. Chem. Commun.*, 1985, 433.
 125. F. Fagès, J.-P. Desvergne, H. Bouas-Laurent, P. Marsau, J.-M. Lehn, F. Kotzyba-Hibert, A.-M. Albrecht-Gary and M. Al-Joubbeh, *J. Am. Chem. Soc.*, 1989, **111**, 8672.
 126. A.P. de Silva and K.R.A.S. Sandanayake, *J. Chem. Soc. Chem. Commun.*, 1989, 1183.
 127. E.U. Akkaya, M.E. Huston and A.W. Czarnik, *J. Am. Chem. Soc.*, 1990, **112**, 3590.
 128. M.E. Huston and A.W. Czarnik, *J. Am. Chem. Soc.*, 1990, **112**, 7054.
 129. L. Fabbrizzi, M. Licchelli, P. Pallavicini, A. Perotti and D. Sacchi, *Angew. Chem. Int. Ed. Engl.*, 1994, **33**, 1975.
 130. L. Fabbrizzi, T.A. Kaden, A. Perotti, B. Seghi and L. Siegfried, *Inorg. Chem.*, 1986, **25**, 321.
 131. R.Y. Tsien in 'Fluorescent Chemosensors for Ion and Molecule Recognition', Ed: A.W. Czarnik, American Chemical Society: Washington, DC, 1993.
Chapter 9.

Chapter 2

CHAPTER 2

Lanthanide Complexes of Tetraazamacrocyclic Ligands Bearing Four Pendent Phosphinate Arms

2.1 Introduction

Octadentate macrocyclic ligands with nitrogen and oxygen donor groups are often well-suited to binding lanthanide(III) ions as discussed in Chapter 1. This is especially true of anionic ligands such as DOTA (4) which forms lanthanide complexes of particularly high thermodynamic stability (Figure 1.7). A further feature of such complexes, especially those based on the 1,4,7,10-tetraazacyclododecane ring ($12N_4$), is their high kinetic stability with respect to metal ion dissociation. This is reflected, for example, in the *in vivo* use of $[Gd:DOTA]^-$ as a contrast agent in magnetic resonance imaging.

A new class of octadentate ligands based on $12N_4$ has been developed at Durham.¹⁻³ These ligands are structurally related to DOTA but contain phosphinic acid as opposed to carboxylic acid pendent groups. The general structure is shown in Figure 2.1. Preliminary results have shown that the ligands form Gd^{3+} and Y^{3+} complexes of high thermodynamic and kinetic stability and are potentially suitable for use *in vivo*.⁴

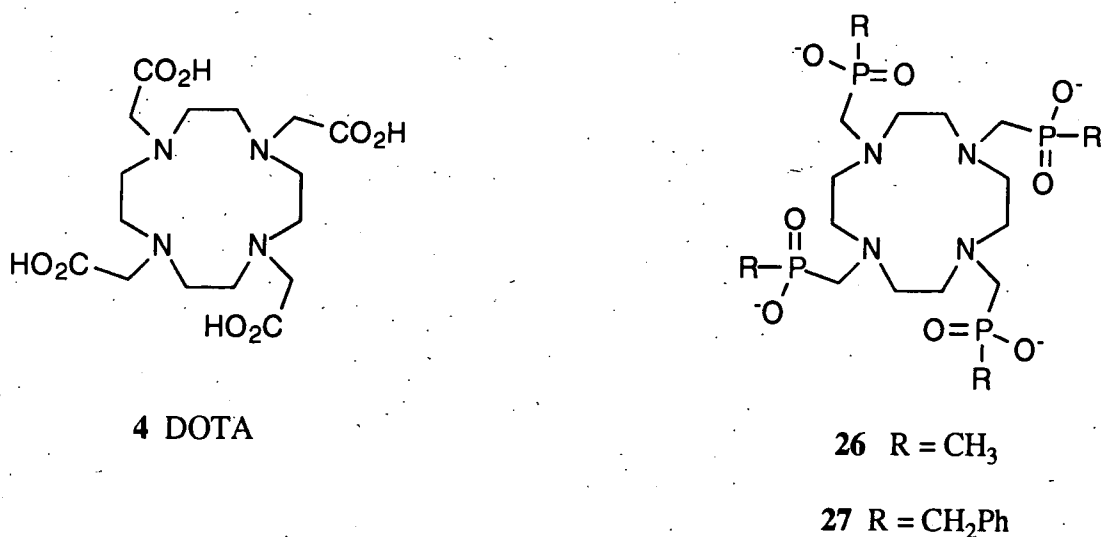
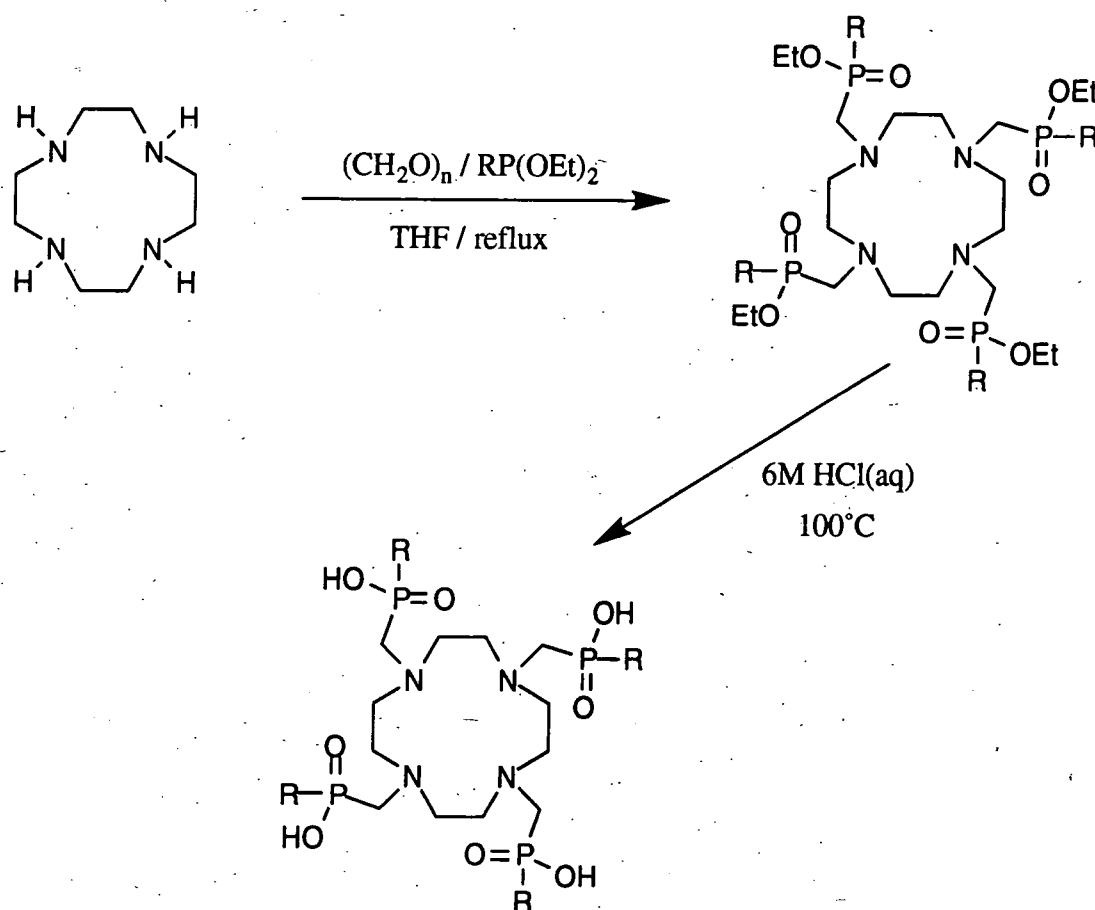


FIGURE 2.1 Structures of the tetraphosphinate ligands and DOTA for comparison

2.2 Ligand Synthesis

The synthetic procedure for preparing these ligands is shown in Scheme 2.1. Condensation of $12N_4$ with paraformaldehyde in dry tetrahydrofuran leads to formation of the electrophilic iminium ion which is subsequently trapped by the appropriately substituted dialkoxyphosphine. An Arbuzov rearrangement occurs to give the tetraphosphinate esters. Acid hydrolysis (6M HCl, 100°C) provides the aminophosphinic acids.



SCHEME 2.1 *The synthetic procedure used in the preparation of the tetraphosphinate ligands*

The dialkoxyphosphines themselves are prepared by reaction of the appropriate Grignard reagent with diethoxychlorophosphonite at -10°C in tetrahydrofuran or diethylether. The phosphines with intermediate boiling points [eg. PhCH₂P(OEt)₂] may be purified by distillation under reduced pressure. The volatility of

diethoxy(methyl)phosphine is such that the solvent co-distills and so this phosphine was used as a solution in THF.

2.3 Complex formation

The preparation of the lanthanide complexes of the tetraphosphinate ligands was carried out by addition of a stoichiometric amount of the appropriate metal oxide (or acetate) to the ligand in water at pH 2. Following dissolution of the oxide (80°C, 3 h), raising of the pH to 6 with aqueous potassium hydroxide led to formation of the metal complexes, which were subsequently crystallised from solution.

2.4 Earlier results concerning the structures of the ligand and its yttrium complex

The tetrabenzylphosphinate ligand **27** was first prepared in 1992 by Dr. Kanthi Pulukkody at the University of Durham. It proved possible to crystallise this ligand as its monohydrochloride salt and an X-ray crystal structure was obtained.⁵ This structure, together with that of the yttrium complex of the ligand, is shown in Figure 2.2.

The structure of the ligand shows that the tetraazacyclododecane ring adopts a square [3333] conformation,⁶ in which the nitrogen atoms are coplanar and lie to one side of the ring, with all adjacent CH₂ units in a staggered configuration. All four side-chains lie on the same side of the ring and one of the oxygen atoms of each phosphinate group is directed inward. These four oxygens, together with the four ring nitrogen atoms (whose lone pairs are also directed inward) form a binding site which is pre-disposed for 8-fold coordination of a metal ion. The ligand could thus be described as preorganised, subject to the caveat that the ligand crystal structure is actually that of the hydrochloride salt.

This is particularly evident from the close similarity of the structure of the Y³⁺ complex to that of the ligand, as illustrated in Figure 2.2: the metal is coordinated to the 4

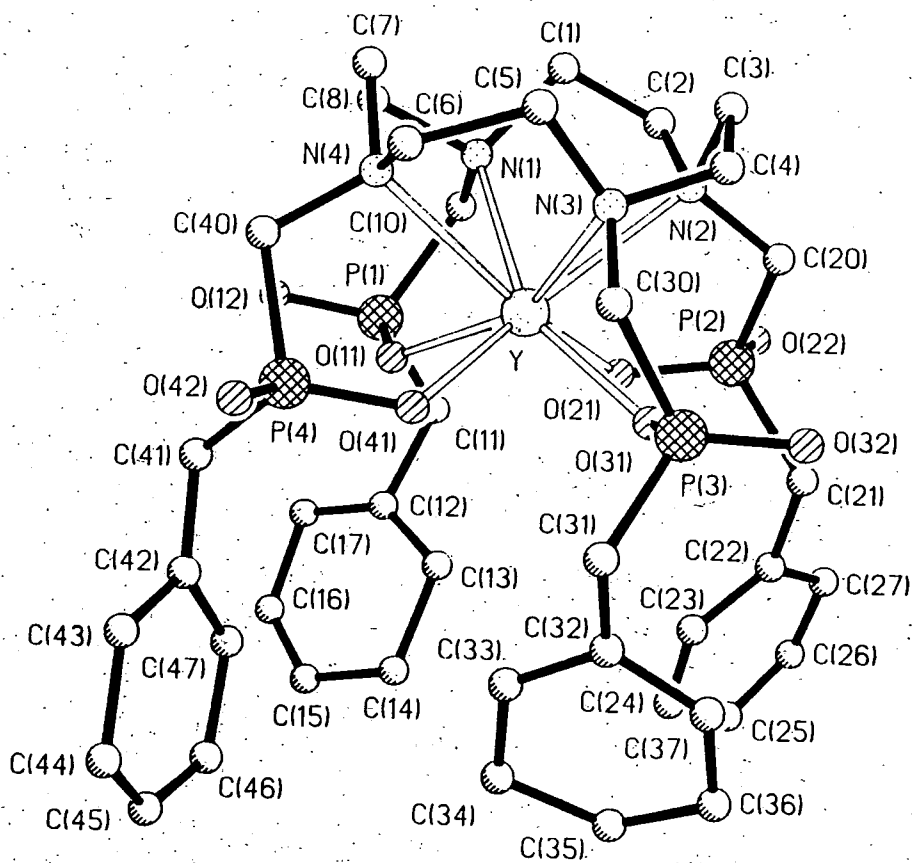
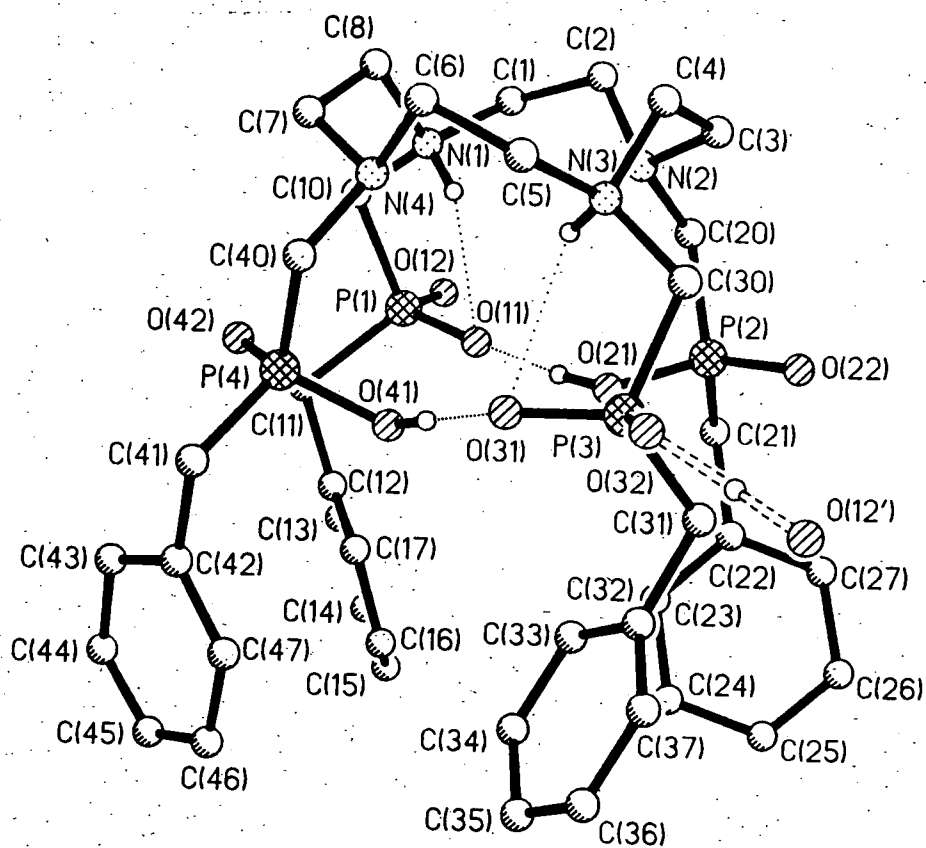


FIGURE 2.2. Molecular structures of $[27H_5]^+Cl^-$ (upper) showing intra- and intermolecular hydrogen bonds and $[Y.27]^-H_3O^+$ (lower). Hydrogen atoms are omitted.

coplanar N atoms and to four phosphinate oxygen atoms which are also coplanar relative to one another. Metal binding does induce some changes, however. Thus, the N_4O_4 polyhedron is contracted in the complex relative to the protonated ligand: the average distance from the vertices of the N_4O_4 core to its centre is 2.44 Å in the complex compared to 2.53 Å in the ligand. The metal ion does not sit at the centre of the polyhedron but is shifted towards the O_4 face, the average Y-O and Y-N distances being 2.26 and 2.66 Å respectively. This reflects the ionic nature of the Y-O bonds as opposed to the 'donor-acceptor' character of the bonds to nitrogen. Such a trend is commonly observed in related complexes, for example those of DOTA.^{7,8}

The coordination geometry of the N_4O_4 cage around the metal is a square prism twisted about the C_4 axis. For a true antiprism, the angle of twist of the O_4 face relative to the N_4 face would be 45°. Here, a value of 29° is observed giving a geometry that is somewhere between a square prism and a square antiprism. This is an interesting point which will be returned to in later sections.

Perhaps the most startling feature of the structure of the complex, however, is the absence of a metal-bound water molecule. This is a most unusual feature for lanthanide complexes of octadentate ligands: in almost all other cases, the metal is nine-coordinate with the ninth coordination site occupied by a water molecule. Only in complexes with the ligand TETA (structure 6 in chapter 1), which is based on a $14N_4$ skeleton, does the metal display a coordination number of 8 with no water molecule in its coordination sphere. In the crystal of $[Y.27]^-$, the nearest water molecule is 5.62 Å away; this compares to a value of 2.48 Å for the distance between the metal and the oxygen of the bound water molecule in $[Eu.DOTA]^-$.⁷

Finally, it is useful to note at this point that, as a consequence of the lanthanide contraction, the ionic radii of the lanthanide ions at the centre of the lanthanide series are very similar to that of Y^{3+} under the same coordination number.⁹ Moreover, yttrium closely resembles the lanthanides in its coordination chemistry in the +3

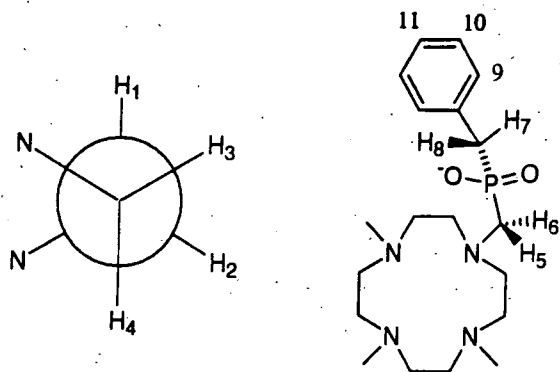
oxidation state (they all belong to the 'rare earth' class). Hence, it is quite likely that structural information obtained on yttrium complexes will also be applicable, in general, to the Eu^{3+} , Gd^{3+} and Tb^{3+} complexes (although some very small changes in bond lengths would be anticipated).

2.5 Solution studies

The information offered by the crystal structure of the yttrium complex is of course very useful. However, it is prudent to bear in mind that such information relates to the solid state and may not necessarily reflect the structure adopted in solution. There are numerous instances in many branches of chemistry where inconsistencies have been observed between solution and solid-state results. It is desirable to pursue techniques which allow the behaviour of lanthanide complexes in solution to be probed. NMR spectroscopy (potentially applicable to all the lanthanide(III) ions except Gd^{3+}), measurement of NMRD profiles (for Gd^{3+}) and luminescence measurements (Eu^{3+} and Tb^{3+}) are three such techniques. These are the methods which have been used in the work described in subsequent sections. Of course, such measurements are also essential in order to assess the suitability of these complexes for the applications in mind.

2.6 NMR studies of complexes in solution

The europium complex of the tetrabenzylphosphinate ligand **27** was prepared: its ^1H NMR spectrum (400 MHz in D_2O) is shown in Figure 2.3, together with the spectrum of the Yb^{3+} complex. The shifting effect of paramagnetic lanthanide ions discussed in Chapter 1 is clearly apparent in the expanded chemical shift ranges in both cases. It is clear that some signals are shifted to high frequencies and others to lower frequency. This is to be expected if there is a dipolar contribution to the shifts, owing to the dependence of dipolar shifts on the quantity $(3 \cos^2\theta - 1) / r^3$ (section 1.8.1) where r and θ are the polar coordinates defining the position of the nucleus under observation. This quantity may change sign depending on the angle θ , thereby giving rise to shifts of both signs.



SCHEME 2.2

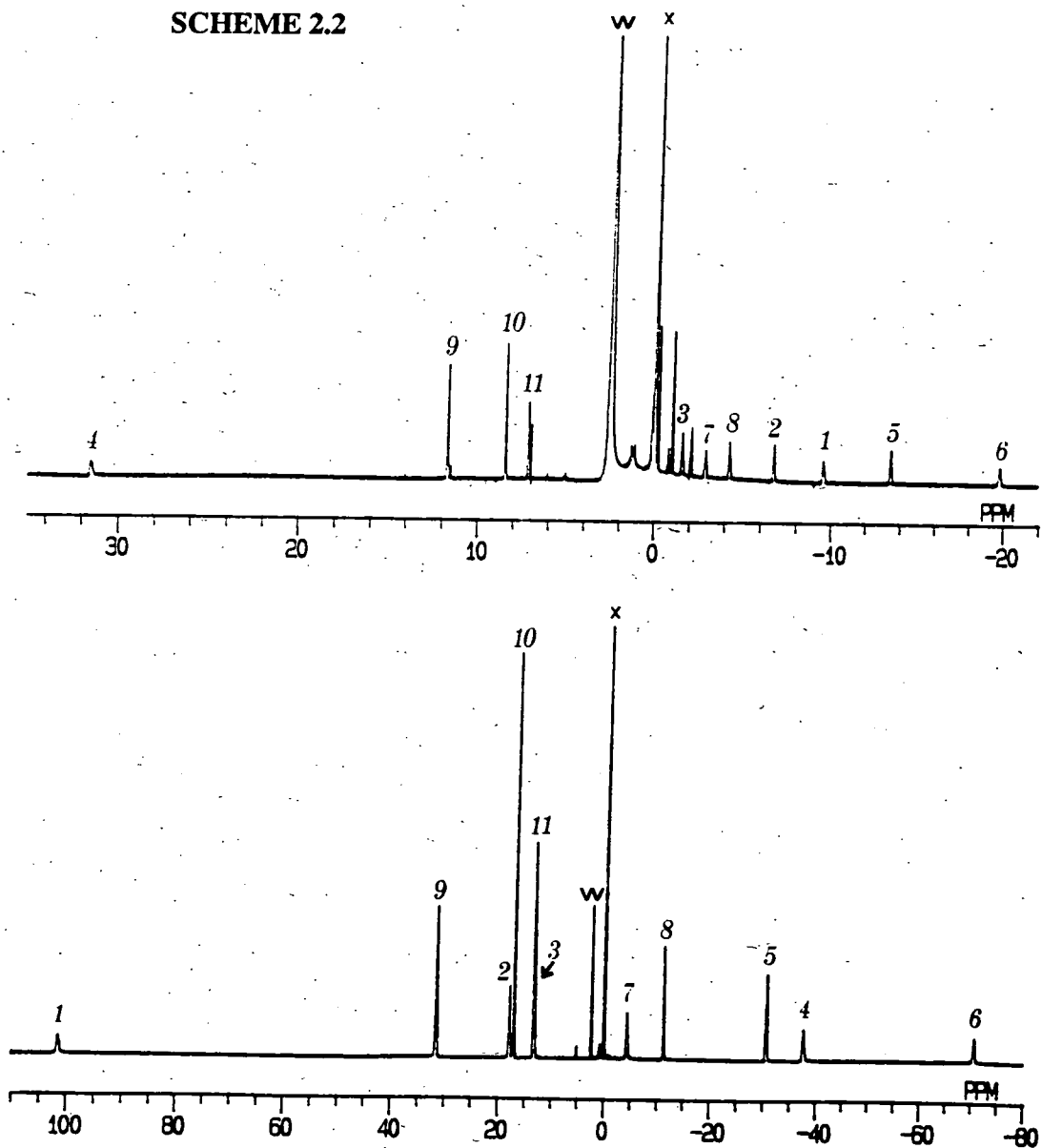


FIGURE 2.3 400MHz ¹H NMR spectra (D₂O, 298K) of (a) [Eu.27] and (b) [Yb.27]. Resonances are labelled according to Scheme 2.2. *tert*-Butanol was added as an internal reference; its signal is denoted by 'x' and that of HOD by 'w'.

In the case of the Eu^{3+} complex, line-broadening was minimal, particularly when lower magnetic field strengths were employed (section 1.8.2) and this allowed the detection of cross-peaks in a two-dimensional ^1H - ^1H COSY experiment at 90 MHz. On the basis of this and by comparison with structurally related complexes of DOTA, it proved possible to assign the observed resonances as indicated by the labelling in Scheme 2.2.

As in the complexes of DOTA, the four protons within each ethylenediamine unit of the ring become inequivalent on binding to the metal (Scheme 2). The distinction between the axial and equatorial protons is readily made on the basis of their coupling patterns. The axial protons should appear as approximate triplets in the one-dimensional spectrum, and showing two cross-peaks in a ^1H - ^1H COSY, as a result of coupling to both the vicinal axial proton and the geminal equatorial proton with similar coupling constants. For example, H_4 couples to the axial H_1 and the equatorial H_3 . The coupling constant to the vicinal equatorial proton H_2 is small, as predicted by the Karplus equations ($\phi \approx 60^\circ$), such that the H_4H_2 coupling is not resolved and does not appear in the two-dimensional spectrum. By the same argument, the equatorial protons (eg. H_2) appear only as doublets (single cross-peak in the COSY spectrum), coupling only to the geminal axial proton (H_1). The vicinal axial and equatorial protons H_3 and H_4 are both oriented at 60° to H_2 , such that coupling to these protons is very small. Some spectra showing these effects more clearly are presented in Chapter 3 for some related complexes.

The assignment is consistent with the presence of just one isomer in solution, as suspected from the ^{31}P spectrum which shows only one resonance (see below).

The lanthanide-induced line-broadening is too severe in the spectrum of the ytterbium complex to allow a two-dimensional COSY experiment to be carried out. However, Yb^{3+} does prove to be a useful ion owing to the fact that the paramagnetic shifts which it induces often approach the limit of a purely pseudocontact interaction, the contact contribution being minimal. This is apparent from Table 1.3 where it can be seen that

the ratio $C_J / \langle S \rangle_{av}$ is higher for Yb^{3+} than for any other ion, with the exception of samarium (which is less useful as it produces shifts which are too small to be helpful in structure elucidation). This feature of ytterbium allows the proton chemical shifts to be correlated with the structural features of the complex since the sign and magnitude of the shift for a given proton will be determined by its position relative to the metal ion through the quantity $(3\cos^2\theta - 1)/r^3$ (Chapter 1, equation 21). The value of r for a given proton under observation may be estimated from its relaxation rate: the paramagnetic contribution to the longitudinal relaxation rate is dependent on the distance r from the paramagnetic centre but not on the angle θ . This then allows the values of θ to be determined from the paramagnetic shifts.

A comprehensive study of the ^1H NMR spectrum of the ytterbium complex of DOTA has previously been carried out by Aime *et al.* and the structure elucidated through an analysis of the observed shifts and relaxation rates.¹⁰ In fact, $[\text{Yb.DOTA}]^-$ was found to exist as a mixture of two isomers in solution. The structural analysis of the major isomer indicated a square antiprismatic coordination geometry about the metal as indicated in Figure 2.4 (a). Such a structure is fully consistent with the X-ray results on Eu, Gd and Y complexes of DOTA. In contrast, the structure deduced for the minor isomer showed a distorted antiprismatic structure containing an inverted layout of the acetate arms with respect to the principal isomer but with the conformation of the macrocycle unchanged, Figure 2.4 (b). The distortion lies towards a prismatic arrangement, with an angle of twist (between the O_4 plane and the N_4 plane) of 29° , substantially less than the value of 45° in a true antiprism. This structural arrangement is referred to in subsequent discussions as an 'inverted square antiprism'.

A convenient way of visualising the distinction between the two structural forms is to consider the view down the C_4 axis from above the N_4 plane. The macrocycle adopts the square [3333] conformation. In the square antiprismatic arrangement (Figure 2.4a), the metal-binding acetate oxygen is seen to approach the metal from the 'side' of the macrocyclic square and the bond to the metal is roughly underneath the C-C bond of

the ring. In contrast, in the alternative inverted square antiprismatic geometry, the acetate oxygen-metal bond lies underneath the N-C bond and the acetate group appears to be approaching from the direction of the corner of the [3333] square.

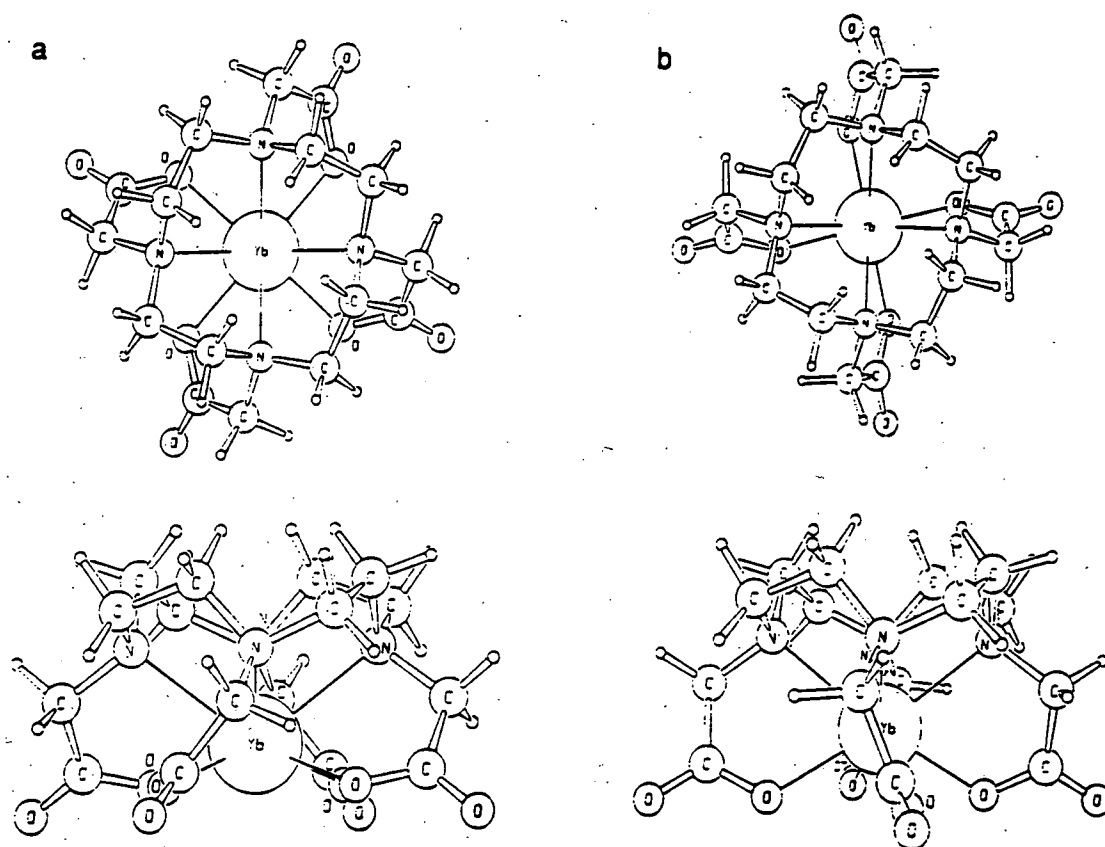


FIGURE 2.4 Top (down the C_4 axis) and side views of the structures for the major (a) and minor (b) isomers of $[Yb.DOTA]^-$ obtained by an analysis of the dipolar shifts (from reference 10).

The 1H NMR chemical shifts of the ring and NCH_2P protons of $[Yb.27]^-$ were found to match closely those of the *minor* isomer of $[Yb.DOTA]^-$. It is reasonable to conclude from this observation that the solution structure of $[Yb.27]^-$ resembles that of the minor isomer of $[Yb.DOTA]^-$ rather than that of the major isomer. This is consistent with the X-ray structure of the yttrium complex of **27** discussed above, where it was pointed out that the twist angle of 29° was well short of the idealised value of 45° for a square antiprism. It is interesting to note that, although this structural geometry is generally less important in the DOTA complexes, it is the only one detectable in the tetrakis(benzylphosphinate) system: there was no evidence in the spectra of either the

Eu^{3+} or Yb^{3+} complexes of any other isomer. Presumably such a structure becomes thermodynamically favoured over the alternative square antiprism in a system containing larger phosphinate groups rather than the smaller acetates of DOTA. Actually, it was noted in the work carried out on the DOTA complexes that for some of the lanthanide ions, for example lanthanum, the square antiprismatic form was the minor isomer. The proportions of the two isomers varied in a rather erratic manner across the series.

In the case of the DOTA complexes, the two isomers were found to undergo exchange; for example, corresponding signals for the two isomers had coalesced by 45°C in the ^{13}C spectrum of $[\text{Nd.DOTA}]^-$. At this temperature, two ethylenic resonances were observed indicating that the rigidity of the macrocycle is maintained under such conditions. This indicates that the interconversion of the two isomers cannot be occurring by a 'flip-flop' motion of the macrocycle but rather through a 'concerted sliding motion' of the 4 oxygen donor atoms, probably passing through an intermediate prismatic arrangement of higher energy.¹⁰ At higher temperatures ($45 - 80^\circ\text{C}$), a second dynamic process is observed averaging the two ethylenic resonances and thus indicative of loss of the rigidity of the macrocyclic ring. Similar conclusions were drawn from an analysis of the variable-temperature ^1H spectra of the Pr^{3+} complex.

In complete contrast, the ^1H NMR spectra of the Eu^{3+} and Yb^{3+} complexes of **27** undergo virtually no change whatsoever over the temperature range $5 - 80^\circ\text{C}$. This indicates that there is a remarkably high rigidity associated with the coordination cage in these complexes which presumably reflects a higher activation barrier to the isomerisation pathways of the type discussed above for complexes of DOTA.

The consecutive occurrence of the sliding motion of the acetate groups and the flipping of the tetraaza ring in the complexes of DOTA leads to a structure which is the enantiomer of the starting structure. Thus, there are a total of 4 possible stereoisomers in the DOTA complexes, consisting of 2 pairs of enantiomers. The relationship

between these and the pathways which interconvert them may be represented schematically as shown in Figure 2.5. Structures A and D constitute one enantiomeric pair, B and C the other.

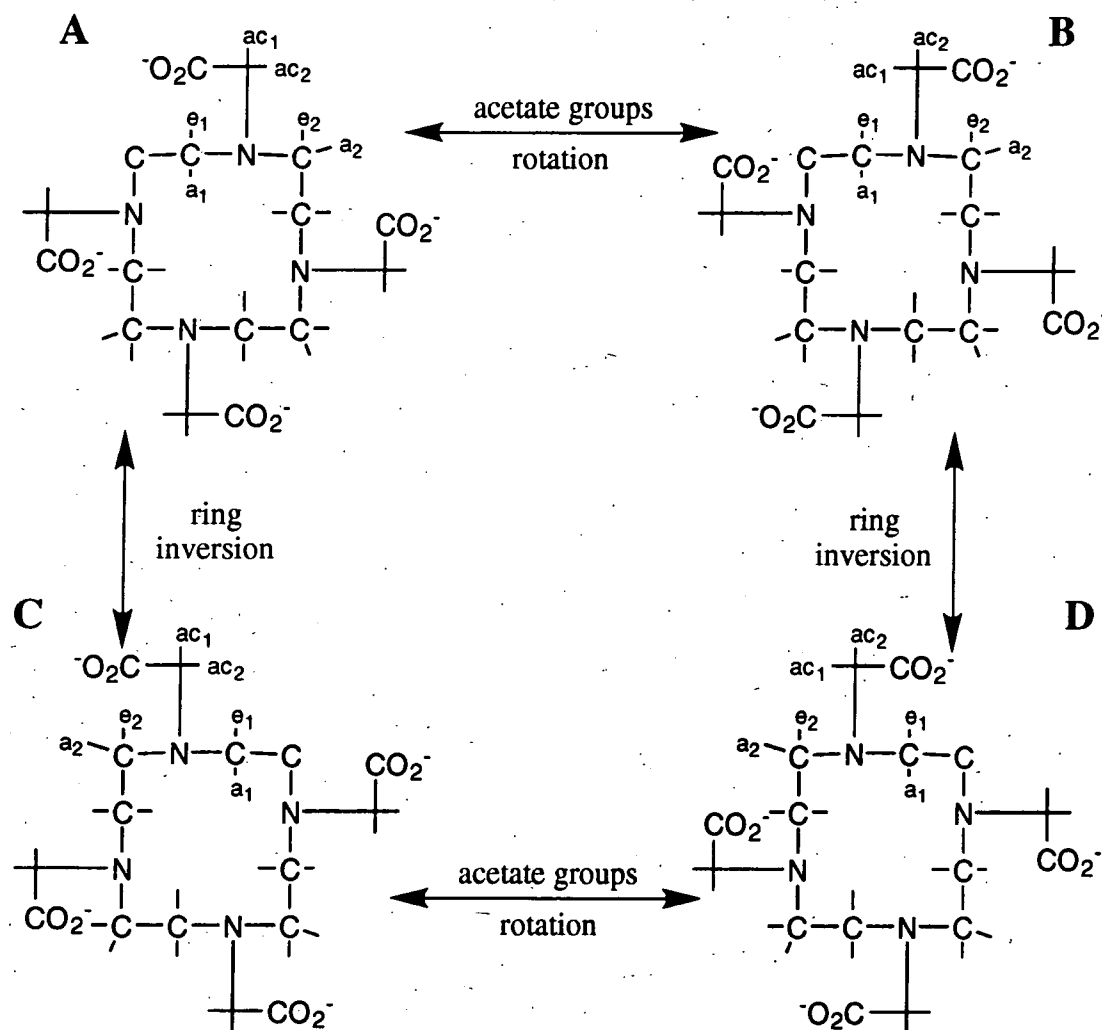


FIGURE 2.5 Schematic representation of the coordination geometries adopted by the lanthanide complexes of DOTA in solution and their interconversion pathways.

In principle, analogous structures and interconversion pathways are open to the tetraphosphinates. In fact, the possibilities here are considerably more complex than for DOTA since the binding of a phosphinate oxygen atom to the metal results in the creation of a new chiral centre at phosphorus. Each phosphorus atom can adopt (at least in principle) either an R or an S configuration, irrespective of the configurations of

the other 3 centres. Thus, for each of the 4 structural types analogous to those of DOTA in Figure 2.5, there may be ~~4~~⁶ different isomers corresponding to the ~~8~~⁶ possible permutations of the R/S configurations of the phosphorus centres in a ring (RRRR, SSSS, RRRS, etc.). Thus there are a total of ~~32~~²⁴ possible stereoisomers. For a given set of phosphorus configurations (eg. RRRR) the structural form D is no longer enantiomeric with that of A (as it was for DOTA); rather D(SSSS) is the enantiomer of A(RRRR). The ~~32~~²⁴ possibilities thus comprise of ~~16~~¹² pairs of enantiomers. A similar structural analysis is pursued in somewhat more detail in Chapter 3, where some related structures are illustrated more explicitly.

In light of the large number of structural possibilities, it is all the more remarkable that only a single species is observed in solution in the NMR studies (obviously, it must consist of a 50/50 mixture of two enantiomers which will be indistinguishable by NMR in an achiral medium). Moreover, the ³¹P spectra of all of the complexes studied show only a single resonance in each case, indicating that the 4 phosphorus atoms are equivalent. On this basis, it seems likely that the major species observed in solution is a mixture of RRRR and SSSS enantiomers in an inverted square antiprismatic structure, in which the P-alkyl substituents are disposed away from the N₄ ring such that the repulsive steric interactions between them are minimised. Such an hypothesis is fully consistent with the X-ray structure of the Y³⁺ complex where the unit cell was found to comprise of a 50/50 mixture of RRRR and SSSS enantiomers, each with an inverted square antiprismatic geometry.

It was pointed out in the preceding section that an analysis of dipolar shifts in a lanthanide complex may potentially provide a good deal of structural information, owing to the dependence of the shifts on the quantity $[(3\cos^2\theta - 1) / r^3]$. As noted above, Yb³⁺ is particularly useful in this respect because the shifts which it induces are largely free of contact contributions for nuclei not directly bound to the metal. However, the method may also be applied to complexes of the other lanthanides, provided that the measured shift for the given nucleus under observation can be

partitioned into the contact and pseudocontact contributions. For nuclei well-removed from the metal and especially for protons, the contact shift is usually negligible.¹¹ For example, the ortho protons of the benzyl groups in the europium and ytterbium complexes of **27** are shifted by 4.3 and 24.6 ppm respectively relative to the diamagnetic yttrium complex (400 MHz in D₂O, 298K). The ratio of these shifts is 0.175, which is in good agreement with the ratio of the theoretical Bleaney C_J values of 0.181 (see Table 1.3). This is probably indicative of a purely dipolar shift and almost identical coordinates of these protons relative to the metal ion in the two complexes.

For nuclei closer to the metal and especially for heteroatoms such as carbon and oxygen, the situation is more complicated and a number of methods have been proposed for evaluating the relative contributions of the dipolar and contact mechanisms to the observed shifts.¹²⁻¹⁴ The most general of these is that proposed by Reilley which relies on the theoretical C_J and <S>_{av} values to separate the components.¹⁴ The total observed shift for a nucleus is given by equation (13) in Chapter 1. After correcting for the diamagnetic contribution to the shift using the yttrium, lutetium or lanthanum complexes as controls, the observed paramagnetic shift (LIS_{obs}) is given by:

$$\text{LIS}_{\text{obs}} = \text{LIS}_{\text{pc}} + \text{LIS}_{\text{c}} \quad (28)$$

where LIS_{pc} and LIS_c are the pseudocontact and contact contributions respectively. Substituting reduced forms of equations (19) and (21) into equation (28) gives:

$$\text{LIS}_{\text{obs}} = G.C_J + F.<S>_{\text{av}} \quad (29)$$

where G is the geometrical term in equation (21) and F contains the hyperfine coupling constant (section 1.8.1). This equation may be rearranged into 2 linear forms:

$$\text{LIS}_{\text{obs}} / <S>_{\text{av}} = G(C_J / <S>_{\text{av}}) + F \quad (30)$$

$$\text{LIS}_{\text{obs}} / C_J = G + F(\langle S \rangle_{\text{av}} / C_J) \quad (31)$$

For a series of isostructural lanthanide complexes, a plot of the observed shifts according to equations (30) or (31) should provide a straight line from which G and F may be evaluated and hence the relative pseudocontact and contact contributions. This then allows the coordinates (r, θ) of the nucleus to be determined. In contrast, significant breaks or abrupt changes in the plots arise if there is a change in the structure of the complex on traversing the series. Reilley has proposed that equation (30) be used when $G \gg F$ and (31) for cases where $F \ll G$.

An analysis of this type could be of interest for the lanthanide complexes of **27**. It is possible that the larger early lanthanides may form complexes which differ in structure from those of europium and ytterbium; for example, they might adopt a square antiprismatic geometry or possess a metal-bound water molecule. The lanthanum complex of **27** has been prepared by Clive Foster at Durham. Interestingly, this complex does indeed appear to contain a significant proportion of a second isomer (most clearly apparent in the ^{31}P spectrum). One of the attractive features of the phosphinate ligands is the presence of the phosphorus atoms. Apart from allowing a greater structural variation (through the P-R group) than is possible for DOTA-based ligands, the ^{31}P nucleus is particularly amenable to NMR studies. It has a natural abundance of 100%, a spin quantum number of 1/2, short relaxation times and a high nuclear magnetic susceptibility.

With this in mind, complexes of ligand **27** with most of the other paramagnetic lanthanide ions have been prepared and their ^{31}P shifts measured in solution in D_2O ($\text{pD} = 6.5$). The shifts relative to the diamagnetic yttrium complex ($\delta_{\text{P}} = 39.2$ ppm) are plotted in Figure 2.6. For comparison, the ^{17}O paramagnetic shifts in the aquo ions, where the shifts are dominated by contact contributions, are plotted in Figure 2.7, together with the ^1H shifts of the $\text{Ln}(\text{dpm})_3$ complexes, where the shifts are exclusively dipolar. It is clear that the ^{31}P shifts do not follow either pattern exactly, but there is

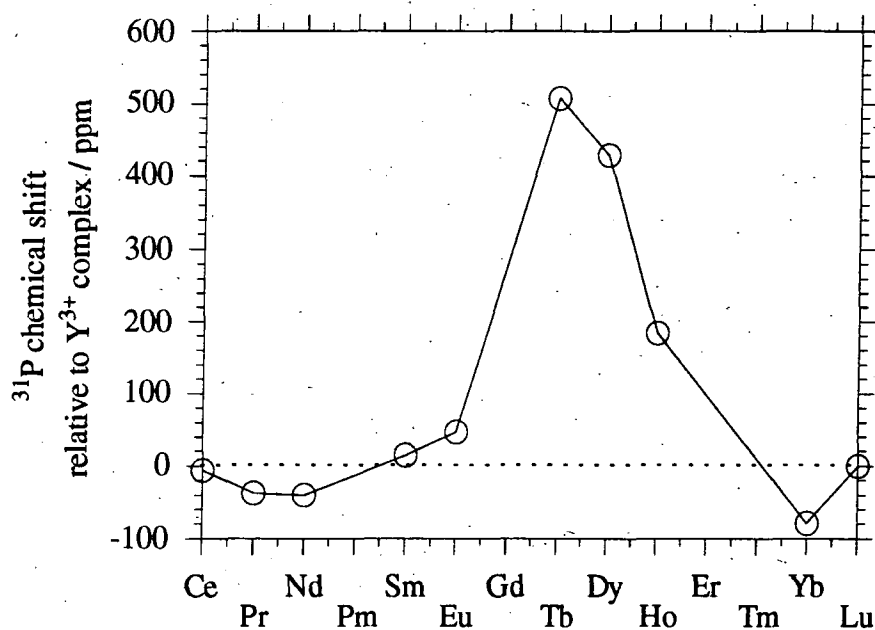


FIGURE 2.6 ^{31}P shifts (101.1 MHz, D_2O , $\text{pD} = 6$, 298K) of the lanthanide complexes of ligand 27, relative to the diamagnetic yttrium complex.

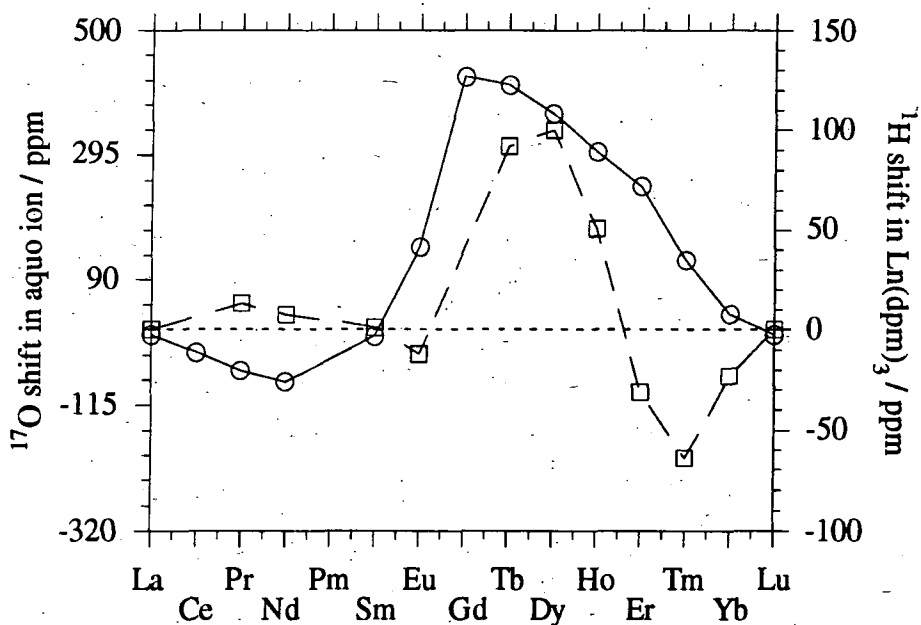


FIGURE 2.7 Paramagnetic ^{17}O shifts in the lanthanide aquo ions (reference 15) and ^1H shifts in the complexes of $\text{Ln}(\text{dpm})_3$ (reference 16). See also Table 1.3 (Chapter 1).

perhaps a closer resemblance to the ^{17}O contact shifts, which suggests that there is a substantial contact contribution to the shifts. This is not surprising bearing in mind the proximity of the phosphorus atoms to the metal and the relatively large spatial extensions of their outer orbitals.

The observed shifts are plotted according to equations (30) and (31) in Figures 2.8 and 2.9. The complexes appear to fall into two groups, with Ce^{3+} , Pr^{3+} and possibly Nd^{3+} showing a different pattern to the remaining later elements, which form a fairly reasonable straight line. This apparent break between the early, larger lanthanides and the later elements could possibly reflect a change in the structure. On the other hand, Peters has shown, through the use of calculated theoretical values of G and F , that such apparent breaks may simply be a consequence of the decrease of the ionic radii across the lanthanide series.¹⁷ Indeed, some results previously ascribed to structural changes have been re-interpreted in this way. The change in ionic radius may be accompanied by small differences in the conformations of the complexes which is reflected in the θ values of the various ligand nuclei. The combined effect of change of r and θ may result in a gradual variation of the G values on going from La^{3+} to Lu^{3+} , which may show up as abrupt changes when the LIS data are plotted according to equations (30) or (31). Significant changes in F are generally considered unlikely, as the hyperfine coupling constant is expected to have a similar value for all of the lanthanide ions.

Thus, the results are rather inconclusive. In fact, the r and θ values for the phosphorus atoms could be very similar in both the square antiprismatic and the inverted square antiprismatic geometries, with the result that the G values may be very similar in both cases. Hence, analysis of the ^{31}P shifts may not be a sufficiently sensitive means of distinguishing between the two possibilities. A study of the magnetic field dependence of the ^{31}P longitudinal relaxation rates would provide more reliable information on the metal-phosphorus distances, as has been carried out for some related complexes (Chapter 3).

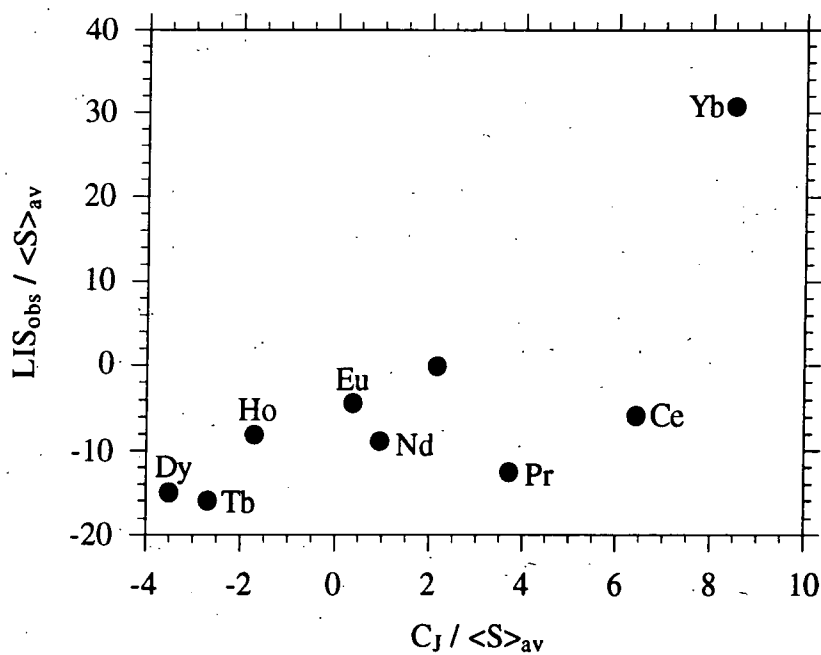


FIGURE 2.8 ^{31}P shifts of the lanthanide complexes of 27 plotted according to equation (30).

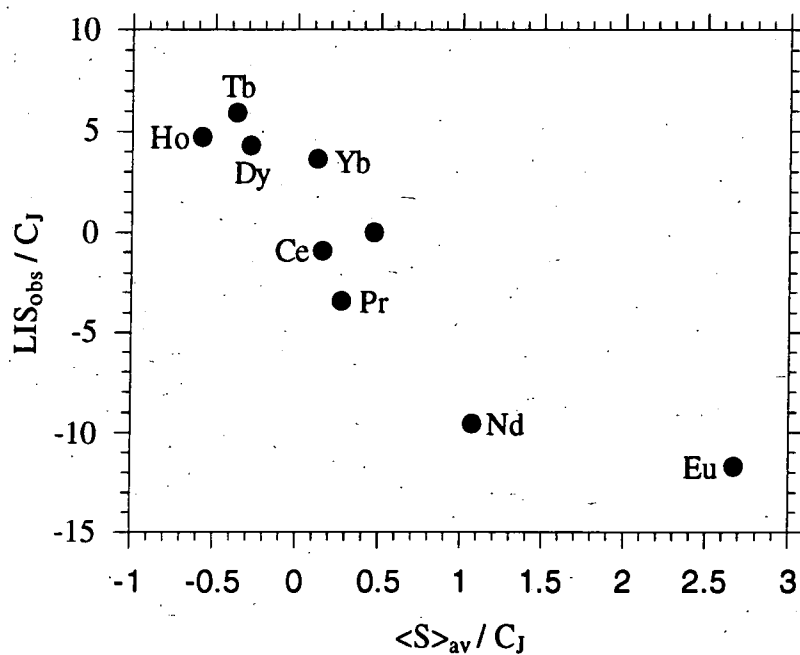


FIGURE 2.9 ^{31}P shifts of the lanthanide complexes of 27 plotted according to equation (31).

2.7 Luminescence of Terbium and Europium complexes

2.7.1 UV absorbance spectra

The absorption and luminescence behaviour of the europium and terbium complexes of ligand **27** have been studied in aqueous solution at room temperature. The UV absorbance spectra resemble that of benzene, with a structured band between 240 and 260 nm ($\lambda_{\text{max}} = 248$ nm, $\epsilon_{\text{Tb}} = 910$, $\epsilon_{\text{Eu}} = 950 \text{ M}^{-1}\text{cm}^{-1}$), as shown in Figure 2.10. This corresponds to the so-called B-band of benzene which is formally forbidden ($\epsilon_{254} = 204 \text{ M}^{-1}\text{cm}^{-1}$ for benzene; the band owes its appearance to the loss of symmetry caused by molecular vibrations). Although weak in terms of organic chromophores, this band is much stronger than the bands observed in the absorption spectra of the free lanthanides, for which ϵ is typically $1 \text{ M}^{-1}\text{cm}^{-1}$ or less (as discussed in Chapter 1) and so it is not surprising that the phenyl absorbance completely dominates the UV spectra of the complexes.

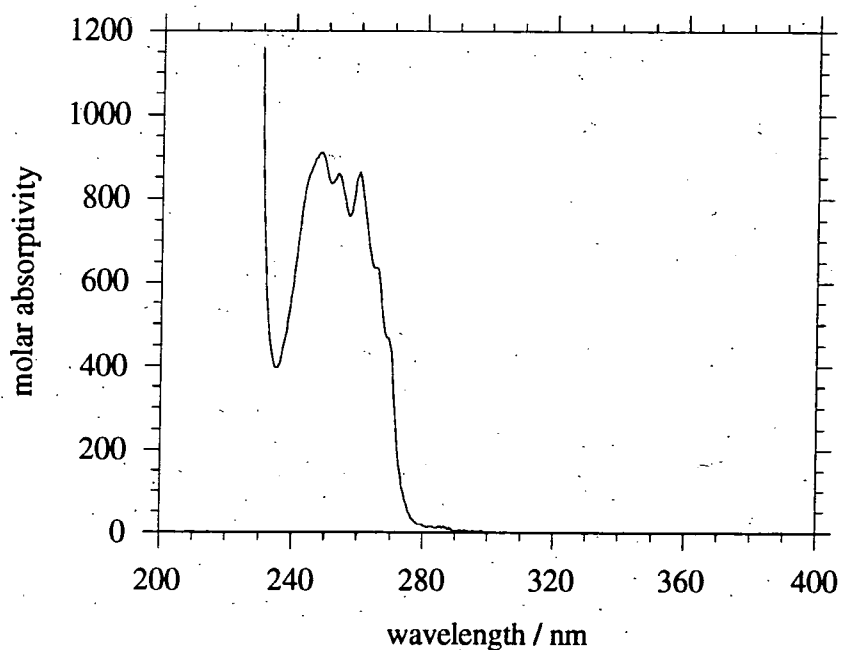


FIGURE 2.10 UV absorbance spectrum of $[\text{Tb.27}]^-$ in aqueous solution (295K).

2.7.2 Luminescence of [Tb.27]⁻

Excitation of the terbium complex of **27** at 250 nm gave rise to intense luminescence characteristic of the metal; a 10^{-4} M solution glowed an apple green colour. The corrected emission spectrum on excitation at 250 nm is shown in Figure 2.11. Four intense bands are observed, the wavelengths of which are consistent with the well-known values for bands arising from transitions from the emissive 5D_4 level to the 7F_6 , 7F_5 , 7F_4 and 7F_3 levels of the ground manifold.¹⁸ Some much weaker bands are also apparent at longer wavelengths; these are due to transitions to the 7F_2 , 7F_1 and 7F_0 levels. A further important feature of lanthanide spectra is also evident, namely the sharpness of the bands as mentioned in section 1.3.1. For example, the $^5D_4 \rightarrow ^7F_5$ band has a half-height width of only 10 nm (using an emission bandpass of 2.5 nm).

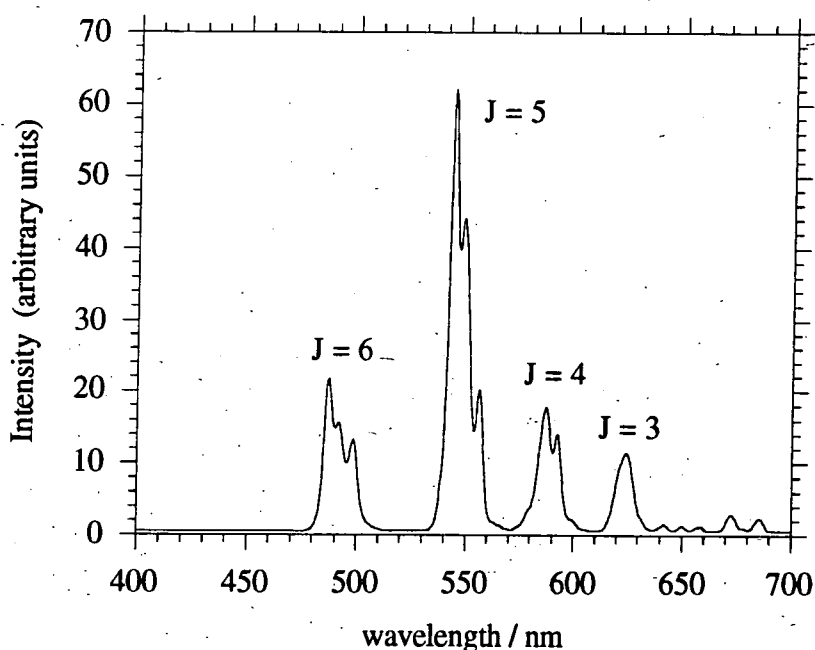


FIGURE 2.11 Metal luminescence emission spectrum of [Tb.27]⁻ in aqueous solution (10^{-4} M, 295K) on excitation at 250 nm. Excitation and emission monochromator slit widths of 2.5 nm were used and a delay of 0.1 ms was set between excitation and measurement of the luminescence intensity. The bands arise from $^5D_4 \rightarrow ^7F_J$ transitions; the J values of the bands are labelled on the spectrum.

Some fine structure is clearly visible in the first three bands. This arises from the removal of the degeneracy of the $2J+1$ states per J level which occurs on bringing a lanthanide ion from the gas phase (or a hypothetical spherical environment) into the complex, where the symmetry is lower. The extent to which the degeneracy is removed depends on the symmetry of the metal's environment: complete loss of degeneracy, giving $2J+1$ non-degenerate sub-levels, only occurs when the symmetry is very low (with a C_2 axis or less). In the complexes of ligand **27**, the local symmetry of the metal is approximately C_4 (from the crystal structure of the Y^{3+} complex). Under these conditions, a $J = 4$ level is predicted to split into 7 non-degenerate sub-levels whilst an energy level with $J = 5$ should give rise to 8 sub-levels.¹⁸ Thus, if we consider the $^5D_4 \rightarrow ^7F_5$ transition, it is apparent that this band should comprise of 56 different transitions. Of course, many of these transitions will have the same or very similar energy; a possible analogy is the overlap of gear ratios which occurs in a bicycle with several front and rear cogs. This is especially true for the lanthanides owing to the weak nature of the interaction of the f electrons with the crystal-field which results in only small separations between these sub-levels. The outcome is that the band does show some structure, as evident from the spectrum in Figure 2.11, but certainly not 56 lines. The large number of possible transitions for terbium bands in general means that it is not normally possible to infer much about the local symmetry of the metal-ion from an analysis of the fine structure of the bands. Europium proves to be a more useful ion for this purpose, owing to the lower J values associated with the observed transitions (see below). Circularly polarised luminescence provides a means of extracting rather more information from the Tb^{3+} spectrum and this is discussed in section 2.9.

The observation of metal emission raises the question of the pathway by which it is induced: does the emission arise from a direct excitation of the metal through some (weak) metal absorbance or charge transfer band at 250 nm, or is there a genuine energy transfer process occurring from the phenyl groups to the metal ion, following excitation into the B-band of the benzene rings? A useful method for distinguishing between these two possibilities is to record a luminescence excitation spectrum. In this

experiment, the emission monochromator of the spectrometer is held constant at a wavelength at which the metal is known to emit and the intensity of emission at this wavelength is monitored as a function of the excitation wavelength. The resulting plot, known as an excitation spectrum, shows the profiles of the band or bands responsible for metal emission.

Such a spectrum was recorded for $[\text{Tb.27}]^-$, using an emission wavelength of 545 nm, at which terbium emits strongly (the $^5\text{D}_4 \rightarrow ^7\text{F}_5$ transition). The result is shown by the dashed line in Figure 2.12. The UV absorbance spectrum has been superimposed on this spectrum (solid line). It is clear that the two spectra match up almost identically over almost the entire wavelength range. The apparent deviation at wavelengths shorter than 230 nm is an artifact arising from a severe inner filter effect (due to the high absorbances at these wavelengths) and from the failure of the spectrometer to correct for the low output of the xenon lamp excitation source at such short wavelengths.

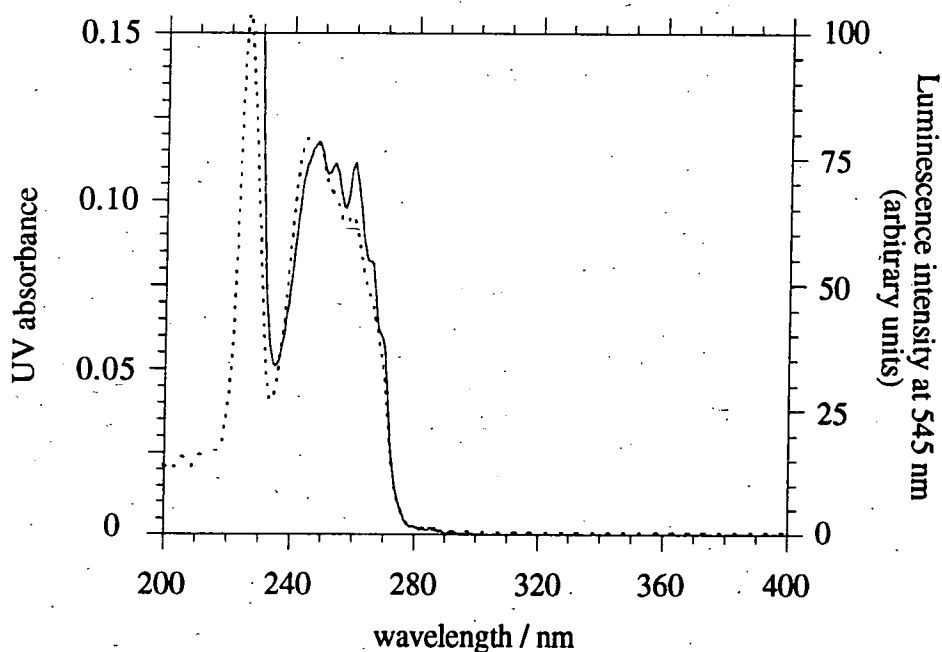


FIGURE 2.12 *Dashed line: Metal luminescence excitation spectrum of $[\text{Tb.27}]^-$ in aqueous solution ($2.6 \times 10^{-4} \text{ M}$, 295K). Emission monitored at 545 nm; excitation and emission monochromator slit widths of 2.5 nm and a delay time of 0.1 ms were used. Solid line: UV absorbance spectrum of this solution.*

The close match of the excitation and absorbance spectra indicates that the metal emission occurs as a result of the absorption of UV light by the phenyl groups. If the emission arose from direct metal excitation, or indeed if the metal ion had dissociated from the ligand following dissolution, then the excitation spectrum would be expected to resemble the line-like UV spectrum of 'free' aqueous terbium(III) (Figure 2.13). Thus, the conclusion is that phenyl-sensitised metal emission is occurring, which must involve an energy transfer process from the benzene rings to the metal.

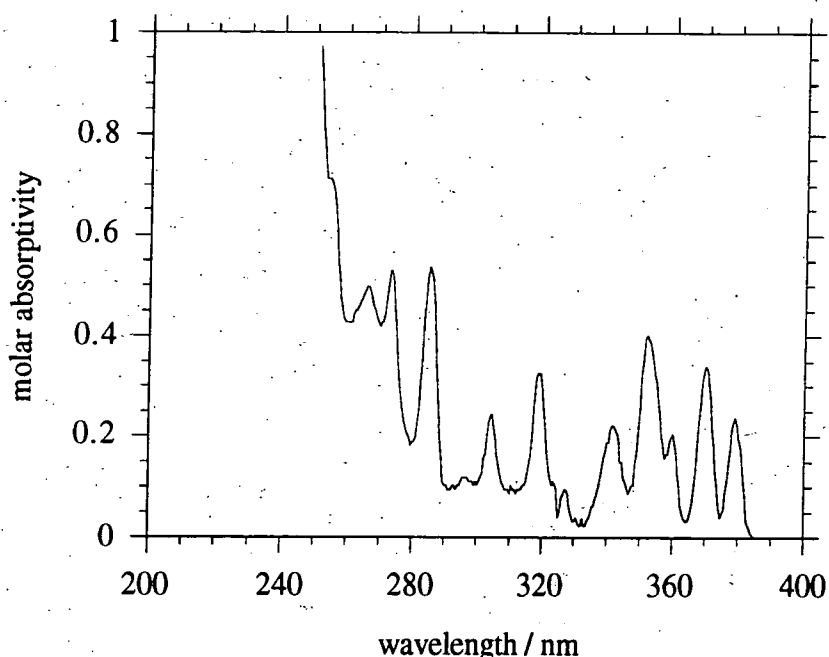


FIGURE 2.13 *UV absorbance spectrum of terbium nitrate in aqueous solution. The rapid rise to short wavelengths is due to the intense $f^8 \rightarrow f^7d^1$ transition at 220 nm. Note the low molar absorptivities of the bands compared to those of [Tb.27]⁻ in Figure 2.10.*

The quantum yield of emission for the complex on excitation at 250 nm in aqueous solution was determined using quinine sulfate (in 1M H₂SO₄) as a standard. An extraordinarily high value of 0.44 was obtained. Some of the factors which are likely to be responsible for this high value are discussed in more detail in subsequent sections. At this point, it is useful to note that the high quantum yield also provides conclusive evidence for an energy transfer process from phenyl to terbium. Bearing in mind that the combined absorbance of 4 phenyl groups at 250 nm is of the order of 1000 times

stronger than that of free terbium at this wavelength, it is clear that an upper limit of about 10^{-3} would apply to the quantum yield if the emission were to arise solely from direct metal excitation, rather than as a result of absorption of UV light by the phenyl groups.

2.7.3 Luminescence of [Eu.27]

To some extent, the europium complex of ligand 27 behaves similarly. Thus, luminescence characteristic of the metal is observed on excitation at 250 nm in aqueous solution (Figure 2.14). The luminescence excitation spectrum (recorded using an emission wavelength of 619 nm, at which the europium complex emits most strongly) again shows a very close resemblance to the UV absorbance spectrum of the complex, being completely dominated by the phenyl absorbance. Again, this indicates that the metal emission arises following absorption by the phenyl groups. A much weaker band at 397 nm was also evident in the excitation spectrum; this is due to a relatively strong absorbance band of europium(III) at this wavelength (ϵ about $3 \text{ M}^{-1}\text{cm}^{-1}$).

The most noticeable difference between the terbium and europium complexes was the much weaker emission of the latter. The emissive quantum yield of this complex was measured using $[\text{Ru}(\text{bipy})_3]\text{Cl}_2$ as a standard and a value of 9×10^{-4} was obtained in water, a very low value when compared to that of 0.44 for the terbium complex. This is discussed further in section 2.11.

It was mentioned briefly in section 2.7.2 that europium emission spectra generally prove to be more useful than those of terbium in terms of the information which they may provide on the symmetry of the metal environment. This reflects the fact that the observed emission bands arise from a non-degenerate $J = 0$ state ($^5\text{D}_0$) and the transitions occur to levels with low J values, such that there are only a small number of possible components per band. In fact, the $^5\text{D}_0 - ^7\text{F}_0$ transition is unique for a given chemical environment, since both the initial and final states are non-degenerate. The number of components observed for this transition is therefore related to the number of

chemically distinct environments of the Eu^{3+} ion. This transition has been used both in excitation and in emission as a probe of sample homogeneity.¹⁸⁻²¹ One problem, however, is that an 0-0 transition is forbidden by all the electronic selection rules and is therefore usually very weak. This is exacerbated when the local symmetry of the metal is high (including D_4 , D_{4h} or D_{4d}) or when an inversion centre is present, as the transition is then formally forbidden by the symmetry selection rule as well. The local symmetry of the metal in $[\text{Eu.27}]^-$ is likely to be C_4 on the basis of the solid state structure of the yttrium complex and, under these conditions, the 0-0 transition is symmetry-allowed through an electric dipole mechanism.¹⁸ The transition is indeed observed as a single, weak band at 579 nm (Figure 2.14). A more highly-resolved spectrum obtained with laser excitation and more sensitive photon-counting equipment (see Figure 3.14 in Chapter 3) shows that there is indeed only one band in this region, consistent with the presence of a single europium species.

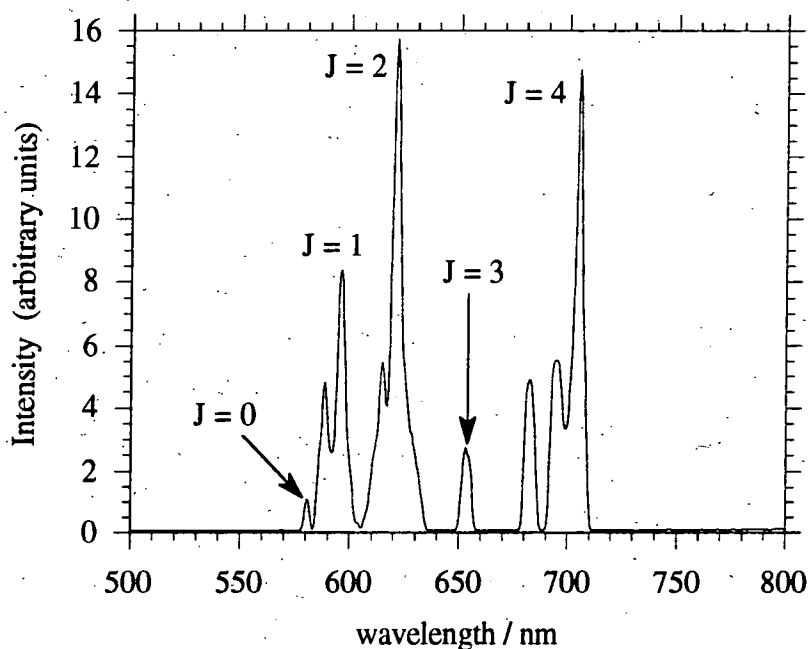


FIGURE 2.14 Metal luminescence emission spectrum of $[\text{Eu.27}]^-$ in D_2O (10^{-4}M , 295 K) on excitation at 250 nm. Excitation and emission monochromator slit widths of 10 and 2.5 nm respectively were used with a delay time of 0.1 ms. The bands arise from $^5\text{D}_0 \rightarrow ^7\text{F}_J$ transitions; the J values of the bands are labelled on the spectrum.

A group theoretical analysis indicates that the 7F_1 level is expected to split into two non-degenerate sub-levels in the presence of a three-fold or higher axis of symmetry (only one in icosahedral or cubic symmetry).¹⁸ The maximum number of three non-degenerate states occurs only for lower symmetry (C_2 axis or lower). Thus, the appearance of two components in the ${}^5D_0 \rightarrow {}^7F_1$ band is consistent with a 4-fold symmetry axis for the complex, as expected on the basis of the X-ray structure of the Y^{3+} analogue. However, some caution must be exercised in drawing conclusions from the number of observed bands. Thus, whilst the appearance of three components in the ${}^5D_0 \rightarrow {}^7F_1$ band would be very strong evidence for a low-symmetry environment, the observation of only two bands cannot necessarily be used to infer higher symmetry as a third, unresolved band could be present. On the other hand, there is no evidence for a shoulder or any other distortion of the observed components of the ${}^5D_0 \rightarrow {}^7F_1$ band in the more highly-resolved spectrum obtained by direct metal excitation and shown in Figure 3.13 (Chapter 3) and so the spectrum is certainly not inconsistent with a 4-fold symmetry axis. Furthermore, the ${}^5D_0 \rightarrow {}^7F_2$ transition is also predicted to display two components under C_4 symmetry and indeed it does.

It may also be possible to draw some conclusions regarding the coordination environment of the metal from the relative intensities of the bands. This point is deferred until Chapter 3, where some comparisons with related complexes are made and some apparent trends are noted.

2.7.4 Excited state lifetimes

Luminescence lifetimes were measured by monitoring the emission intensity after a number of pre-set time intervals following the excitation pulse (experimental details are given in Chapter 6). The result of a typical experiment for an aqueous solution of $[Tb.27]^-$ ($10^{-4}M$) is shown in Figure 2.15, where the open circles represent the observed data points.

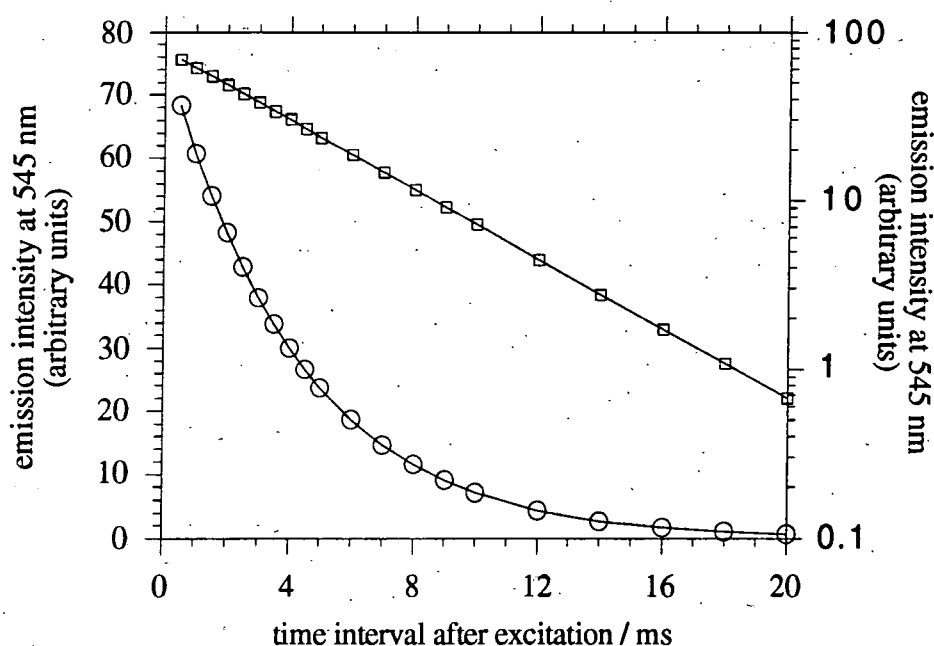


FIGURE 2.15 Metal luminescence decay curve for $[\text{Tb.27}]^-$ in aqueous solution ($3 \times 10^{-4} \text{ M}$, 295K) on excitation at 250 nm. The open circles represent the measured data points; the solid line is the best fitting monoexponential curve through these points: $I(t) = 77 \times \exp(-0.242.t)$. The squares represent the same data points plotted on a logarithmic scale.

The data have been fitted to a monoexponential equation of the form

$$I(t) = I(0)\exp(-k_{\text{obs}}t) \quad (6)$$

as outlined in Chapter 1 (section 1.6.3). The solid line represents the best fit of the data to such a curve. The good match between the curve and the observed points (the difference between the two, the residual, is extremely small and purely random) indicates that the luminescence decay is monoexponential. In other words, the $^5\text{D}_4$ emissive state displays first-order kinetics of deactivation and the value of the observed first-order rate constant, k_{obs} , was found to be 242 s^{-1} from the equation of the fitted curve. As mentioned in section 1.6.3, it is usual to quote the luminescence lifetime, τ , which is simply the reciprocal of k ; thus, the lifetime of emission for $[\text{Tb.27}]^-$ in H_2O is 4.13 ms. This is a particularly long lifetime, indeed it appears to be the longest lifetime reported to date for a terbium complex in aqueous solution. This long value indicates that competitive, non-radiative deactivation pathways for the metal emissive state are

minimal in this compound. In particular, it implies that the ligand is shielding the metal very efficiently from solvent water molecules (which are able to deactivate the emissive state by energy transfer into O-H vibrations, section 1.3.2). This effect was further investigated by measuring the luminescence lifetime in D₂O. In this case, a value of 4.44 ms was obtained, which is only marginally higher than the value of 4.13 ms in water. Use of the Horrocks parameter²² for estimating the hydration state, *q*, through:

$$q = A_{Ln} (\tau_{H_2O}^{-1} - \tau_{D_2O}^{-1}) \quad (5)$$

(where $A_{Tb} = 4.2$ and $A_{Eu} = 1.05$, section 1.3.3), gave a value of 0.07 for the hydration state. This is very strong evidence for the lack of any metal-bound water molecules in [Tb.27]⁻ in aqueous solution. This remarkable observation is consistent with the X-ray structure of the yttrium complex discussed earlier, where the nearest water molecule was 5.6 Å away. Of course, in the present instance, the conclusion applies to the behaviour in solution. It seems likely, then, that the structure of the complex is not substantially changed on dissolution.

A similar conclusion was reached for the europium complex: the measured lifetimes were 1.59 and 2.07 ms in H₂O and D₂O respectively, giving a *q* value of 0.15. Again, this value is close to zero, suggesting the absence of metal-bound water molecules. Bearing in mind the similarity of the ionic radii of Eu³⁺ and Tb³⁺ and the apparent similarity of the structures adopted by the europium and ytterbium complexes deduced from the NMR studies, it is reassuring to observe similar behaviour for the two complexes. On the other hand, a surprisingly large difference in solubility was noticed between the two complexes, that of terbium being significantly the more soluble.

The luminescence lifetimes of the Eu³⁺ and Tb³⁺ complexes of ligand **26** were also measured, both in H₂O and in D₂O. A hydration state, *q*, of 0.27 was observed for both complexes. Again, such a value is consistent with a lack of inner-sphere water molecules or, at least, a long metal-nearest-water distance (section 3.5.4 discusses this

point in more detail). This observation implies that low hydration states are a feature of the $12N_4$ -tetrakisphosphate motif in general, rather than an effect specific to the tetrabenzylphosphinate system alone (i.e. it is not, for example, just a steric effect arising from the bulk of the 4 benzyl groups). It is possible that this difference, as compared to related tetraamide and tetracarboxylate complexes, which all display one metal-bound water molecule, reflects the greater ability of the PRO_2^- group over the carbonyl and carboxylate groups to function as a σ -donor to the metal. Of course, the phosphinate groups are also rather bulkier than the carboxylates and so there may also be a steric effect hindering the approach and binding of the water molecule.

The luminescence information for the four complexes is summarised in Table 2.1.

TABLE 2.1 *Luminescence results for the europium and terbium complexes of ligands 26 and 27.*

Complex	τ (298K) / ms		ϕ (298K)		q^c
	D ₂ O	H ₂ O	D ₂ O	H ₂ O	
[Eu.DOTA] ⁻	2.13 ^a	0.60 ^a	---	---	1.2
[Tb.DOTA] ⁻	2.54 ^b	1.51 ^b	---	---	1.1
[Eu.26] ⁻	1.85	1.25	1.0×10^{-3}	0.59×10^{-3}	0.27
[Tb.26] ⁻	3.71	2.96	10×10^{-3}	9.0×10^{-3}	0.29
[Eu.27] ⁻	2.07	1.59	1.5×10^{-3}	0.9×10^{-3}	0.15
[Tb.27] ⁻	4.44	4.13	0.49	0.44	0.07

a) reference 56. b) this work.

c) q is the hydration state determined according to equation (5), chapter 1.

2.8 Other methods for probing the hydration state in solution

2.8.1 ^{17}O Paramagnetic shifts

The contact contribution to the paramagnetic shift experienced by a lanthanide-bound ^{17}O nucleus has been shown to be almost independent of the nature of the ligand in question and also of the other ligands coordinated to the metal.²³ This observation has been exploited as a means of determining information regarding the coordination properties of the ligand, the stoichiometry of the complex and also the number of metal-bound water molecules.²³ As explained in Chapter 1, the ^{17}O shift of lanthanide-coordinated water molecules is probably dominated by the contact contribution for all of the lanthanides. In the case of dysprosium, the ^{17}O shift (d.i.s. - dysprosium induced shift) is thought to arise from a contact contribution of greater than 85%. Dysprosium is therefore particularly well-suited to the studies in question, as a partitioning of the observed shift into contact and pseudocontact contributions is not required.

For a lanthanide complex in aqueous solution, the lability of metal-bound water molecules is high and exchange of water is much faster than the ^{17}O NMR time-scale. Consequently, the effect of the metal is transferred to the bulk water and this is reflected by a shift in the ^{17}O resonance of the solvent water molecules (cf. the effect of Gd^{3+} on the relaxation rate of water protons, section 1.8.3). The magnitude of the effect will be dependent on the concentration of the complex and is predicted to follow the relationship given in equation (32).

$$\text{d.i.s.} = q \Delta [\text{Dy}(\text{ligand})_n(\text{H}_2\text{O})_q] [\text{H}_2\text{O}] \quad (32)$$

where q is the number of metal-bound water molecules and Δ is the shift per inner-sphere water molecule (in units of ppm M^{-1}). Since the complex concentrations in such an experiment are relatively low, $[\text{H}_2\text{O}]$ will be virtually constant and so a plot of the observed d.i.s. versus the concentration of the complex should be linear, with a gradient of $q\Delta[\text{H}_2\text{O}]$, provided that q is independent of concentration. If the complex lacks sufficient stability, the dissociation of the metal from the ligand may become significant at low concentrations. Under these conditions, q clearly becomes concentration-dependent and so a deviation from linearity will be observed.

In order to evaluate q , it is necessary to obtain a value for the quantity Δ , (the shift per metal-bound water molecule). This can be achieved by examining the behaviour of a complex which has a well-defined number of inner-sphere water molecules. The lanthanide complexes of DOTA and DTPA are suitable for this purpose, both of which are known to possess one metal-bound water molecule.^{7,8} Thus, the ratio of the gradient obtained for the complex under investigation to that obtained for $[\text{Dy.DOTA}]^-$ or $[\text{Dy.DTPA}]^-$ will directly provide a value of q for the complex of interest.

Some experiments of this type were carried out and the results are shown in Figure 2.16. The ratio of the gradient for $[\text{Dy.26}]^-$ to that of $[\text{Dy.DOTA}]^-$ was found to be 0.15. This value, which is close to zero, again provides further evidence that in the complexes of these tetraphosphinate ligands, there is no metal-bound water molecule. Clearly, a q value of exactly zero would not be expected by this method, as there is certain to be some dipolar contribution to the observed shift, albeit minimal, through an effect on non-coordinated water molecules.

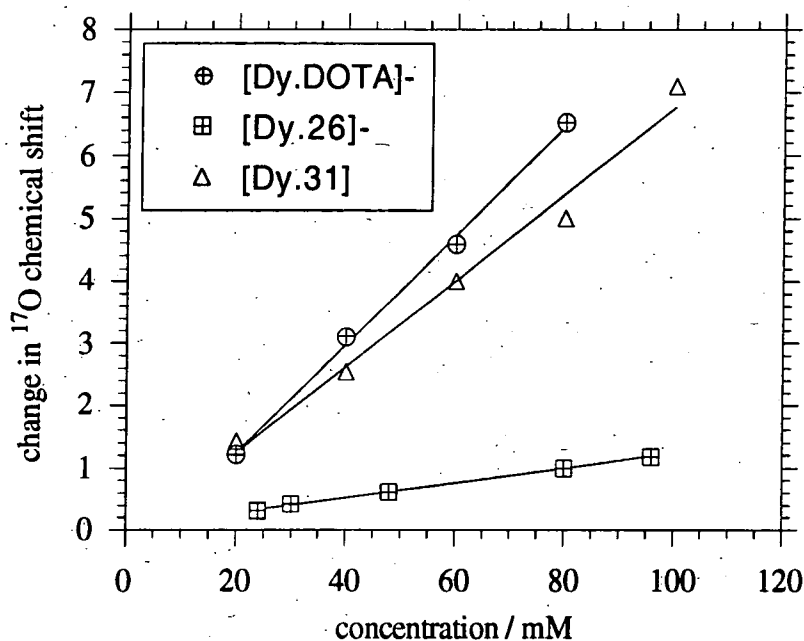


FIGURE 2.16 Plots of the dysprosium induced shifts of the ^{17}O resonance of water as a function of the concentration of the dysprosium complexes of DOTA and 27 (31 is a ligand from Chapter 3 and is discussed there).

2.8.2 Relaxivity of the gadolinium complexes

The Gd^{3+} complexes of ligands **26** and **27** were prepared by Dr. Kanthi Pulukkody at Durham with a view to examining their potential as paramagnetic contrast agents in magnetic resonance imaging. The relaxivities and NMRD profiles for the two complexes have been measured by Professor Silvio Aime and coworkers at the University of Turin. As explained in Chapter 1, the NMRD profiles may provide a large amount of structural and dynamic information on the complexes. The magnitude of the relaxivity over the entire magnetic field range and the shape of the profiles (Figure 2.17) indicate that neither complex possesses a metal-bound water molecule and are able to catalyse the relaxation of solvent water protons through outer-sphere effects only. This is in marked contrast to the behaviour of the Gd^{3+} complexes of structurally related ligands based on the tetraazacyclododecane ring with carboxylate and phosphonate pendent groups, where the NMRD profiles show that there is one metal-bound water molecule present. For example, the relaxivity at 20 MHz for $[\text{Gd.27}]^-$ is about $2 \text{ mM}^{-1}\text{s}^{-1}$, which compares to values of 4 - 6 $\text{mM}^{-1}\text{s}^{-1}$ for complexes such as $[\text{Gd.DOTA}]^-$ or $[\text{Gd.DTPA}]^{2-}$.

The observation of purely outer-sphere behaviour for the tetraphosphinate complexes is consistent with the X-ray structure of the Y^{3+} complex, the luminescence results of the Eu^{3+} and Tb^{3+} complexes and the ^{17}O shifts of water for the dysprosium complex, all of which indicate the lack of inner-sphere water molecules.

Figure 2.17 shows that the two complexes have rather different NMRD profiles. Fitting of the observed data points to Freed's theoretical expression for outer-sphere relaxivity (Chapter 1) indicates that this difference arises primarily from a difference in the value of the parameter a for the two complexes; i.e. the distance of closest approach of diffusing water protons to the paramagnetic centre. Values of 4.25 and 3.82 Å were calculated for the complexes of **27** and **26** respectively. The difference may be accounted for by the steric bulk of the benzyl groups in **27**. These values are returned

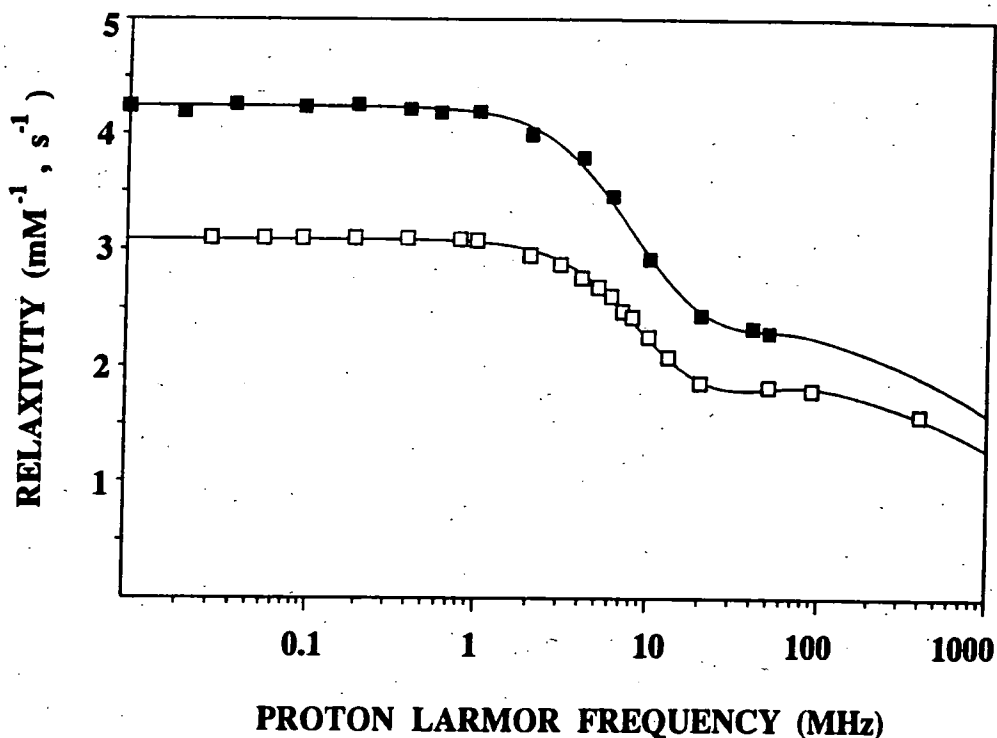


FIGURE 2.17 Experimental NMRD profiles for $[Gd.26]^-$ (solid squares, 296K) and $[Gd.27]^-$ (open squares, 298K) in aqueous solution (pH 7.3). The solid lines through the data are best-fitting curves obtained using the theory described in Chapter 1.

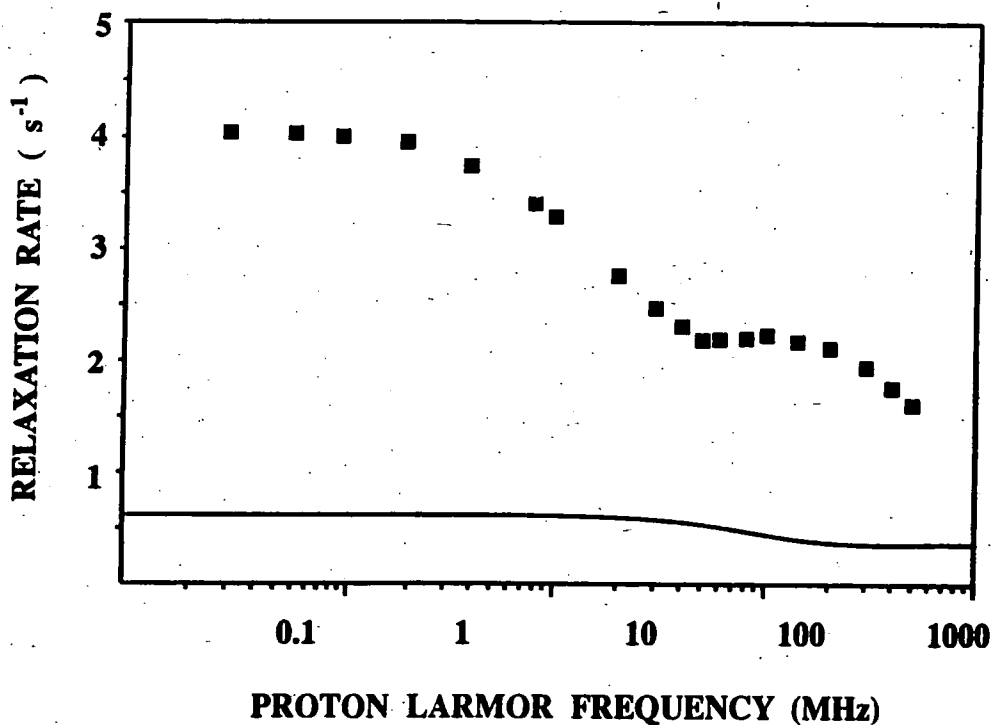


FIGURE 2.18 Experimental NMRD profile for $[Gd.27]^-$ (aqueous solution, 0.2 mM, 298K), in the presence of bovine serum albumin (1.8 mM). The solid line at the bottom is the calculated profile for the same concentration of the complex in the absence of protein.

to in Chapter 3 where an attempt is made to correlate the NMRD data to that obtained from luminescence.

Preliminary MRI experiments have shown that $[\text{Gd.27}]^-$ gives rise to a remarkably high signal enhancement in liver and bile.⁴ *In vitro* studies were carried out on the effect of binding of $[\text{Gd.27}]^-$ to a representative protein (bovine serum albumin). A large increase in solvent proton relaxation rate compared to the value for unbound complex was observed, as shown in Figure 2.18. Complexes containing *inner-sphere* water molecules are expected to display substantial enhancements in relaxivity on binding to large molecules such as proteins, owing to the longer rotational correlation times τ_R of large molecules, which lead to an increase in τ_C and hence an increase in the inner-sphere relaxivity (equations 25-27 in Chapter 1). This is known as a Proton Relaxation Enhancement (PRE) effect.^{27,28} In contrast, purely outer-sphere complexes (eg. $[\text{Gd.27}]^-$) are not expected to show such a large change in relaxivity under such conditions and so the magnitude of the observed effect is rather surprising. (There are a few other examples of high relaxation enhancements in complexes with $q = 0$ ²⁸).

In order to investigate the suggestion that this might be due to a change in the structure of the complex on binding to the protein, in such a way that the hydration state q is increased, some luminescence experiments were performed on the terbium complex in the presence of the same protein. A solution of the terbium complex of **27** (10^{-4}M) in H_2O (phosphate buffered saline at pH 7.4) containing bovine serum albumin (10^{-3}M) was prepared. Under these conditions, and assuming a value of $2.8 \times 10^{-4}\text{M}$ for the dissociation constant of the $[\text{Gd.27}]^-$ -protein adduct (estimated from the PRE measurements), the concentration of protein-bound complex will be approximately three times that of the unbound complex. The measured luminescence lifetime will thus be an average for that of the bound and unbound complex, weighted towards that of the protein-bound complex. (Exchange between the two environments is expected to be much faster than the lifetime of Tb^{3+} emission). Luminescence lifetimes were determined in both H_2O and D_2O and values of 3.7 and 3.9 ms were obtained

respectively. Although these values are very slightly lower than those found in the absence of the protein, they suggest a hydration state of 0.06 (using the Horrocks parameter) which is fully consistent with that obtained from the unbound complex. This observation provides firm evidence that the hydration state of the complex is unperturbed by protein binding. Some other theories which may account for the unexpectedly high relaxivity of the protein-bound Gd^{3+} complex have been put forward.⁵

2.9 Circularly Polarised Luminescence

Chiroptical spectroscopic methods, such as optical rotation, optical rotatory dispersion, circular dichroism and circularly polarised luminescence, potentially offer a good deal of additional information on the coordination environment of metal ions in complexes compared to conventional spectroscopic techniques.²⁹⁻³¹ These methods are particularly sensitive to details of molecular stereochemistry, and the double-signed nature of the spectral features may be exploited to provide higher resolution. Moreover, the intensities are governed by mechanisms and selection rules which are different to those of conventional spectroscopic bands and this may allow further information to be extracted.

The properties of polarised light are normally described in terms of the behaviour of the electric vector. An unpolarised light beam propagating along the z axis contains electric vectors whose directions span all possible angles within the xy plane. In the case of linearly polarised light (also known as plane-polarised light), the transverse electric vectors are all constrained to vibrate in a single plane. Linearly polarised light may be visualised as consisting of two circularly-polarised components. The right circularly polarised component's electric vector spirals to the right (E_r) along the direction of propagation and thus may be thought of as sweeping out a right spiral on the surface of a cylinder of radius equal to E_r , whereas the left circularly polarised component spirals to the left. These two components of equal magnitude add vectorially to produce plane-polarised light (Figure 2.19a).

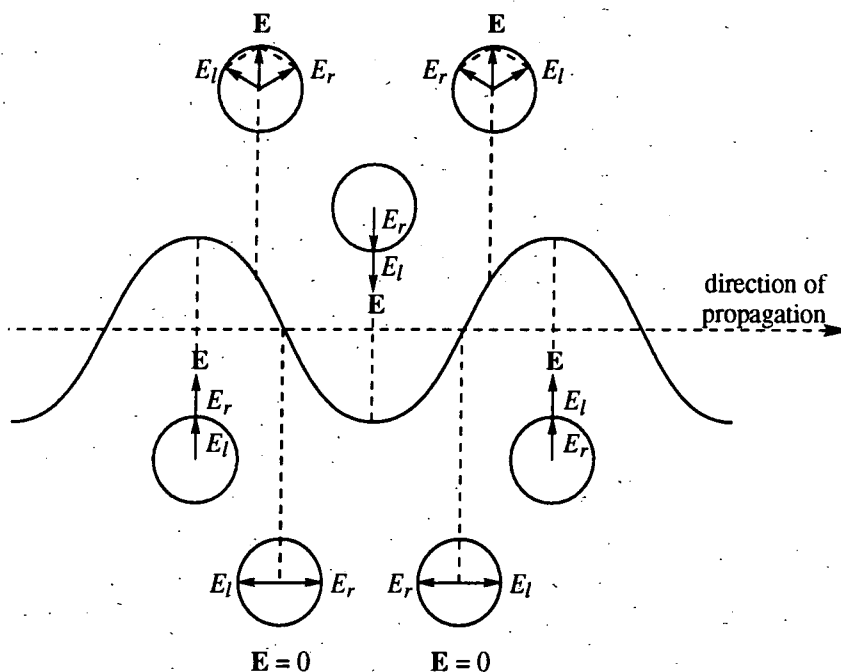
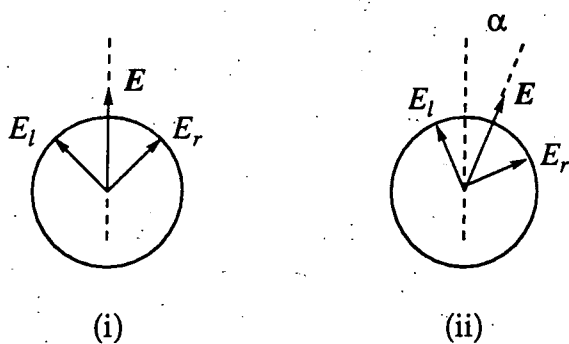


FIGURE 2.19 (a) A beam of plane-polarised light viewed from the side (sine wave) and along the direction of propagation at specific times (circles), where the resultant electric vector E and the circularly polarised components E_l and E_r are shown. Adapted from a diagram in reference 32.



(b) Plane-polarised light before entering (i) and after emerging (ii) from an optically active substance

The two components travel with the same velocity in an optically inactive medium but, in an optically active medium, one component is slowed relative to the other owing to a difference in the indices of refraction ($n_l \neq n_r$). Since one component is retarded more than the other, the resultant vector will be rotated through an angle α after passing through an optically active medium (Figure 2.19b). This is the basis of the widely-observed property of optical rotation.

Optical rotation and its variation with wavelength (known as optical rotatory dispersion or ORD) are readily interpreted through such a description, provided that the wavelength of observation does not coincide with an absorption band of the compound. Within an absorption band, not only is the phase angle between the two projections of the two components altered by passage through the chiral medium, but their amplitudes are modified according to the degree of absorption experienced by each component. This differential absorption of left and right circularly polarised light by a chiral substance is termed circular dichroism (CD).

In order to measure the circular dichroism of a sample, it is necessary to generate circularly polarised light. This is achieved by passing linearly polarised light through what is called a quarter-wave plate - a material that is able to produce a 90° phase difference between the left and right circularly polarised components. A dynamic quarter wave plate alternately modulates the incoming linearly polarised light into left and right circularly polarised light. This device may be a Pockels cell (in which stresses are created in a crystal of ammonium dideuterium phosphate through application of AC high voltage) or a photoelastic modulator (which relies on the piezoelectric effect). The circularly polarised light is passed through the sample and the emerging light is detected by a photomultiplier tube, the output of which is converted into two signals. One of these consists of an alternating signal (at the frequency of the quarter wave plate) proportional to the circular dichroism and arising from the differential absorbance by the sample of one component over the other. The other signal is averaged and is related to the mean light absorption. The quantity of interest, and the one which is normally quoted, is the absorption dissymmetry factor (g_{abs}^{λ}) which is effectively the ratio of these two signals, being defined through equation (33).

$$g_{\text{abs}}^{\lambda} = \frac{\Delta\epsilon}{\epsilon} = \frac{\epsilon_{\text{L}} - \epsilon_{\text{R}}}{\frac{1}{2}(\epsilon_{\text{L}} + \epsilon_{\text{R}})} \quad (33)$$

where $\Delta\epsilon$ is the difference in extinction coefficients for left and right circularly polarised components (ϵ_{L} and ϵ_{R}) and ϵ is the average extinction coefficient.

Whereas circular dichroism is concerned with the differential *absorption* of right and left circularly polarised light, the technique of circularly polarised luminescence spectroscopy (CPL) is concerned with the measurement of the difference in intensity of left versus right circular polarisation in the *emission* spectrum.^{33,34} As for CD, in the absence of perturbing static electric or magnetic fields, differential emission will arise only if the molecular species of interest is chiral. CPL is complementary to CD as it provides a measure of the chirality of the luminescent excited state as opposed to the ground state.

Circularly polarised luminescence has not caught on to the same extent as the widely-used technique of circular dichroism. This reflects the fact that its applicability is rather more limited, being confined to systems which are quite strongly emissive. A few reports of its application to transition metal complexes {Cr(en)₃³⁺, Ru(bipy)₃²⁺ and Ru(phen)₃²⁺} have been reported in the literature³⁵⁻³⁷ but, in general, transition metals are not very well suited to CPL measurements, owing to the fact that strong emission from appropriate complexes only occurs at low temperatures in frozen glasses. In order to measure CPL from such low-temperature systems, it is necessary to make strain-free glasses to avoid depolarisation of the emitted light. This proves to be quite difficult.³⁸

The luminescent lanthanide ions, on the other hand, and especially Eu³⁺ and Tb³⁺, prove to be ideal candidates for use in CPL spectroscopy, owing to the intense emission which they display under ambient conditions. Moreover, good quality CD spectra are generally inaccessible for complexes of the lanthanide ions owing to the low absorptivities of the ions. A number of reviews of the application of CPL to lanthanide complexes have appeared.^{29,30,33,34,39}

No commercial instrumentation is available for the measurement of CPL. The instrumental set-ups which have been described in the literature are essentially identical to an ordinary fluorescence spectrometer but with the addition of a circular analyser between the sample and the emission monochromator.³⁹ As for CD, a photoelastic

modulator (PEM) or Pockels cell quarter wave plate is used for this purpose, but here its task is the reverse: during one half-cycle of the modulation it converts left circularly polarised light into linearly polarised light and then, during the other half-cycle, right circularly polarised light is transformed. Thus the two components are successively converted into linearly-polarised light and passed onto the monochromator to be detected.

In the experimental arrangement used to acquire the spectra shown below, detection is achieved using a photomultiplier tube, the signal from which is passed to an amplifier which outputs photopulses to a differential photon counter.³⁹ This device is linked to the PEM controller in such a way that the counter adds the photopulses that enter when left circularly polarised light is passing through the PEM and subtracts the pulses when right circularly polarised light intensity is being measured. A second counter counts every pulse. Thus one counter provides a number which is proportional to ΔI and the other a number proportional to I , where:

$$\Delta I = I_L - I_R \quad \text{and} \quad I = I_L + I_R$$

By analogy with CD, it is usual to define a luminescence (or emission) dissymmetry ratio, g_{lum}^λ , as:

$$g_{lum}^\lambda = \frac{\Delta I}{\frac{1}{2} I} \quad (34)$$

Of course, ΔI and I apply to a single wavelength only. A CPL spectrum is a plot of ΔI versus wavelength. The form of the variation of ΔI (both its magnitude and its sign) with wavelength may be used to obtain information on the chirality of the excited state of the molecule and may provide a 'fingerprint' which is unique for a given structural geometry.

The techniques of CD and CPL as described above require the use of a sample consisting of a single enantiomer or, failing that, an excess of one enantiomer over the other. A racemic mixture is no use as the effects for the two enantiomers will be equal and opposite and therefore cancel each other out (cf. the lack of optical rotation for a

racemic mixture). However, Professor Jim Riehl of Michigan Technological University and his collaborators have pioneered a method of overcoming this limitation of CPL by making use of circularly polarised excitation of the sample. A quarter-wave plate is placed in the excitation beam, between the source (an arc lamp or a laser) and the sample, such that the excitation beam becomes circularly polarised. If the sample consists of a racemic mixture, then one enantiomer will be preferentially excited over the other, to an extent which is determined by the values of g_{abs} at the excitation wavelength used. This enantioselective excitation means that circularly polarised emission may then be detected in the same way as if there were an excess of this enantiomer in the mixture. Using this experimental method, the measured luminescence dissymmetry factor, g_{obs} , is given by:

$$g_{\text{obs}} = \frac{1}{2} \cdot g_{\text{abs}}^{\lambda_{\text{ex}}} \cdot g_{\text{lum}}^{\lambda_{\text{em}}} \quad (35)$$

where g_{abs}^{λ} and g_{lum}^{λ} have the meanings given earlier. In effect, the technique combines the properties of circular dichroism and circularly polarised emission.

The circularly polarised luminescence properties of the Eu^{3+} and Tb^{3+} complexes of ligand **27** have been examined by Professor Riehl and coworkers using this technique. As mentioned earlier, the complexes were thought to consist of a 50/50 mixture of enantiomers (RRRR and SSSS in the inverted square antiprismatic geometry). Separation of the two enantiomers has not been achieved to date and so the use of circularly polarised excitation is essential if any CPL is to be detected. For lanthanide(III) ions, it has been shown that transitions which obey magnetic dipole selection rules, that is $\Delta J = \pm 1$, often possess quite large values for $|g_{\text{lum}}|$, typically greater than 0.01.³⁹ (Note that the theoretical maximum value is 2 from equation 34, and likewise for g_{abs} , equation 33). $\text{Eu}(\text{facam})_3$ displays the strongest CPL effect of any Eu^{3+} complex studied to date, with a g_{lum} value of about 0.5.³⁹

The experiments performed on $[\text{Eu.27}]^-$ were carried out by excitation of the ${}^7\text{F}_2 \rightarrow {}^5\text{D}_1$ transition at 553 nm, using a tunable dye laser with a power output of 1W. This approach has not been reported previously. Although the ${}^7\text{F}_2$ state is only about 1% populated at room temperature, the transition satisfies the $\Delta J = \pm 1$ selection rule and this imparts a high degree of circular dichroism to the transition; i.e. a high g_{abs}^λ , reflected in large discriminations between the two possible circular polarisations. The circularly polarised emission spectra of the ${}^5\text{D}_0 \rightarrow {}^7\text{F}_1$ and ${}^5\text{D}_0 \rightarrow {}^7\text{F}_2$ bands were recorded. The former is shown in Figure 2.20, together with the corresponding total emission spectrum.

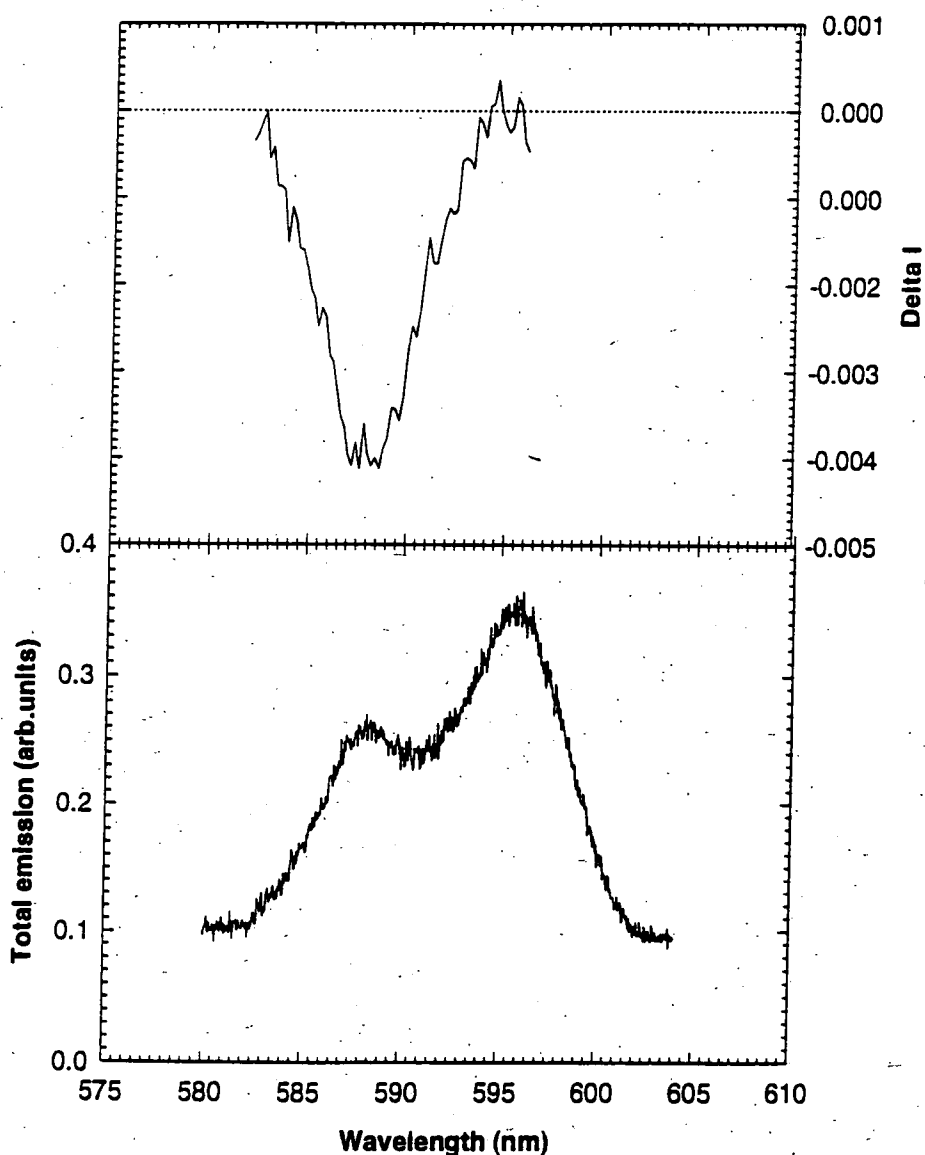


FIGURE 2.20 Circularly polarised and total luminescence emission spectra of the ${}^5\text{D}_0 \rightarrow {}^7\text{F}_1$ band of $[\text{Eu.27}]^-$ in aqueous solution on excitation at 553 nm (298K).

Although the circularly-polarised luminescence (ΔI) is relatively weak (maximum g_{obs} is -0.016 for ${}^5\text{D}_0 \rightarrow {}^7\text{F}_1$) it is clearly present. This indicates that the environment of the europium is indeed chiral. Moreover, in the absence of the excitation PEM, no CPL was observed which is consistent with a racemic mixture of the two enantiomers.

A similar experiment was also carried out on the terbium complex of **27**. In this case, the 488 nm line of an argon ion laser was used to excite the ${}^7\text{F}_6 \rightarrow {}^5\text{D}_4$ transition. This transition has $\Delta J = -2$ and is therefore not ideal for use in this technique. However, the ${}^7\text{F}_5$ energy is too high for this level to be significantly populated at room temperature and so excitation from ${}^7\text{F}_5$ to ${}^5\text{D}_4$ ($\Delta J = -1$) is not viable. Despite the low enantioselectivity (low g_{abs}^{λ}) expected for the ${}^7\text{F}_6 \rightarrow {}^5\text{D}_4$ transition, some surprisingly strong CPL was observed for the ${}^5\text{D}_4 \rightarrow {}^7\text{F}_5$, ${}^7\text{F}_4$ and ${}^7\text{F}_3$ emission bands (Figure 2.21). Maximum g_{obs} values were about 0.03, 0.015 and 0.014 respectively. Clearly, this indicates that the *emission* dissymmetry factor must be very high for this compound. Again, this is conclusive evidence for the chirality of the terbium environment and shows that there is no interconversion of enantiomers during the excited state lifetime of the terbium.

The CPL spectra are clearly quite complex in appearance and there are no theories available to account for the relative signs or magnitudes of the effect for different components within a given emission band. However, the spectra unambiguously show that the complexes are indeed chiral and provide useful 'fingerprints' of the specific coordination environment. A further point relates to the higher resolution which CPL spectra may provide as compared to conventional luminescence spectra. This is perhaps most evident for the terbium ${}^5\text{D}_4 \rightarrow {}^7\text{F}_3$ transition where the presence of 4 components to the band is much clearer in the CPL spectrum than in the total emission spectrum, even though the latter was measured at higher resolution (Figure 2.21).

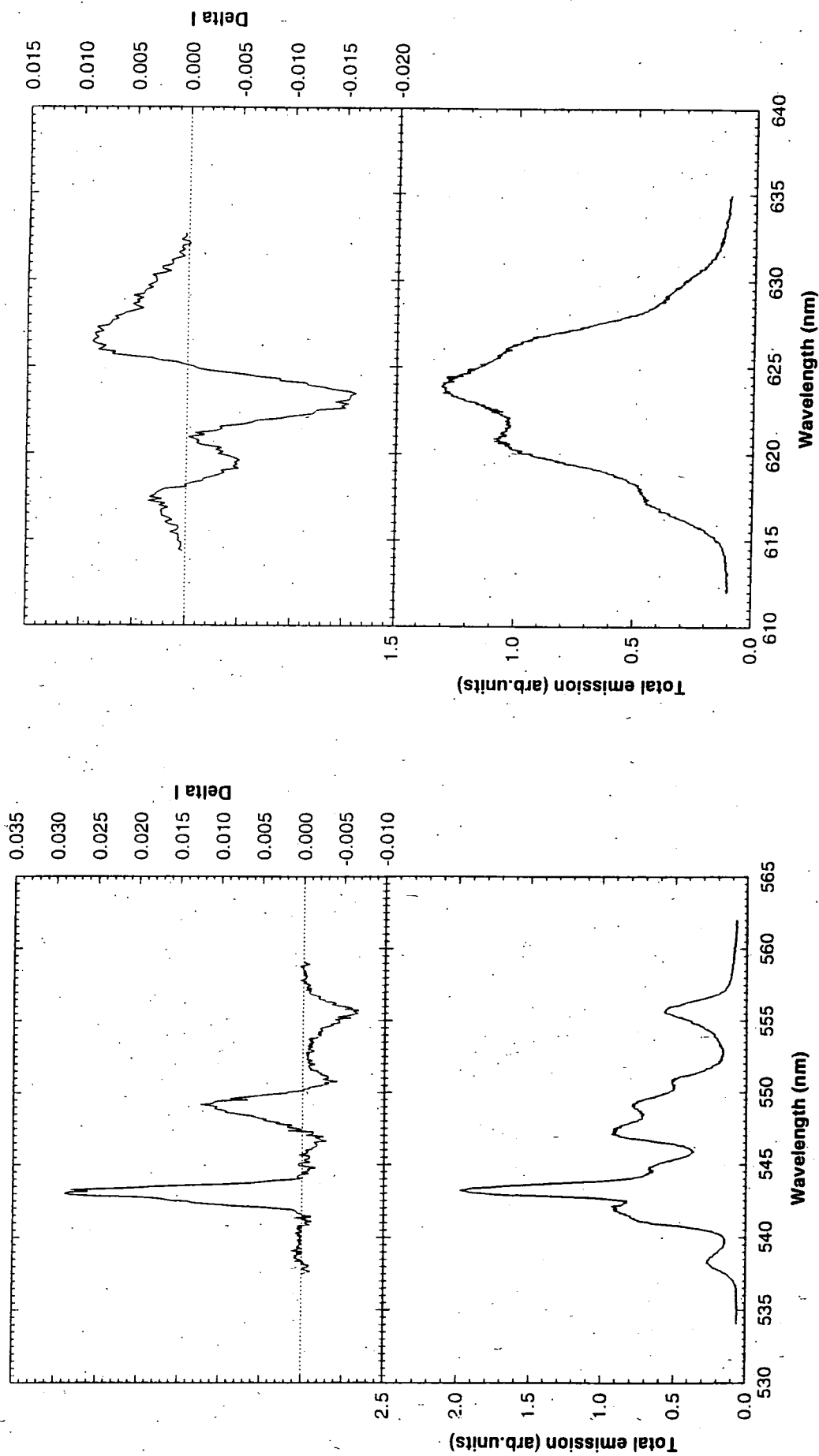
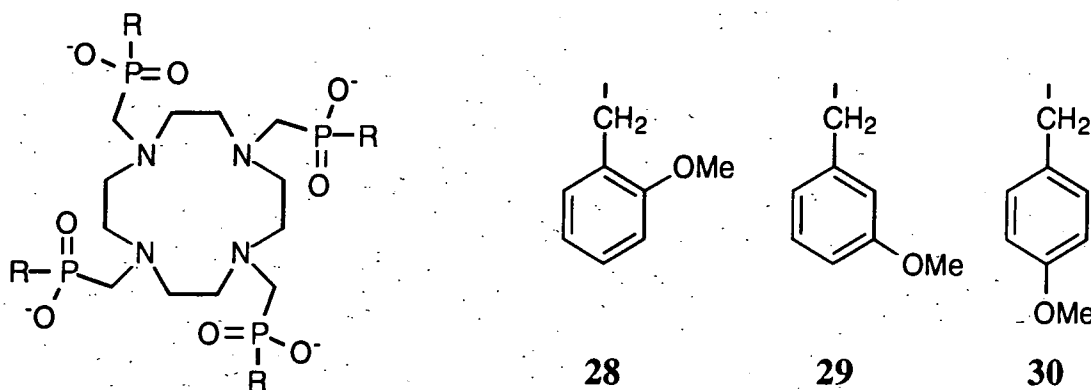


FIGURE 2.21 Circularly polarised luminescence (upper) and total luminescence (lower) of [Tb.27]⁻ in aqueous solution (298K) following excitation at 488 nm. The spectral regions displayed are those of the ⁵D₄ → ⁷F₅ transition of terbium (left) and the ⁵D₄ → ⁷F₃ (right).

2.10 Methoxybenzylphosphinate complexes

A series of ligands related to **27**, but in which the benzene rings carry a methoxy substituent, have been prepared at Durham. The europium and terbium complexes of ligands **28** - **30** were provided by Dr. Tim Norman, Clive Foster and Dr. Steven Faulkner respectively. The syntheses proved to be rather more arduous than that of the tetrabenzylphosphinate, **27**, owing in large part to the instability of the intermediate dialkoxyphosphines.



The UV absorbance spectra of the 6 complexes in aqueous solution showed bands characteristic of the methoxybenzene chromophore ($\lambda_{\text{max}} = 274 \text{ nm}$, $\epsilon = 3800 \text{ M}^{-1}\text{cm}^{-1}$) in each case. However, it was noted that the bands for the *para* isomer were less sharply defined than for the other isomers and a pronounced tailing of the long wavelength band to wavelengths in excess of 300 nm was observed. In each case, the metal luminescence excitation spectra (recorded using emission wavelengths of 545 nm for the terbium complex and 619 nm for those of europium) closely resemble the UV absorbance spectra, providing conclusive evidence that the metal emission arises following absorption by the methoxybenzene chromophores (Figure 2.22).

Luminescence lifetimes and quantum yields for the three terbium complexes in aqueous solution were determined on excitation at 277 nm. In all cases, strictly monoexponential decay of the luminescence was observed. Lifetimes were of the order of 4.0 ms in water (Table 2.2) and only marginally higher in D₂O, again indicative of the absence of inner-sphere water molecules ($q < 0.1$ in each case). Quantum yields

comparable to those of [Tb.27]⁻ were observed for the ortho and meta substituted complexes (Table 2.2). That of the *para* isomer was somewhat lower, although still very respectable. In each case, the form of the emission spectra (i.e. fine structure and relative intensities of the bands) were very similar to that of [Tb.27]⁻.

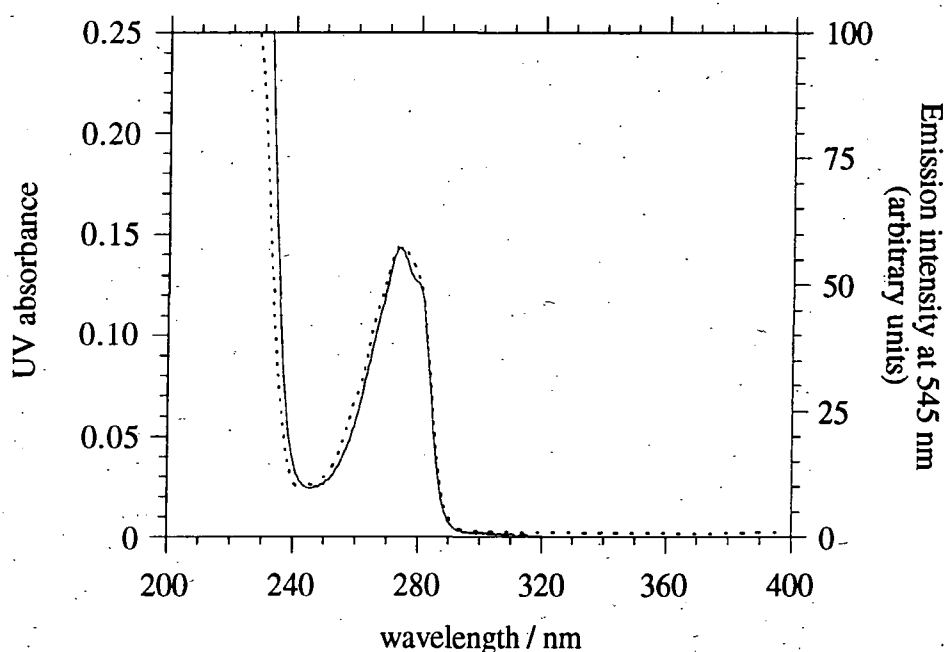


FIGURE 2.22 *Dashed line: Metal luminescence excitation spectrum of [Tb.28]⁻ in aqueous solution (3×10^{-5} M, 295K). Emission monitored at 545 nm; excitation and emission monochromator slit widths of 2.5 nm and a delay time of 0.1 ms were used. Solid line: UV absorbance spectrum of this solution.*

The terbium complexes of **28** and **29** do, however, offer two significant advantages over [Tb.27]⁻, namely the longer excitation wavelength ($\lambda_{\text{max}} = 274$ nm compared to 249 nm) and the higher extinction coefficients (3800 compared to $910 \text{ M}^{-1}\text{cm}^{-1}$) at the respective absorbance maxima. Both of these properties are attractive as far as potential applications are concerned, as discussed in Chapter 1 (section 1.6.2). Unfortunately, however, the methoxybenzyl complexes suffer from a problem of very low solubility in water (or indeed in other solvents such as methanol).

This drawback also afflicts the analogous europium complexes. Here, the low solubility, coupled with the weakness of the emission for the europium complexes,

resulted in an excessive amount of scatter in the luminescence decay curves, preventing the determination of reliable lifetimes. The quantum yields of emission were estimated to be of the order of 10^{-3} - 10^{-4} .

TABLE 2.2 *Luminescence results for the terbium complexes of the methoxybenzylphosphinate ligands 28 - 30.*

Complex	τ (298K) / ms		q	ϕ (298K)		ϕ_{fl}^a
	D ₂ O	H ₂ O		D ₂ O	H ₂ O	
[Tb.28] ⁻	4.33	3.97	0.09	0.52	0.44	1.00
[Tb.29] ⁻	4.42	4.08	0.08	0.46	0.40	0.91
[Tb.30] ⁻	4.32	4.00	0.08	0.08	0.07	0.54
[Tb.27] ⁻	4.44	4.13	0.07	0.49	0.44	---

(a) *Relative* fluorescence quantum yields, with that of [Tb.28]⁻ arbitrarily set to 1.00. The fluorescence of the phenyl groups in [Tb.27]⁻ is extremely weak.

Table 2.2 also shows the relative fluorescence quantum yields for the methoxybenzyl chromophore in the three terbium complexes. Their measurement relative to a standard is unreliable, owing to the very short wavelength of the emission ($\lambda_{max}^{em} = 298$ nm); consequently, only relative values are given, with the value for the *ortho* compound arbitrarily set to 1.00. The *ortho* and *meta* isomers are seen to display similar fluorescence intensities; that of the *para*-substituted complex is again somewhat lower. The most informative point as far as the fluorescence is concerned is the close similarity in ϕ_{fl} for the terbium and gadolinium complexes of the ligands. Bearing in mind that the observed gadolinium emission was extremely weak, indicating almost negligible energy transfer from the singlet state of the chromophore to the metal, this observation indicates that the intense metal luminescence observed for the terbium complexes is unlikely to arise from energy transfer from the singlet state of the methoxybenzyl group. If this were the case, then ϕ_{fl} for the terbium complex would be expected to be substantially lower than that of the gadolinium analogue. Clearly this is



persuasive evidence for the involvement of the triplet state in the energy transfer process.

2.11 Accounting for the high luminescence quantum yields

Bearing in mind the extraordinarily high luminescence quantum yields measured for the terbium complexes of the benzyl and methoxybenzylphosphinate ligands (27 - 30), it is appropriate to attempt to provide some explanation for the high luminescence efficiencies and also for the very weak emission common to all of the europium complexes discussed so far.

The low emissive quantum yields of the europium complexes probably reflect the occurrence of photoinduced electron transfer (PET) from the excited state of the chromophore (the benzyl or methoxybenzyl groups) to the metal. Of course, such a process will provide an additional deactivation pathway for the aryl excited state, thereby reducing the proportion of the absorbed energy which may reach the metal through the slower process of energy transfer. Photoinduced electron transfer is favoured here owing to the relative ease of reduction of Eu^{3+} to Eu^{2+} . Indeed, Abusaleh and Meares have examined the Eu^{3+} complexes of benzyl and methoxybenzyl substituted EDTA and encountered a similar problem.⁴³ They estimated the free energy change for photoinduced electron transfer to be -140 kJ mol^{-1} and -88 kJ mol^{-1} for methoxybenzyl and benzyl substituents respectively. In some other cases, for example the europium cryptates alluded to in section 1.7.1,⁴⁰⁻⁴¹ low emissive quantum yields have been ascribed to the presence of LMCT states which are apparent in the absorbance spectrum. Competitive absorption into these states does not lead to Eu^{3+} emission and so such bands do not appear in the metal excitation spectrum. In the present instance, the equivalence of the excitation and absorbance spectra of the europium complexes (sections 2.7.3 and 2.10) implies that no CT states are present over the wavelengths examined. LMCT differs from PET in that the charge transfer occurs from an immediate neighbour (eg. a bound N atom) to the metal *during* light absorption and hence appears in the absorbance spectrum.

Clearly one factor contributing to the high terbium quantum yields is the long lifetime of the emission. This in turn reflects the efficient shielding of the metal by the ligand from the solvent water molecules and minimal deactivation of the emissive state through other non-radiative deactivation pathways. The emissive quantum yield for a lanthanide complex is also dependent on two other variables, namely the efficiency of formation of the energy level of the antenna from which energy transfer occurs, ϕ_T , and the efficiency of the energy transfer process itself, η_{et} . The importance of these quantities is apparent from equation 12 in Chapter 1 (section 1.6.5):

$$\phi_{em} = \phi_T \cdot \eta_{et} \cdot k^0 \cdot \tau_{obs} \quad (12)$$

Here, k^0 is the natural radiative rate constant of the metal. Bearing in mind that the energy levels of a lanthanide ion which are derived from an f^n configuration are largely unperturbed by the ligand, k^0 would not be expected to show very significant variations between one complex and another.

This leaves the quantities ϕ_T and η_{et} . The majority of the photophysical studies which have been carried out on luminescent lanthanide complexes to date have concluded that the energy transfer process occurs from the triplet state of the antenna, probably owing to its inherently longer lifetime compared to the singlet (section 1.3.4). Indeed, flash photolysis studies carried out during this work with naphthalene as the antenna, as described in Chapter 4, have also shown clearly the involvement of the triplet. The quantum yields of formation of the triplet states of the four ligands would be very difficult to measure. However, some idea of their values may be obtained by considering some model compounds. Thus, toluene is probably a suitable model for the antenna in **27**, whilst methoxybenzene may be a reasonable approximation for the antennae in **28** - **30**. The literature quantum yields of formation of the triplet states of toluene and methoxybenzene are 0.45 and 0.64 respectively.⁴⁴ These values are high. If anything, the analogous values in the lanthanide complexes would be expected to be higher still, owing to the large spin-orbit coupling constants for the lanthanide ions

which may enhance the rate of singlet-triplet inter-system crossing in the nearby chromophore. Moreover, the literature values for the model compounds were obtained in non-polar, benzenoid solvents. For many systems, ϕ_T values are higher in polar solvents than in non-polar solvents and so it is possible that the values in the complexes will be further enhanced when in aqueous solution. With these points in mind, it is clear that the ϕ_T values are likely to be high, representing an important contribution to the high metal luminescence quantum yields observed.

Finally, it is necessary to consider the remaining parameter, namely the efficiency of the energy transfer process. Two limiting theories for the mechanism of energy transfer processes in general have been put forward. These are discussed in turn below, together with their potential applicability to luminescent lanthanide complexes.

Förster's theory describes the energy transfer in terms of a purely electrostatic interaction between the donor and the acceptor.⁴⁵⁻⁴⁶ A useful starting point for this theory is to consider the 'trivial' case of radiative electronic energy transfer whereby emission of a quantum of light by one molecule is followed by absorption of the emitted photon by a second molecule. Here, the rate of energy transfer will depend on the emissive quantum yield of the donor, the concentration of the acceptor, the light-absorbing ability of the acceptor and the overlap of the emission spectrum of the donor with the absorption spectrum of the acceptor. This last factor may be quantitated in terms of a spectral overlap integral J :

$$J = \int I_D(\nu) \cdot \epsilon_A(\nu) \cdot d\nu \quad (36)$$

where I_D is a graph of the experimental emission of the donor and ϵ_A a graph of the experimental absorption spectrum of the acceptor.

This radiative form of energy transfer does not apply to intramolecular energy transfer or, usually, to intermolecular transfer, because the distances over which the energy transfer occurs are much shorter than the wavelength of the light involved. In the Coulombic (Förster) mechanism of energy transfer, an electronically excited molecule is regarded as producing an oscillating electric field analogous to that associated with a photon of light. For light absorption to give rise to excitation of a molecule A to an excited state A*, the resonance condition $\Delta E(A \rightarrow A^*) = h\nu$ must be fulfilled and coupling of the electrons of A with the oscillating electric field of the light wave occurs. In the case of Coulombic energy transfer, the resonance condition is $\Delta E(D^* \rightarrow D) = \Delta E(A \rightarrow A^*)$ and the coupling occurs between the excited electron of the donor D* and the electrons of ground state A. As such, the mechanism is a purely through-space effect, which does not require orbital overlap of the donor and the acceptor.

Förster has shown that the rate of energy transfer by such a dipole-dipole mechanism is given by:

$$k_{ET} = C \cdot \frac{\kappa^2 \cdot k_D^0}{R_{DA}^6} \cdot J(\epsilon_A) \quad (37)$$

Here, C is a constant which includes, for example, the refractive index of the medium, and κ^2 reflects the dependence of the interaction of two dipoles on their relative orientation in space and has a value of 2/3 for a random distribution of interacting dipoles. k_D^0 is the natural radiative rate of the donor and R_{DA} is the separation of donor and acceptor. The term $J(\epsilon_A)$ is a spectral overlap integral similar to that defined in equation (36) and incorporating the extinction coefficient of the acceptor in the integration. Experimentally, the efficiency of energy transfer, rather than the rate constant, is measured. It is usual to define a critical separation, R_0 , at which the rate of energy transfer is equal to the sum of the rates of all other processes deactivating the excited state of the donor. In other words, R_0 is the distance for 50% energy transfer. Under these conditions, the experimentally observed efficiency of energy transfer is related to R_0 through equation (38).

$$\eta_{\text{et}} = [1 + (r/R_0)^6]^{-1} \quad (38)$$

It is clear from the preceding discussion that the Förster energy transfer efficiency will be favoured by high dipole oscillator strengths for the two transitions, $D^* \rightarrow D$ and $A \rightarrow A^*$ (in other words where k_D^0 and ϵ_A are high). If one or both of the transitions is spin-forbidden, then the efficiency of energy transfer would be expected to be much lower. This, of course, is the situation for ligand triplet-sensitised lanthanide emission, where both the donor transition [$D^*(T) \rightarrow D(S)$] and the acceptor transition (${}^7F_J \rightarrow {}^5D_J$) are both formally spin-forbidden. However, the presence of the heavy lanthanide ion and its high spin-orbit coupling constant leads to a breakdown of such simple selection rules; S is not a good quantum number for lanthanide ions. Hence it is likely that a Förster mechanism may still be applicable in lanthanide complexes.

Extensive use of the Förster theory has been made in estimating distances between fluorescent donors and acceptors in large molecules.⁴⁸ The approach is to calculate R_0 from the theory, by using the fluorescence emission spectrum of the donor and the absorbance spectrum of the acceptor to calculate the spectral overlap integral J . When used in conjunction with the measured experimental energy transfer efficiency, this allows the donor-acceptor separation, R , to be evaluated. In most cases, strongly fluorescent donors and strongly absorbing acceptors have been used. Comparison with X-ray structural information, where available, has frequently shown that the method is quite reliable.

The replacement of calcium by terbium or europium in calcium-binding proteins such as parvalbumin has been mentioned in Chapter 1. Terbium emission sensitised by nearby aromatic amino acids is observed in these cases. Horrocks has attempted to apply Förster theory to these energy transfer processes and the evaluation of amino acid-metal distances.⁴⁹⁻⁵¹ Despite the reasonable agreement of the values obtained with those found from X-ray data, the approach seems to be flawed. For example, in

calculating the spectral overlap integral, the fluorescence emission spectrum of the tryptophan donor was used. This appears to ignore the conclusions of nearly all previous studies where terbium sensitisation was attributed to energy transfer from the *triplet* state. On this basis, it would surely be preferable to use the *phosphorescence* spectrum of the amino acid donor. Indeed, the authors themselves note that the introduction of terbium into the protein causes a negligible effect on the intensity of the tryptophan donor's fluorescence, which is evidence in itself that the terbium sensitisation is unlikely to be occurring from the singlet state of the amino acid. The absorbance spectrum of Tb^{3+} in the protein is clearly unobtainable and that of a model compound, $[\text{Tb.DTPA}]^{2-}$, had to be used in calculating J . The distances between the relevant amino acids and the metal were of the order of 10\AA , which is not so large as to completely preclude some Dexter (*vide infra*) contribution to the energy transfer (though this is probably unlikely). With these limitations in mind, it is quite possible that the good agreement with the X-ray results may be largely fortuitous.

The second mechanism of energy transfer is that of electron exchange, known as Dexter theory.⁵² This mechanism requires a significant overlap of the electron clouds of the two species (D^* and A); electron exchange may occur in the region of overlap. Roughly speaking, the rate of energy transfer by this mechanism is expected to fall off exponentially as the separation of donor and acceptor increases, since electron densities usually fall off exponentially as the distance between the electron and the nucleus is increased. Dexter has proposed that the rate of electron transfer, k_{ET} , by this mechanism is given by:

$$k_{\text{ET}} \propto J \cdot \exp(-2R_{\text{DA}}/L) \quad (39)$$

where R_{DA} is the donor-acceptor separation relative to the sum of their van der Waals radii L . J is a spectral overlap integral similar to that defined earlier (equation 36). However, in contrast to the overlap integral in the Förster theory, here J does not depend on the magnitude of ϵ_{A} . In other words, k_{ET} is predicted to be independent of the absorbance characteristics of A in this case. It is also independent of the dipole

oscillator strength for $D^* \rightarrow D$ and, from this point of view, it might be expected to be an important mechanism for luminescent lanthanide complexes. It is often stated that energy transfer by the Dexter mechanism becomes insignificant for donor-acceptor separations in excess of 5 - 10 Å. This is not necessarily true, however, as the effect may be transmitted through the several bonds. For example, a number of systems have been examined where the donor and acceptor groups are separated by rigid bridging groups of varying length, such as those based on norbornylogous or steroidal-type structures.⁵³⁻⁵⁴ In these cases, experiments have shown that the Dexter mechanism may apply over 20 bonds or more.

It is clear from the above discussions that it is far from simple to partition an observed energy transfer phenomenon into contributions from the two theoretical mechanisms. This is especially true when the donor-acceptor separation is small, as it is for [Tb.27] for example. Here, the X-ray structure of the yttrium analogue gives a value of 5.48 Å for the distance from the metal to the centre of the plane of each phenyl ring and 4.74 Å to the phenyl edge. This distance is too small to allow a Dexter mechanism to be completely ruled out, although it is worth remembering that the f orbitals of lanthanide ions do not have large radial extensions.

An independent method of assessing the likelihood of a Dexter contribution would be very useful. One possibility might be to consider whether or not there is a contact contribution to the lanthanide-induced proton or carbon shifts of the antenna group in the ^1H or ^{13}C NMR spectra. Contact shifts are determined by the f electron density of the lanthanide ion at the nucleus under observation, according to the hyperfine coupling constant, A (section 1.8.1). Dexter energy transfer is determined by the extent to which the f electron density overlaps with the molecular orbitals of the antenna. It is possible, therefore, that its magnitude may bear some reflection of the magnitude of the contact shift. Obviously it would be very difficult to prove whether or not there is any empirical relationship between these two quantities and there have been no attempts to do so. It is interesting to note, however, that there is apparently no contact contribution

to the shifts of the benzyl protons in the complexes of **27**, as discussed in section 2.6. It may not be completely unreasonable to infer from this that the Dexter contribution to the energy transfer is minimal.

In summary, it is clear that the mechanism of energy transfer is not easy to predict. Indeed, it is likely that in many cases, both mechanisms may contribute. Irrespective of the mechanism which is operative, however, the energy transfer will be dependent on a spectral overlap integral, J , and will therefore be favoured by a matching of the energy of the excited donor level with the excited state of the acceptor. On the other hand, in the case of luminescent lanthanide complexes, Sato and Wada (and others) have shown that if the energies are too close (but still corresponding to an exothermic forward energy transfer pathway) then a thermally-activated back energy transfer process becomes efficient, leading to a reduced quantum yield of emission⁵⁵ (see also Chapter 4).

Figure 2.23 shows the triplet energies of the model compounds, toluene and methoxybenzene, relative to the energy of the emissive 5D_4 state of terbium. It is clear that the energy gaps here are very large and so, at first sight, it seems surprising that the energy transfer in the complexes of **27-30** is so efficient (as it must be, in order to account for the high quantum yields). However, this ignores the fact that the terbium ion has other, higher excited electronic states to which energy transfer could occur. In particular, the 5D_3 level, with an energy of 313 kJ mol^{-1} (relative to the 7F_6 ground state), is well-matched with the triplet levels of toluene and methoxybenzene (346 and 338 kJ mol^{-1} respectively). The energy gaps are such that the forward energy transfer processes are exothermic. Once populated, the 5D_3 state will undergo rapid internal conversion and vibrational relaxation to the 5D_4 state. There have been few investigations into the role of the 5D_3 state in terbium luminescence, probably reflecting this high rate of deactivation to the 5D_4 . This is in contrast to europium, where emission from higher states ($^5D_{1,2,3}$) may be observed in the solid state.¹⁸

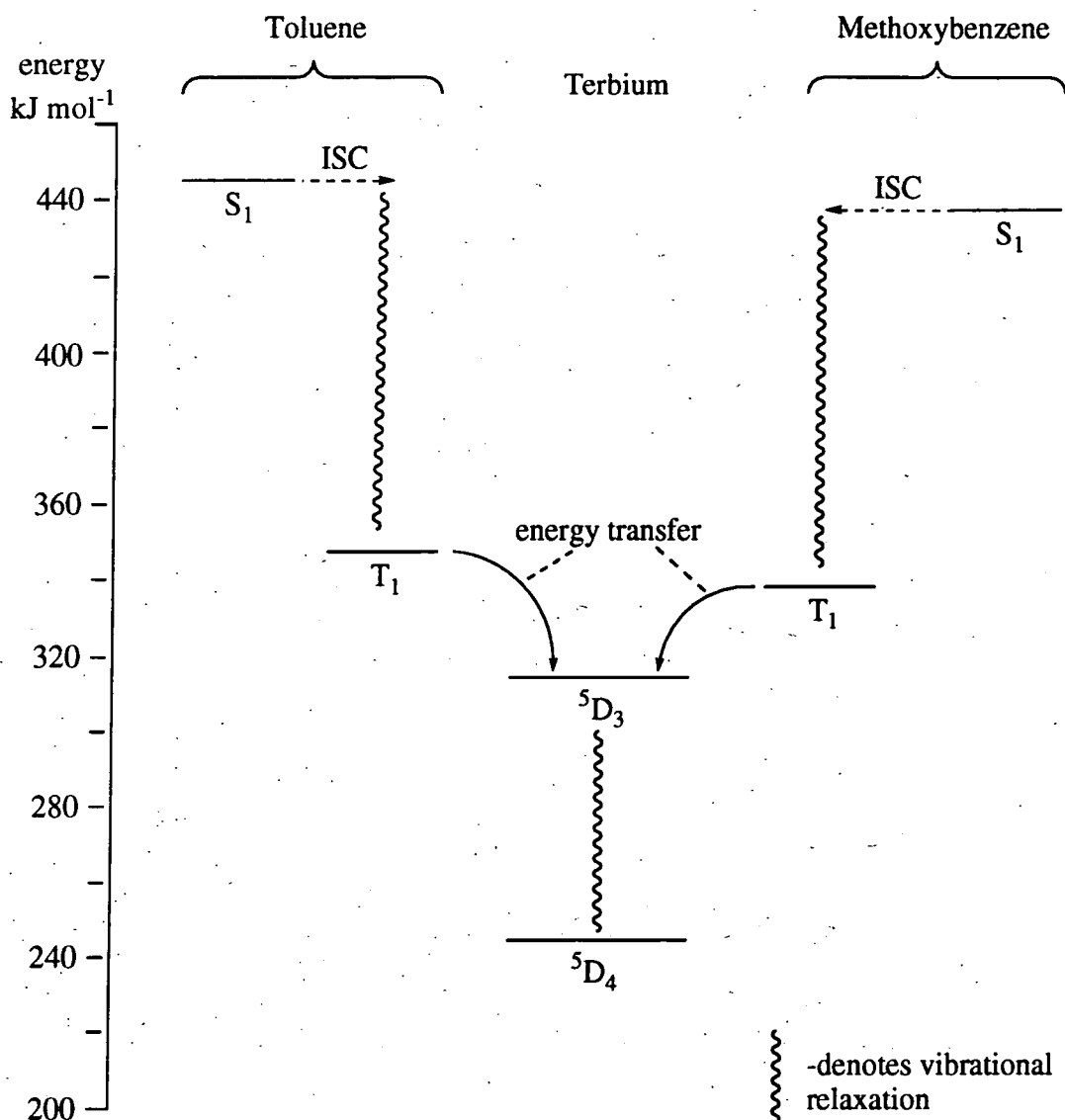


FIGURE 2.23 Showing the relative energies of the singlet and triplet levels of methoxybenzene and toluene and the 5D_4 and 5D_3 excited states of terbium. It is proposed that energy transfer occurs from the triplet level of the chromophore to the 5D_3 state of the metal, followed by rapid relaxation to the emissive 5D_4 state.

In conclusion, the high luminescence quantum yields observed for the terbium complexes arise from a combination of minimal non-radiative deactivation of the metal emissive state, a high quantum yield of formation of the triplet state of the antenna group and thirdly, an efficient energy transfer process favoured by the good match of donor and acceptor energy levels and the proximity of the antenna group to the metal.

References for Chapter 2

1. K. Pulukkody, T.J. Norman, D. Parker, L. Royle and C.J. Broan, *J. Chem. Soc., Perkin Trans. 2*, 1993, 605.
2. D. Parker, K. Pulukkody, T.J. Norman, A. Harrison, L. Royle and C. Walker, *J. Chem. Soc., Chem. Commun.*, 1992, 1441.
3. C.J. Broan, E. Cole, K.J. Jankowski, D. Parker, K. Pulukkody, B.A. Boyce, N.R.A. Beeley, K. Millar and A.T. Millican, *Synthesis*, 1992, 63.
4. A. Harrison, L. Royle, C. Walker, C. Pereira, D. Parker, K. Pulukkody and T.J. Norman, *Magn. Reson. Imaging*, 1993, **11**, 761.
5. S. Aime, A.S. Batsanov, M. Botta, J.A.K. Howard, D. Parker, K. Senanayake and G. Williams, *Inorg. Chem.*, 1994, **33**, 4696.
6. J. Dale, *Isr. J. Chem.*, 1980, **20**, 3.
7. M.-R. Spirlet, J. Rebizant, J.F. Desreux and M.-F. Loncin, *Inorg. Chem.*, 1984, **23**, 359.
8. D. Parker, K. Pulukkody, F.C. Smith, A. Batsanov and J.A.K. Howard, *J. Chem. Soc., Dalton Trans.*, 1994, 689. M.S. Konings, W.C. Dow, D.B. Love, K.N. Raymond, S.C. Quay and S.M. Rocklage, *Inorg. Chem.*, 1990, **29**, 1489.
9. A.G. Sharpe, 'Inorganic Chemistry', 2nd edition, Longman: Harlow, 1986.
10. S. Aime, M. Botta and G. Ermondi, *Inorg. Chem.*, 1992, **31**, 4291.
11. A.D. Sherry and C.F.G.C. Geraldès in 'Lanthanide Probes in Life, Chemical and Earth Sciences', eds: J.-C.G. Bünzli and G.R. Choppin, Elsevier: Amsterdam, 1989. Chapter 4.
12. C.D. Barry, J.A. Glasel, A.C.T. North, R.J.P. Williams and A.V. Xavier, *Nature*, 1971, **232**, 236.
13. C.M. Dobson, R.J.P. Williams and A.V. Xavier, *J. Chem. Soc., Dalton Trans.*, 1973, 2662.
14. C.N. Reilley, B.W. Good and R.D. Allendoerfer, *Anal. Chem.*, 1976, **48**, 1446.
15. W.B. Lewis, J.A. Jackson, J.F. Lemons and H. Taube, *J. Chem. Phys.*, 1962, **36**, 694.

16. H. Donato, Jr. and R.B. Martin, *J. Am. Chem. Soc.*, 1972, **94**, 4129.
17. J.A. Peters, *J. Magn. Reson.*, 1986, **68**, 240.
18. J.-C.G. Bünzli in 'Lanthanide Probes in Life, Chemical and Earth Sciences', eds: J.-C.G Bünzli and G.R. Choppin, Elsevier: Amsterdam, 1989. Chapter 7.
19. J.-C.G. Bünzli and A. Giorgetti, *Inorg. Chim. Acta.*, 1985, **110**, 225.
20. D. Harrison, A. Giorgetti and J.-C.G. Bünzli, *J. Chem. Soc., Dalton Trans.*, 1985, 885.
21. M. Albin and W. DeW. Horrocks, Jr., *Inorg. Chem.*, 1985, **24**, 895.
22. W. DeW. Horrocks, Jr. and D.R. Sudnick, *Acc. Chem. Res.*, 1981, **14**, 384.
23. M.C. Alpoim, A.M. Urbano, C.F.G.C. Geraldés and J.A. Peters, *J. Chem. Soc., Dalton Trans.*, 1992, 463.
24. A.D. Sherry, R.D. Brown, C.F.G.C. Geraldés, S.H. Koenig, K.-T. Kuan and M. Spiller, *Inorg. Chem.*, 1989, **28**, 620.
25. S. Aime, M. Botta, G. Ermondi, F. Fedeli and F. Uggeri, *Inorg. Chem.*, 1992, **31**, 1100.
26. S. Aime, P.L. Anelli, M. Botta, F. Fedeli, M. Grandi, P. Paoli and F. Uggeri, *Inorg. Chem.*, 1992, **31**, 2422.
27. M.F. Tweedle in 'Lanthanide Probes in Life, Chemical and Earth Sciences', eds: J.-C.G Bünzli and G.R. Choppin, Elsevier: Amsterdam, 1989. Chapter 5.
28. R.B. Lauffer, *Chem. Rev.*, 1987, **87**, 901.
29. F.S. Richardson and J.P. Riehl, *Chem. Rev.*, 1977, **77**, 1773.
30. H.G. Brittain in 'Lanthanide Probes in Life, Chemical and Earth Sciences', eds: J.-C.G Bünzli and G.R. Choppin, Elsevier: Amsterdam, 1989. Chapter 8.
31. H.G. Brittain, *Photochem. Photobiol.*, 1987, **46**, 1027.
32. B. Douglas, D.H. McDaniel and J.J. Alexander, 'Concepts and Models of Inorganic Chemistry', 2nd edition, John Wiley and Sons: New York, 1983. Chapter 8.
33. H.G. Brittain, *Coord. Chem. Rev.*, 1979, **28**, 213.
34. J.P. Riehl and F.S. Richardson, *Chem. Rev.*, 1986, **86**, 1.

-
35. G. Hilmes, H.G. Brittain and F.S. Richardson, *Inorg. Chem.*, 1977, **16**, 528.
 36. A.F. Gafni and I.Z. Steinberg, *Isr. J. Chem.*, 1977, **15**, 102.
 37. P.M.L. Blok, P.S. Cartwright, H.P.J.M. Dekkers and R.D. Gillard, *J. Chem. Soc., Chem. Commun.*, 1987, 1232.
 38. P.M.L. Blok and H.P.J.M. Dekkers, *Appl. Spectrosc.*, 1990, **44**, 305.
 39. J.P. Riehl and F.S. Richardson, *Methods Enzymol.*, 1993, **226**, 539.
 40. B. Alpha, R. Ballardini, V. Balzani, J.-M. Lehn, S. Perathoner and N. Sabbatini, *Photochem. Photobiol.*, 1990, **52**, 299.
 41. N. Sabbatini, M. Guardigli and J.-M. Lehn, *Coord. Chem. Rev.*, 1993, **123**, 201.
 42. W.T. Carnall, 'The Absorption and Fluorescence Spectra of Rare Earth Ions in Solution', in 'Handbook on the Physics and Chemistry of Rare Earths', eds: K.A. Gschneider, Jr. and L. Eyring, North-Holland Publishing Company, 1979.
 43. A. Abusaleh and C. Meares, *Photochem. Photobiol.*, 1984, **39**, 763.
 44. I. Carmichael and G.L. Hug in 'CRC Handbook of Organic Photochemistry', Volume I, ed. J.C. Scaiano, CRC Press Inc., Boca Raton, Florida, 1989. Chapter 16.
 45. N.J. Turro, 'Modern Molecular Photochemistry', University Science Books: Mill Valley, California, 1991. Chapter 9.
 46. J.B. Birks, 'Photophysics of Aromatic Molecules', John Wiley: New York, 1970. Chapter 11.
 47. F. Scandola and V. Balzani, *J. Chem. Educ.*, 1983, **60**, 814.
 48. L. Stryer, *Annu. Rev. Biochem.*, 1978, **47**, 819.
C.F. Meares and T.G. Wensel, *Acc. Chem. Res.*, 1984, **17**, 202.
 49. W. DeW. Horrocks, Jr. and W.E. Collier, *J. Am. Chem. Soc.*, 1981, **103**, 2856.
 50. J. Bruno, W. DeW. Horrocks, Jr. and R.J. Zauhar, *Biochemistry*, 1992, **31**, 7016.

-
51. W. DeW. Horrocks, Jr. and D.R. Sudnick, *Acc. Chem. Res.*, 1981, **14**, 384.
 52. D.L. Dexter, *J. Chem. Phys.*, 1953, **21**, 836.
 53. Norbornylogous bridges: H. Oevring, J.W. Verhoeven, M.N. Paddon-Row, E. Cotsaris and N.S. Hush, *Chem. Phys. Lett.*, 1988, **143**, 488. *Idem, ibid.*, 1988, **150**, 179.
 54. Steroid-type bridges: G.L. Closs, P. Piotrowiak, J.M. McInnis and G.R. Fleming, *J. Am. Chem. Soc.*, 1988, **110**, 2657. G.L. Closs, M.D. Johnson, J.R. Miller and P. Piotrowiak, *ibid.*, 1989, **111**, 3751.
 55. S. Sato and W. Wada, *Bull. Chem. Soc. Jpn.*, 1970, **43**, 1955.
 56. C.C. Bryden and C.N. Reilley, *Anal. Chem.*, 1982, **54**, 610.

Chapter 3

CHAPTER 3

Lanthanide Complexes of Tetraazamacrocyclic Ligands Incorporating One Carboxamide and Three Phosphinate Coordinating Arms

3.1 Introduction

The amide carbonyl oxygen is known to be an effective ligating group for cations of high charge density such as Ca^{2+} .¹⁻² Bearing in mind the similarity of the lanthanide ions to calcium as far as their coordination properties are concerned and their high charge densities, it is reasonable to expect that an amide group will be able to function as an efficient donor to a lanthanide ion. Some recent studies on polyazapolycarboxylic ligands containing one or more amide groups have shown this to be the case. Lanthanide complexes of high thermodynamic stability have been obtained, although it may be noted in passing that, in many cases, their kinetic stabilities are insufficient for use *in vivo* (eg. for magnetic resonance imaging purposes).³⁻⁵

The replacement of one of the phosphinate groups by an amide substituent in the tetrakisphosphinate structure of Figure 2.1 will provide a tribasic ligand, as shown in Figure 3.1. Here, binding of a trivalent lanthanide ion will give a charge-neutral complex. Provided that the amide carbonyl group does bind strongly to the metal ion, a neutral complex of this type may be expected to display some advantages over the anionic complexes of tetrakisphosphinate ligands. For example, acid-catalysed dissociation of the metal ion from the ligand is expected to be reduced in a charge-neutral complex compared to an anionic complex, on simple electrostatic grounds. In the case of the potential *in vivo* use of Gd^{3+} complexes in magnetic resonance imaging, a charge neutral complex may be advantageous in that it may be more readily transported into cells.⁶ Moreover, the introduction of an amide carbonyl group into the coordination environment of the metal might be expected to allow a water molecule to approach closer to the metal than in the tetrakisphosphinate complexes. Clearly, this should lead to an enhancement of the relaxivity of the Gd^{3+} complexes.

Some preliminary results on the yttrium complexes of ligands of the type illustrated in Figure 3.1 have shown that the *in vivo* stabilities of such complexes are indeed high, being comparable to those of [Y.DOTA]⁻⁶

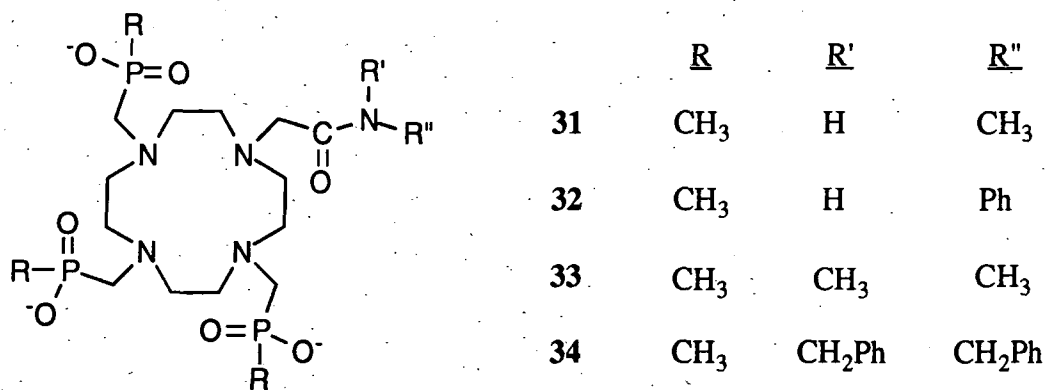
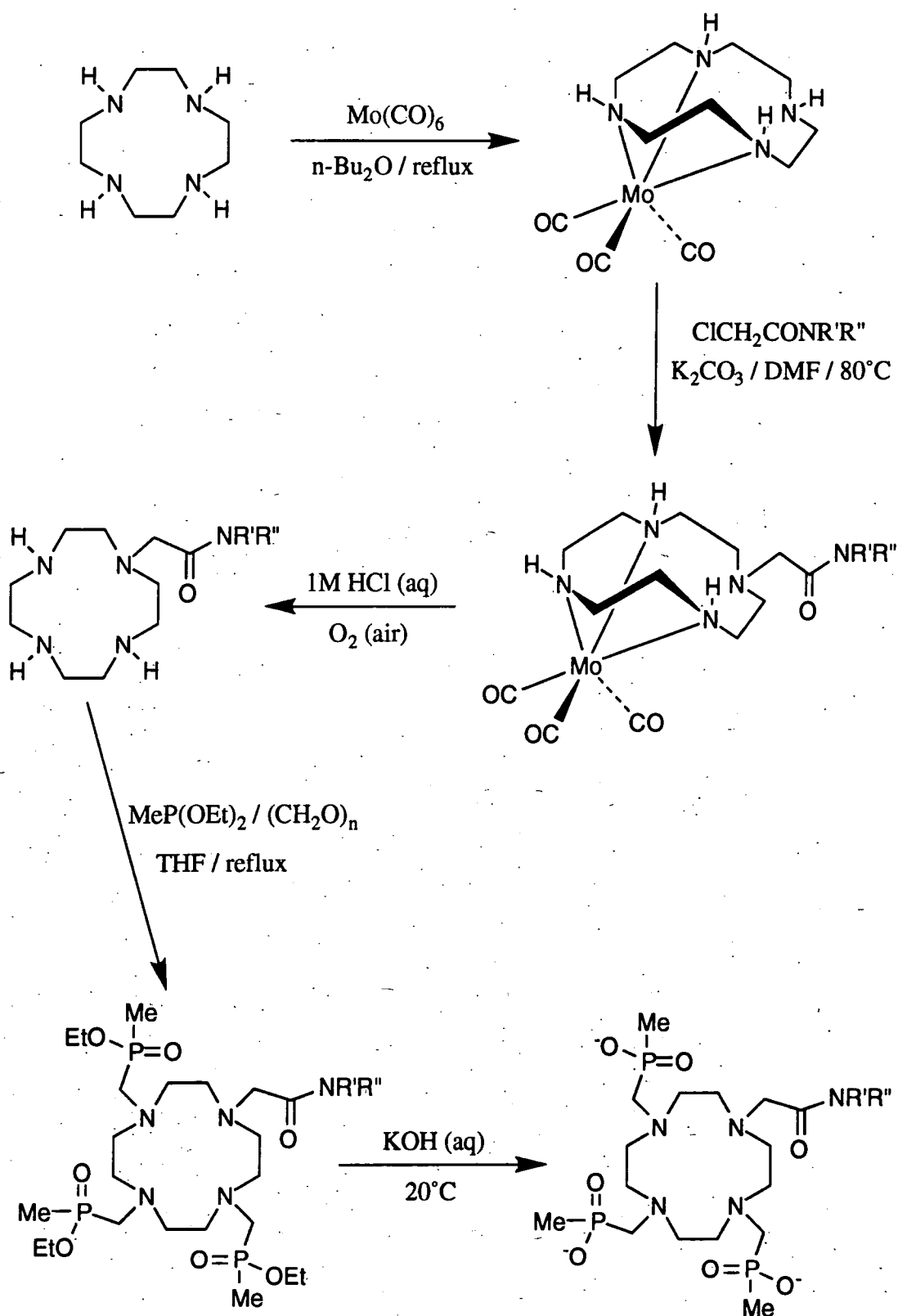


FIGURE 3.1 General structure of the amide-tris-phosphinate ligands discussed in this chapter

3.2 Synthesis of the Amide Ligands

In the past, the introduction of one substituent onto just one of the four equivalent nitrogen atoms of 12N₄ has been achieved through the use of a large excess of the cycle followed by a rather laborious purification procedure, often requiring extensive use of preparative HPLC.⁵ A preferable approach is to make use of a protection procedure. The method which has been employed in this work entails the use of the molybdenum tricarbonyl complex of 12N₄, in which three of the four ring nitrogen atoms of the cycle are bound to the molybdenum in an octahedral complex (Scheme 3.1) leaving the fourth free to react. Other members of the Durham group have found this approach to be preferable to the use of the analogous tricarbonyl-chromium complex which had been reported previously.⁷

The [Mo(CO)₃.12N₄] complex was readily prepared from the cycle by reaction with Mo(CO)₆ in n-butyl ether under argon at 140°C, in quantitative yield. Alkylation of the free ring nitrogen with the appropriate chloro- or bromo-amide was carried out under argon in dimethylformamide, with potassium carbonate as the base. Removal of the



SCHEME 3.1 The synthetic procedure used in the preparation of ligands 31 - 34.

Mo(CO)₃ protecting group was accomplished by vigorous stirring in aqueous HCl (1M), in contact with air, allowing the isolation of the monofunctionalised cycles in high yields (Scheme 3.1). Subsequent reaction with paraformaldehyde and diethoxy(methyl)phosphine, as described in Chapter 2, led to the amide-triesters. Selective hydrolysis of the phosphinate esters was achieved on treatment with aqueous potassium hydroxide at room temperature, leaving the amide group intact.

3.3 Complex formation

The preparation of the lanthanide complexes of the amide ligands was carried out in a similar manner to that outlined for the tetraphosphinate ligands in Chapter 2. In this case, however, attempts to crystallise the complexes have not proved successful. Fortunately, purification of these neutral complexes is straightforward through the use of alumina column chromatography.

The amide ligands **31** - **34** (Figure 3.1) have been prepared during the course of this work using the method described above. The europium and terbium complexes have been isolated in each case, together with the ytterbium complexes of **32** - **34** and the gadolinium complex of **32**.

3.4 Solution NMR Studies

3.4.1 Introduction

High-resolution ¹H, ¹³C and ³¹P spectroscopy has been performed on the europium and ytterbium complexes of ligands **32** - **34** in aqueous solution. This work has been carried out in collaboration with Professor Silvio Aime and Dr. Mauro Botta at the University of Turin. The results on the complexes of the N,N-dimethyl amide ligand **33** are discussed in subsequent discussions. The corresponding spectra of the complexes of the other ligands are all very similar (other than the expected differences arising from the change of the substituents on the amide functionality).

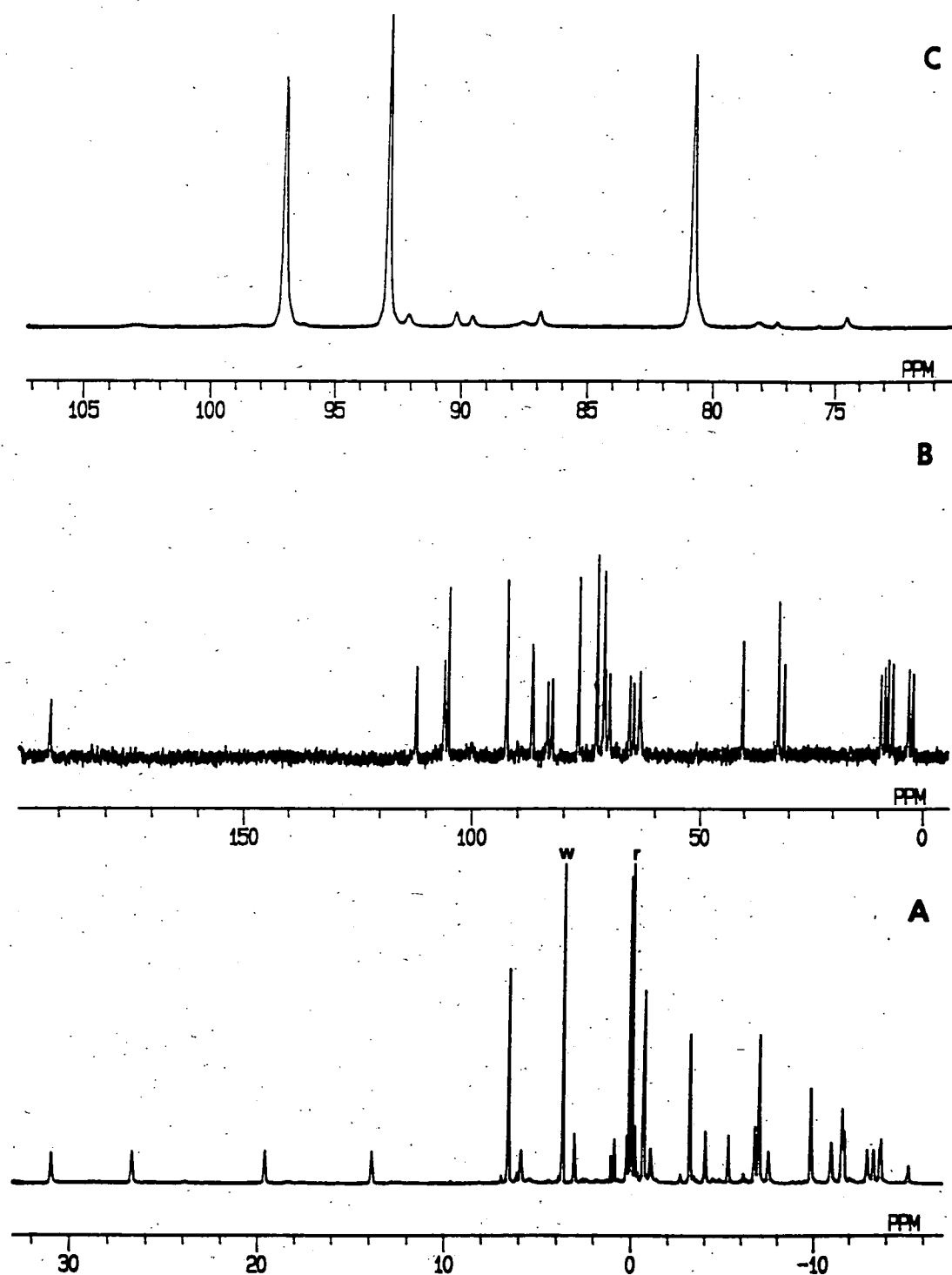


FIGURE 3.2 The ¹H (A), ¹³C{¹H} (B) and ³¹P{¹H} (C) NMR spectra of [Eu.33] (D₂O, 298K, 9.4 T). The labels w and r refer to the solvent and ¹BuOH (1% internal reference) peaks respectively.

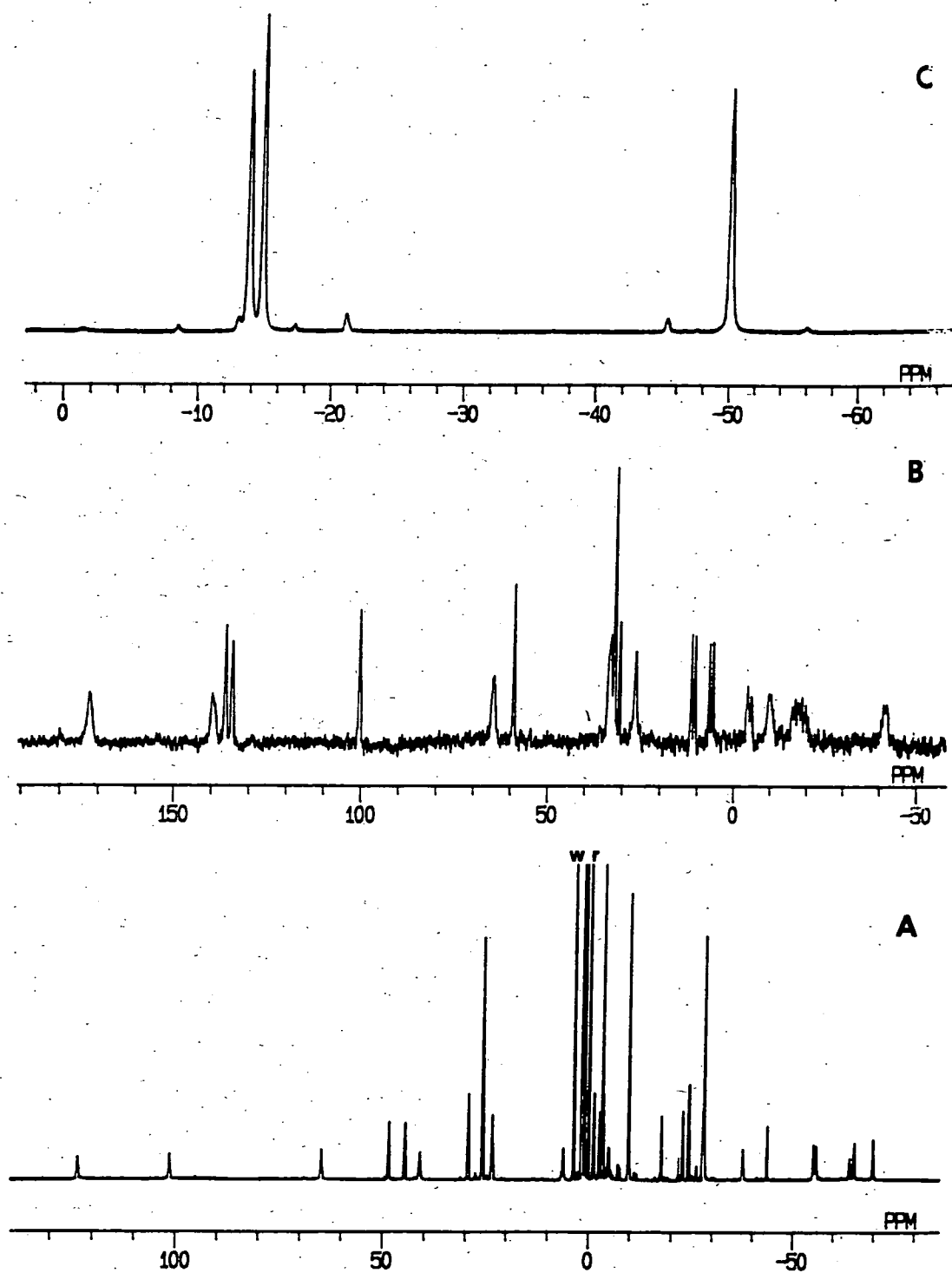


FIGURE 3.3 The ^1H (A), $^{13}\text{C}\{^1\text{H}\}$ (B) and $^{31}\text{P}\{^1\text{H}\}$ (C) NMR spectra of [Yb.33] (D_2O , 298K, 9.4 T). Labels as in Figure 3.2.

The ^1H , ^{13}C and ^{31}P spectra of the europium and ytterbium complexes of **33** are shown in Figures 3.2 and 3.3. The ^{31}P spectra of the complexes show one main set of three, equally intense resonances, which suggests that there is one predominant isomer in solution, with three non-equivalent phosphorus nuclei. Twelve peaks of much lower intensity are just visible in the spectrum of the europium complex, suggesting that at least four other isomers may be present in small proportions.

3.4.2 Structural possibilities

In attempting to understand the experimental information, it is useful to consider the possible structural geometries which are potentially accessible to the complexes. The discussion of the tetraphosphinate structures in Chapter 2 is a useful starting point for this purpose. Again, four possible structural models exist (Figure 3.4), corresponding to the square antiprismatic and inverted square antiprismatic geometries observed for DOTA complexes (Figure 2.5). For each of these four structural types, there are 8 possible stereoisomers arising from the 8 possible permutations of the phosphorus centres (RRR, RRS, RSR etc.). This gives rise to a total of 32 distinct structures available to the complexes. As before, an isomer of type A (Figure 3.4) with phosphorus configurations RRR is enantiomeric with the isomer having a D-type structure and the opposite configurations at phosphorus, namely SSS, and so on. Thus, the 32 possibilities comprise of 16 enantiomeric pairs. The situation is thus analogous to the case of the tetraphosphinates.

The relationships between the 32 possibilities are illustrated schematically in Figure 3.6. Here, the structures are arranged into 8 groups, numbered according to the 8 possible permutations of the configurations at phosphorus. Each group consists of 4 isomers corresponding to the 4 DOTA-like structural models A - D. A schematic illustration of the structures of the 16 diastereoisomers of groups 1 - 4 is provided in Figure 3.5 arranged according to the coordination geometries A, B, C and D.

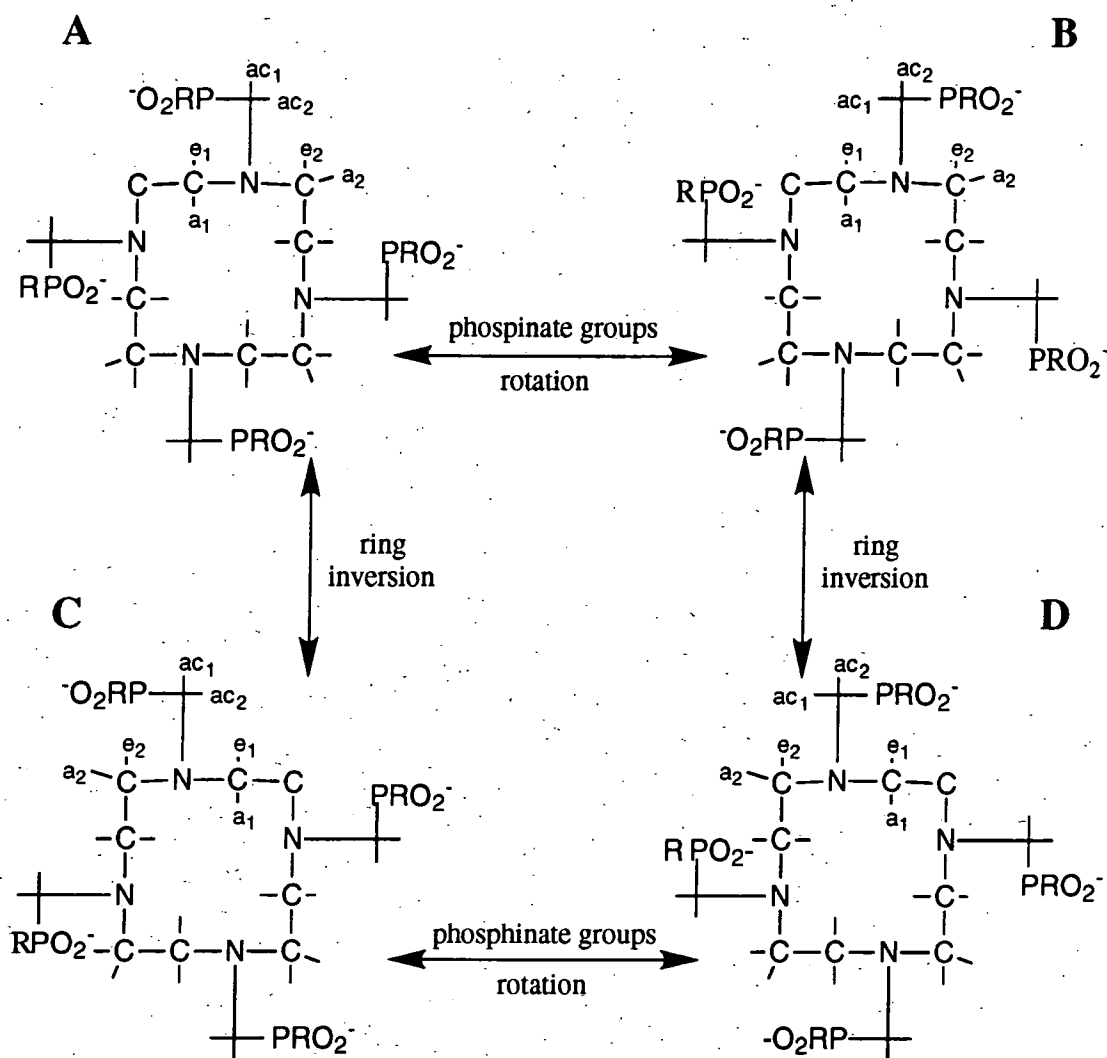


FIGURE 3.4 Schematic representation of the two distinct coordination geometries which are accessible, in theory, to the complexes of 31 - 34. The stereochemistry at phosphorus is not defined here.

It is apparent from the ^{31}P NMR spectra that only one pair of enantiomers predominates (indistinguishable by NMR), which is similar to the conclusion reached for the tetraphosphinates in Chapter 2. In the latter case, however, there was no evidence for the presence of any minor isomers in the ^{31}P spectra of the europium and ytterbium complexes (although some additional peaks were observed in the yttrium complex). In the present instance, small proportions of other isomers are evident and this could reflect a less stringent steric effect disfavouring other geometries, on passing to a system where one of the four relatively bulky phosphinate groups has been replaced by an amide. This may also account for the difference in behaviour of the two systems at

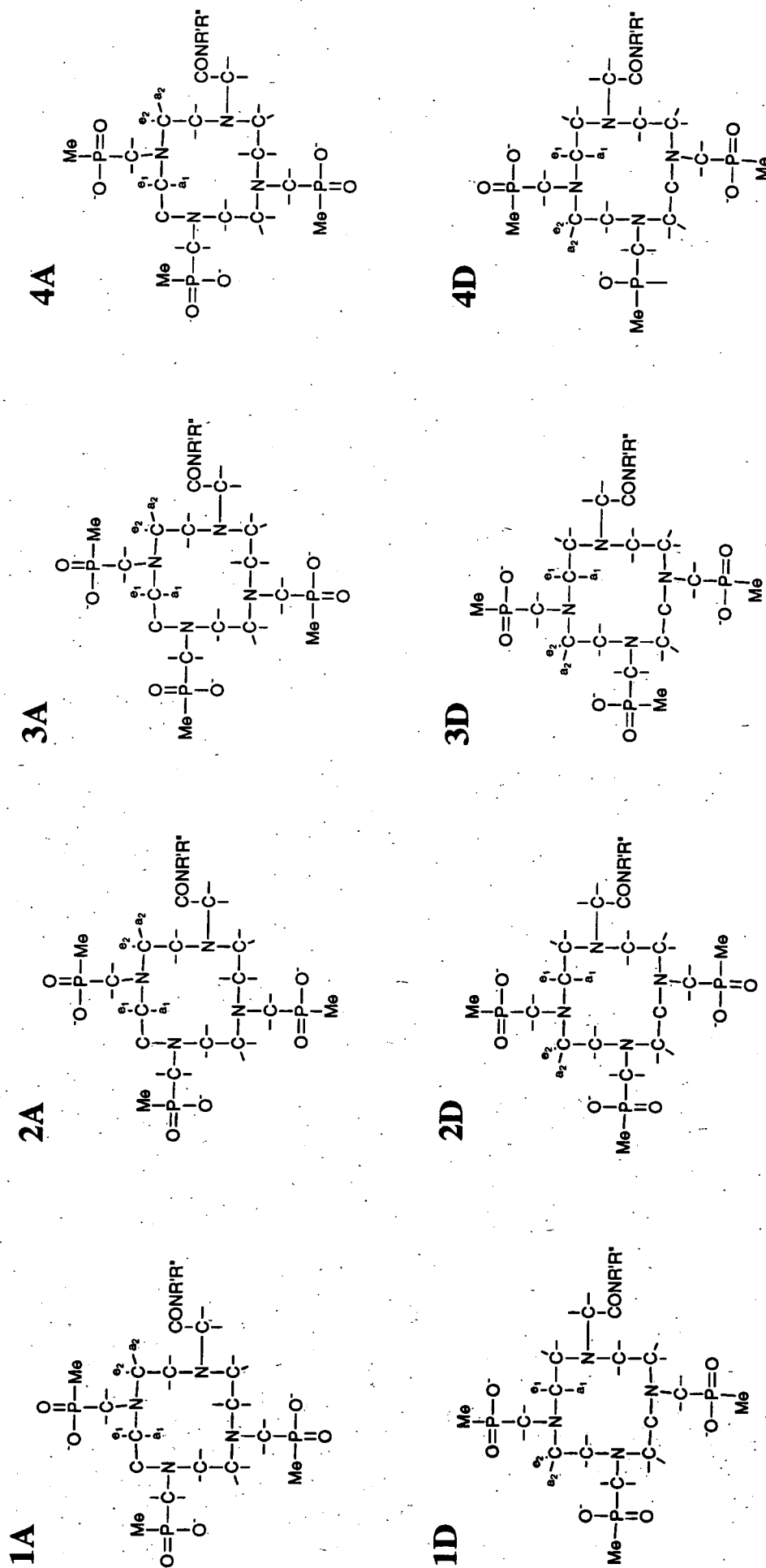


FIGURE 3.5 (a) Schematic representation of the four distinct stereoisomers characterised by an A-type structural model (upper) and by a D-type model (lower)

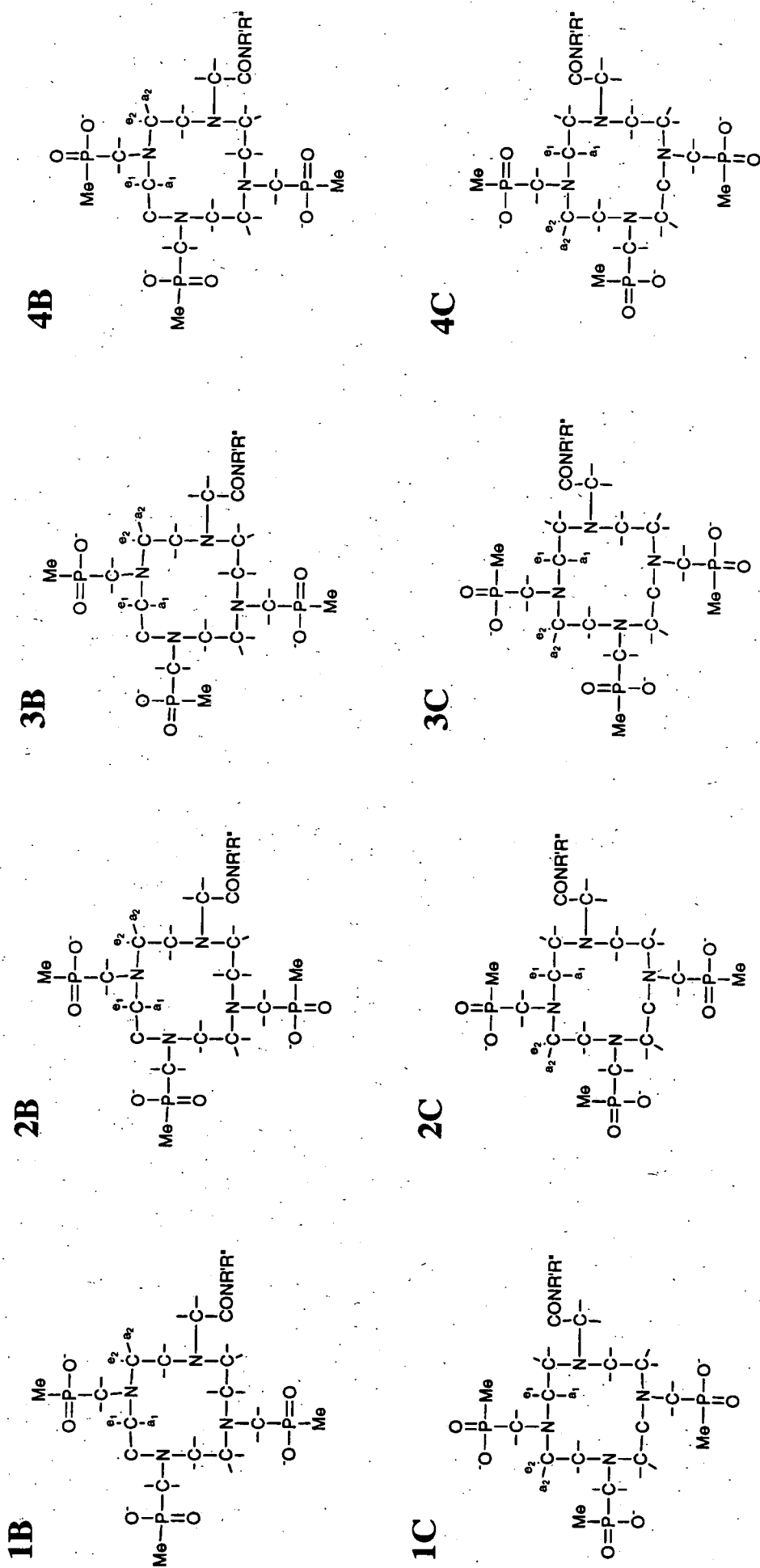


FIGURE 3.5 (b) Schematic representation of the four distinct stereoisomers characterised by a B-type structural model (upper) and by a C-type model (lower)

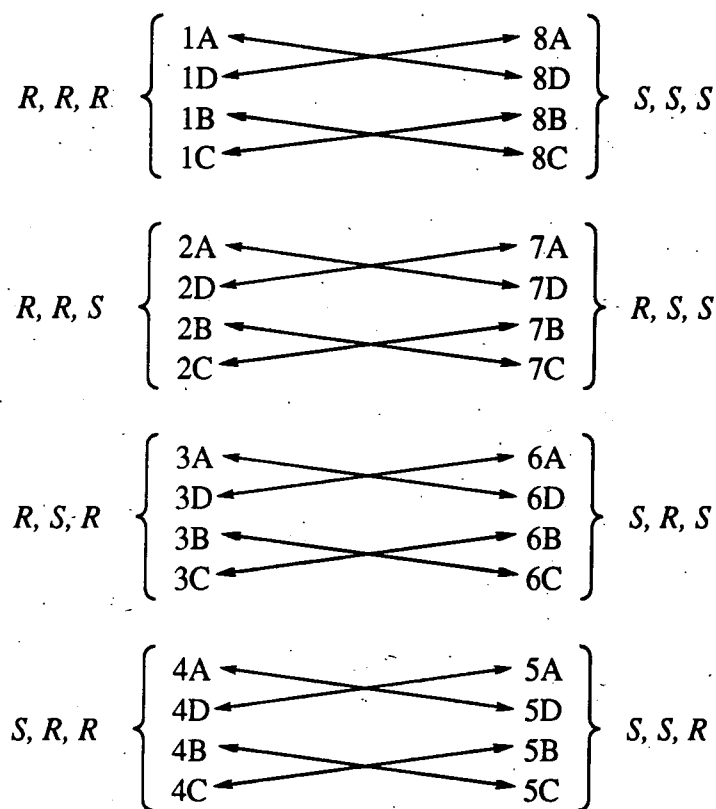


FIGURE 3.6 Symbolic representation of the 32 possible stereoisomers for the lanthanide complexes of 31 - 34. Arrows connect enantiomeric pairs.

elevated temperatures. The variable temperature ^1H and ^{31}P NMR spectra of the amide complexes indicate that an exchange process involving the different isomers takes place over the range 20 - 90°C. Bearing in mind the kinetic inertness of lanthanide-oxygen bonds which has been observed in structurally-related systems to date,⁸ it seems likely that this exchange process occurs through a 'sliding motion' of the phosphinate and amide arms or through an inversion of the tetraaza ring with the pendent arms held fixed in their positions. In contrast to this observation, the spectra of the complexes of the tetrabenzylphosphinate (27) were unchanged over the same temperature range which implies that the activation energies to such motions are too high in this case.

Unfortunately, no structural conclusions can be drawn from the ^1H and ^{13}C spectra as to the identity of the predominant isomer. However, on steric grounds alone, one might suspect the enantiomeric pairs 1D/8A and 1B/8C (Figure 3.5) to be the most favoured

possibilities since in these structures, all of the P-methyl groups are directed away from the coordination cage. By analogy with the tetrphosphinates discussed in Chapter 2, it also seems probable that the inverted square antiprism will be favoured over the alternative square antiprismatic structure. Thus, the enantiomeric pair 1B/8C is likely to be the predominant form.

3.4.3 Partial Assignment of the Europium Spectra

The 4-fold axial symmetry of the complexes of DOTA and the tetrphosphinates leads to relatively simple ^1H and ^{13}C spectra. In contrast, the lack of axial symmetry in the amide complexes leads to much more complicated spectra. However, a partial assignment of the proton and carbon NMR spectra of the europium complex has been achieved, thanks to the limited line-broadening induced by europium, coupled with the expanded chemical shift range. The coupling pattern is clearly detectable at low magnetic field (2.11 T or 90 MHz), as shown in Figure 3.7, and a ^1H - ^1H COSY has been recorded (Figure 3.8). As explained in Chapter 2, the axial protons of the ring are expected to appear as triplets (due to coupling to the geminal equatorial proton and to the vicinal axial proton) whereas the equatorial protons couple only to the geminal axial proton and should therefore be doublets. Eight triplets are indeed detected, attributable to the eight non-equivalent axial protons of the ring. These having been identified, the COSY spectrum allows the doublets arising from the eight equatorial protons to be assigned. Three doublets of relative intensity 3 are clearly visible, corresponding to the phosphinate methyl groups in which coupling to phosphorus occurs. Two singlets of relative intensity 3 are also observed; these are due to the N-methyl groups of the amide. This leaves four pairs of mutually-coupled multiplets which are due to the NCH_2P and NCH_2CO protons. A heteronuclear ^{13}C - ^1H COSY experiment was also recorded, allowing the assignment of the carbon resonances, as shown in Figure 3.7.

Comparison of the ^1H spectra in Figures 3.7 and 3.2 clearly shows the adverse effect of using stronger magnetic fields in the acquisition of NMR spectra of lanthanide complexes. Thus, at 400 MHz, most of the ^1H signals appear only as singlets. This, of

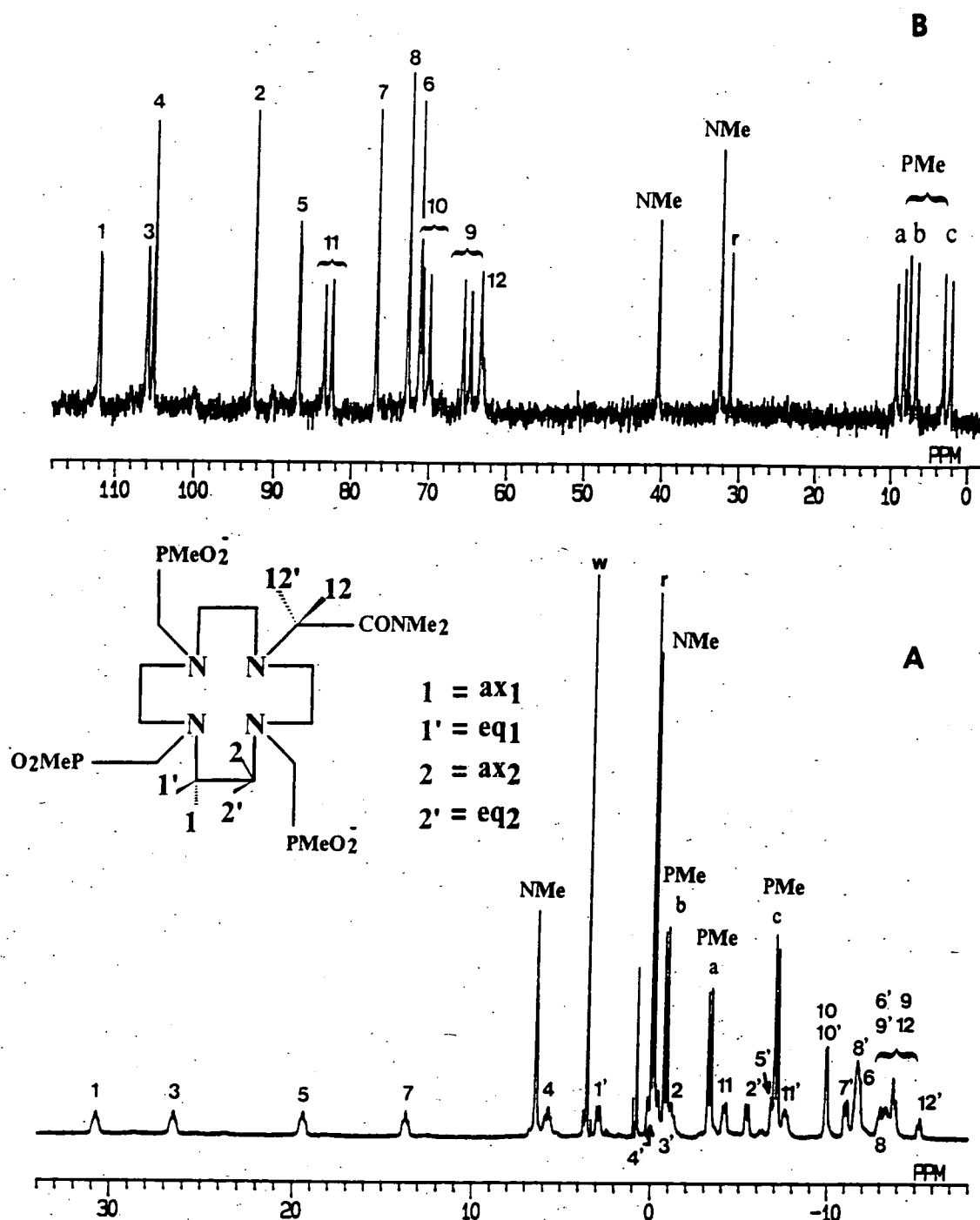


FIGURE 3.7 The 90 MHz ^1H (a) and 100.6 MHz $^{13}\text{C}\{^1\text{H}\}$ (b) NMR spectra (298K, D_2O) of [Eu.33] with partial assignment of the resonances. In (a) the primed numbers indicate equatorial hydrogen atoms, unprimed numbers axial hydrogen atoms. In (b), only the region of the protonated carbon atoms is shown. Peaks 1-8 and 9-11 correspond to the macrocyclic and to the methylenephosphinic carbon atoms or protons respectively. Assignment to a specific ethylenediamine unit is not possible. The resonances labelled with w and r refer to the solvent and $^1\text{BuOH}$ ($\delta_{\text{H}} = 0$, $\delta_{\text{C}} = 31.3$ ppm), respectively.

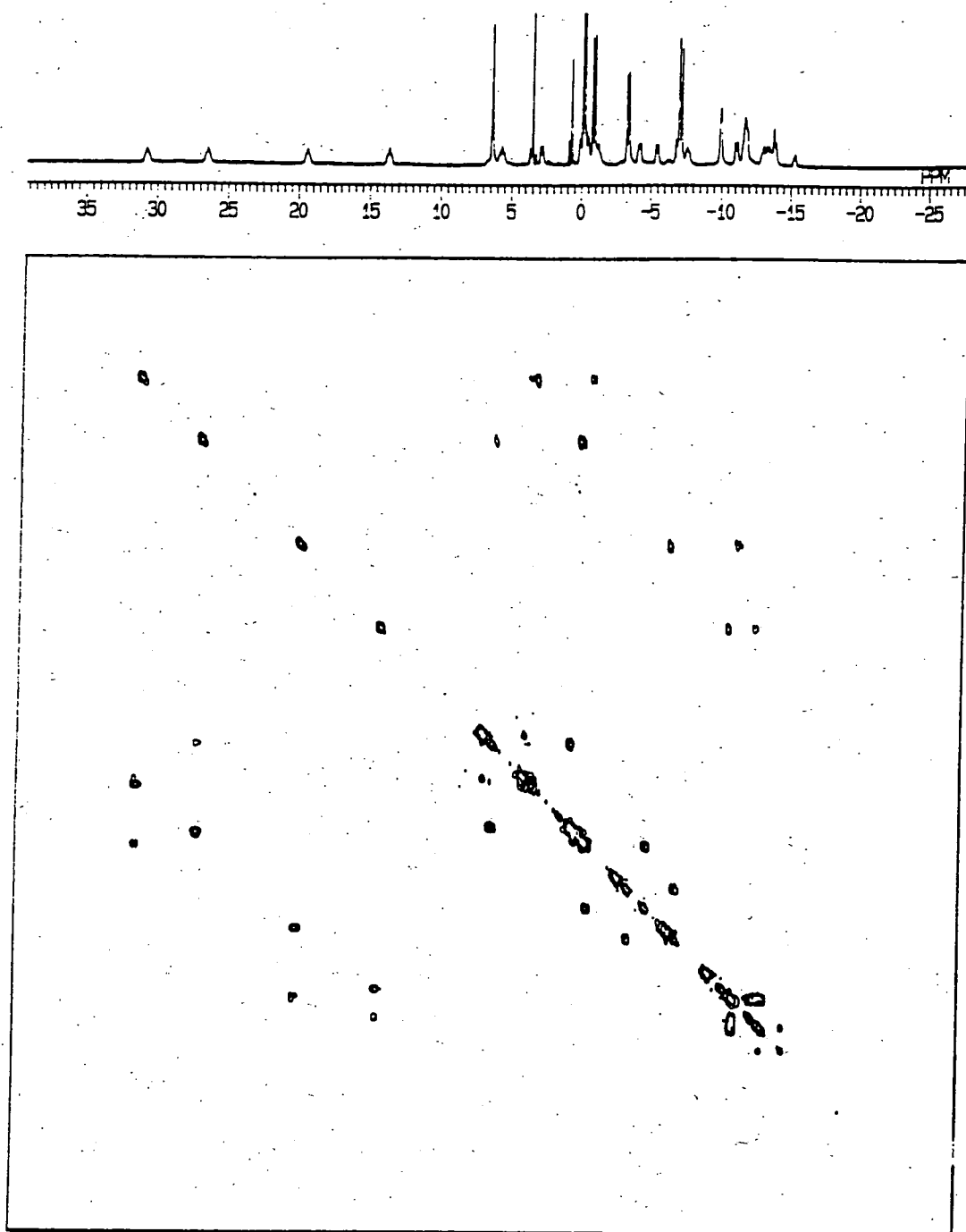


FIGURE 3.8 The 90 MHz $^1\text{H} - ^1\text{H}$ two-dimensional COSY spectrum (298K) of [Eu.33], allowing the resonances to be assigned as shown in Figure 3.7.

course, reflects the more pronounced line-broadening which occurs at higher magnetic field strengths, as discussed in Chapter 1. The usual advantage of high-field instruments, namely the higher resolution provided, is of little importance for europium complexes since the shifting effect of the metal is sufficient to provide almost complete resolution of the signals at low fields.

3.4.4 Determination of Yb-P distances by T_1 measurements

In the case of the ytterbium complexes, even at low magnetic field strengths, line-broadening is too severe for coupling to be discerned in the one-dimensional spectra or for a complete set of cross-peaks to be detected by two-dimensional experiments. It was pointed out in Chapter 2 that the paramagnetic shifts induced by ytterbium, for nuclei not directly bound to the metal, are almost solely dipolar in origin, allowing the chemical shifts of such nuclei to be related to their geometrical coordinates. On this basis, the observation of three well-separated resonances in the ^{31}P spectra of the ytterbium complexes may be indicative of small differences in the metal-phosphorus distances. Estimates of the Yb-P distances have been made by investigating the magnetic-field dependence of the Curie contribution to the ^{31}P T_1 relaxation times. The paramagnetic contribution $(1/T_1)_p$ to the measured relaxation rate has the form given in equation (40).⁹

$$\left(\frac{1}{T_1}\right)_p = \frac{20}{15} \frac{\gamma_p^2 g_J^2 \beta^2 J(J+1)}{r^6} \tau_S + \frac{6}{5} \frac{\omega_p^2 g_J^4 \beta^4 J^2(J+1)^2}{r^6 (3kT)^2} \left[\frac{\tau_R}{1 + \omega_p^2 \tau_R^2} \right] \quad \text{-----(40)}$$

Here, τ_S is the electronic relaxation time for the metal (ca. 10^{-13} s for Yb^{3+}) and τ_R the reorientational correlation time of the complex; r is the Yb-P distance. The Larmor frequency of the phosphorus atom is denoted by ω_p ; γ_p is the gyromagnetic ratio of phosphorus and β is the Bohr magneton. The Landé factor, g_J , has a value of 8/7 for Yb^{3+} and $J = 7/2$.

The first term of equation (40) is the electron-nuclear dipolar contribution to $(1/T_1)_p$ and is independent of the applied field. The second term is the Curie-spin term and is dependent on the square of the magnetic field through ω_p^2 . For most species of interest in solution, τ_R^{-1} is of the order 10^{10}s^{-1} and, since ω_p is in the region 10^8 Hz , this means that $\omega_p^2 \tau_R^2 \ll 1$. Thus, equation (40) can be simplified to the form given in equation (41).

$$\left(\frac{1}{T_1}\right)_p = D_1 \tau_S + \frac{\chi_1 \tau_R H_0^2}{r^6} \quad (41)$$

where $D_1 \tau_S$ is the first term of equation (40), H_0 is the applied field and

$$\chi_1 = \frac{6}{5} \frac{\gamma_p^2 g_J^4 \beta^6 J^2 (J+1)^2}{h (3kT)^2}$$

Hence a plot of the measured relaxation rates for a given phosphorus atom as a function of the square of the applied magnetic field (H_0^2) should yield a straight line.⁹ The value of the Yb-P distance, r , may then be estimated from the gradient of the line, provided that a reliable estimate of the reorientational correlation time, τ_R , is available.

Figure 3.9 shows the results of such an experiment for the three phosphorus resonances of the ytterbium complex of **34**. It is immediately clear from the relative magnitudes of the relaxation rates of the three phosphorus nuclei (at any given magnetic field strength) that the metal-phosphorus distances must lie in the order $P2 < P1 < P3$. Analysis of the NMRD profiles of similar Gd^{3+} complexes indicates that τ_R is about 100 ps at 298K. Using this value and the gradients of the lines in Figure 3.9, the Yb-P distances may be estimated by means of equation (41). The values obtained in this way for the three complexes are shown in Table 3.1 and may be compared to the average value of 3.35 Å for the yttrium complex of the tetraphosphinate ligand **27**, as determined from the X-ray crystal structure. The non-equivalence of the three metal-phosphorus distances in each

complex indicates that the amide group is causing some distortion of the coordination cage. Curiously, the effect is most pronounced for the complex of the N,N-dimethyl ligand 33.

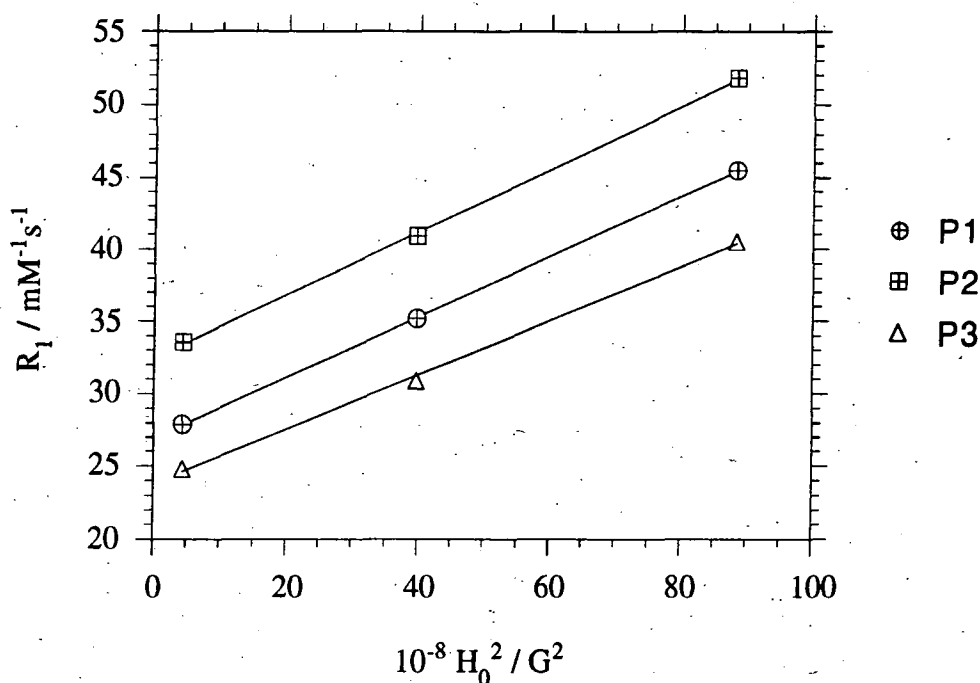


FIGURE 3.9 Plot of the longitudinal relaxation rates of the ^{31}P resonances for [Yb.34] against the square of the magnetic field strength. Data recorded at 2.1, 6.3 and 9.4 T and 298K in D_2O . The phosphorus nuclei are labelled according to Table 3.1.

TABLE 3.1 ^{31}P NMR shifts^a and calculated metal-phosphorus distances^b of the ytterbium complexes with 32 - 34.

	[Yb.32]		[Yb.33]		[Yb.34]	
	δ_P / ppm	$r / \text{\AA}$	δ_P / ppm	$r / \text{\AA}$	δ_P / ppm	$r / \text{\AA}$
P1	-34.3	3.46	-13.7	3.43	-25.0	3.35
P2	-40.4	3.51	-14.8	3.61	-35.2	3.32
P3	-43.0	3.38	-50.3	3.82	-41.3	3.40

(a) ^{31}P shifts measured in aqueous solution at 9.4 T, 298K and referenced to 85% H_3PO_4 . (b) From data measured at 2.1, 6.3 and 9.4 T.

3.4.5 Spectral resolution of the enantiomeric complexes

It was noted in section 3.4.2 that the predominant isomer observed in solution for the neutral amide complexes is actually a racemic mixture of enantiomers (probably corresponding to structure **1B** in Figure 3.5 and its enantiomer). Being enantiomeric, they cannot be distinguished directly by NMR spectroscopy. However, an interaction with a suitable enantiomerically pure substrate will result in non-equivalent, diastereoisomeric adducts. Provided that the association constant for such adduct formation is sufficiently large, it may be possible to observe these two diastereoisomers by NMR.

Cyclodextrins (CDs) are chiral host molecules which form inclusion complexes with a very large number of organic molecules. Owing to the chirality of the CD cavity, complexation with enantiomeric pairs results in the formation of diastereoisomeric complexes. A number of ^1H NMR studies have been reported in which CDs have been used as chiral complexing agents for enantiomeric purity determinations of pharmaceutically important molecules.¹⁰⁻¹² The presence of the benzyl groups in the complexes of **34** may allow such adduct formation with cyclodextrins. Addition of a small excess of β -CD to an aqueous solution of [Yb.**34**] resulted in the splitting of the ^{31}P resonances, as shown in Figure 3.10. Chiral resolution of the two enantiomeric forms of the complex is thereby effected: the two diastereoisomeric inclusion adducts formed on binding to the CD are characterised by a different set of NMR resonances.

Chiral resolution of this type does not necessarily require a selective binding of one enantiomer over the other. This has been shown, for example, by a study of the interaction of α -pinene with peracetylated β -CD, where slow exchange conditions apply and equally intense resonances are observed for both of the complexed enantiomers.¹⁰

In principle, if the two enantiomers can be discriminated by NMR using a particular CD, then it is likely that it should be possible to separate them chromatographically using

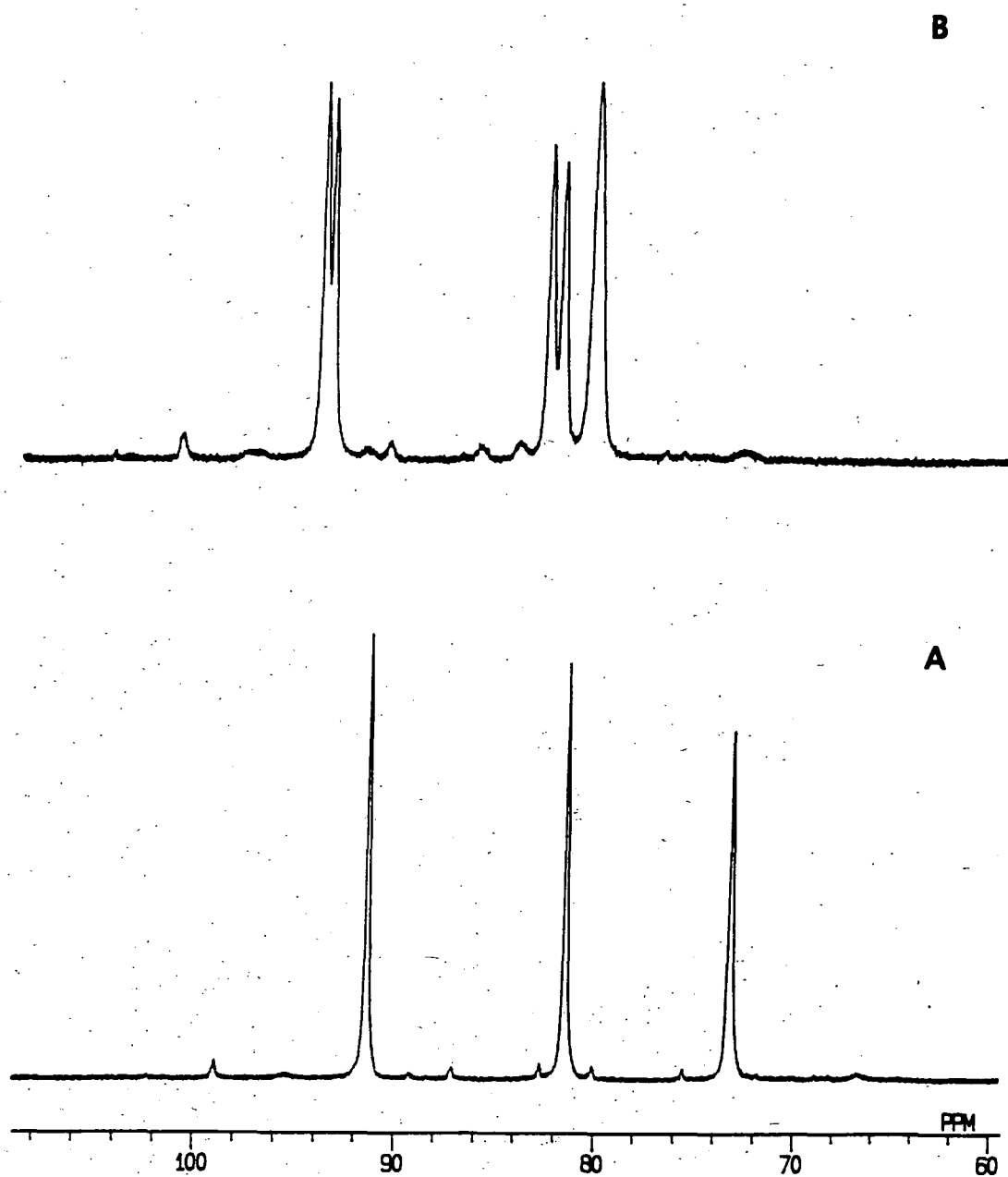


FIGURE 3.10 The ^{31}P NMR spectra (9.4T, 298K) of $[\text{Yb.33}]$ (10^{-2}M in D_2O) in the absence (A) and in the presence (B) of a small excess of β -cyclodextrin.

the same CD. The ytterbium complex of **34** was therefore examined by analytical HPLC using a cyclodextrin-based column with methanol as the eluant and detection by monitoring of the absorbance at 250 nm. Only one peak was observed, indicating no separation of the enantiomers. An attempt using a different type of chiral column, based on a helical polymethacrylate (Chiralpak OT⁺) appeared to show some splitting of the detected peak. Since the two components were of very different intensity, however, this could not reflect enantiomeric separation, but could possibly arise from a separation of the minor isomers from the major isomer. On this basis, preparative HPLC was carried out using this column type, with cooling to 10°C. Unfortunately, the fractions collected, corresponding to the early and late portions of the peak, were found to have identical ³¹P spectra.

3.5 Luminescence of the europium and terbium complexes

3.5.1 Terbium spectra

The UV spectra of the terbium complexes of **32** and **34** showed structured bands in the region 250 - 260 nm. Such bands are to be expected owing to the presence of the phenyl groups in the ligands. In contrast, the N,N-dimethyl and N-methyl ligands do not possess such chromophores and it was surprising, therefore, to find that the terbium complexes of these ligands displayed a relatively intense (ϵ 220), unstructured band centred at 250 nm (Figure 3.11). Its absence, in the spectrum of [Tb.26]⁻ and in the spectra of the corresponding europium complexes, indicates that the band must arise from the specific combination of an amide group bound to terbium. The possibility that this is due to a CT state may be dismissed as the band also appears in the metal luminescence excitation spectrum (see below): absorption by CT states should not lead to metal emission. The band is probably too narrow to arise from a π - π^* transition associated with the amide.

One possible explanation is that the band arises from a transition from the ground state of the f^8 configuration to an f^7d^1 configuration. Such a transition occurs at 220 nm for an aqueous solution of terbium perchlorate, with a high extinction coefficient of

$270 \text{ M}^{-1}\text{cm}^{-1}$. It is conceivable that the position of this band might be significantly shifted in the amide complex relative to its position in the aquo ion, although the magnitude of the shift which would be required, 5500 cm^{-1} , is difficult to believe.

Excitation of these two complexes at 250 nm led to quite intense metal luminescence, with quantum yields of the order of 0.1 (Table 3.3). The metal luminescence excitation spectra closely resembled the UV absorbance spectra, again dominated by an unstructured band centred at 250 nm (Figure 3.11). Thus, whatever the origin of this band, the efficiency of conversion of the state so-formed into the $^5\text{D}_4$ emissive state of terbium must be high.

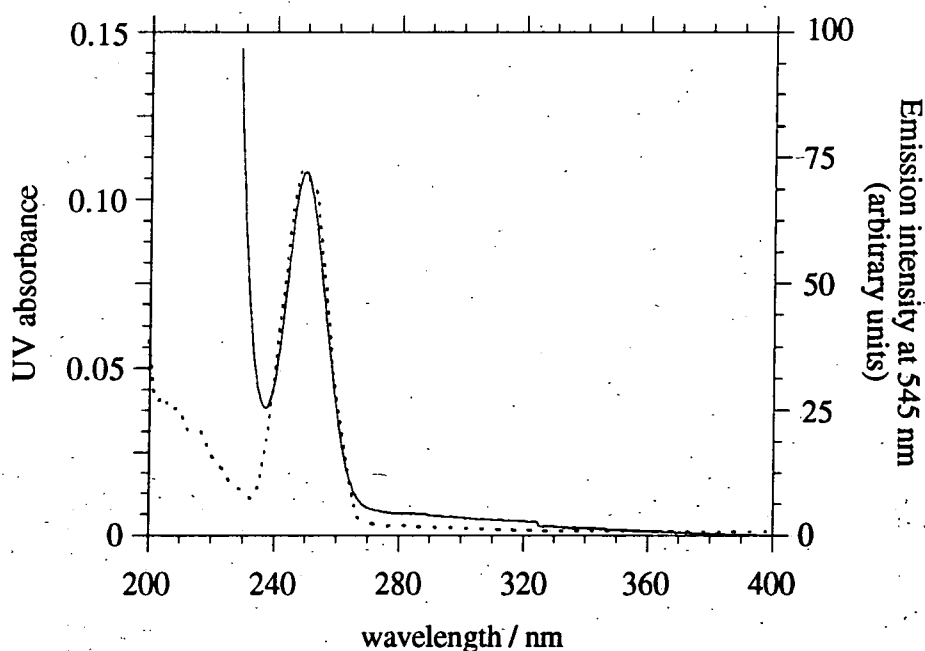


FIGURE 3.11 *Solid line: UV absorbance spectrum of $[\text{Tb}.33]$ ($4 \times 10^{-4} \text{ M}$ in H_2O). Dashed line: Metal luminescence excitation spectrum of this solution. Emission monitored at 545 nm. Excitation and emission monochromator slit widths of 2.5 nm were used with a delay time of 0.1 ms.*

If the band is a general effect related to coordination of terbium by an amide, then it should be observed in complexes with simpler amides. In this respect, dimethylformamide could be a useful model. A concentrated solution of $\text{Tb}(\text{NO}_3)_3$ in

DMF was prepared and its UV spectrum recorded. This showed no evidence of a band at 250 nm although this was not completely conclusive as the absorbance of even the best quality DMF available is >1 at wavelengths less than 270 nm. A more useful and more conclusive experiment, however, is the measurement of the metal luminescence excitation spectrum. This showed the characteristic line-like spectrum of 'free' terbium, with no evidence of a broader more intense band at 250 nm. Thus the band observed in the complexes of **31** - **34** must be a more specific effect.

The N,N-dibenzyl complex [Tb.**34**] showed a similar, apparently unstructured band in its metal luminescence excitation spectrum. This would seem to suggest at first sight that the phenyl groups are not undergoing energy transfer to the metal, as they were in [Tb.**27**]⁻. On the other hand, the quantum yield of metal emission was found to be identical to that of the N,N-dimethyl complex. Since the phenyl groups will be absorbing at 250 nm in competition with the 250 nm unstructured band, this observation indicates that either the amide-Tb 250 nm band is substantially stronger in the dibenzyl complex than in the dimethyl analogue *or* that the benzyl groups are also involved, either undergoing energy transfer directly to the metal or into the amide-Tb band. Involvement of the benzyl groups is perhaps the more likely explanation. It is possible that the non-equivalence of the two benzyl groups, together with the superposition of the amide-Tb band, simply inhibits any fine structure from being detected in the excitation spectrum. On the other hand, the band in [Tb.**34**] is just as narrow as that for [Tb.**33**], whereas it should be broader if the benzyl groups are involved.

In contrast, the quantum yield of [Tb.**32**] is much lower (Table 3.3). This seems to indicate that competitive absorption by the phenyl group in this compound is not followed by energy transfer to the metal.

The appearance of the metal emission spectra was very similar for all four complexes and closely resembled that of the tetraphosphinates; eg. [Tb.**27**]⁻ (Figure 2.11). This

close similarity is also evident in the CPL spectra on direct metal excitation (using circularly polarised light at 488 nm). Those of the $^5D_4 \rightarrow ^7F_5$ transition for [Tb.27]⁻ and [Tb.33] are shown in Figure 3.12, together with the corresponding total emission profiles. The resemblance is striking. Bearing in mind the difference in the local symmetry and coordination environment of the terbium in the two types of complex, it is rather surprising that the spectra are so similar. This behaviour contrasts with that of europium, where some significant changes are observed, as discussed below. Again, the very observation of a CPL spectrum indicates that the complex is chiral. The maximum value of g_{abs} in the $^5D_4 \rightarrow ^7F_5$ band is 0.016, similar to the value found for [Tb.27]⁻.

3.5.2 Europium spectra

Excitation of the Eu^{3+} complexes of the amide ligands at 250 nm gave rise to the characteristic europium emission but, as in the case of the tetraphosphinates, the emission intensity was very low. Quantum yields are shown in Table 3.3. The metal luminescence excitation spectra were largely featureless curves, rising steadily with decrease in wavelength and resembling the UV spectra. There were no significant bands at 250 nm in these complexes.

As pointed out in Chapter 2, europium emission spectra tend to be more informative than those of terbium, as the low J values ensure that there are only a small number of possible transitions per band, allowing conclusions regarding the local symmetry of the metal to be reached. The $^5D_0 \rightarrow ^7F_0$ transition is unique for a given chemical environment, the initial and final states both being non-degenerate. When observed, the transition invariably occurs between 578 and 580 nm, but is always weak, being forbidden by electronic selection rules.¹³ Under conditions of high symmetry, (eg. D_4 , D_{4h} , D_{4d} and higher), the transition is further forbidden by the symmetry selection rule. The amide complexes lack axial symmetry and the transition is allowed through both electric and magnetic dipole mechanisms. Its intensity (relative to the other bands) is higher than in the C_4 symmetric complexes of the tetraphosphinates, as is shown clearly

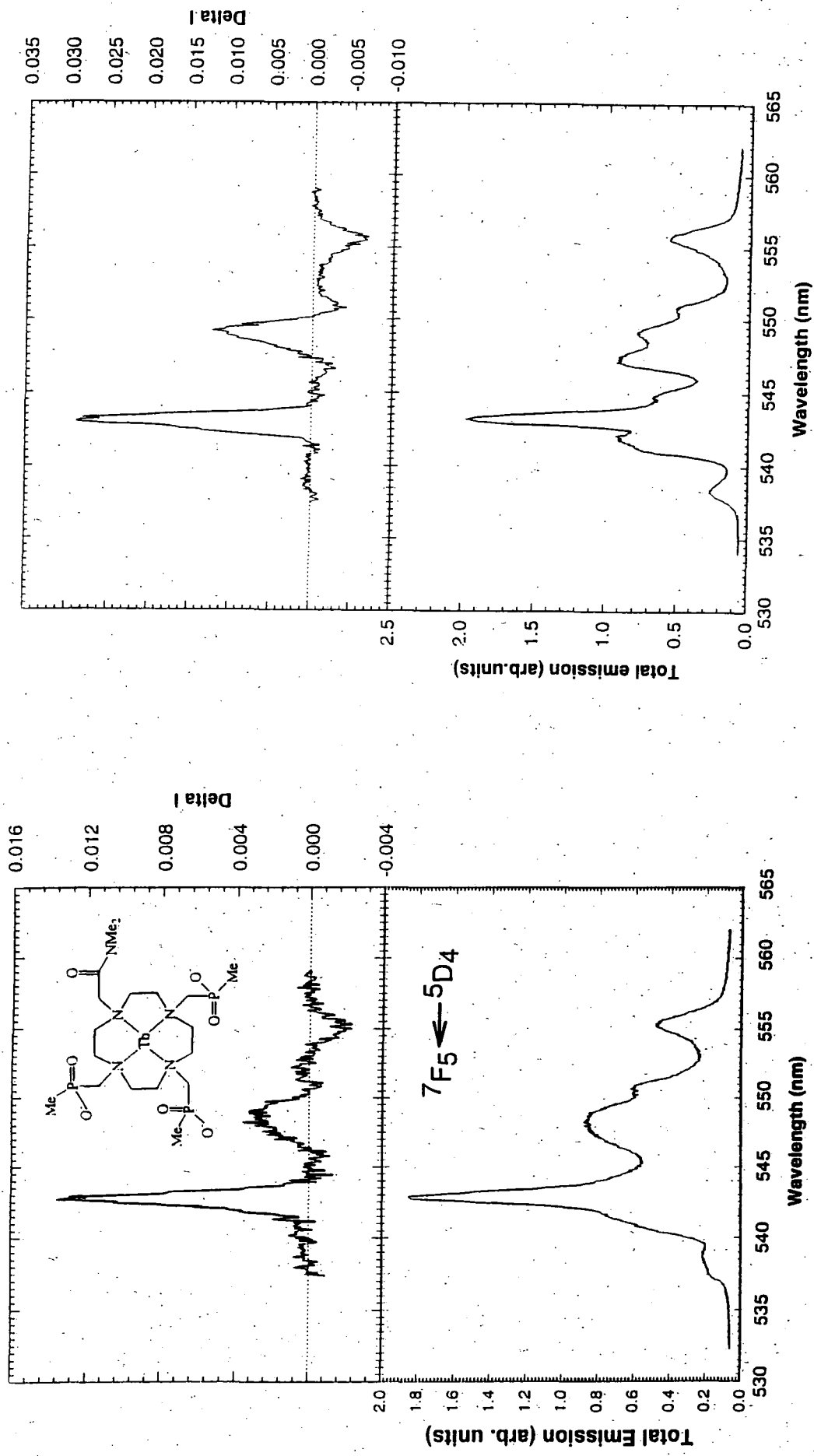


FIGURE 3.12 Circularly polarised luminescence (upper) and total luminescence (lower) of [Tb.33] (left) and [Tb.27] (right) in water (298K), following excitation of the ${}^7F_6 \rightarrow {}^5D_4$ transition at 488 nm. The spectral regions displayed correspond to the ${}^5D_4 \rightarrow {}^7F_5$ transition of terbium.

by the spectra obtained upon direct laser excitation of the metal at 553 nm (Figure 3.13).

The spectra measured using the fluorimeter are not really sufficiently well-resolved to conclude that there is only one ${}^7F_0 \rightarrow {}^5D_0$ transition. However, this portion of the spectrum was examined by Professor Riehl and co-workers under higher resolution, using laser excitation. The results for [Eu.27]⁻ and [Eu.33] are shown in Figure 3.14. It is clear that in both cases only a single band is present, confirming that there is only one predominant species in solution. The band for the tetraphosphinate lies slightly to higher energy than that of the amide complex; the positions are 579.26 nm (17263 cm⁻¹) and 579.34 nm (17261 cm⁻¹) respectively. Albin and Horrocks have proposed an empirical relationship to relate the energy of the ${}^5D_0 \rightarrow {}^7F_0$ transition to the sum, q , of the formal negative charges of the ligands directly bonded to the europium ion:¹⁴

$$\nu \text{ (cm}^{-1}\text{)} = 17273 + 2.29q - 0.76q^2 \quad (T = 296\text{K}) \quad (42)$$

However, such relationships are of relatively little value in general, being derived from only a limited number of ligand systems and completely ignoring any covalent contributions to the bonding. Thus, the energies predicted for ligands with $q = -4$ and $q = -3$ are 17251.7 and 17259.3 cm⁻¹ respectively. Whilst the agreement with the observed value for [Eu.33] ($q = -3$) is reasonable, the value predicted for [Eu.27]⁻ is substantially lower than that which is observed. Indeed, even the relative energies are predicted incorrectly.

The ${}^5D_0 \rightarrow {}^7F_1$ transition of the europium ion has a purely magnetic dipole character and, as such, is largely insensitive to the coordination environment of the metal. As explained in Chapter 2, under low symmetry (C_2 axis or less), the 7F_1 level splits into the maximum number of three non-degenerate sub-levels such that, in principle, three transitions should be observable in such complexes. In the presence of a 3-fold or

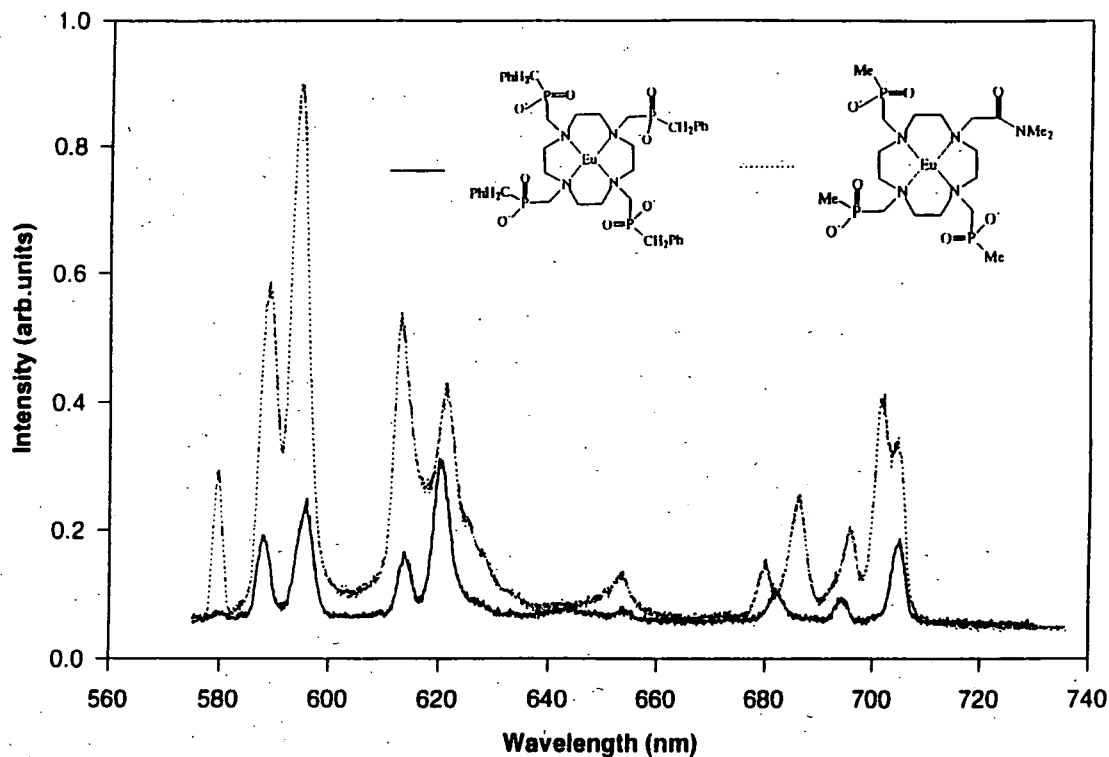


FIGURE 3.13 Total emission spectra (uncorrected) of $[Eu.27]^-$ (solid line) and $[Eu.33]$ (dotted line) under high resolution following direct laser excitation of the ${}^7F_2 \rightarrow {}^5D_1$ transition at 553.43 nm (H_2O , 298K).

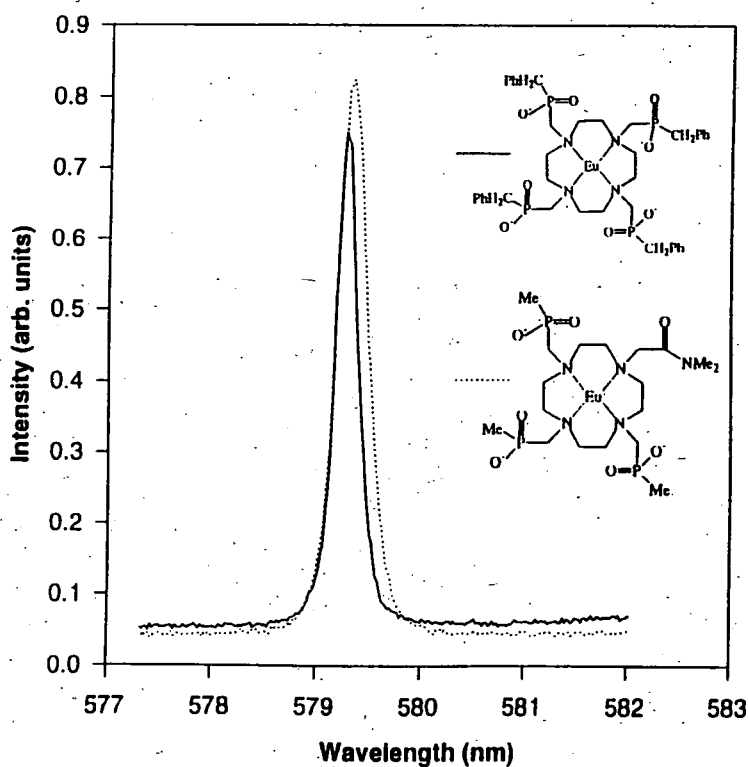


FIGURE 3.14 High resolution emission spectra of the 0-0 transition of $[Eu.27]^-$ (solid line) and $[Eu.33]$ (dotted line) following excitation of the metal at 553.43 nm (H_2O , 298K). The bands have been normalised to similar intensities for comparison.

higher axis of symmetry, only two bands are expected.¹³ In fact, for all of the complexes studied, only two components were observed in the $^5D_0 \rightarrow ^7F_1$ band and, in each case, their relative intensities were similar (Figure 3.15; see also Figure 3.13 at higher resolution).

In contrast, the $^5D_0 \rightarrow ^7F_2$ transition is allowed through an electric-dipole mechanism. It is well-known that its intensity is very sensitive to the metal environment and particularly to the polarisability of the ligating atoms. Thus, it is perhaps not surprising to find that its intensity, relative to the $\Delta J = 1$ transition, varies considerably in the complexes studied. The trend is shown by the spectra in Figure 3.15, where the spectrum of DOTA is also included. The relative intensities of the bands are listed in Table 3.2. In all of the complexes examined, two components were observed for this transition ($^5D_0 \rightarrow ^7F_2$), although more are predicted. In fact, the relative intensities of these two components also showed a marked variation through the series of complexes, as shown in Figure 3.15 and Table 3.2.

Two limiting cases may be discerned, namely those of $[\text{Eu.DOTA}]^-$ and $[\text{Eu.27}]^-$. In the former case, the $\Delta J = 2$ transition is weaker than the $\Delta J = 1$ and, within the $\Delta J = 2$ band, the intensity of the shorter wavelength component greatly exceeds that of its longer wavelength neighbour. Both of these features are reversed for $[\text{Eu.27}]^-$. It is difficult and perhaps impossible to provide a theoretical explanation for these observations but it seems reasonable to propose that the difference arises from the different solution structures of the two complexes. As discussed in Chapter 2, $[\text{Eu.DOTA}]^-$ adopts a square antiprismatic structure whereas $[\text{Eu.27}]^-$ possesses an inverted square antiprismatic geometry.

Figure 3.15 and Table 3.2 show that the behaviour of the complexes of ligands **31** - **34**, where an amide donor is present, are intermediate between these two extremes. Moreover, the identity of the amide substituent has a significant effect. Indeed, there appears to be some correlation between the $\Delta J = 1 / \Delta J = 2$ intensity ratio (Table 3.2)

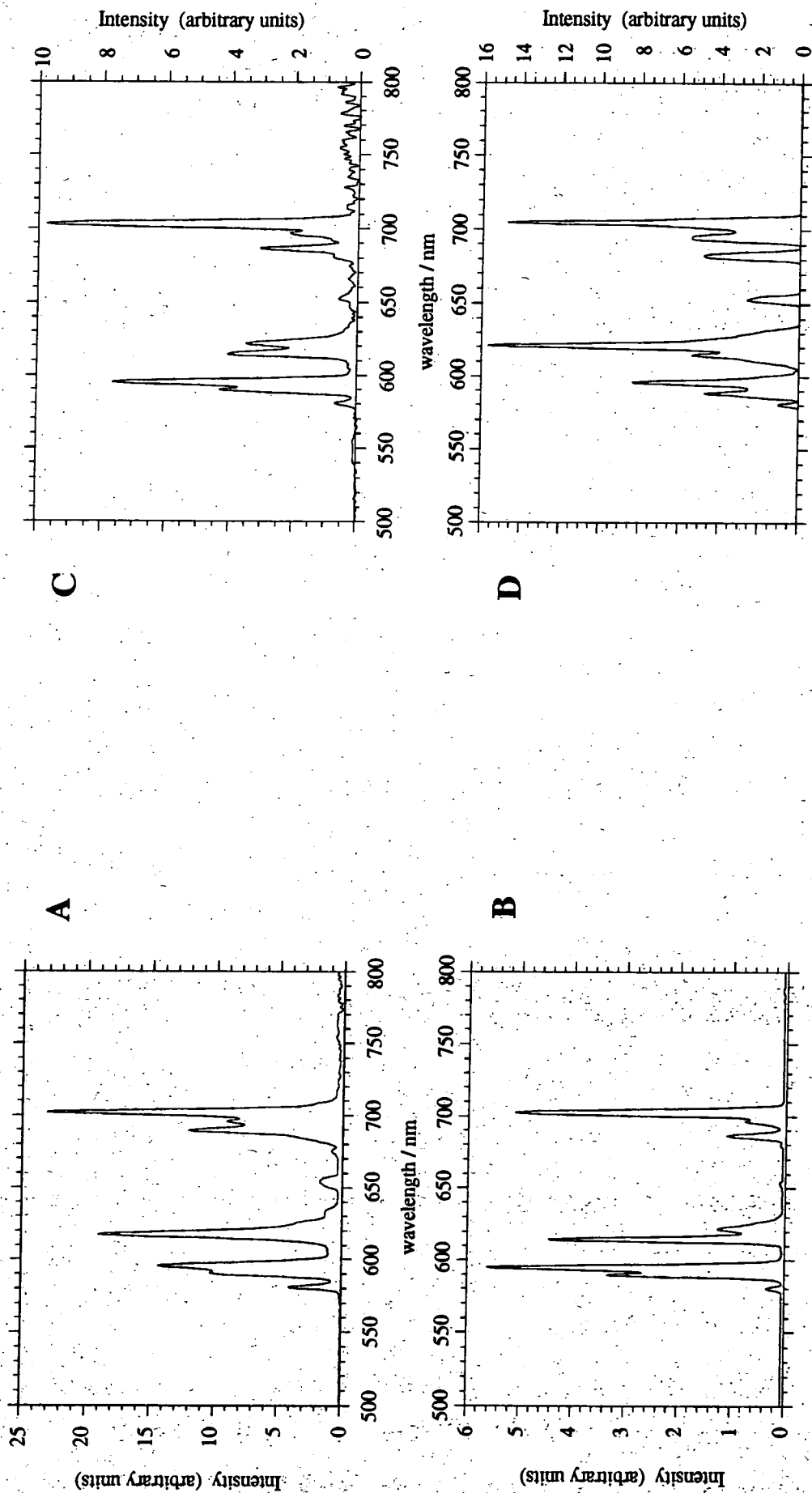


FIGURE 3.15 Corrected metal emission spectra for [Eu.DOTA] (A), [Eu.33] (B), [Eu.27] (C) and [Eu.27] (D) in D_2O (293K). $\lambda_{ex} = 250$ nm for B, C and D; 397 nm for A. Excitation and emission slit widths of 10 and 2.5 nm respectively were used.

and the steric bulk of the amide substituents: the ratio progressively decreases from the bulky N,N-dibenzyl amide through to the smallest NH-methyl system. This could possibly reflect the differing degrees of distortion of the coordination cage induced by the amide group. It is clear from the ^{31}P NMR studies of the corresponding Yb^{3+} complexes, discussed in section 3.4.4, that the different amide groups do indeed result in significant but different changes in the metal-phosphorus distances.

TABLE 3.2 Characteristics of the $\Delta J = 2$ transition of the europium complexes (295K, H_2O).

Complex	$\Delta J = 2$ band: relative intensities of the two components (610 / 619 nm)	Relative Overall Intensity $\Delta J = 1 / \Delta J = 2$
[Eu.DOTA] ⁻	5 : 1	1.7
[Eu.34]	2.6 : 1	1.44
[Eu.33]	1.1 : 1	1.25
[Eu.32]	1.3 : 1	1.15
[Eu.31]	1.25 : 1	0.90
[Eu.26] ⁻	0.5 : 1	0.71
[Eu.27] ⁻	0.3 : 1	0.71

The $^5\text{D}_0 \rightarrow ^7\text{F}_3$ transition is reported to be weak in all cases reported to date, as is observed here. The $^5\text{D}_0 \rightarrow ^7\text{F}_4$ band has a similar total intensity to that of the $\Delta J = 1$ band in all of the complexes studied. This is also the case for [Eu.DOTA]⁻ and [Eu.TETA]⁻, which also have four nitrogen atoms bound to the metal, although only a qualitative comparison with this work can be made as the literature spectra were not corrected for wavelength-dependent detection sensitivity.¹⁵ It has been proposed that the intensity of this band may be related to the number of bound nitrogen atoms; thus, the europium complexes with ligands such as NOTA, EDTA, DTPA, CyDTA and DPA (where there are fewer nitrogen atoms) display $^5\text{D}_0 \rightarrow ^7\text{F}_4$ bands of much lower

intensity than that of the $\Delta J = 1$ band.¹⁵ Perhaps a more likely explanation lies in the lower axial symmetry of the latter group of complexes. The $\Delta J = 4$ band is predicted to split into seven components under C_4 symmetry and the maximum of nine components when the axial symmetry is C_2 or lower. Although not all of the transitions are resolved, it is clear from the spectra in Figure 3.13 that more components are observed for the low-symmetry complex of **33** than for $[\text{Eu.27}]^+$, which has C_4 symmetry.

3.5.3 Lifetimes and hydration states

Excited state lifetimes were measured for the europium and terbium complexes of the amide ligands **31** - **34** in both H_2O and D_2O . The hydration state, q , was estimated using the Horrocks parameters (equation 5 in Chapter 1). The results are shown in Table 3.3, together with the values for the tetrakisphosphate complexes for comparison. Two trends are immediately apparent. All of the neutral amide complexes display non-integral q values between 0 and 1, which are significantly higher than those obtained for the tetrakisphosphate complexes (where it was concluded that there are no metal-bound water molecules, Chapter 2). Secondly, the values obtained for the europium complexes are found to be consistently higher than those of the terbium complexes, by about 0.5. An explanation for these observations is desirable.

One possibility is to simply dismiss the non-integral q values as arising from the error inherent in the Horrocks method: Horrocks quotes an error of ± 0.5 in q .¹⁶ Clearly, this is most unsatisfactory. The precision of the lifetime measurements in this work is high; in most cases, the lifetimes are reproducible to within ± 0.1 ms, which would correspond to a maximum error in q of about ± 0.2 for the europium complexes and rather less for the longer-lived terbium complexes. The reliability of the Horrocks A_{Ln} parameter is therefore called into question. It should be noted that this is a purely empirical parameter, derived from a study of a very limited number of complexes and a correlation with the number of metal-bound water molecules as obtained from X-ray crystal structure analyses. The plots were derived from complexes where q took integral values from 0 to 9 in the solid state but there is no guarantee that the behaviour

in solution will be the same as that in the solid state. The possibility of N-H / N-D or C-H / C-D exchange was not considered in complexes where it could conceivably be occurring.

TABLE 3.3 *Luminescence Data for the Europium and Terbium Complexes Discussed in Chapters 1 and 2*

Complex	τ (298K) / ms		ϕ (298K)		$\Delta k^a/\text{ms}^{-1}$	q^b
	D ₂ O	H ₂ O	D ₂ O	H ₂ O		
[Eu.31]	1.85	0.76	1.3×10^{-3}	0.5×10^{-3}	0.78	0.81
[Tb.31]	4.30	3.20	0.28	0.16	0.08	0.34
[Eu.32]	2.03	0.70	0.35×10^{-3}	0.10×10^{-3}	0.94	0.98
[Tb.32]	4.13	3.09	4.4×10^{-3}	4.7×10^{-3}	0.081	0.34
[Eu.33]	1.97	0.84	1.4×10^{-3}	0.74×10^{-3}	0.68	0.72
[Tb.33]	4.30	3.53	0.12	0.10	0.05	0.21
[Eu.34]	1.93	0.80	1.4×10^{-3}	0.60×10^{-3}	0.73	0.77
[Tb.34]	4.03	3.32	0.11	0.10	0.053	0.22
[Eu.26] ⁻	1.85	1.25	1.0×10^{-3}	0.59×10^{-4}	0.26	0.27
[Tb.26] ⁻	3.71	2.96	9.1×10^{-3}	10×10^{-3}	0.068	0.29
[Eu.27] ⁻	2.07	1.59	1.5×10^{-3}	0.93×10^{-3}	0.15	0.15
[Tb.27] ⁻	4.44	4.13	0.49	0.44	0.017	0.07
[Eu.DOTA] ⁻	2.44 ^c	0.64 ^c	---	---	1.19	1.2
[Tb.DOTA] ⁻	2.54	1.51	---	---	0.27	1.1

(a) $\Delta k = k_{\text{H}_2\text{O}} - k_{\text{D}_2\text{O}}$ where k is the observed first order rate constant for deactivation of the metal emissive state. (b) q is the hydration state determined using the Horrocks parameter (equation 5). (c) From reference 15.

Ultimately, however, the Horrocks relationship and the A_{Ln} parameters are of little importance here. Irrespective of such empirical correlations, we are left with a group of complexes which display values of Δk (i.e. $(k_{H_2O} - k_{D_2O})$, where k is the first order rate constant for depopulation of the emissive state) which are intermediate between those observed for the complexes of **27** (no metal-bound water molecules) and those of DOTA (one metal-bound water water), as indicated in Table 3.3. This *must* reflect a degree of deactivation by water O-H bonds that is rather less than in a model 'one bound water' complex (eg. those of DOTA) but is more significant than in purely outer-sphere complexes such as those of **27**. One possibility is that the equilibrium position of the nearest water molecule is further away from the metal than in DOTA complexes. In assessing this possibility, the information provided by an analysis of the NMRD profiles of related Gd^{3+} complexes may prove to be very useful.

3.5.4 Hydration states and the correlation of Gd^{3+} NMRD information with luminescence measurements

The Gd^{3+} complex of **32** has been prepared during this work and that of **34** had been prepared previously. Gadolinium complexes of ligands closely related to **31** and **33** were available (see footnote to Table 3.4). The $1/T_1$ NMRD profiles of these complexes have been recorded at Turin and analysed in terms of the theories discussed in Chapter 1. All of the complexes show similar behaviour and the profile for one of them is shown in Figure 3.16. The shape of the profile is typical of small Gd^{3+} complexes possessing a single coordinated water molecule. However, the magnitude of the relaxivity is substantially lower across the entire magnetic field range than that which is measured for inner-sphere complexes such as $[Gd.DOTA.H_2O]^-$, where the relaxivity passes from 8 - 12 in the low-field region to about 4 - 6 $mM^{-1}s^{-1}$ at 20 MHz (section 2.8.2). For the complexes studied here, the relaxivities are about one-half of these values (eg. about 2.9 $mM^{-1}s^{-1}$ at 20MHz). On the other hand, the behaviour is inconsistent with purely outer-sphere properties, as is clear from Figure 3.16, which also shows the profile for a typical outer-sphere complex such as $[Gd.27]^-$. In order to account for the observed profile under the constraint of $q = 0$, a significantly shorter

molecular radius would have to be invoked, compared to the tetraphosphinate, or a large change of the diffusional dynamics in aqueous solution, neither of which possibilities is realistic. Evidently, there are contributions from both inner and outer sphere mechanisms.

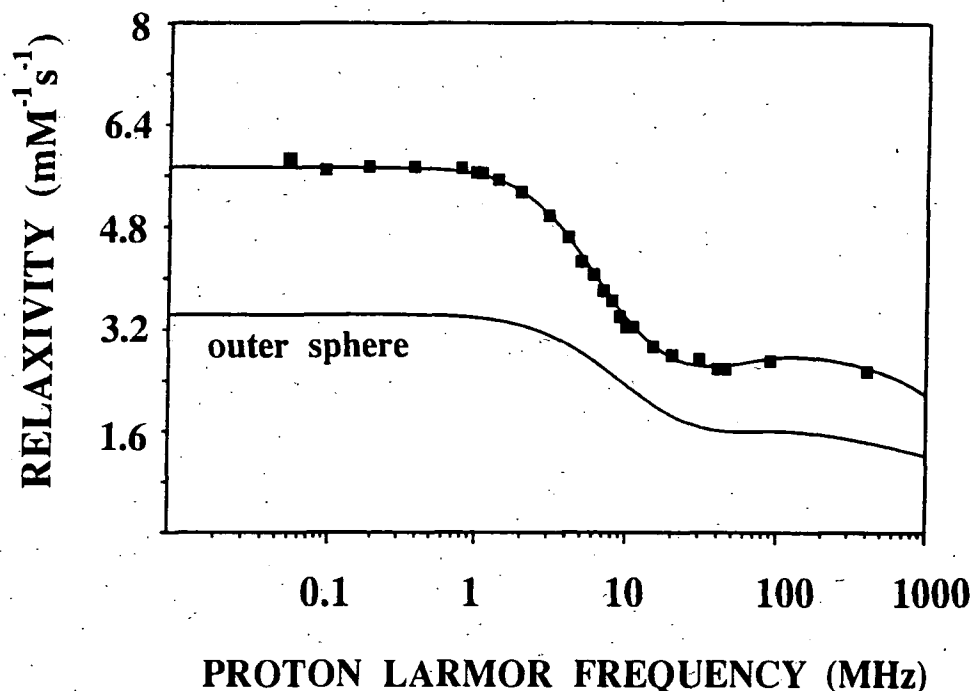
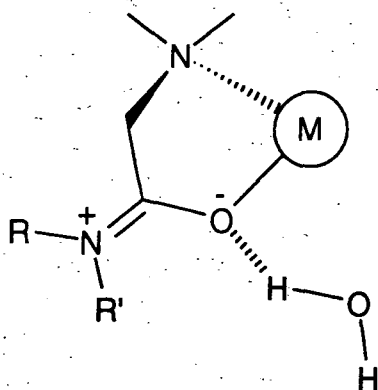


FIGURE 3.16 Representative $1/T_1$ NMRD profile of the gadolinium complexes of the amide-trisphosphinate ligands in aqueous solution (1mM, 298K, pH 7). The solid line is the simulated behaviour using a best-fitting procedure to the equations for inner and outer sphere relaxation discussed in Chapter 1. The lower curve represents the outer-sphere component.

The relaxivity in the high-field region is about $2.4 \text{ mM}^{-1}\text{s}^{-1}$ for the purely outer-sphere $[\text{Gd.27}]^-$ under these conditions, which suggests that the inner-sphere contribution to the relaxivity is of the order of $0.5 \text{ mM}^{-1}\text{s}^{-1}$. This leads to estimates in the range 3.4 - 3.6 Å for the Gd-H distances of the coordinated water molecules in these complexes (Table 3.4). These values are significantly longer than those of 3.0 - 3.2 Å found for Gd^{3+} complexes of macrocyclic polyamino-polycarboxylic ligands such as DOTA, but considerably shorter than the value of 3.82 Å for the distance of closest approach to the metal of protons on diffusing water molecules for the outer-sphere complex $[\text{Gd.26}]^-$.

The most obvious conclusion from these observations is that the substitution of a phosphinate group by a carboxamide results in the binding of a water molecule at an equilibrium distance from the metal which is somewhat longer than that in 'conventional' inner-sphere complexes, but the residence lifetime, τ_M , of this water molecule is significantly longer than the time necessary for solute and solvent to diffuse apart. It seems reasonable to propose that this may reflect the formation of a hydrogen bond between the carbonyl oxygen atom and a water molecule as shown in Scheme 3.2. The water molecule could be referred to as occupying the 'second coordination sphere' of the metal ion, but this is perhaps a rather artificial distinction. It is probably preferable to think in terms of a continuum of metal-water proton distances, ranging from ca. 3.1 Å in a complex such as [Gd.DOTA]⁻ to > 4 Å in outer-sphere complexes.



SCHEME 3.2

It is worth commenting at this point that an estimate of the hydration state of the complexes of one of the amide ligands (31) was also made using the method of the dysprosium induced shift of the ¹⁷O nucleus of water, as discussed in Chapter 2 (section 2.8.1). The result is shown in Figure 2.16. The behaviour here is seen to be very similar to that of [Dy.DOTA]⁻, suggesting that the hydration states are similar. In light of the results discussed above, this seems somewhat surprising, as a gradient intermediate between that of [Dy.27]⁻ and [Dy.DOTA]⁻ might have been expected.

The conclusions reached above from the analyses of the NMRD profiles are obviously of direct relevance to the luminescence results discussed earlier. The efficiency of an

energy transfer process decreases rapidly as the distance between the energy donor and the acceptor increases (section 2.11). Thus, the extent to which the europium or terbium emissive states are deactivated through energy transfer into O-H vibrations is likely to display a sensitive dependence on the equilibrium distance of the metal from the nearest water molecule. It is therefore not unreasonable to expect non-integral q values, between 0 and 1, according to the exact value of this metal-water distance. If this is the case, then one would predict some correlation between the luminescence q values and the metal-water-proton distances obtained from the gadolinium NMRD profiles. Table 3.4 and Figure 3.17 show that there is indeed quite a reasonable correlation.

It is worth noting that there is an alternative explanation for the observed behaviour of the luminescent complexes and of the gadolinium complexes, namely that there is a mixture of isomers in solution, some of which have $q = 0$ and others having $q \geq 1$. The observed q values would then be averages, determined by the proportions of these isomers in solution. Such an explanation can probably be dismissed on the grounds that the solution NMR studies have shown that there is only one major isomer in solution (see for example the ^{31}P spectra of [Eu.33] and [Yb.33] in Figures 3.2 and 3.3). Moreover, as pointed out in section 3.5.2, only one $\Delta J = 0$ transition is observed in the emission spectra of the europium complexes, which is also very strong evidence for the presence of a single predominant isomer.

Reference to Tables 3.3 and 3.4 shows that the complexes of the secondary amide ligands **31** and **32** display very similar luminescence behaviour to one another, with consistently larger Δk and q values than those of the tertiary amides. A possible explanation for this trend is the occurrence of N-H / N-D exchange when in solution in D_2O . The amide N-H bond has a vibrational stretching frequency similar to that of O-H. Hence, it is reasonable to suppose that an N-H bond lying close to the metal will be able to deactivate the lanthanide emissive states in a similar manner to O-H, whilst N-D will have little effect. The net effect would be a q value which is higher than that

TABLE 3.4 Correlation of Gd-H (H of water) distances, r , determined from NMRD profiles with the hydration state, q , determined by luminescence measurements (295K, H_2O).

Complex	Eu	Tb	Gd(NMRD)
	q	q	$r / \text{\AA}$
[Ln.27] ⁻	0.15	0.07	4.25
[Ln.26] ⁻	0.27	0.29	3.82
[Ln.34]	0.77	0.22	3.56
[Ln.33]	0.72	0.21	3.53 ^a
[Ln.32]	0.98	0.34	3.42
[Ln.31]	0.81	0.34	3.42 ^b
[Ln.DOTA] ⁻	1.2	1.1	3.13

(a) for the *N,N*-dibutylamide analogue. (b) the related $\text{CONH}(\text{CH}_2)_4\text{NH}_3^+$ derivative.

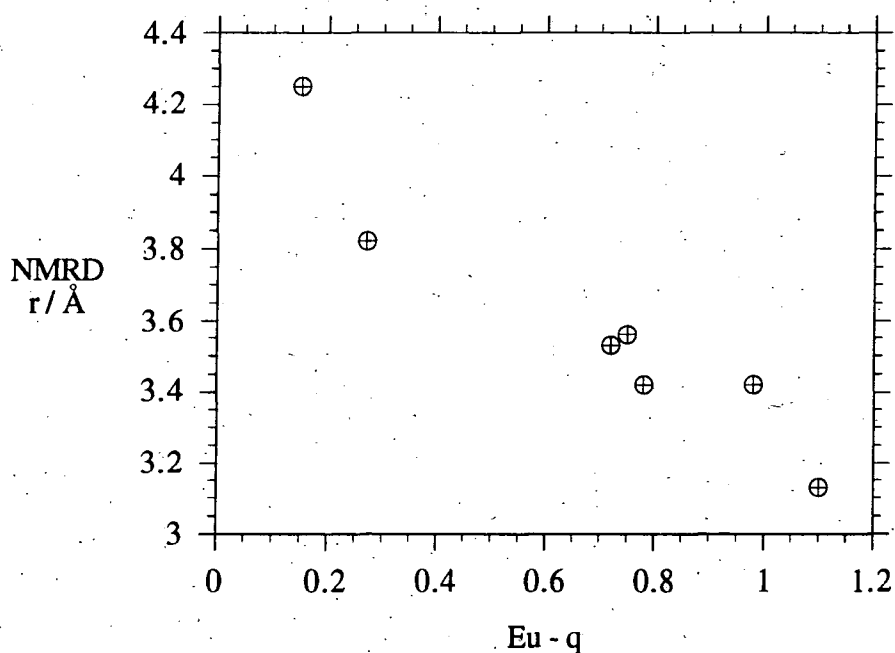


FIGURE 3.17 Correlation between the q value measured by luminescence methods for the europium complexes and the distance of closest approach of a water molecule for the corresponding gadolinium complex determined by NMRD methods.

observed for a similar tertiary amide, with no N-H. During the course of this work, such an effect has been demonstrated explicitly for some related tetraamide complexes containing 4 amide N-H bonds and is discussed in Chapter 4. It was estimated that 4 such N-H bonds contribute about $350 - 400 \text{ s}^{-1}$ to the value of k for the europium complexes in H_2O , a contribution which is absent in D_2O . This amounts to about $90 - 100 \text{ s}^{-1}$ per N-H oscillator and this is indeed largely consistent with the present observations. For example, the difference in Δk for [Eu.31] (-NHMe) compared to [Eu.33] (-NMe₂) is 100 s^{-1} , or a difference in q of 0.09 (Table 3.3). Similarly, the q values for the secondary amide Tb^{3+} complexes are higher by about 0.1 than those of the tertiary amide analogues.

The possibility of C-H / C-D exchange of the NCH_2CO protons when in solution in D_2O was also considered. Again, the vibrational stretching frequency of C-H is only a little lower than that of O-H so that the C-H bond may be able to deactivate the metal emissive state, an effect which would be lost on deuteration. However, if this were to occur, then the amide NCH_2CO protons should not appear in the proton spectra of the complexes or at least they should have diminished intensity relative to the NCH_2P protons. It is clear from the NMR work (Figures 3.2 and 3.7) that this is not the case. In fact, the possibility of Ln^{3+} deactivation by C-H bonds has not been investigated previously, although some authors have speculated that it may be operative.¹⁷ In an attempt to ascertain whether C-H bonds can act in this way, [Eu.DOTA]⁻ was prepared, as previously reported,¹⁸ and the luminescence decay was examined in D_2O at pD 6.5 following excitation at 397 nm. A value of k of 574 s^{-1} was obtained. The pD of the solution was then raised to 11 by addition of KOD in D_2O and the solution heated at 45°C for 8 h. Under these conditions, the NCH_2CO protons are expected to undergo exchange to give CD_2CO . The pD was then lowered to 6.5 (DCl in D_2O) and the luminescence decay was monitored once again. A k value of 414 s^{-1} was observed in this case. The tentative conclusion from this experiment is that the rate constant for the decay of the Eu^{3+} excited state is significantly reduced on deuteration of the acetate protons, from which it is apparent that C-H bonds are indeed able to deactivate the

excited state. The effect of 160 s^{-1} would amount to an average of 20 s^{-1} per C-H bond; this is probably a minimum value as the deuteration may not have gone to completion. A value of this order of magnitude does not seem unreasonable: clearly, the lower vibrational stretching frequency of C-H (ca. 2970 cm^{-1}) compared to N-H or O-H would be expected to give rise to a smaller effect than that observed for these latter oscillators. The effect is currently being pursued in more detail by other workers within the group.

It was also apparent that this exchange process does not take place at neutral pH (even over several days). Consequently, provided that solutions of the complexes do not become basic at any point, there is no reason to suspect that C-H / C-D exchange will have any effect on the q values (as the C-H bonds will be present in D_2O as well as in H_2O). This is consistent with the NMR observations mentioned above.

This still leaves the question of the difference between the q values obtained using the europium and terbium complexes. This does not simply reflect random error in the measurements as the difference is too consistent: the value calculated using the europium lifetimes is about 0.5 higher than the terbium value in each case. Again, this could be dismissed as arising from the empirical nature of the Horrocks parameters discussed earlier. As before, however, it is preferable to consider the Δk values without recourse to these parameters. Perhaps a more reliable approach would be to compare the Δk values obtained with those of a closely-related model compound where the behaviour is well-understood. The complexes of DOTA are potentially useful here, as it is well-known that all of the lanthanide complexes of DOTA have one metal-coordinated water molecule. The Δk values for the complexes of **33** (as a representative of the amide complexes) and of DOTA, together with the ratios of these values, are shown in Table 3.5. Since Δk should be directly proportional to the number of O-H oscillators in the coordination sphere of the complex (see section 1.3.2) and, since DOTA complexes contain one metal-bound water molecule, these ratios should be equal to the number of inner-sphere water molecules. They might be expected to be

rather more reliable than the q values obtained using the Horrocks numbers, where the method is based on Δk values for structurally unrelated complexes, some having several metal-coordinated water molecules.

As before, non-integral values are obtained, which may be accounted for as discussed above. Again, however, the value for terbium is seen to be significantly smaller than that for europium. This seems to imply that the difference is indeed real. One possibility is that there is a change in the solution structure on going from europium to terbium, the complex of the former having a metal-bound water molecule which is not present in the complex of the smaller terbium ion. Such breaks in structure as the lanthanide series is traversed are not unprecedented. An example is provided by the complexes of the hexadentate polyazapolycarboxylic ligand NOTA where ^{17}O NMR results have shown a water coordination number of 3 for the larger early lanthanides and two for the later elements.¹⁹ However, the behaviour here may be due to the fact that the NOTA ligand is rather too small to accommodate the larger ions efficiently. In the case of octadentate ligands based on 12N_4 , such an abrupt change in the number of coordinated water molecules seems less likely.

TABLE 3.5 Values of Δk , (i.e. $k_{\text{H}_2\text{O}} - k_{\text{D}_2\text{O}}$, where k is the observed rate of depopulation of the emissive state of the metal) for the europium and terbium complexes of 33, 27 and DOTA.

	Δk [Ln.33]	Δk [Ln.DOTA]	Δk [Ln.27]	$\frac{\Delta k \text{ [Ln.33]}}{\Delta k \text{ [Ln.DOTA]}}$
	ms^{-1}	ms^{-1}	ms^{-1}	
Eu	0.68	1.19 ^a	0.15	0.57
Tb	0.05	0.27	0.017	0.19

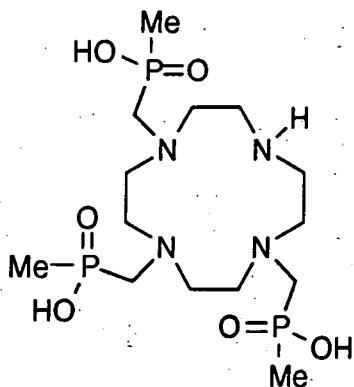
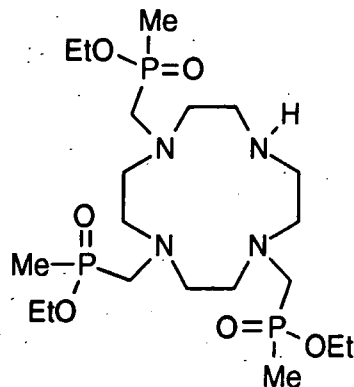
(a) Reference 15.

In fact, there is no need to invoke an abrupt structural change of this sort if the argument proposed earlier to account for the non-integral q values is employed. Thus, the difference in the hydration states for europium and terbium could simply reflect a

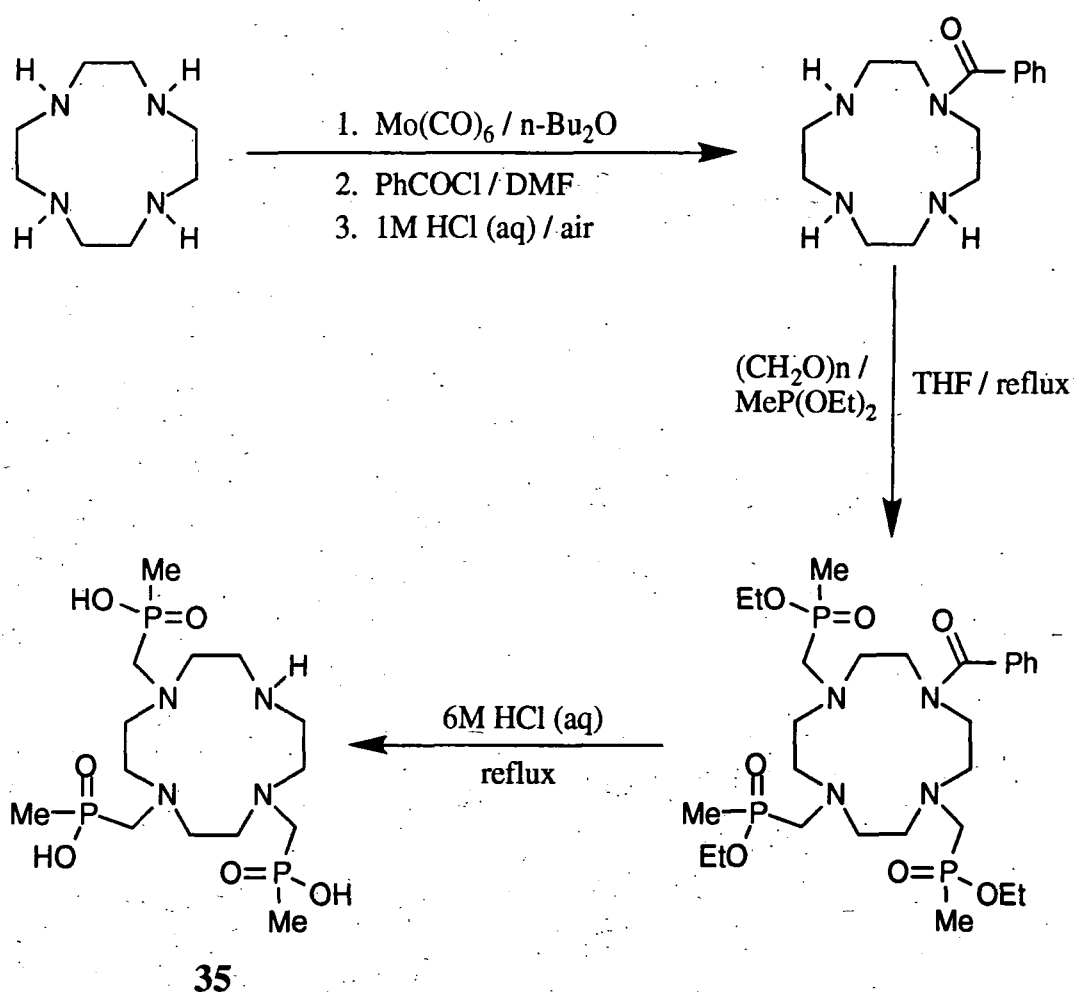
change in the equilibrium distance of the nearest water-molecule. The larger size of europium compared to terbium may allow the water molecule to approach closer to the metal in the Eu^{3+} complex, so that the O-H deactivating effect is proportionately higher. Certainly, the energy transfer into O-H vibrations will be strongly distance-dependent. A theoretical treatment suggests that O-H mediated deactivation of the emissive $^5\text{D}_0$ state will display a dependence on the metal-to-O-H distance which is governed by the J'' level to which the deactivation occurs. A minimum of an r^{-6} dependence is predicted. Thus, it is clear that small changes in the metal-water distances may give rise to quite large differences in the O-H deactivating effect. Such changes are quite plausible as the lanthanide series is traversed and the ions become smaller.

Appendix to Chapter 3: Routes to Trisphosphinate Esters and Acids of 12N_4

Although the synthetic procedure discussed in section 3.2 is ideal for the preparation of mono-amide ligands, it is not so well-suited to the introduction of other substituents such as ketone groups. Thus, although reaction of $[12\text{N}_4.\text{Mo}(\text{CO})_3]$ with RCOCH_2Br , for example, would indeed yield the macrocycle mono-N-alkylated with a ketone group, this could be followed by condensation of the ketone carbonyl group with a neighbouring amine nitrogen in the ring, giving a bicyclic compound. Ideally, the formation of ketone-trisphosphinate esters or acids requires the use of **35** or **36** as intermediates. Two possible routes were investigated.

**35****36**

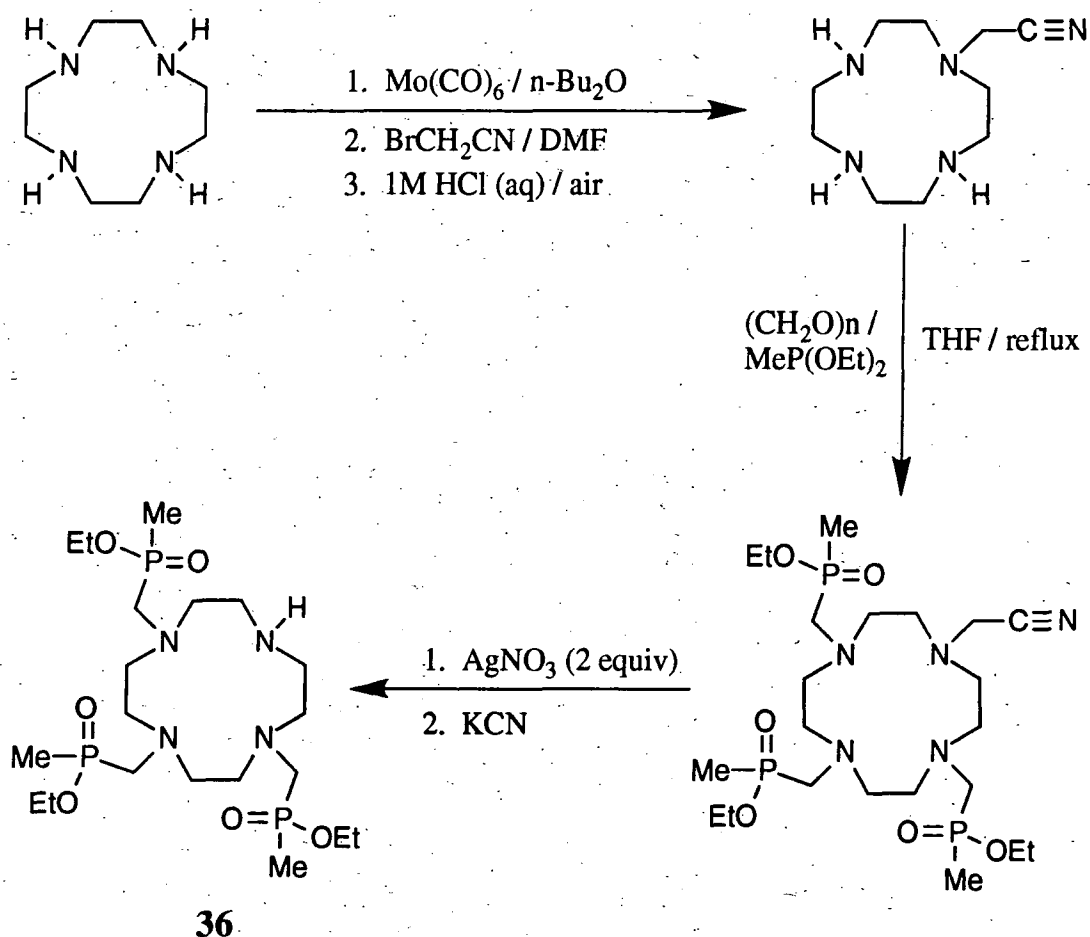
The first of these is shown in Scheme 3.3 and involves the conversion of one of the amine nitrogens of $12N_4$ into an amide, via the $[12N_4.Mo(CO)_3]$ complex. Hydrolysis of the amide was accomplished on refluxing in aqueous 6M HCl which, of course, also leads to hydrolysis of the phosphinate esters. Unfortunately, attempts to N-alkylate the resulting compound (35) with, for example, 2-bromomethylnaphthalene were unsuccessful, possibly owing to the difficulty of deprotonating the amine nitrogen in the presence of the three phosphinic acid groups.



SCHEME 3.3 The synthetic procedure used to obtain the trisphosphinate (35)

The tris-phosphinate ester 36 was recognised as being a more desirable intermediate. Following the report of the use of a cyanomethyl group as a protecting group for an amine, which may be removed on treatment with Ag^+ , the strategy shown in Scheme

3.4 was attempted. Unfortunately, the yield of the monoalkylated product was surprisingly low and the purity of the cyanomethyl-trisphosphinate, after alumina column chromatography, was poor, as judged by proton NMR. Nevertheless, treatment of this compound with two equivalents of AgNO_3 , followed by KCN to precipitate the amine-bound silver ions as AgCN , did indeed result in the conversion of the compound (38) to the desired product (36), as shown clearly by the DCI mass spectra and ^{13}C NMR spectra. Owing to the low purity of the product, however, this strategy was not pursued further.



SCHEME 3.4 The synthetic procedure investigated as a route to the tris-phosphinate ester (36)

References for Chapter 3

1. R. Kataký, K.E. Matthes, P.E. Nicholson, D. Parker and H.-J. Buschmann, *J. Chem. Soc., Perkin Trans. 2*, 1990, 1425.
2. R. Kataký, D. Parker, A. Teasdale, J.P. Hutchinson and H.-J. Buschmann, *J. Chem. Soc., Perkin Trans. 2.*, 1992, 1347.
3. D. Parker, K. Pulukkody, F.C. Smith, A. Batsanov and J.A.K. Howard, *J. Chem. Soc., Dalton Trans.*, 1994, 689.
4. M.S. Konings, W.C. Dow, D.B. Love, K.N. Raymond, S.C. Quay and S.M. Rocklage, *Inorg. Chem.*, 1990, **29**, 1489.
5. J.P.L. Cox, Ph.D. Thesis, University of Durham, 1989.
6. A. Harrison, L. Royle, D. Parker and T. Norman, *Nucl. Med. Biol.*, 1995, *in press*.
7. J.-J. Yaouanc, N. Le Bris, G. Le Gall, J.-C. Clement, H. Handel and H. des Abbayes, *J. Chem. Soc., Chem. Commun.*, 1991, 206.
8. S. Aime, M. Botta and G. Ermondi, *Inorg. Chem.*, 1992, **31**, 4291.
9. S. Aime, L. Barbero, M. Botta and G. Ermondi, *J. Chem. Soc., Dalton Trans.*, 1992, 225.
10. A. Botsi, K. Yannakopoulou, E. Hadjoudis and B. Perly, *J. Chem. Soc., Chem. Commun.*, 1993, 1085.
11. A.F. Casy and A.D. Mercer, *Magn. Reson. Chem.*, 1988, **26**, 765.
12. D. Greatbanks and R. Pickford, *Magn. Reson. Chem.*, 1987, **25**, 208.
13. J.-C.G. Bünzli in 'Lanthanide Probes in Life, Chemical and Earth Sciences', eds: J.-C.G Bünzli and G.R. Choppin, Elsevier: Amsterdam, 1989. Chapter 7.
14. M. Albin and W. DeW. Horrocks, Jr., *Inorg. Chem.*, 1985, **24**, 895.
15. C.C. Bryden and C.N. Reilley, *Anal. Chem.*, 1982, **54**, 610.
16. W. DeW. Horrocks, Jr. and D.R. Sudnick, *Acc. Chem. Res.*, 1981, **14**, 384.
17. L. Prodi, M. Maestri, R. Ziessel and V. Balzani, *Inorg. Chem.*, 1991, **30**, 3798.

-
18. M.-R. Spirlet, J. Rebizant, J.F. Desreux and M.-F. Loncin, *Inorg. Chem.*, 1984, **23**, 359.
 19. A.D. Sherry, M. Singh and C.F.G.C Geraldes, *J. Mag. Reson.*, 1986, **66**, 511.

Chapter 4

CHAPTER 4

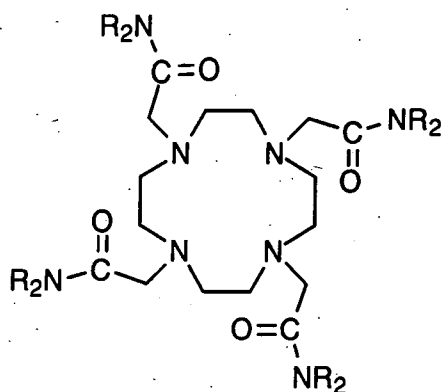
Luminescence Properties of Tetraazamacrocyclic Ligands Incorporating Four Pendent Amide Arms and Their Complexes with Lanthanides and Other Ions

4.1 Introduction

The subject of fluorescence detection of metal ions was introduced in Chapter 1. It was pointed out that many of the systems which have been studied to date comprise simple fluorescent aryl groups, as reporter units, linked to polyamine or polyoxo ionic receptors. The basis of their operation lies in the fact that the binding of a metal ion may disfavour the rate of amine-to-aryl photoinduced electron transfer as a quenching process, with a resulting enhancement of the fluorescence intensity. This effect arises from a perturbation of the amine oxidation potential on binding of metal ions or protons and is discussed in more detail in subsequent sections. The further development of such systems lies in the pursuit of two important goals, namely a search for more *selective* ionic or molecular receptors which may be coupled to suitable lumophores and, secondly, the extension of the applicability of such systems to allow their use in aqueous media or at an aqueous interface in neutral or acidic conditions. It is only with the attainment of these objectives that development for clinical or environmental monitoring applications becomes realistic.

It is clear from the preceding chapters that N-substituted octadentate ligands based on the 1,4,7,10-tetraazacyclododecane ring are predisposed to bind large metal ions that favour a coordination number of 8. Such behaviour is not just confined to systems bearing acidic pendent groups such as DOTA and the tetraphosphinates. Ligands bearing four amide groups, such as **37** and **38** for example, show related coordination properties. Such ligands are particularly versatile, forming complexes of high stability with a number of different metal ions, especially those which prefer a square antiprismatic geometry. Thus, ligand **37** has been found to display a marked preference for Ca^{2+} over alkali metal ions¹ ($\log K_{\text{ML}}$ for the Ca^{2+} complex is 6.80 at 298K, 0.1 M

NMe₄NO₃), whilst complexation of lanthanides by **38** has been investigated.^{2,3,5} A stability constant of 10.05 has been measured for the gadolinium complex (298K, 0.1M NaNO₃).⁵ This ligand also binds strongly the toxic metal ions Cd²⁺ and Pb²⁺, with a lower limit of 19 for log K_{ML}.^{4,5} In terms of stability constants, high selectivity over zinc is observed, for which a much lower value of 10.47 was obtained under the same conditions.⁵ Importantly, these values apply to aqueous solution and, indeed, for lead and cadmium, complexes were fully formed even at pH 0.3.



37 R = Me

38 R = H

With these points in mind, a series of 12N₄-based tetraamide ligands have been prepared bearing one or more naphthyl groups in differing arrangements. These are shown in Figure 4.1. The effect of metal complexation on their fluorescence properties has been investigated. The europium and terbium complexes of these ligands have also been prepared where both the metal luminescence and the naphthyl fluorescence behaviour have been studied. This aspect is discussed in the second half of the chapter.

4.2 Ligand Syntheses

The mononaphthyl ligand **39** was prepared using a similar strategy to that for the amide-trisphosphinates in Chapter 3. Thus, selective protection of three of the four nitrogen atoms of 12N₄ was achieved through formation of the molybdenum tricarbonyl complex, as discussed in section 3.2. Alkylation of the fourth nitrogen atom with chloro-N-2-(naphthylmethyl)ethanamide **43** in dimethylformamide yielded the monosubstituted cycle **44** (Scheme 4.1). Subsequent reaction with 3 equivalents of

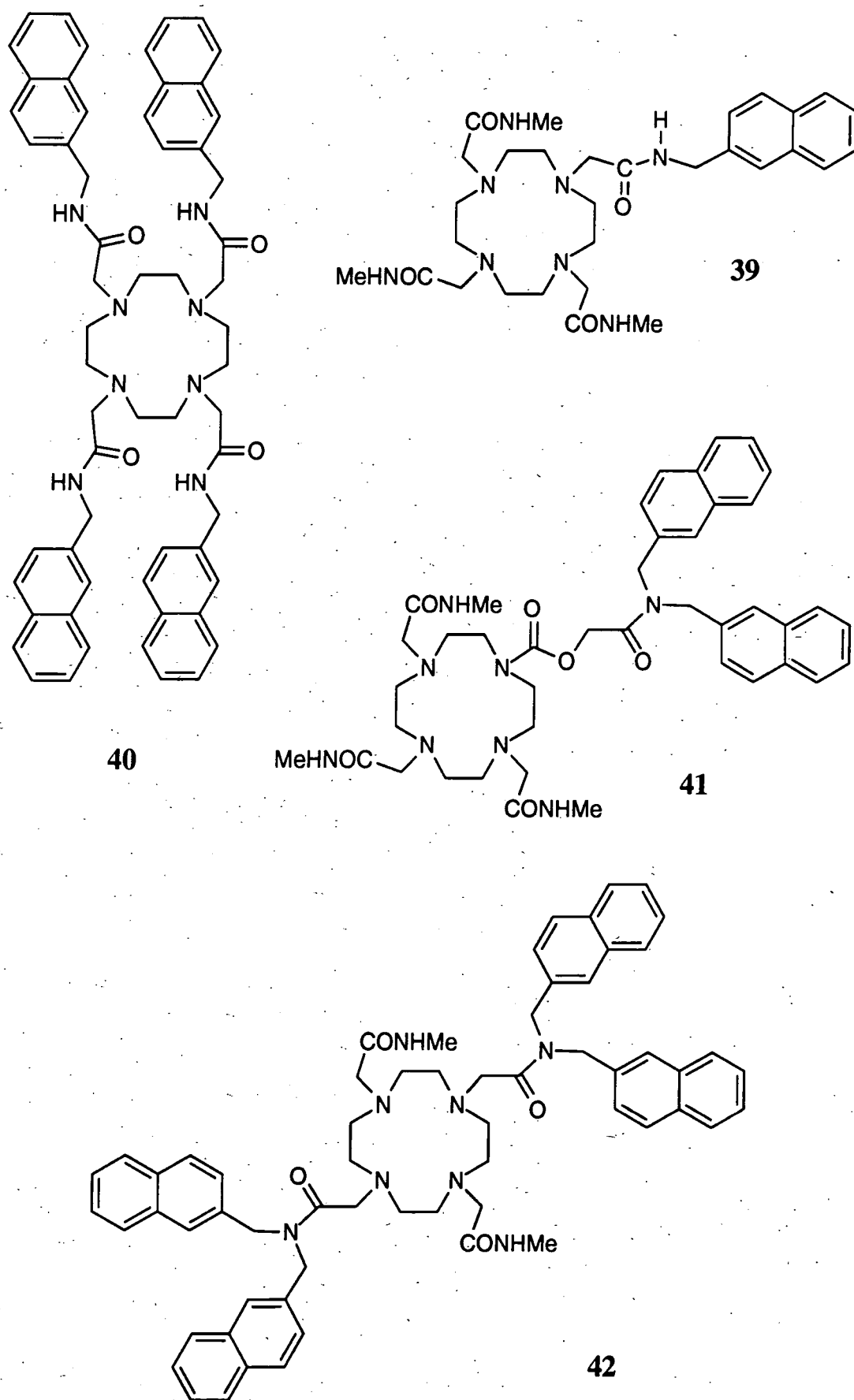
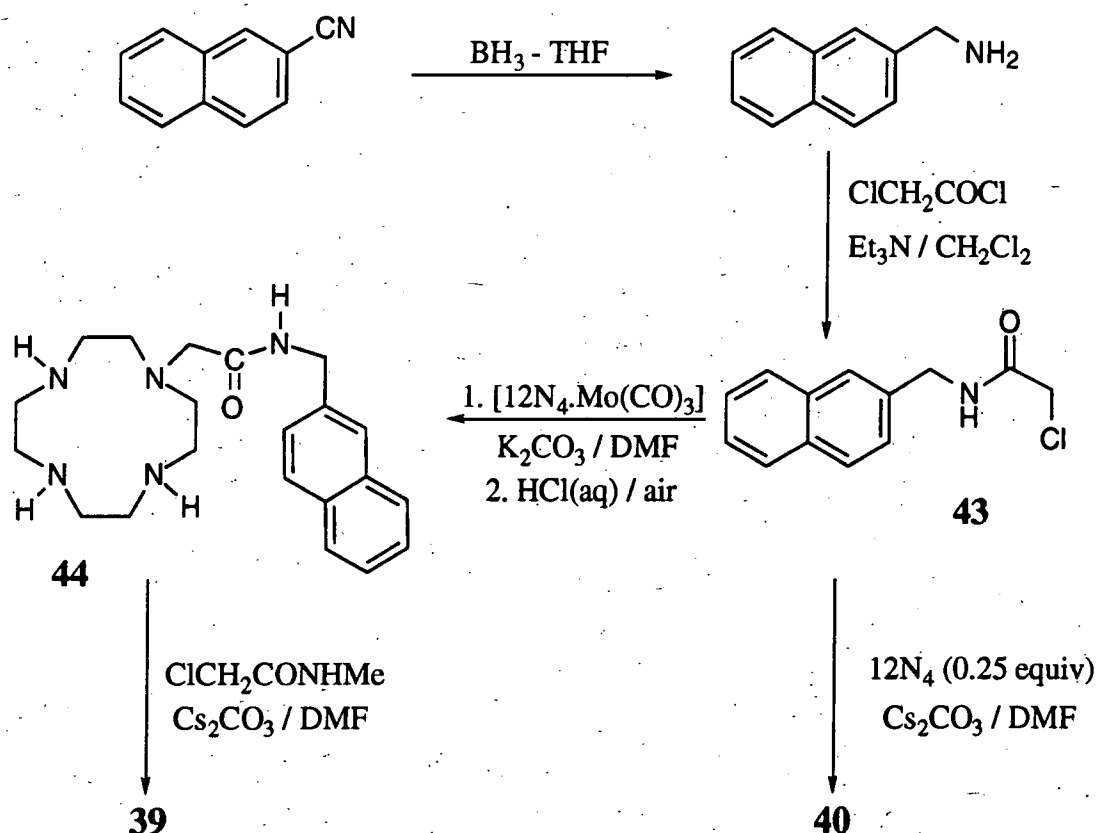


FIGURE 4.1 Structures of the naphthyl-containing ligands described in this Chapter

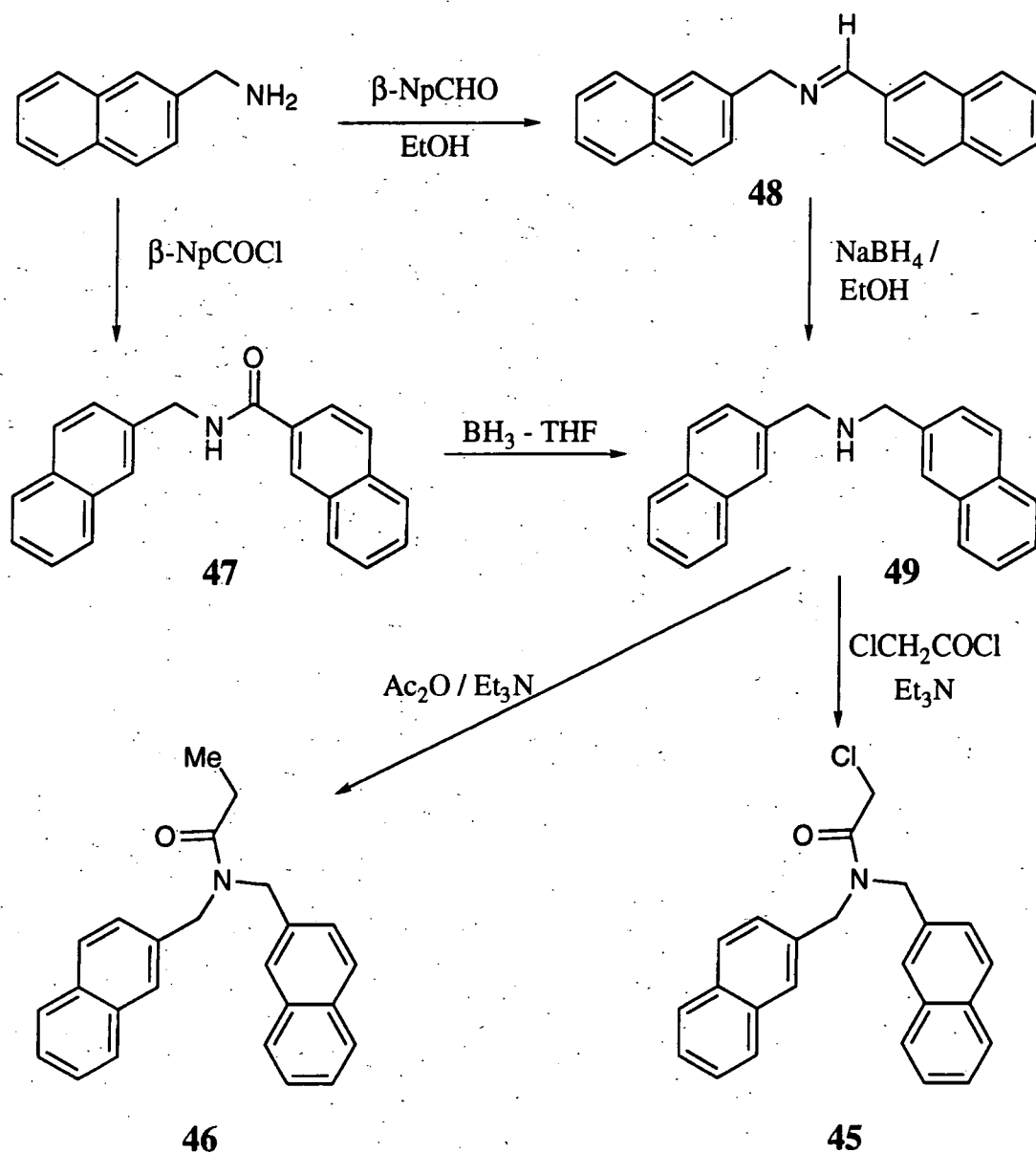
chloro-*N*-methylethanamide in dimethylformamide in the presence of Cs_2CO_3 gave the tetraamide **39**, which was purified by chromatography on neutral alumina. The naphthyl alkylating agent itself (**43**) was prepared from 2-aminomethylnaphthalene as shown in Scheme 4.1. The latter was readily obtained through reduction of 2-cyanonaphthalene with borane-THF complex.

The tetranaphthyl amide ligand **40** was prepared in 71% yield by direct reaction of 12N_4 with **43** in DMF in the presence of caesium carbonate and precipitated as a fine, colourless solid. It may be noted that the use of $\text{EtOH} / \text{Et}_3\text{N}$ as solvent and base in place of $\text{DMF} / \text{Cs}_2\text{CO}_3$ led only to a mixture of di- and tri-alkylated material. The compound **40** displayed extremely limited solubility in all common solvents but, when protonated by adding one or more equivalents of an acid (eg. TFA, AcOH, triflic acid or HPF_6), dissolved readily in organic solvents and, to an appreciable extent also in water.



SCHEME 4.1 The synthetic procedure used in the preparation of ligands **39** and **40**

The introduction of a bis-naphthyl fragment onto $12N_4$ (as in **41** and **42**) necessitated the preparation of the bis-naphthyl amide **45** (Scheme 4.2). Two routes to this compound were investigated, as shown in Scheme 4.2. The first of these, on the left hand side of the scheme, entailed the reaction of 2-aminomethylnaphthalene with β -naphthoyl chloride. Unfortunately, borane reduction of the resulting amide **47** did not proceed satisfactorily and only a small amount of the bis-naphthyl amine **49** was isolated. The use of $LiAlH_4$ may have proved to be preferable for this reduction.



SCHEME 4.2 Illustrating the two routes to the bis-naphthyl alkylating agent **45**

However, an alternative high-yielding strategy was adopted instead, involving the intermediacy of the bis-naphthyl imine **48**, prepared in quantitative yield by reaction of 2-aminomethylnaphthalene with 2-naphthaldehyde. Reduction of the imine with NaBH_4 gave the bis-naphthyl amine **49** in high yield. Acylation in the usual manner provided the required compound **45** or the model compound **46**.

Alkylation of the $\text{Mo}(\text{CO})_3$ complex of 12N_4 with the bis-naphthyl chloroamide **45** was expected to proceed in the usual manner to provide the intermediate monoalkylated system **50** (Figure 4.2). However, a most curious reaction was found to occur in this case: the compound **51** was isolated, where there had been an apparent insertion of " CO_2 " giving a carbamate. Moreover, the reaction was repeatable when a second attempt was made using freshly prepared starting materials.

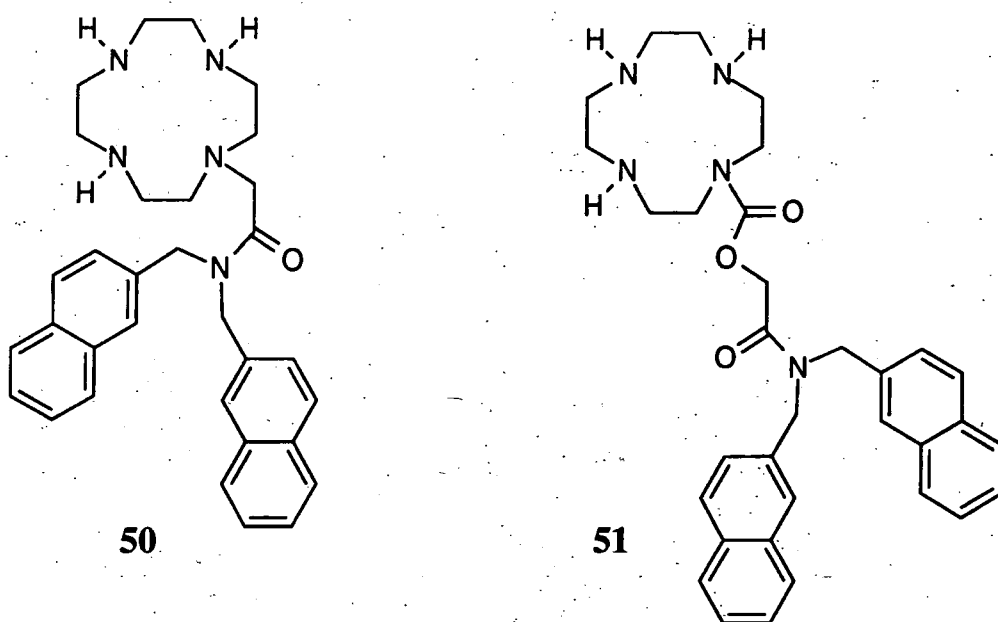


FIGURE 4.2 *The expected product (50) and the product obtained (51) on reaction of $[12\text{N}_4.\text{Mo}(\text{CO})_3]$ with 45.*

The mechanism of this strange reaction remains unclear. One possible explanation would involve the migration of one of the carbonyl groups of $[12\text{N}_4.\text{Mo}(\text{CO})_3]$ to the nitrogen of the ring. However, this still requires a second oxygen atom, the source of which is uncertain, but could possibly arise from trace water. Potassium carbonate is

used as the base in this reaction and could conceivably be a source of CO_2 . On the other hand, 1.5 equivalents was used and so the product of reaction with H^+ should be HCO_3^- with no further reaction to give CO_2 . A possible means of determining whether a carbonyl group of the $\text{Mo}(\text{CO})_3$ moiety is involved would be to prepare $[\text{12N}_4\text{Mo}(\text{13CO})_3]$ and examine whether or not the ^{13}C nucleus becomes incorporated into the carbamate.

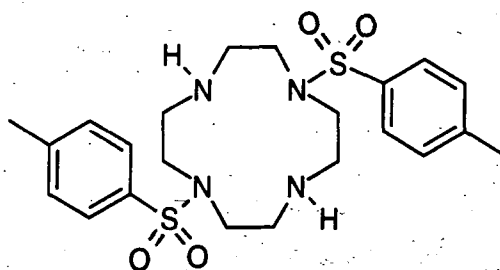
An alternative explanation is that the bis-naphthyl amide is so hindered that reaction had not actually occurred when the work-up procedure commenced. The first step of the work-up involves stirring the residue in aqueous HCl (1M). Clearly, the action of acid on the potassium carbonate will result in generation of $\text{CO}_2(\text{aq})$ which could possibly react with the free ring nitrogen giving $\text{R}_2\text{N-CO}_2^-$. This would be expected to undergo rapid decarboxylation under acidic conditions, but an alternative fate would be alkylation by the chloroamide **45**, thereby leading to **51**. This does not seem a very convincing explanation.

There is a third, rather naïve possibility, again assuming that reaction had not occurred initially. It has been reported that carbamates $\text{R}_2\text{NCOOR}'$ can be obtained from secondary amines R_2NH on treatment with CO , O_2 and an alcohol $\text{R}'\text{OH}$ in the presence of platinum and iodide ion.⁶ This bears some relation to the present instance, where an amine, O_2 and a source of CO are present, together with an alkyl halide which may undergo hydrolysis to give the alcohol. Of course, such an analogy would require that the combination of Mo and Cl^- could function in a similar manner to Pt and I^- and, on the basis of the proposed mechanism, this seems unlikely. Moreover, the cited reaction requires the use of high pressures of CO and O_2 .

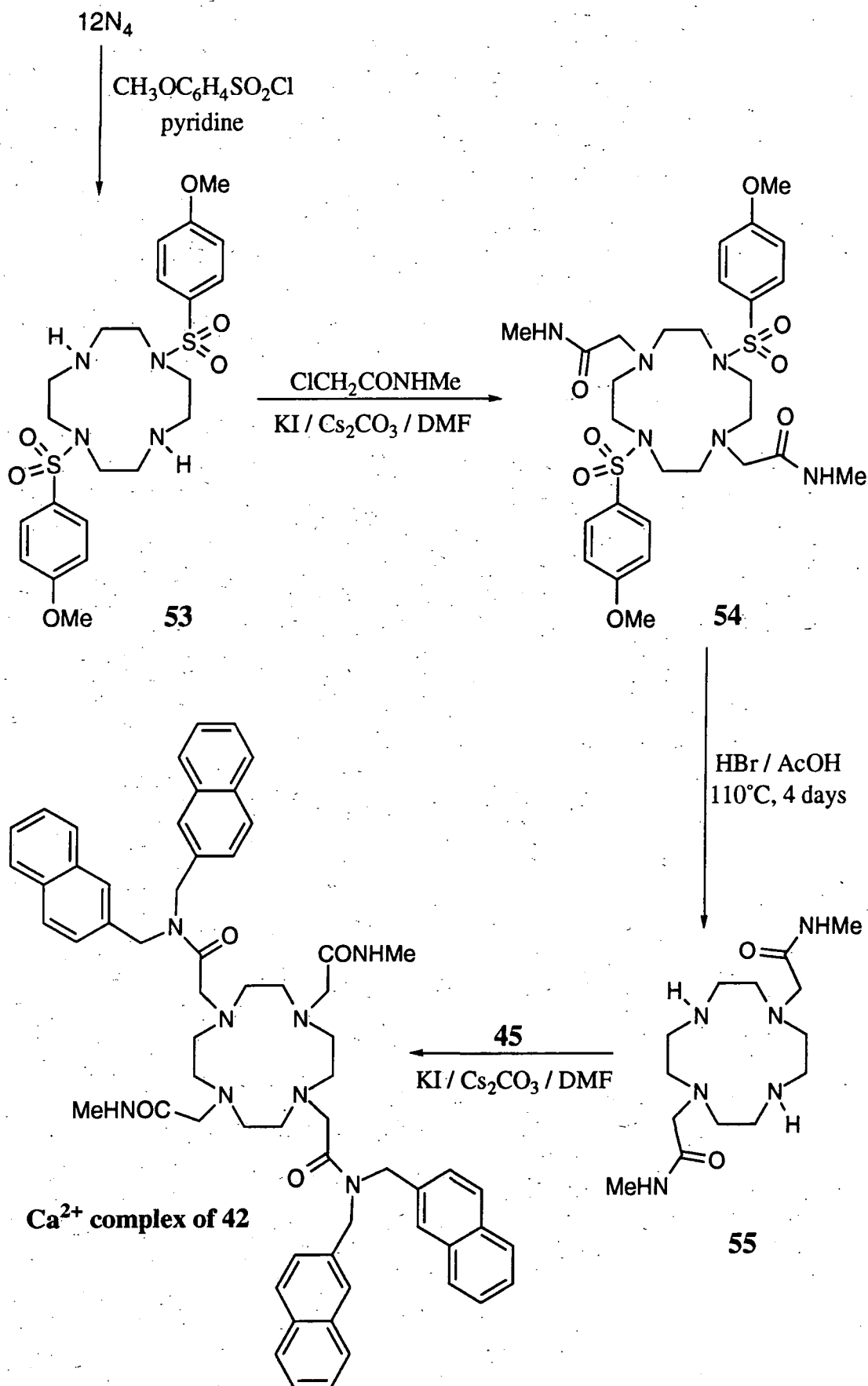
Irrespective of the mechanism of the reaction, the compound **51** was the product. In fact, purification at this stage by preparative HPLC was not completely successful and some $(\text{NpCH}_2)_2\text{NCOCH}_2\text{OH}$ remained. However, reaction with 3 equivalents of

MeNHCOCH₂Cl led to the compound **41**, the purification of which proved to be straightforward using silica column chromatography.

Ligand **42** is related to **40** in that it contains 4 naphthyl groups but, in this case, they are arranged as two pairs bound to *trans*-related nitrogen atoms of the ring. The synthesis of such a system clearly requires the selective protection of two such *trans*-related nitrogens allowing the other two to be alkylated first, either with **45** or with MeNHCOCH₂Cl. Desreux has reported that reaction of 12N₄ with two equivalents of toluenesulfonyl chloride in pyridine leads exclusively to the *trans*-functionalised compound **52**.⁷ This effect is specific to pyridine as the solvent, for reasons which are not clear. The use of other solvents (eg. CHCl₃ with Et₃N as the base) gives the usual mixtures of mono-, di- (*cis* and *trans*), tri- and tetra-alkylated material. Since the tosyl groups can subsequently be removed using, for example, concentrated H₂SO₄ or HBr / AcOH or by means of a dissolving metal reduction, the use of pyridine then provides a means for the selective protection of the 1 and 7 positions of 12N₄.

**52**

With this in mind, the compound **53** (Scheme 4.3) was prepared by an analogous procedure using 4-methoxybenzenesulfonyl chloride. This compound is likely to display some advantage over **52** in that the 4-methoxybenzenesulfonamides are generally more sensitive to acid cleavage than the tosyl analogues. Clearly, the bis-naphthyl amide **45** is a much more valuable reagent than MeNHCOCH₂Cl (which is simply prepared from methylamine and chloroacetylchloride). Hence, **53** was alkylated with the latter as shown in Scheme 4.3, thereby postponing the use of **45** until the end



SCHEME 4.3 The synthetic procedure for the preparation of ligand 42

of the sequence. Deprotection was subsequently achieved by treatment with a 33% solution of HBr in AcOH at 110°C for 4 days. The use of lower temperatures and shorter reaction times failed to provide complete removal of the sulfonamides. Although reaction with HBr / AcOH did indeed result in formation of the desired intermediate **55**, a significant proportion of the monoamide was also formed (ca. 20%) even though the purity of **54** had been high. This curious result has since been observed independently in the group. Fortunately, it proved possible to separate the required compound **55** by precipitation from toluene, giving a colourless solid.

Reaction of the bis amide **55** with the bis-naphthyl chloroamide **45** was carried out in dimethylformamide in the presence of caesium carbonate, in the expectation that the desired ligand **42** would be formed. Potassium iodide was added in an attempt to catalyse the reaction and the product was purified by silica column chromatography. Astonishingly, the compound isolated was the Ca^{2+} complex of the required ligand, with iodide as the counterion, as evidenced by the elemental analysis (C, H, N, I, Ca) and the positive ion electrospray mass spectrum, which consistently displayed a 100% peak at 515 (mass of $[\text{42.Ca}]^{2+} = 1030$). This is a remarkable result and seems to indicate that the ligand had leached out trace Ca^{2+} from the silica during chromatography. The kinetics of dissociation must be very slow, perhaps reflecting the steric bulk of the four naphthyl groups and the restricted rotation about the N-C(O) bonds at room temperature. This latter point was clearly apparent from the variable temperature ^1H NMR spectra of the compound in d_6 -DMSO (400 MHz). At 25°C, 4 broad signals, each of relative intensity 2, were observed between 4.4 and 5.2 ppm due to the non-equivalence of the 4 sets of $\text{NCH}_2\text{C}_{10}\text{H}_7$ protons. By 70°C, the resonances had coalesced to give a single signal at 4.81 ppm. Similarly, two resonances were observed for the $\text{NCH}_2\text{CON}(\text{CH}_2\text{C}_{10}\text{H}_7)_2$ protons at low temperature but these had also coalesced by 70°C. Removal of the calcium was achieved through treatment with acid to induce dissociation, followed by re-complexation by DOTA, which forms a water-soluble complex of exceptionally high thermodynamic stability with Ca^{2+} ($\log K_{\text{ML}} = 17.2$ (H_2O , 298K)⁸).

4.3 UV absorbance spectra of 39 - 42

The UV absorbance spectra of the four ligands all resembled that of naphthalene, $\lambda_{\max} = 276$ nm (Figure 4.3) and extinction coefficients were consistent with the number of naphthyl groups present. There were no significant differences in water compared to acetonitrile and there was no evidence for any additional bands arising from interaction of ground state naphthalene groups in ligands 40 - 42.

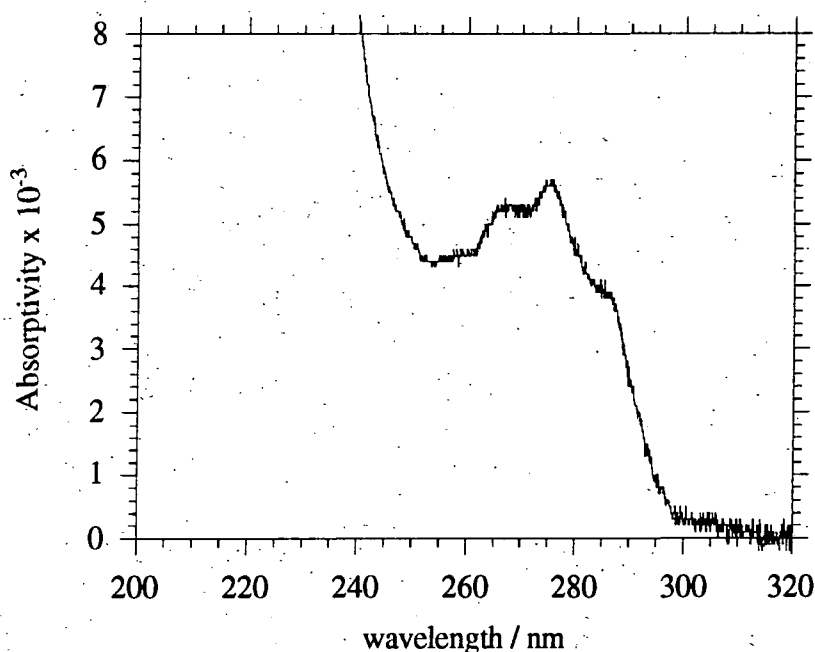


FIGURE 4.3 UV absorbance spectrum of ligand 39 in MeCN acquired at high resolution.

4.4 Fluorescence of 39

Ligand 39 contains a single naphthyl group. Its fluorescence spectrum on excitation at 270 nm in acetonitrile closely resembled that of naphthalene, $\lambda_{\max}^{\text{em}} = 337$ nm (see Figure 4.9). Addition of an excess of trifluoroacetic acid to 39 in acetonitrile resulted in a 50% increase in the fluorescence intensity. This behaviour can be interpreted in terms of the theory outlined in Chapter 1, whereby fluorescence quenching may occur through intramolecular photoinduced electron transfer from an amine nitrogen to the excited aryl group. Protonation of the nitrogen raises the amine oxidation potential, thereby

disfavouring the reduction of the aryl excited singlet state, leading to an enhancement in the fluorescence intensity.

The theory of Rehm and Weller⁹ may be used to attempt to provide a rather more quantitative description of this effect. As in some related theories,¹⁰ it is proposed that there exists a relation between the activation energy change, ΔG^\ddagger , for the charge transfer reaction and the final, overall free energy change, ΔG , thereby allowing the rate constant for charge transfer to be related to ΔG . The extent to which electron transfer is able to compete with fluorescence is then directly related to ΔG . It is proposed that the value of ΔG associated with the electron transfer process is determined by the difference in the energy of the excited singlet state of the chromophore and that required to bring about the electron transfer process, as calculated from the appropriate reduction and oxidation potentials. An additional term also has to be taken into consideration, namely the attractive potential energy between the radical ion pair formed, $-e^2/\epsilon r$, which favours the PET process. The Weller equation for the combination of an amine and an aryl group is then:

$$\Delta G_{\text{ET}} = F \{ [E_{\text{ox}}(\text{amine}) - E_{\text{red}}(\text{aryl})] - E_s - (e^2/\epsilon r) \} \quad \text{J mol}^{-1} \quad (43)$$

where E_{ox} (amine) is the oxidation potential of the amine group (V), E_{red} (aryl) the reduction potential of the aryl group (V), E_s is the singlet energy in eV and F is the Faraday constant. 2-Methylnaphthalene is perhaps a suitable model for the naphthyl group in **39**. Reference to Table 4.1 shows that $E_{1/2}^{\text{red}}$ for this compound is -2.460 V and the first excited singlet state energy is 3.87 eV. The amine groups in compound **39** might be expected to display oxidation potentials of similar magnitude to that of triethylamine, for which $E_{1/2}^{\text{ox}}$ is 1.15V (in CH_3CN versus SCE). Finally, the parameter $e^2/\epsilon r$ is likely to be of the order 0.1 - 0.2 eV. On this basis, ΔG_{ET} is predicted to be about -34 kJ mol^{-1} . Clearly, this is only a very rough-and-ready value as all of the quantities involved are solvent dependent and may display quite different values in the real system as compared to the model compounds, but it does perhaps

serve as some guide. Protonation of the amine nitrogen atoms, or complexation by a metal ion, will inevitably result in a substantial increase in the amine oxidation potential, possibly even to the extent that ΔG becomes positive and the electron transfer process thermodynamically unfavourable. Clearly, since the electron transfer process results in a deactivation of the excited singlet state, any process that disfavours electron transfer (eg. protonation) should lead to an increase in fluorescence intensity, as observed.

In water, the fluorescence intensity of **39** was significantly greater than in acetonitrile. Quantum yields of 3.10 and 1.39 were obtained respectively, relative to naphthalene in aerated acetonitrile. In part, this may be accounted for by the fact that two of the ring nitrogens will be protonated in water at pH 7 (the first two pK_a for **39** are about 11

TABLE 4.1 *Some useful photophysical data for naphthalene in non-polar benzenoid solvents, values for polar solvents in parenthesis (compiled from references 11 and 12)*

	Singlet	Triplet
Energy / kJ mol^{-1}	385 (384) ^e	253 (255) ^f
Lifetime	96 (105) ^g ns	175 (1800) μs
ϕ_{fl} or ϕ_{T} (a)	0.19 (0.21) ^h	0.75 (0.80) ⁱ
$k_{\text{Q}}^{\text{O}_2} / \text{M}^{-1}\text{s}^{-1}$ (b)	2.7×10^{10} (cyclohexane) ^j	1.5×10^9 (PhH) 2×10^9 (MeCN)
$\lambda_{\text{S}}(0-0)$ or $\lambda_{\text{T}}^{\text{max}}$ / nm (c)	311	425 (415)
		$\epsilon = 13\,200$ (24\,500)

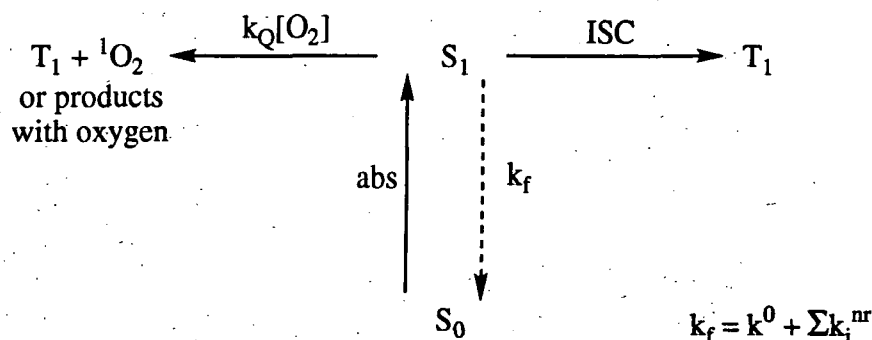
$E_{1/2}^{\text{ox}}$, CH_3CN versus SCE (d): +1.70 V^k

$E_{1/2}^{\text{red}}$, 75% dioxane-water versus SCE (d): -2.437 V^l

(a) ϕ_{fl} is the fluorescence quantum yield of the first excited singlet state; ϕ_{T} the quantum yield for triplet formation. (b) $k_{\text{Q}}^{\text{O}_2}$ is the bimolecular rate constant for quenching by dissolved molecular oxygen. (c) $\lambda_{\text{S}}(0-0)$ is the wavelength of the $v'' = 0 \rightarrow v' = 0$ transition; $\lambda_{\text{T}}^{\text{max}}$ is the wavelength of the absorbance maximum in the triplet-triplet absorption spectrum. (d) redox potentials of the first excited singlet state. Values for 2-methylnaphthalene: (e) 376 (374) kJ mol^{-1} (f) (254) kJ mol^{-1} (g) 59 (47) ns (h) 0.27 (0.16) (i) 0.56 (j) $2.5 \times 10^{10} \text{ M}^{-1}\text{s}^{-1}$ (k) +1.45 V (l) -2.460 V.

and $10^{1,2}$). However, the intensity was also substantially higher than for a solution of the ligand in CH_3CN (20 μM) containing 50 equivalents of trifluoroacetic acid, conditions under which the ligand would also be diprotonated. The explanation probably lies in the effect of dissolved molecular oxygen.

Quenching of triplet states by molecular oxygen is, of course, commonly encountered and was alluded to in Chapter 1. However, under ambient conditions, significant quenching of singlet states (and therefore of fluorescence) by O_2 only occurs for compounds for which the lifetime of the singlet state is relatively long. Scheme 4.4 serves to illustrate this.



SCHEME 4.4

Clearly, the extent to which quenching by oxygen can compete with fluorescence and other non-radiative processes will depend on the relative magnitude of $k_Q[\text{O}_2]$ compared to k_f (where k_f is the observed decay rate in the absence of oxygen). The bimolecular rate constant for quenching by O_2 , k_Q , is of the order $10^{10}\text{M}^{-1}\text{s}^{-1}$ in most organic solvents. Moreover, for typical organic solvents in equilibrium with air at 760 mmHg pressure (i.e. 0.21 atm O_2), the concentration of dissolved oxygen, $[\text{O}_2]$, is usually about $2 \times 10^{-3}\text{M}$. Thus, the rate of quenching by oxygen is of the order of $2 \times 10^7 \text{ s}^{-1}$. Consequently, singlet states with decay rates (k_f) of the order of $10^8 - 10^9 \text{ s}^{-1}$ will not be efficiently quenched under such conditions. Most commonly-encountered fluorescent compounds have lifetimes in the range 1 - 10 ns, such that no significant differences in fluorescence intensity are observed upon degassing solutions of such

compounds. Naphthalene is rather unusual in this respect as it has a particularly long singlet lifetime of about 100 ns (Table 4.1); i.e. $k_f \approx 10^7 \text{ s}^{-1}$. This is seen to be of the same order of magnitude as $k_Q[\text{O}_2]$ and so significant quenching by oxygen is expected in this case. Indeed, upon degassing a solution of the protonated ligand **39** in acetonitrile, the fluorescence intensity increased 3-fold, in line with this prediction. In fact, the difference in fluorescence intensities between aerated and degassed solutions allows an approximate estimate of the fluorescence lifetime (τ_f) for compound **39** to be obtained through application of the Stern-Volmer equation:

$$\frac{\phi_f}{\phi_f^Q} = 1 + \tau_f \cdot k_Q[\text{Q}] \quad (44)$$

where ϕ_f and ϕ_f^Q are the quantum yields in the absence and in the presence of the quenching species and $[\text{Q}]$ is the concentration of the quencher. Since $\phi_f(\text{degassed}) \approx 3\phi_f(\text{aerated})$ and $[\text{O}_2] = 1.9 \times 10^{-3} \text{ M}$ (Table 4.2) then, using a k_Q value of $2.7 \times 10^{10} \text{ M}^{-1} \text{ s}^{-1}$ (Table 4.1), we can crudely estimate τ_f to be 39 ns. Whilst this is rather less than the literature value of 105 ns for naphthalene, it is close to that of 47 ns reported for 2-methylnaphthalene, which is probably the better model anyway.

The above discussion may appear to be irrelevant to the question of the difference in behaviour in water and acetonitrile. However, reference to Table 4.2 shows that this is not the case. It can be seen that the equilibrium concentration of O_2 in water at 760 mmHg air is much smaller than in MeCN. This is perhaps rather counter-intuitive but it has particular significance here. Thus, $k_Q[\text{O}_2]$ is only of the order of $3 \times 10^6 \text{ s}^{-1}$ in water and so quenching by molecular oxygen is much less significant in this solvent. This then probably accounts for the higher fluorescence intensity observed in aqueous solution. Obviously there may be other effects contributing as well, such as a decrease in the efficiency of other non-radiative deactivation pathways in water, although such effects are likely to be of less significance.

It should be noted that the spectra shown in subsequent sections, together with the relative quantum yields reported, apply to aerated solutions unless otherwise stated. This is appropriate since any practical application in mind will necessarily entail the use of the compounds under ambient conditions.

TABLE 4.2 O_2 concentration in solvents

Solvent	Temperature / °C	$[O_2] / 10^{-3} \text{ mol dm}^{-3}$	$[O_2] / 10^{-3} \text{ mol dm}^{-3}$
		(1 atm O_2) ^a	(0.21 atm O_2) ^{a, b}
Acetonitrile	24	9.1	1.9
Ethanol	25	9.92	2.1
Water	20	1.39	0.29
	25	1.27	0.27

(a) From reference 11. (b) Values calculated from those at 1 atm partial pressure of O_2 , assuming Henry's Law holds.

4.5 Fluorescence of 41 and 42

Compounds **41** and **42** were prepared in the hope that they would exhibit excimer emission. This did indeed prove to be the case: in addition to the usual fluorescence band (λ_{max} 337 nm), these compounds displayed a second, unstructured, longer-wavelength band (λ_{max} 397 - 401 nm), attributable to a naphthyl excimer, $[Np\dots Np]^*$. Some background information on the phenomenon of excimer emission is given in Box 4.1. The ratio of excimer to monomer intensities ($I_{\text{ex}} / I_{\text{m}}$) is a useful parameter in such systems. Here, it was found to be independent of concentration in a given solvent (for concentrations $< 10^{-4} \text{ M}$), which is indicative of *intramolecular* excimer formation. In other words, an excited state naphthyl group in the $-N(\text{CH}_2\text{C}_{10}\text{H}_7)_2$ unit is able to interact with the other naphthyl group in its ground state to form the excited dimer. This then subsequently decays to two ground state naphthyl groups, with long wavelength emission characteristic of the dimer.

BOX 4.1 Excimer Emission

The first report of emission from an excimer (an excited dimer) was made by Förster and Kaspar in 1954.¹³ They found that as the concentration of pyrene in cyclohexane solution was increased, the usual structured fluorescence band (λ_{max} 395 nm) gave way to a broad structureless emission with $\lambda_{\text{max}} \approx 480$ nm. This was interpreted in terms of the formation of a complex from 2 pyrene molecules, formally one in its first electronically excited state and the other in the ground state.¹⁴ The process has since been shown to be common to most aromatic hydrocarbons and is illustrated schematically in Figure 4.4.

As two ground state molecules are brought together, they experience a mutual repulsion at small internuclear separations. In contrast, the interaction of an excited state molecule with a ground state molecule results in a net stabilisation at such short distances and a weakly-bound dimer results, characterised by the upper potential energy curve in Figure 4.4. It is clear from the diagram that the emission from such a dimer will be of lower energy than that from isolated excited state monomers. Moreover, since the lower state is repulsive, the molecules fly apart after emission and the observed band therefore shows no vibrational structure.

The stabilisation of an excimer depends strongly on the overlap of the orbitals of the two aryl groups. Theoretical calculations have led to a picture of the excited state complex in which the 2 chromophores are at an optimum distance of 3.5 Å in a plane-parallel orientation.¹⁵

Excimer formation is not confined to intermolecular interactions. *Intramolecular* excimer emission is well-documented, having been reported originally in 1963 by Yanari¹⁶ and by Hirayama,¹⁷ following an examination of the fluorescence spectrum of polystyrene. The intramolecular effect requires that two aryl groups within the molecule can attain an appropriate conformation with respect to one another within the lifetime of the excited state. A number of studies have shown that this is most likely to be achieved if the two groups are separated by 3 methylene (or analogous) units.¹⁸ Excimer emission is often strongly dependent on a number of environmental factors including the viscosity of the solvent and the temperature.¹⁹

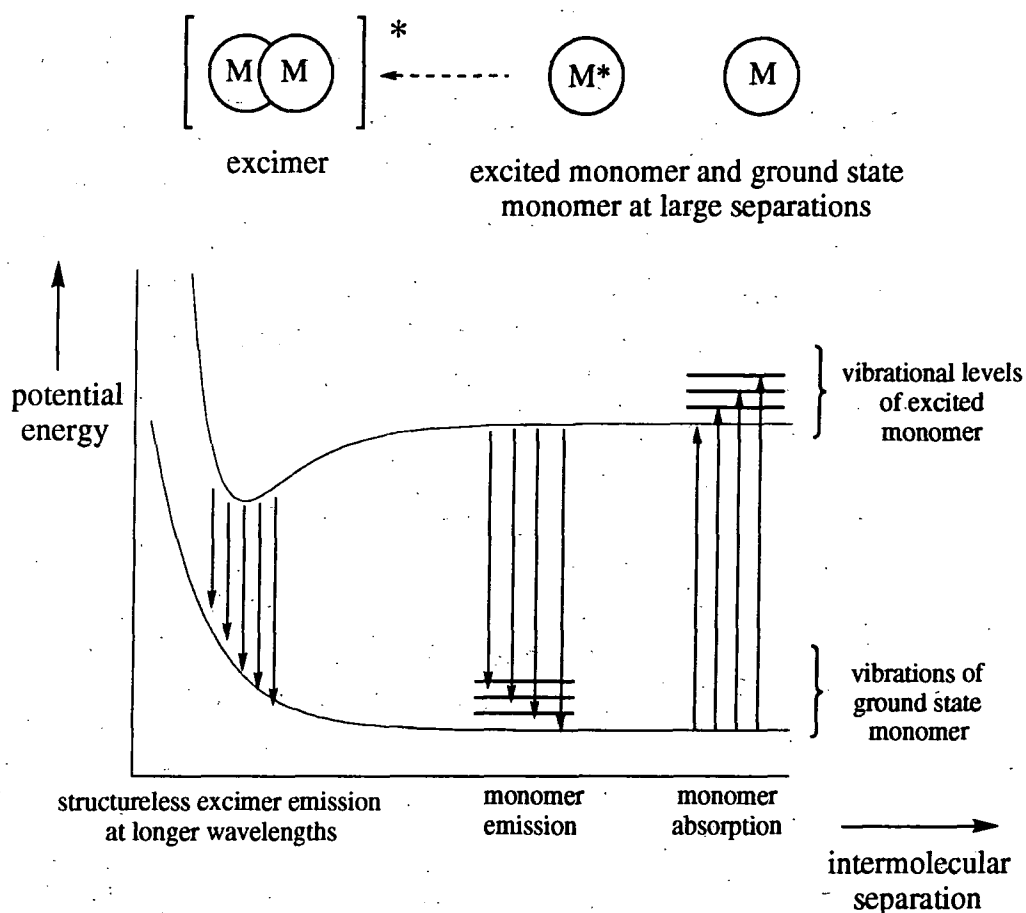
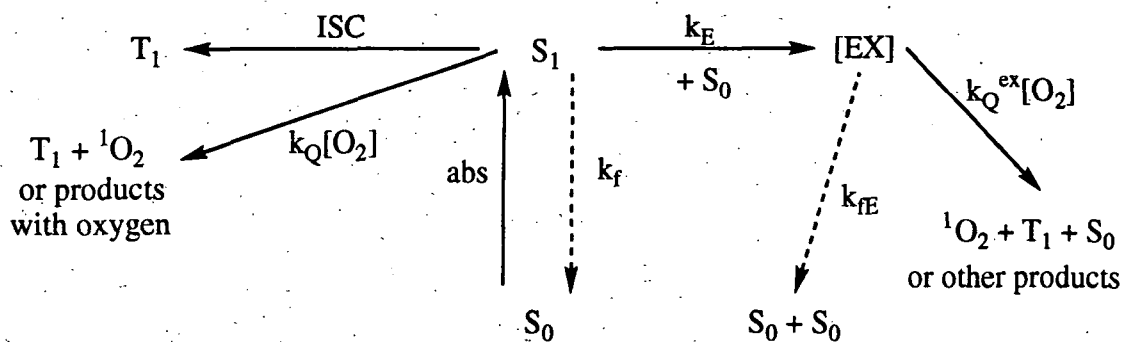


FIGURE 4.4 Schematic illustration of excimer emission in terms of potential energy curves. The lower curve represents the interaction between two ground state molecules and the upper curve that of a molecule in the first excited state with another in its ground state.

For aromatic groups linked by several methylene units, it has generally been found that excimer emission is most likely to be observed when there are three CH_2 groups between the two aryl groups.¹⁸ This reflects the requirement for the naphthyl groups to adopt a mutually plane-parallel arrangement, with an optimum interplanar distance of 3.5 \AA .¹⁵ This conclusion was also expected to apply in the present instance, where there are again three atoms in the linking chain, although of course one of them is now the nitrogen of the amide. The observation of intense excimer emission vindicates this prediction. It is interesting to note in passing that, whilst there has been a good deal of work on intramolecular excimer formation for α -substituted naphthalenes {eg. (α - NpCH_2) $_2\text{NH}_2^+$ }, there is relatively little information available on the β -substituted analogues.

In subsequent discussions, the ratio of the maximum fluorescence intensity of the excimer (between 390 and 401 nm) to that at 337 nm is used as a measure of $I_{\text{ex}} / I_{\text{m}}$. This is not strictly correct, as the two bands overlap to some extent. However, the overlap is small at these two wavelengths and so the approximation is largely justified.

Solutions of **41** and **42** in aerated acetonitrile displayed $(I_{\text{ex}} / I_{\text{m}})$ values of about 1.4 (from the *corrected* emission spectra; Figure 4.5). Degassing of the solutions resulted in a net increase in the fluorescence intensity, as expected, but the excimer band increased to a greater extent, leading to an $I_{\text{ex}} / I_{\text{m}}$ ratio of 2.3. This is consistent with the original observations of Hirayama,¹⁷ who found that oxygen had a more pronounced effect on the excimer in the fluorescence spectra of diphenyl and triphenyl alkanes. In the present instance, there are two possible reasons for the greater increase in the excimer band. Firstly, excimer emission is generally longer-lived than monomer emission. Unfortunately, there is little information available on naphthyl excimer lifetimes but a value of 143 ns has been measured for the *intermolecular* excimer formed by 1,6-dimethylnaphthalene.²⁰ This compares to the value of 47 ns for τ_{f} of 2-methylnaphthalene (Table 4.1). As outlined earlier, the effect of quenching by molecular oxygen is more significant for compounds having long decay lifetimes and will therefore be more significant for the excimer than for the monomer. Secondly, oxygen quenching of the monomer will also result in a decrease in excimer intensity (in addition to the monomer) as this process will be in competition with excimer formation (Scheme 4.5).



SCHEME 4.5

In fact, for $\beta\text{Np}-(\text{CH}_2)_3-\beta\text{Np}$, the rate constant for excimer formation, k_E , has a value of $2.4 \times 10^8 \text{ s}^{-1}$, which compares to $5 \times 10^7 \text{ s}^{-1}$ for $k_Q[\text{O}_2]$ at 760 mmHg and a value of k_f for monomer naphthalene of $2.13 \times 10^7 \text{ s}^{-1}$. These values indicate that the removal of monomer quenching is likely to have a more significant effect on the intensity of monomer fluorescence than on the extent of excimer formation and so the increase in $I_{\text{ex}} / I_{\text{m}}$ probably arises solely from the first explanation, namely the longer lifetime of the excimer.

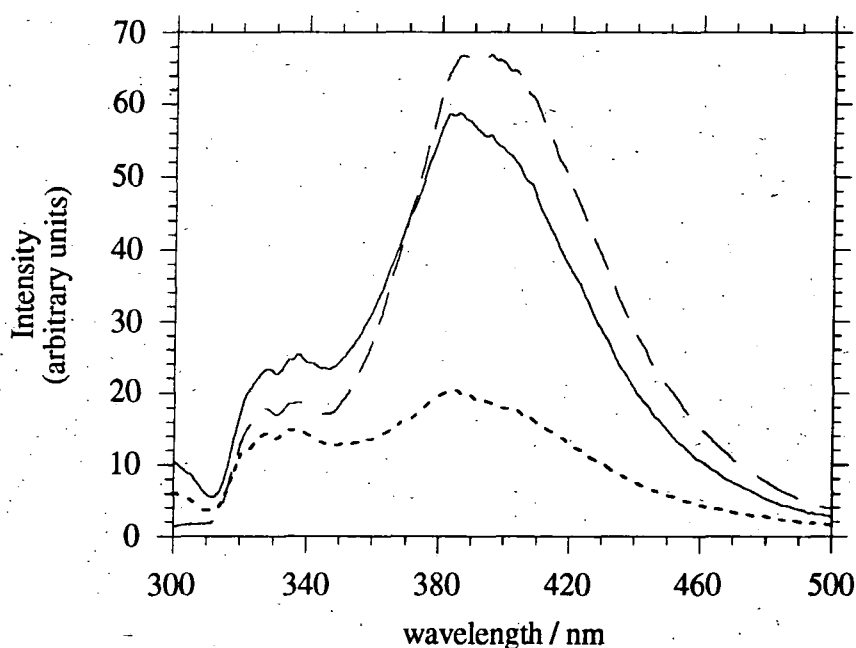


FIGURE 4.5 The fluorescence emission spectrum of ligand **41** in degassed acetonitrile (solid line), aerated acetonitrile (dotted line) and in water (dashed line) at a concentration of 10^{-5} M . Ligand **42** displayed similar behaviour.

In solution in water (90% H_2O / 10% CH_3CN), the $I_{\text{ex}} / I_{\text{m}}$ ratio had a higher value of about 3.5 for both **41** and **42** and also for the model compound **46**. According to the discussion above, a higher $I_{\text{ex}} / I_{\text{m}}$ ratio would be expected in water compared to acetonitrile (under aerated conditions), simply on the basis of the lower oxygen content of water compared to organic solvents under 760 mmHg pressure of air (Table 4.2). Surprisingly, this particular effect of change in solvent appears to have gone unnoticed in previous work on naphthyl excimers, possibly because most of the work has been

carried out in non-aqueous media and perhaps also since most of the comprehensive photophysical work has been carried out using exclusively degassed solutions.

Actually, the effect here of changing from acetonitrile to water must be more profound than simply a change in oxygen concentration alone since $I_{\text{ex}} / I_{\text{m}}$ is still substantially higher in aerated water than in degassed acetonitrile (the values are about 3.5 and 2.3 respectively). The reasons for this are unclear. Intensity measurements on a nanosecond timescale would be required in order to investigate the effect of solvent on the lifetimes of the monomer and excimer and the rate of excimer formation, k_{E} . It is possible that the excimer is stabilised slightly in water relative to CH_3CN (the emission maxima were at 396 and 391 nm respectively) which might be reflected in an increase in k_{E} in water.

4.6 Fluorescence of 40

The fluorescence spectrum of **40** ($5 \mu\text{M}$ in CH_3CN) in the presence of added protons ($\geq 30 \text{ mM}$) displayed not only the expected monomer emission at 337 nm but also a broad, structureless band centred at 401 nm, again typical of a naphthyl excimer and characterised by an excitation spectrum identical to that of the monomer. The relative intensity of excimer and monomer emission bands ($I_{\text{ex}} / I_{\text{m}}$) was independent of ligand concentration in the range $0.5 - 50 \mu\text{M}$ and was also insensitive to the nature of the acid used (eg. trifluoroacetic acid, trifluorosulfonic acid, AcOH , HPF_6). This behaviour is consistent with formation of an intramolecular excimer, requiring a plane-parallel conformation of two naphthyl groups in the protonated ligand, with an interplanar separation of the order of 3.5 \AA .

The value of $I_{\text{ex}} / I_{\text{m}}$ for protonated **40** in aerated acetonitrile was 0.6. Upon degassing of this solution, the total fluorescence intensity was substantially increased, as expected in light of the earlier discussions (section 4.4). However, in this case, degassing barely had any effect whatsoever on the $I_{\text{ex}} / I_{\text{m}}$ ratio, in complete contrast to the bis-naphthyl compounds **41** and **42**. The reason for this intriguing difference is not clear but it

would appear to indicate that in the present instance, there is relatively little difference in the lifetimes of the monomer and excimer. Clearly, decay measurements on a nanosecond timescale at 337 nm and 401 nm would be required to confirm or disprove this possibility. However, it is interesting to note that where data are available, intermolecular excimers generally exhibit lifetimes which are substantially shorter than those of their intramolecular analogues. An example is provided by pyrene, where the intermolecular excimer has a lifetime of 67 ns²¹ compared to 140 ns for the intramolecular case in 2-pyr-CH(CH₃)-CH₂-CH(CH₃)-2-pyr.²² It does not seem unreasonable to suppose that the excimer in ligand **40** may show behaviour more akin to an intermolecular excimer than the intramolecular systems of **41** and **42** (it does, after all, have a large number of atoms intervening between each pair of naphthyl groups). This might then account for the different observations concerning the effect of oxygen on $I_{\text{ex}} / I_{\text{m}}$.

The relative intensities of the excimer and monomer bands was again found to be much higher in water than in acetonitrile (Figure 4.6). In fact, the change here was much greater than for the bis-naphthyl compounds, with an $I_{\text{ex}} / I_{\text{m}}$ value of 3.3 (compared to 0.6 in CH₃CN). On the basis of the above discussion concerning degassed and aerated solutions in acetonitrile, it is clear that such a change *cannot* be attributed here to the lower oxygen concentration in water. This was further apparent from a study of $I_{\text{ex}} / I_{\text{m}}$ in a number of other solvents, where the ratio displayed no correlation whatsoever with the literature values for equilibrium oxygen concentrations under ambient conditions. Clearly, there must be other effects at work here. In fact, there is quite a reasonable correlation between the percentage of excimer emission and the polarity of the solvent, as measured by Reichardt's normalised $E_{\text{T}}(30)$ scale²³ (Figure 4.7). The more polar solvents, with a high E_{T} value, displayed the most excimer emission. Somewhat similar behaviour has been noted for a tetrapyrenyl-18-crown-6 tetraamide, where it was observed that the proportion of excimer emission was higher in polar solvents such as MeOH than in non-polar media (eg. THF).²⁴ No explanation for this behaviour was provided. In contrast, a bis-pyrenyl functionalised calixarene displayed stronger

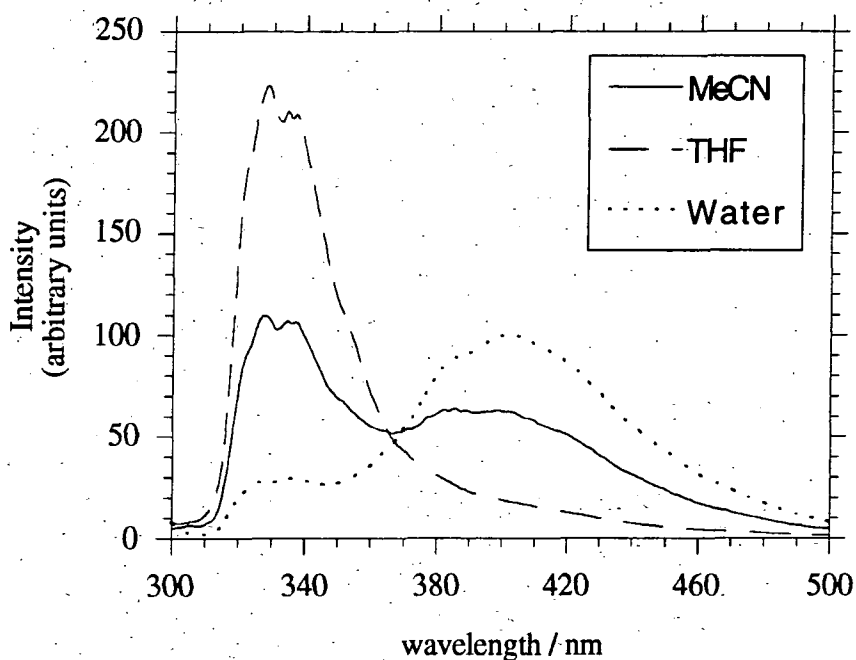


FIGURE 4.6 Corrected fluorescence emission spectra for **40** in MeCN (solid line), THF (dashed line) and water (dotted line). $[40] = 5 \mu\text{M}$, $[\text{CF}_3\text{CO}_2\text{H}] = 250 \mu\text{M}$, $\lambda_{\text{exc}} = 270 \text{ nm}$.

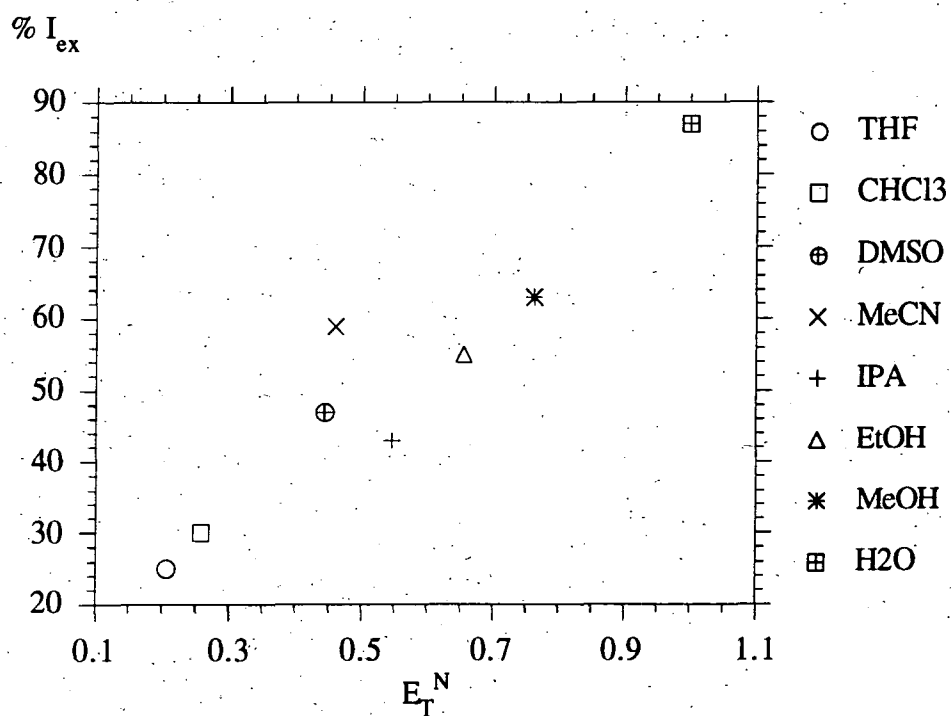


FIGURE 4.7 Variation of excimer emission intensity (% I_{ex}) with the normalised E_T solvent polarity parameter.

monomer emission in the more polar solvents. In the latter case, the trend was thought to reflect a change in the proportions of the two distinct conformations adopted by the calixarene in solution. The form which is favoured in the more polar solvents has a geometry which disfavours the close approach of the pyrene units.

In the present instance it is not clear why the polarity of the solvent should have such a profound effect. The lack of any significant changes in the excimer emission wavelength ($\lambda_{\max}^{\text{em}}$) in the various solvents seems to rule out an effect of selective stabilisation of the excimer in the more polar solvents. One possibility is that the more polar solvents disfavour *intramolecular* hydrogen bonding, perhaps allowing the molecule to adopt the required conformation for excimer formation. A somewhat related viewpoint is that the solvophobic naphthyl groups are forced closer together in polar solvents to give a larger contribution from excimers. Similar behaviour is seen in solvent effects on polymer molecules. The lack of variation of $I_{\text{ex}} / I_{\text{em}}$ over the 100-fold concentration range mentioned above suggests that intermolecular effects are absent. On the other hand, aggregation cannot be completely ruled out as there is always the possibility of a critical aggregation concentration at values lower than the range examined.

4.7 Effect of metal ions on the fluorescence of **39**

4.7.1 In solution in acetonitrile

Addition of 5 equivalents of anhydrous zinc or cadmium triflates to a solution of the mononaphthyl ligand **39** in MeCN (20 μM) at 20°C led to a two-fold increase in the intensity of the naphthyl fluorescence (Figure 4.9). This is readily interpreted in terms of a 'chelation enhanced fluorescence effect', similar to that discussed earlier arising from protonation and reflecting an increase in the oxidation potential of the amine groups on binding to a metal. The increase in the fluorescence intensity was directly proportional to the concentration of added metal ion (for ≤ 1 equivalent of the metal). For example, when cadmium triflate was added to **39** in acetonitrile, I_{fl} was a maximum when the ratio of ligand to added Cd^{2+} ions was unity (Figure 4.8), consistent with formation of a strong 1:1 complex.

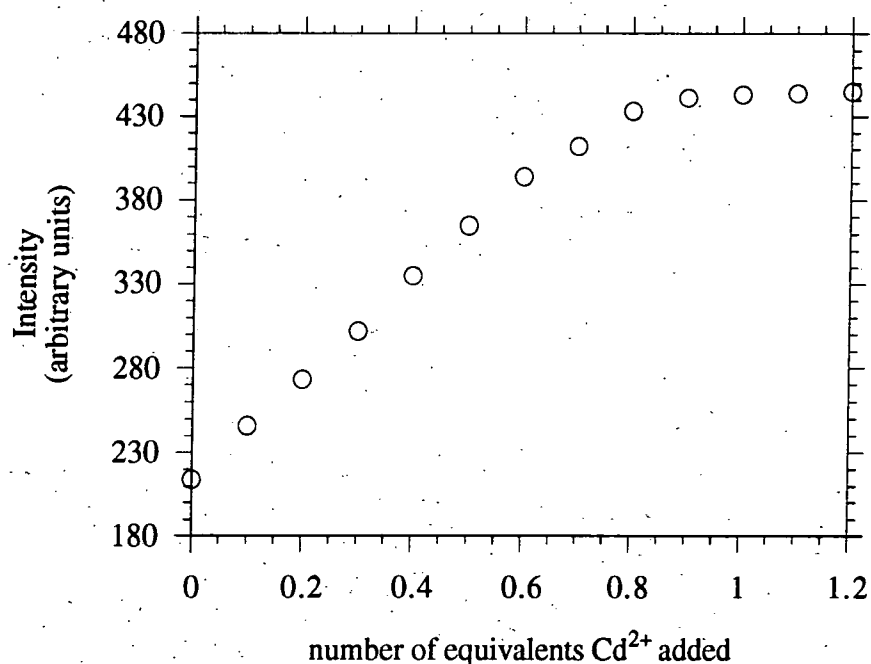


FIGURE 4.8 Effect of adding $\text{Cd}(\text{CF}_3\text{SO}_3)_2$ on the fluorescence emission intensity of **39** ($\lambda_{em} = 337 \text{ nm}$, $[\mathbf{39}] = 18 \mu\text{M}$).

Different behaviour was noted following addition of 5 equivalents of Pb^{2+} ions (Figure 4.9). Here, a reduction in fluorescence intensity of 25% was observed, accompanied by a 250% increase in the absorbance at 270 nm. The UV spectrum of the resulting lead complex displayed an intense band at 258 nm ($\epsilon = 1.8 \times 10^4 \text{ M}^{-1}\text{cm}^{-1}$) which obscures the weaker naphthyl band. This is presumably due to a charge-transfer transition and is reminiscent of the UV spectrum of $[\text{Pb.DOTA}]^{2-}$ ($\lambda_{max} 257, \epsilon 10000^{26}$). Complexation of lead must again disfavour the photoinduced electron transfer pathway of naphthyl deactivation. However, in this case, the resulting chelation enhanced fluorescence effect that might be expected must be outweighed by the quenching effect of the nearby heavy lead atom. The large spin-orbit coupling constant of lead, together with its proximity to the naphthyl chromophore, probably enhances singlet-triplet inter-system crossing and promotes non-radiative deactivation of the naphthyl excited singlet state. Similar behaviour in the presence of Pb^{2+} ions has been observed with a monoanthryl-linked 18- N_4O_2 cycle in methanol solution.²⁷

Quenching of excited states by the paramagnetic Cu^{2+} and Ni^{2+} ions is well-known.²⁸ Addition of 5 equivalents of copper triflate to **39** in acetonitrile caused an immediate 95% reduction in ligand fluorescence intensity (Figure 4.9). This compares to a much smaller reduction of 20% for the purely intermolecular quenching of pure naphthalene by Cu^{2+} under the same conditions of solvent and concentration. The quenching effect of added copper ions may be considered to occur either by means of an energy transfer process (probably involving electron exchange) or by a Cu^{II} -to-naphthyl electron transfer process, which requires stabilisation of the resultant Cu^{III} complex. Nickel(II) is expected to induce qualitatively similar changes. Indeed, addition of 5 equivalents of nickel triflate in acetonitrile to the ligand **39** caused a 65% reduction in I_{fl} .

For all of the divalent ions mentioned above, the forward rates of metal binding in acetonitrile were too fast to allow the estimation of relative rates of complexation.

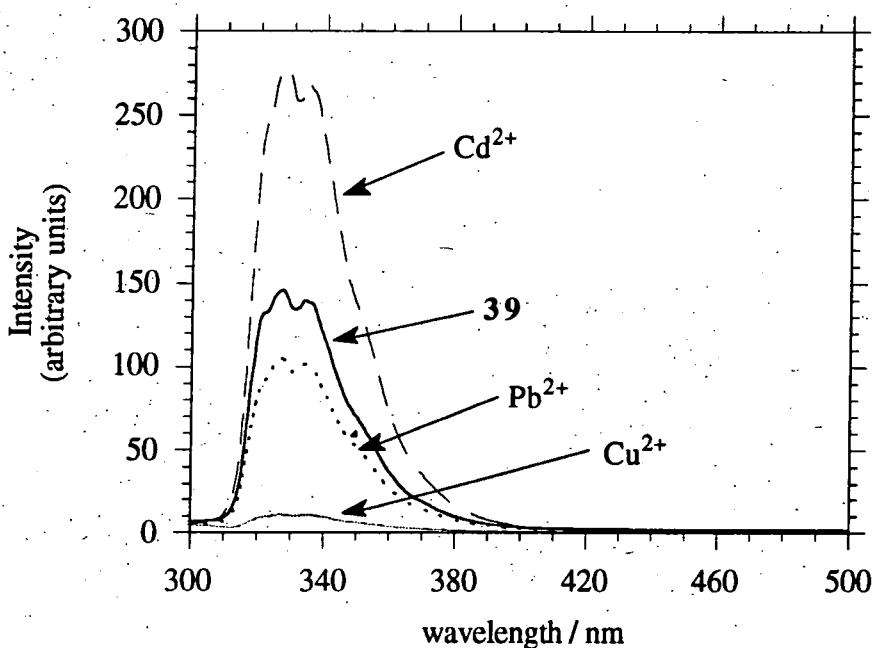


FIGURE 4.9 Corrected fluorescence emission spectra for **39** in the presence of excess metal ions: free ligand **39** (thick solid line); Cd^{2+} (dashed line); Pb^{2+} (dotted line); Cu^{2+} (thin solid line). $\{[\mathbf{39}] = 20 \mu\text{M}$ in CH_3CN ; $[M(\text{CF}_3\text{SO}_3)_2] = 100 \mu\text{M}$; $\lambda_{\text{exc}} = 270 \text{ nm}$; 298K]

4.7.2 In water

As noted earlier, the fluorescence intensity of ligand **39** was substantially higher in water than in CH_3CN , reflecting both the protonation of two of the ring nitrogen atoms in aqueous solution (reducing the photoinduced electron transfer mechanism of deactivation) and the lower equilibrium concentration of oxygen in water compared to acetonitrile. This second point probably also accounts for the higher fluorescence intensities observed for the metal complexes in aqueous solution compared to acetonitrile (see also Table 4.4).

The rates of complexation of added metal ions were slower in water and this allowed the changes in the fluorescence spectra to be monitored as a function of time. A higher free energy of activation in water compared to acetonitrile is to be expected, since the approach of a metal cation to a protonated ligand is Coulombically inhibited and deprotonation at nitrogen prior to complexation is necessary, at least for the ions favouring 8-coordination (Pb^{2+} , Cd^{2+} ; lanthanides). At a ligand concentration of $20\mu\text{M}$, reaction with $200\mu\text{M}$ of added metal triflates (i.e. pseudo-first-order conditions) was still too fast to measure with the available instrumentation but when 5 equivalents were added, the rates were sufficiently slow to allow the calculation of comparative observed rate constants at a constant pH of 5.5 (Table 4.3). Under these conditions, the observed changes approximate to pseudo-first-order behaviour and the rate constants k have been obtained through fitting to appropriate monoexponential equations of the form $I_t = c + A \exp(-kt)$ (for the quenching ions, Pb^{2+} , Ni^{2+} and Cu^{2+}) or $I_t = c - A \exp(-kt)$ (for the enhancing ions, Cd^{2+} and Zn^{2+}). (Here, I_t is the intensity at time t , c is an offset and A is a constant).

Addition of copper triflate again rapidly caused almost complete (ca. 95%) quenching of the naphthyl fluorescence emission. In contrast, addition of nickel triflate had very little effect, as shown in Figure 4.10b: metal binding is very slow in this case. This behaviour provides an interesting means of distinguishing between Cu^{II} and Ni^{II} ions in aqueous solutions based on their relative rates of complexation with the ligand,

notwithstanding the fact that both are intrinsically quenching ions. This contrasts with the system mentioned in Chapter 1 (section 1.9.2) wherein these ions were distinguished according to the pH-dependence of their binding to an anthryl-linked dioxatetraaza unit.²⁸

TABLE 4.3 *Effect of added divalent metal ions^a on naphthyl fluorescence emission^b with the 12N₄ mononaphthyl ligand 39 (293K, H₂O).*

Metal ion	$k_{\text{obs}} / 10^{-2} \text{ s}^{-1}$	Comment
Cd ²⁺	1.27	Fluorescence enhancement observed
Zn ²⁺	0.2	Fluorescence enhancement observed
Ni ²⁺	<0.0001	Only 1% decay of fluorescence observed after 5 min ^c
Cu ²⁺	1.14	> 95% fluorescence quenching
Pb ²⁺	5.00	Rapid fluorescence quenching to 40% of original I_{fl}

(a) [39] = 2×10^{-5} M; [M²⁺] as the triflate salt = 10^{-4} M. (b) The emission at 337 nm was monitored ($\lambda_{\text{exc}} = 270$ nm). (c) Under similar conditions in acetonitrile, a 65% reduction in I_{fl} was observed within 30s of addition of Ni(CF₃SO₃)₂.

The addition of lead triflate caused a decrease in I_{fl} of 60% under parallel conditions (Table 4.3 and Figure 4.10b). This is a proportionately larger decrease than that observed in acetonitrile and simply reflects the fact that the change from a diprotonated ligand to [Pb.39]²⁺ gives a proportionately smaller chelation enhanced fluorescence effect, so that the 'heavy atom' quenching effect of the lead ion is more marked. Binding of the lead ion was the fastest of the ions studied here. This is consistent with the high affinity reported for related 8-coordinating tetraamide ligands for this heavy metal ion.^{4,5} The cadmium complex of such tetraamides is also reported to be very stable, even at pH 1.^{4,5} Complexation of Cd²⁺ ions by 39 in water was somewhat slower than with Pb²⁺ and was distinctive in that a fluorescence enhancement was observed (Figure 4.10a). Obviously, the effect is rather less pronounced here than in CH₃CN since the 'free' ligand is already diprotonated in water, thereby reducing the initial extent of PET deactivation. The effect should be proportionately greater at

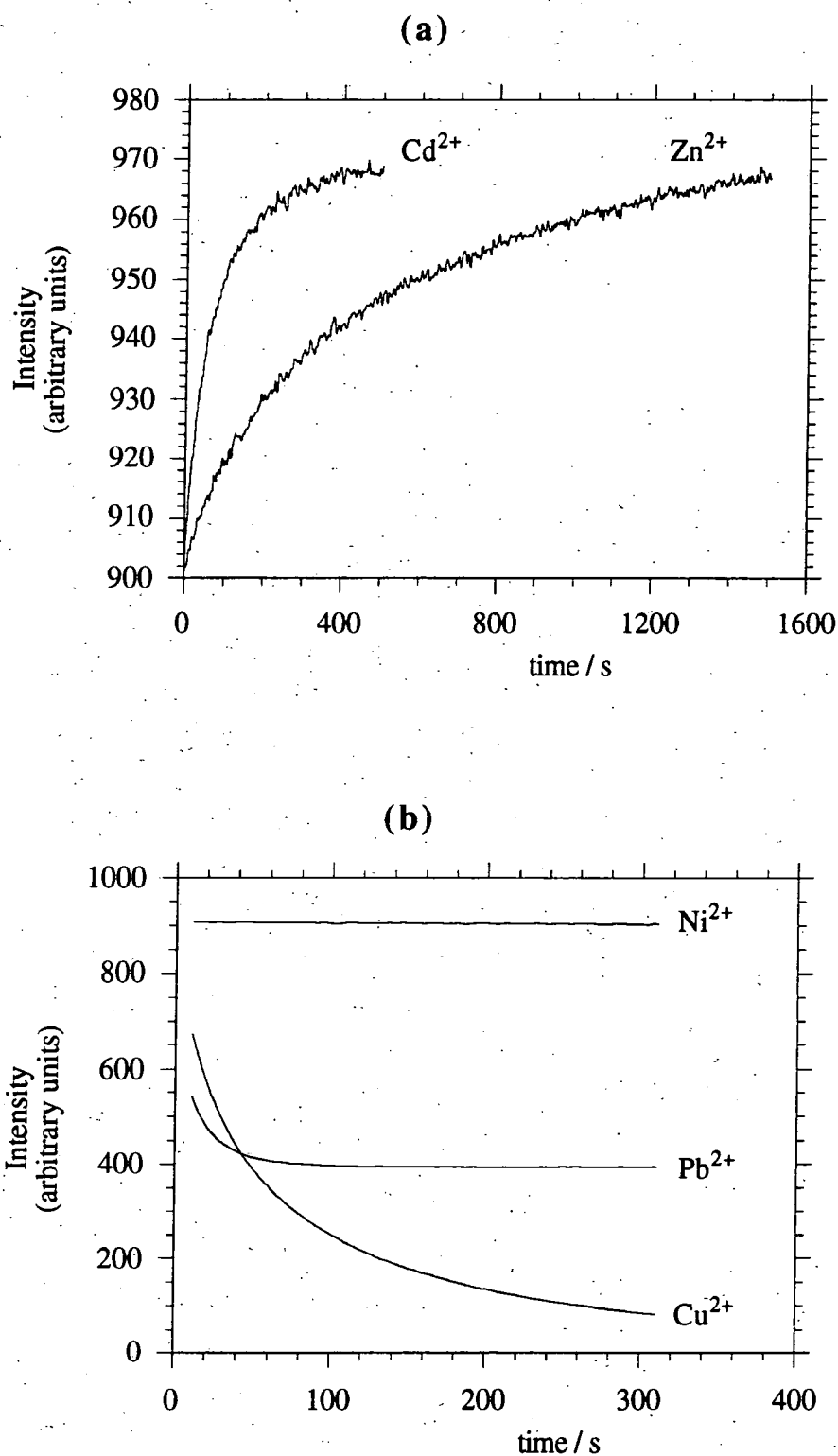


FIGURE 4.10 Effect of adding metal trifluoromethanesulfonate salts (5 equiv.) on the fluorescence emission intensity of ligand **39** in water (a) Cd²⁺, Zn²⁺; (b) Ni²⁺, Pb²⁺ and Cu²⁺ {[**39**] = 20 μ M, pH 5.5, 293K}.

higher pH values. A chelation enhanced fluorescence effect of comparable magnitude was also observed upon addition of zinc triflate, although at a reduced rate (Figure 4.10a).

4.8 Effect of metal ions on the fluorescence of 40

Addition of 50 equivalents of zinc triflate to a solution of the protonated ligand **40** in acetonitrile ($20\ \mu\text{M}$) caused no significant change in the fluorescence spectrum over a period of at least 6h. In contrast, when 5 equivalents of cadmium triflate was added to the protonated ligand $\{[\mathbf{40}] = 5\ \mu\text{M}, [\text{H}^+] = 50\ \mu\text{M}\}$, the monomer emission increased rapidly and, at the same time, the excimer band decayed (Figure 4.12). The rates of monomer increase and excimer decay were identical (Figure 4.11) and a first order dependence of these rates on ligand and cadmium concentration (for up to 1 equivalent of Cd^{2+}) was observed (see also the experimental section). In the more polar solvents MeOH and H_2O , the rate of excimer decay was at least 10 times slower and addition of an excess of acid also reduced this rate.

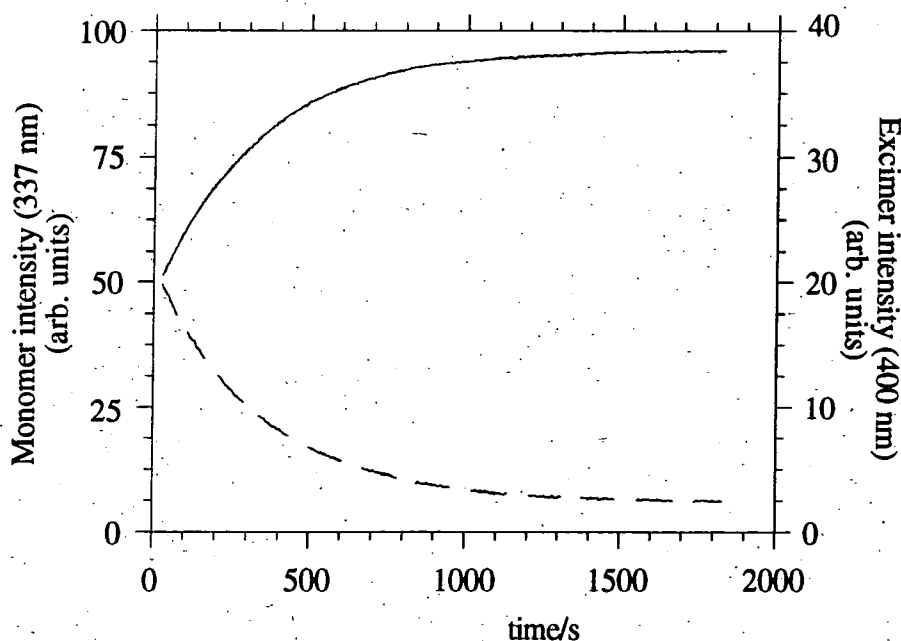


FIGURE 4.11 Increase in monomer emission (337 nm) and decay in excimer emission (401 nm) for ligand **40** (MeCN, $[\mathbf{40}] = 5\ \mu\text{M}$, $[\text{CF}_3\text{CO}_2\text{H}] = 100\ \mu\text{M}$), following addition of $\text{Cd}(\text{CF}_3\text{SO}_3)_2$ ($50\ \mu\text{M}$).

This behaviour is consistent with the formation of a 1:1 complex, $[\text{Cd.39}]^{2+}$, involving expulsion of the ring protons. The cadmium complex was prepared and isolated independently (see section 4.11 for further details) and gave a fluorescence spectrum identical to that of the complex prepared *in situ*. A single C=O stretching band was observed in the IR spectrum, both in the solid state (KBr disc) and in methanol solution, and shifted by 30 cm^{-1} to lower frequency compared to the free ligand $\{\nu_{\text{CO}}(\text{MeOH})$: **40** 1672 cm^{-1} , $[\text{Cd.40}]^{2+}$ 1641 cm^{-1}). This is indicative of simultaneous coordination of each amide carbonyl oxygen and hence an 8-coordinate complex in solution, with all of the nitrogen and amide carbonyl oxygens bound to the Cd^{2+} ion. This coordination type contrasts with that of the zinc complexes of **39** and **40**, for which two carbonyl stretching bands were observed, both in the solid state and in methanol solution; eg. for $[\text{Zn.39}]^{2+}$, $\nu_{\text{CO}} = 1665$ and 1636 cm^{-1} for free and bound carbonyls respectively. This is consistent with 6-coordination for the smaller zinc ion, leaving two amide carbonyls unbound in the complex.

The loss of the excimer band and the concomitant increase in monomer emission on binding of cadmium almost certainly reflect a structural change. Presumably, binding of the metal changes the mutual arrangement of the amide groups in such a way that the naphthyl groups are shifted apart and are inhibited from attaining the plane-parallel conformation required for excimer emission. The alternative possibility, namely that the change in the fluorescence spectrum represents a selective quenching of the excimer over the monomer, can be dismissed on the grounds that this would not give rise to an increase in the monomer emission. Clearly, the rise in the monomer occurs at the expense of the excimer. This is also apparent from the quantum yield of the cadmium complex (Table 4.4) which is seen to be little different from that of the protonated ligand.

The behaviour of lead was found to be quite different. Addition of an excess of Pb^{II} to protonated **40** in acetonitrile $\{[\text{40}] = 5\text{ }\mu\text{M}, [\text{H}^+] = 50\text{ }\mu\text{M}\}$ again resulted in a rapid decay of the excimer emission but, in this case, there was virtually no change in the

monomer intensity. In other words, the total emission intensity (the area under the corrected spectra) was substantially reduced. This can be rationalised once again in terms of the heavy-atom effect of lead enhancing singlet-triplet inter-system-crossing and hence non-radiative deactivation of the naphthyl singlet excited state. Complexation of lead could be further distinguished from cadmium by the appearance of an intense charge transfer band in the UV spectrum (λ_{max} 260 nm, ϵ $2.8 \times 10^4 \text{ M}^{-1} \text{ cm}^{-1}$). This band contributes significantly to the absorbance at 270 nm in the complex, which results in a quantum yield lower than that expected from a comparison of the fluorescence intensities of solutions of the ligand and lead complex at the same concentration (Table 4.4 cf. Figure 4.12).

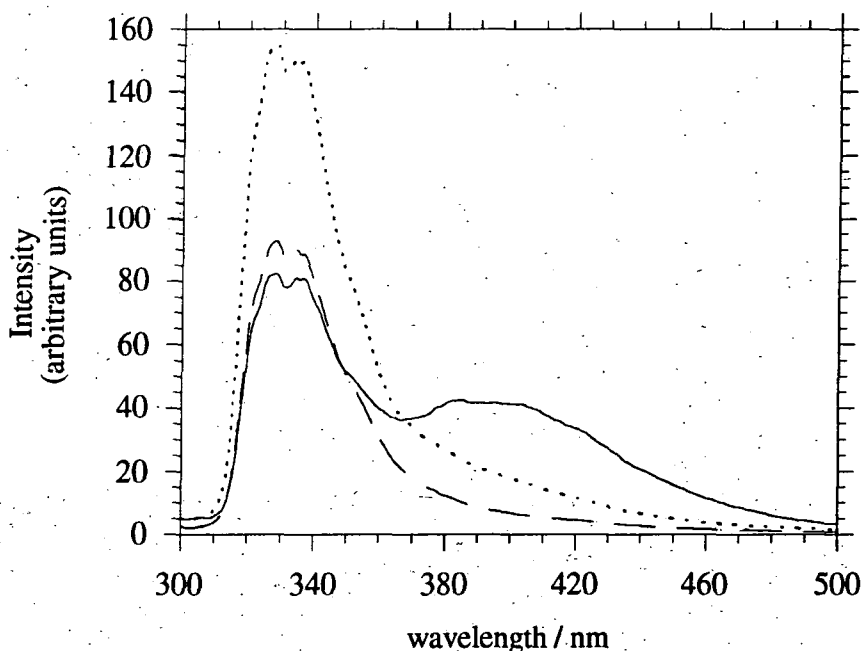


FIGURE 4.12 Corrected fluorescence emission spectra ($\lambda_{\text{exc}} = 270 \text{ nm}$) for **40** (solid line, $5 \mu\text{M}$ in CH_3CN in the presence of $0.1 \text{ mM CF}_3\text{CO}_2\text{H}$) and after addition of 5 equivalents of lead triflate (dashed line) or cadmium triflate (dotted line).

That quenching by lead is an *intramolecular* effect was demonstrated by addition of 10 equivalents of the anionic complex $[\text{Pb.DOTA}]^{2-}$ to the protonated ligand in MeOH: no diminution of the excimer emission was observed. As for **39**, binding of lead was found to occur at a somewhat faster rate than complexation of cadmium. At a ligand

concentration of $5\mu\text{M}$ and in the presence of 20 equivalents of TFA in acetonitrile, addition of 10 equivalents of the metal triflates caused excimer quenching with observed pseudo-first-order rate constants of $4.8 \times 10^{-3} \text{ s}^{-1}$ and $2.9 \times 10^{-3} \text{ s}^{-1}$ for lead and cadmium respectively.

TABLE 4.4 Fluorescence quantum yields for ligands **39**, **40** and selected isolated triflate complexes.

Species (39)	Solvent	$\phi_{\text{fl}}(\text{rel})^{\text{a}}$	Species (40)	$\phi_{\text{fl}}(\text{rel})^{\text{a}}$ CH ₃ CN
39	CH ₃ CN	1.39	[40.H_n] ⁿ⁺	1.04
[39.H₂] ⁺	H ₂ O	3.10	[Tb. 40] ³⁺	0.96
[Tb. 39] ³⁺	CH ₃ CN	1.18	[Eu. 40] ³⁺	0.12
[Eu. 39] ³⁺	CH ₃ CN	0.20	[Y. 40] ³⁺	1.21
[Tb. 39] ³⁺	H ₂ O	2.1	[Cd. 40] ²⁺	0.88
[Eu. 39] ³⁺	H ₂ O	0.49	[Pb. 40] ²⁺	0.31

(a) Values are relative to naphthalene (aerated solution in acetonitrile, $\phi = 0.06$).

The quenching of excimer emission by lead ions was also monitored in the presence of increasing quantities of added zinc ions. At a ligand concentration of $5\mu\text{M}$ in CH₃CN and in the presence of $100\mu\text{M}$ of acid (CF₃CO₂H), excimer quenching was still observed and the equilibrium fluorescence spectrum matched that of the isolated lead complex. The effect of added zinc was to slow down the rate at which this equilibrium was reached. Thus, in the absence of added zinc ($[\text{40}] = 5\mu\text{M}$, $[\text{Pb}^{2+}] = 50\mu\text{M}$), excimer emission was completely quenched (i.e. lead complexation had occurred) within about 5 minutes. In the presence of 10, 20 and 50 equivalents of added zinc ions, the rate of formation of the lead complex slowed to about 10, 20 and 45 minutes, respectively. Parallel experiments carried out with a zinc background following cadmium complexation showed a more marked interference effect. The rate of excimer quenching by added cadmium was 10 times slower in the presence of added zinc and, at

higher added zinc concentrations, total excimer quenching was not observed. This indicates that the ligand binds lead most avidly and with good selectivity over zinc.

The effect of metal ions on the fluorescence of **40** is of significance for at least three reasons. Firstly, it has long been recognised that practicable fluorescence detection of metal ions or other species is favoured if the emission or excitation spectrum can be monitored at two different wavelengths, the intensities of which are perturbed to differing extents on binding of the analyte.²⁹ This then allows detection and quantification to be achieved through the ratio of the intensities at these two wavelengths. This avoids a number of problems associated with detection by the monitoring of absolute emission intensities, such as variations in illumination intensity and detection efficiency and the problem of varying amounts of other species absorbing at the excitation wavelength, which serve to reduce I_{fl} . The present compound incorporates this desired feature in that the intensities at 337 nm and 401 nm are affected to differing extents and the ratio of these intensities may therefore be used to monitor the metal binding. The second point relates to the fact that the changes observed are dependent on the identity of the metal ion. The behaviour of lead is very different from that of cadmium and, in principle, it would be possible to monitor both simultaneously. Moreover, potentially interfering ions, such as Zn^{2+} , Mg^{2+} and alkali metal ions have no effect on the fluorescence spectrum and so the system exhibits high selectivity. Thirdly, the metal binding occurs in water (albeit at a reduced rate compared to acetonitrile). This is an important point: as mentioned in Chapter 1, applications of such systems are almost always intended for use in aqueous solution but water is a difficult medium in which to obtain efficient metal binding. It may be noted in passing that there have been a few other reports of metal ion detection making use of the quenching or triggering of excimer emission following conformational changes induced by metal ion binding.^{25,30,31} However, all of these studies were carried out in solvents such as methanol in the absence of acid and it is very likely that none would operate in aqueous solution.

4.9 Effect of metal ions on the fluorescence of 41 and 42

The concept of exploiting a ratio of emission intensities was also in mind for the ligands **41** and **42**. Here, the bis-naphthyl moiety is extrinsic to the metal-binding part of the system and so structural changes on metal binding would not be expected to have a significant effect on $I_{\text{ex}} / I_{\text{m}}$. However, it was pointed out in section 4.5 that the lifetime of a naphthyl excimer is likely to be substantially longer than that of the monomer (i.e. $k_{\text{fE}} < k_{\text{f}}$), with the result that excimer emission displays a more sensitive dependence on the presence or absence of quenching species. Thus, one might reasonably expect the binding of suitable quenching ions to have a more significant effect on the excimer band than on the monomer emission, in such a way that $I_{\text{ex}} / I_{\text{m}}$ is reduced. By the same token, complexation of an enhancing ion (which reduces the efficiency of the PET process) may be expected to have a more significant effect on the excimer, especially if k_{ET} has a value intermediate between that of k_{f} and k_{fE} . Of course, in both cases, the total fluorescence intensity should also be affected, providing a further parameter to be monitored.

The effect of adding 5 equivalents of the metal triflates to ligand **41** in CH_3CN (10^{-5} M) was investigated. The results are shown in Table 4.5 where the $I_{\text{ex}} / I_{\text{m}}$ ratios before and after complexation are given, together with the changes in the total fluorescence intensity I_{total} expressed as a percentage of the initial intensity. Some of the spectra are shown in Figure 4.13.

It is clear that the quenching ions, Cu^{2+} , Pb^{2+} , Ni^{2+} and Eu^{3+} do indeed result in a reduction of the total fluorescence intensity in a manner which resembles, at least qualitatively, the behaviour of **39**. Again, Cu^{2+} is the most efficient quencher and Pb^{2+} and Ni^{2+} cause similar changes to one another (ca. 36% reduction). However, in addition to these changes in I_{total} , the $I_{\text{ex}} / I_{\text{m}}$ ratios are also affected to differing extents. Thus, binding of a given metal ion is characterised by a unique pair of values for the parameters $I_{\text{ex}} / I_{\text{m}}$ and I_{total} . For all of these quenching ions, the $I_{\text{ex}} / I_{\text{m}}$ value is reduced on metal binding. This fulfils the prediction above, namely that the excimer

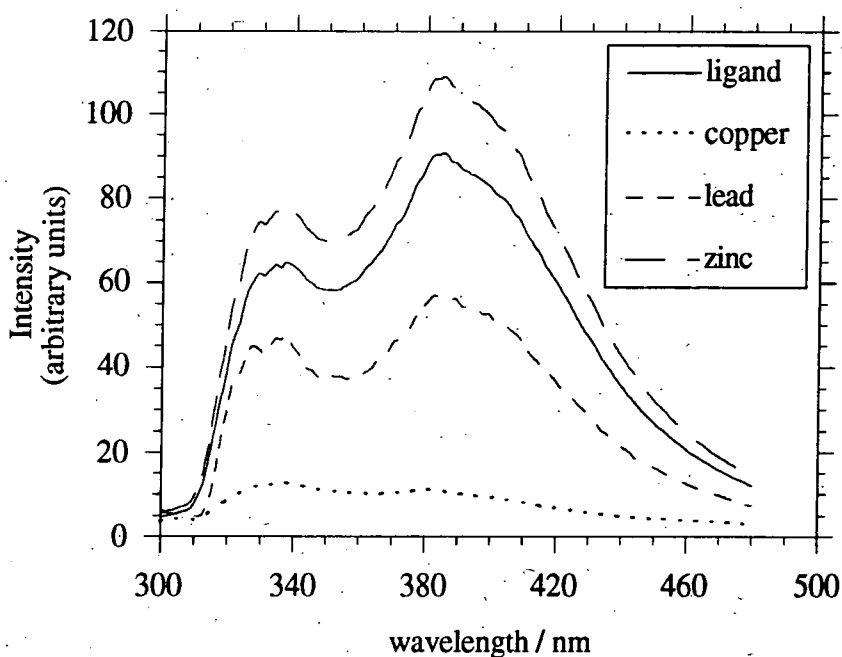


FIGURE 4.13 The fluorescence spectrum of ligand 41 in CH_3CN ($10 \mu\text{M}$) and after addition of 5 equivalents of metal triflates ($M = \text{Zn}^{2+}$, Pb^{2+} and Cu^{2+}).

TABLE 4.5 Effect of metal ions (5 equivalents) on the excimer-to-monomer intensity ratio ($I_{\text{ex}}/I_{\text{m}}$) and on the total fluorescence intensity (I_{total}) for ligand 41 ($10 \mu\text{M}$).

	acetonitrile solution		aqueous solution	
	$I_{\text{ex}}/I_{\text{m}}^{\text{a}}$	$I_{\text{total}}(\%)^{\text{b}}$	$I_{\text{ex}}/I_{\text{m}}^{\text{a}}$	$I_{\text{total}}^{\text{(b)}}$
Free ligand	1.41	100	3.34	100
Zinc	1.40	119	(c)	(c)
Cadmium	1.31	106	3.47	97
Lead	1.20	64	2.68	61
Nickel	1.03	63	(d)	(d)
Copper	0.85	14	2.32	25
Europium	1.14	25	3.28 ^e	90 ^e

(a) The ratio of the maximum emission intensities of excimer and monomer was used, as obtained from the corrected emission spectra. (b) I_{total} is the total emission intensity expressed as a percentage of that measured for the free ligand. (c) No effect observed. (d) Binding of nickel was very slow; complexation of the other metals was effectively instantaneous in both solvents. (e) Probably an intermolecular effect.

emission is expected to be affected to a greater extent than that of the monomer in the presence of a quenching species, owing to its longer lifetime. The trend in $I_{\text{ex}} / I_{\text{m}}$ follows that of I_{total} to some extent but not precisely. For example, nickel and lead both induce similar changes in I_{total} (37 and 36% reductions respectively) but the former causes a significantly larger decrease in $I_{\text{ex}} / I_{\text{m}}$. Europium, on the other hand, has a proportionately larger effect on the total intensity than on the excimer / monomer ratio. These differing observations probably arise from the relative rates of quenching (be it through electron or energy transfer, as for Cu^{2+} say, or through enhanced inter-system crossing, eg. for lead), monomer emission k_{f} , excimer formation k_{E} and excimer emission k_{fE} . Thus, one can envisage one extreme where the quenching rate constant is intermediate between k_{f} and k_{fE} , in which case I_{ex} will be reduced to a significantly greater extent than I_{m} . This would be reflected in a substantial decrease in $I_{\text{ex}} / I_{\text{m}}$, without the total emission intensity being affected to the same extent. This is perhaps the case for Ni^{2+} say. On the other hand, if the quenching rate constant is much larger than both k_{f} and k_{fE} then a large decrease in I_{total} would be expected but the effect on the monomer will be almost as large as the effect on the excimer, such that $I_{\text{ex}} / I_{\text{m}}$ is not greatly affected. This probably accounts for the behaviour of europium. The bimolecular rate constant, k_{Q} , for quenching of the first excited singlet state of naphthalene by Eu^{3+} ions has a value of $7.2 \times 10^9 \text{ M}^{-1}\text{s}^{-1}$ (in CH_3CN , see section 4.12). The local concentration $[\text{Q}]$ of Eu^{3+} is high in the complex and so quenching is likely to compete very efficiently with both monomer and excimer fluorescence (k_{f} ca. $2 \times 10^7 \text{ s}^{-1}$, k_{fE} ca. $7 \times 10^6 \text{ s}^{-1}$ for possible model compounds, see section 4.5). Thus, quenching will cause a substantial fall in I_{total} with relatively little discrimination between excimer and monomer, such that $I_{\text{ex}} / I_{\text{m}}$ is not affected to such a large extent.

Zinc causes a modest increase in I_{total} , consistent with a 'chelation enhanced fluorescence effect'. This is rather less dramatic than for compound **39** in CH_3CN , which probably reflects a proportionately smaller PET deactivation in **41** compared to **39**. This may be related to the fact that the ring nitrogen nearest to the naphthyl groups

in **41** is a carbamate nitrogen, which will have a much higher oxidation potential than the corresponding amine nitrogen in **39**.

Actually, the lone pair of this nitrogen atom will be delocalised into the neighbouring carbonyl group and so will not be available for binding to the metal. Moreover, the naphthyl amide C=O is now too far from the cycle to act as donor to the bound metal. Thus, **41** is only a hexadentate ligand and this will of course disfavour binding of the larger ions such as lead and europium, which prefer octacoordination. However, this does not seem to be a problem in acetonitrile: binding of all six of the metal ions investigated, including lead and europium, occurred very rapidly (within the time required to record the spectrum).

Very rapid binding was also observed for most of the metal ions in *aqueous* solution: equilibrium had again been attained before the spectra could be acquired. This contrasts with the behaviour of **39**, where metal binding was substantially slower in water than in CH₃CN. There are probably two contributing factors to the faster rates of complexation in water for **41** compared to **39**. Firstly, since one of the ring nitrogen atoms of **41** is incorporated into a carbamate, the pK_a values of this ligand are likely to be somewhat lower than those of **39** with the result that the deprotonation required prior to metal binding may occur more readily in the former. Secondly, the bis-naphthyl unit of **41** is further away from the metal binding site than the naphthyl group in **39**, so that there is less steric hindrance to the approach of the metal ion in **41**. Again, nickel was found to bind only very slowly: a 10% reduction in I_{total} was observed over 30 minutes. Europium appeared not to bind at all in aqueous solution. This is probably not surprising bearing in mind the high affinity of lanthanide ions for water molecules as ligands and the fact that **41** is only a hexadentate and charge-neutral ligand (protonated in water).

Binding of Cu²⁺ and Pb²⁺ in aqueous solution induced similar changes to those observed in acetonitrile. (Of course, the I_{ex} / I_m ratio is higher than in MeCN, both

before and after complexation, owing in part to the lower concentration of dissolved oxygen as explained earlier). Both the total fluorescence intensity and the $I_{\text{ex}} / I_{\text{m}}$ values were affected and to extents which were dependent on the identity of the metal ion (Table 4.5). Binding of zinc gave rise to no detectable effect. This is not surprising, since the chelation enhanced fluorescence effect was small in MeCN and will be smaller still in water, owing to the fact that the ligand is initially protonated (as discussed for 39).

In summary, ligand 41 is of significance for a number of reasons. There appear to have been no previous studies on the use of a 'built-in' excimer for fluorescence detection of metal ions or other species. Where excimer emission has been exploited, it is normally through some form of geometrical change affecting the relative positions or orientations of a pair of aryl groups. Whilst the changes in $I_{\text{ex}} / I_{\text{m}}$ are not as large in the present system as those in some previously reported compounds (or indeed for ligand 40), it is important to note that the extent to which $I_{\text{ex}} / I_{\text{m}}$ is affected shows a sensitive and reproducible dependence on the identity of the metal ion. The total fluorescence intensity (as measured by the area under the fluorescence spectrum) is also affected to differing extents (in a similar manner to 39). Thus, there are *two* parameters characterising the binding of a specific metal ion. This should allow, in principle, the simultaneous detection of two different metal ions (eg. Pb^{2+} and Cu^{2+} in aqueous solution). In this respect, 41 offers a significant advantage over 39. A further point relates once again to the fact that the system operates effectively in aqueous solution and, importantly, at a very fast rate. This is a property which is clearly desirable in any practical system.

The behaviour of ligand 42 to added metal ions was also investigated. Unfortunately, for this compound, metal binding was extremely slow, even in solution in MeCN. Several days were required for equilibrium to be attained, even for lead. This slow rate of binding probably reflects the steric hindrance of the two bulky bis-naphthyl groups to the approach of the metal ion, coupled with the restricted rotation about the N-C(O)

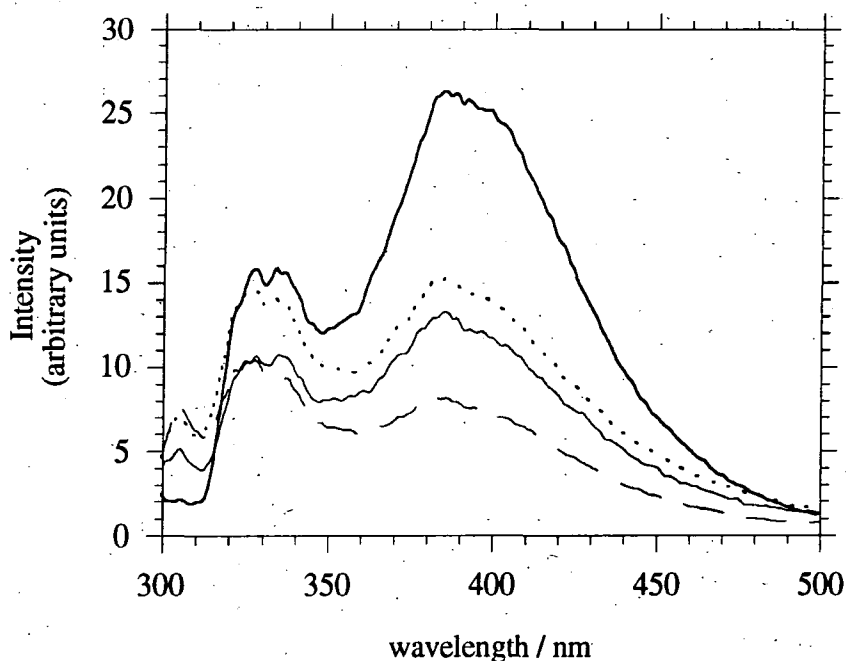


FIGURE 4.14 Corrected fluorescence emission spectra of ligand **42** in acetonitrile at a concentration of $5 \mu\text{M}$ (thick solid line) and the spectra 72h after addition of Pb^{2+} (dotted line), Cu^{2+} (thin solid line) or Eu^{3+} (dashed line) (as their triflate salts, 5 equivalents).

TABLE 4.6 Effect of metal ions (5 equivalents) on $I_{\text{ex}}/I_{\text{m}}$ and on I_{total} for ligand **42** in CH_3CN ($5 \mu\text{M}$).

	$I_{\text{ex}}/I_{\text{m}}^{\text{a}}$	$I_{\text{total}} (\%)^{\text{b}}$
Free ligand 42	1.66	100
Copper	1.25	58
Lead	1.04	69
Europium	0.79	40

(a). The ratio of the maximum emission intensities of excimer and monomer was used, as obtained from the corrected emission spectra. (b) I_{total} is the total emission intensity expressed as a percentage of that measured for the free ligand.

bonds. Such behaviour is consistent with the kinetic inertness noted for the Ca^{2+} complex formed initially (section 4.2), where metal ion dissociation is hindered for the same reasons. The observed effects of Cu^{2+} , Pb^{2+} and Eu^{3+} are shown in Table 4.6 and Figure 4.14. The pattern is somewhat different to that of **41**. This could be due to the differing distance dependencies of the quenching rates: the naphthyl groups in **42** are closer to the metal binding site than in **41**.

4.10 Effect of added β -cyclodextrin on naphthyl fluorescence

As pointed out in Chapter 3 in connection with spectral resolution of enantiomers (section 3.4.5), cyclodextrins are able to form non-covalently bound adducts with a very large number of organic molecules containing aryl groups. β -Cyclodextrin is well known to form relatively stable complexes with simple naphthyl derivatives ($\log K \approx 10^3 \text{ M}^{-1}$). It has also been observed that deactivation of aryl excited states may be inhibited through binding of the aromatic moiety within the cavity of an appropriately sized cyclodextrin.³² When bound within the cyclodextrin, the aryl group is shielded from solvent vibrational quenching and has less conformational freedom so that non-radiative deactivation processes such as internal conversion are disfavoured. Under such circumstances, an enhanced fluorescence emission intensity may be observed.

With these points in mind, the fluorescence characteristics of ligand **39** and selected complexes were examined in the presence of varying concentrations of β -cyclodextrin. The ligand itself showed an increase in fluorescence emission (Table 4.7) and the effect was greater for both higher concentrations of ligand or of added cyclodextrin. This is consistent with the fact that at higher concentrations of added CD or of ligand, more of the ligand naphthyl groups will be bound at equilibrium. A similar variation in I_{fl} with concentration was noted for the zinc, terbium and the more weakly fluorescent europium complexes of **39** (Table 4.7). The europium complex gave the highest increase. In this complex, the main naphthyl excited-state deactivation pathway is likely to involve a charge-transfer transition mechanism of energy capture by the easily reduced Eu^{3+} ion (section 4.12). It is possible that this process is disfavoured slightly

on binding of the naphthyl group to the cyclodextrin (eg. through a small perturbation of the oxidation potential of the naphthyl singlet excited state), which could account for the higher fluorescence enhancement. A small increase of the metal-based luminescence was also observed. The effect of cyclodextrin binding on the terbium luminescence is discussed in section 4.13.4.

Parallel experiments were attempted with ligand **40** and its complexes in aqueous solution, but addition of β -cyclodextrin (up to 100-fold excess over complex at 20 μ M) caused no changes at all in I_{fl} . In this case, the proximity of three adjacent naphthyl groups in the ligand and its complexes prevents the close approach of the cyclodextrin molecule to a given naphthyl group.

TABLE 4.7 Effect of added β -cyclodextrin on the fluorescence of **39** and its complexes (H₂O, 293K).

Species	Concentration (μ mol dm ⁻³)	Added β -CD (equivalents)	% Increase in I_{fl} ^(a)
[39]	7.3	50	10
[39]	18.2	10	4
[39]	18.2	50	18
[Zn. 39] ²⁺	7.3	50	9
[Eu. 39] ³⁺	7.3	50	16
[Zn. 39] ³⁺	18.2	50	16
[Eu. 39] ³⁺	18.2	50	25
[Zn. 39] ³⁺	18.2	10	4
[Eu. 39] ³⁺	18.2	10	8
[Tb. 39] ³⁺ (b)	18.2	50	13 ^c

(a) Monitoring fluorescence emission at 336 nm. Values quoted are the mean of four separate measurements; the variation in the % increases was less than 1%.

(b) Solution was degassed using four freeze-pump-thaw cycles before and after addition of the cyclodextrin. (c) Terbium luminescence emission was enhanced by 44% and the lifetime of emission was increased from 0.67 ms to 0.85 ms.

4.11 Preparation, isolation and characterisation of metal complexes of **39** and **40**

The europium and terbium complexes of **39** and **40** were prepared, along with the Cd^{2+} , Pb^{2+} and Y^{3+} complexes of **40** and the Zn^{2+} complex of **39**. The use of metal triflate salts has been reported in the synthesis of complexes of structurally-related tetraamide ligands.² The triflate counterion imparts solubility in both aqueous and organic solvents and, being a 'non-coordinating' anion, is unlikely to affect the properties of the metal complex. The complexes were prepared by addition of a stoichiometric amount of the metal triflate to a solution of **39** in MeCN or a suspension of **40** in DMF, at 60°C. Complexation occurred very rapidly under these conditions and the complexes were isolated by precipitation from diethyl ether.

Infra-red spectroscopy is a useful analytical tool for amide complexes. Metal binding is indicated clearly by a shift in the C=O stretching frequency, usually between 30 and 40 cm^{-1} to lower frequency. As pointed out earlier, 6-coordinate complexes such as $[\text{Zn}(\mathbf{39})]^{2+}$ displayed two bands due to bound and unbound carbonyl groups, whilst the larger ions, forming 8-coordinate complexes, gave only a single band. Such behaviour is consistent with the X-ray structures reported for the Zn^{2+} and Cd^{2+} complexes of the structurally-related ligand **38**.⁵ In the lanthanide complexes, the C=O stretching band was shifted from 1674 cm^{-1} (ligand) to 1628 cm^{-1} . For a given ligand, the IR spectra for the Eu^{3+} , Tb^{3+} and Y^{3+} complexes were indistinguishable.

A ^1H - ^1H COSY NMR spectrum was obtained for the diamagnetic yttrium complex of **40** (CD_3OD , 400 MHz, 298K), which revealed that the tetraaza ring in the complex again adopts the [3333] conformation, as outlined in Chapter 2. Thus, two triplets were observed, corresponding to the two non-equivalent axial protons within each of the four equivalent ethylenediamine units, together with two doublets attributable to the equatorial protons. A second pair of mutually coupled doublets was also detected ($^2J = -17$ Hz) arising from the protons of the NCH_2CO unit, which are non-equivalent on binding to the metal. The carbon spectrum was consistent with this interpretation, displaying two signals for the ring carbons. The room temperature proton and carbon

spectra of the Cd^{2+} and Pb^{2+} complexes displayed broader signals indicating the onset of a fluxional process analogous to that observed in DOTA complexes (Chapter 2), leading to an averaging of the ring carbons and protons. This is consistent with recently reported results on the cadmium and lead complexes of ligand **38**.⁴

A further technique which has been found to be particularly useful for characterising the cationic complexes of these ligands is that of electrospray ionisation mass spectrometry. Electrospray ionisation has emerged over the past decade as a powerful tool for the production of intact ions from large and complex species in solution.³³ It allows mass spectrometric analyses to be applied to large, fragile and involatile polar molecules and, in this application, is greatly superior to the more conventional "soft" ionisation methods such as fast atom bombardment (FAB). Levels of internal excitation of the ions are generally low when generated through the electrospray technique, such that fragmentation is reduced. Multiple charging allows molecules of very high mass to be detected (well in excess of 100 kDa).

In the present instance, electrospray ionisation mass spectra were carried out using very dilute samples in 50% MeOH / H₂O and the spectra were acquired in the positive ion detection mode. The compounds show multiple charging where the observed mass is found at $[M+nA+bH] / x$, where M is molecular mass of the cation, A the mass of the anion, n the number of anions associated with the cation, x is the observed charge on the spectrum ion and $b = x - \sum_{\text{charge}} (\text{cation} + n. \text{anion})$.

A representative example is shown in Figure 4.15, which is the spectrum obtained for $[\text{Tb.39}]^{3+}(\text{CF}_3\text{SO}_3^-)_3$. The molecular mass of the cation is 741. Due to the tripositive charge, the cation may have associated with it up to three triflate anions (each anion has a charge of -1 and a mass of 149). Thus, the singly charged ion peaks expected are:

$$[741 + (0 \times 149) + (1 - (3 + 0)) \times 1] / 1 = 739 \text{ m/z (observed)}$$

$$[741 + (1 \times 149) + (1 - (3 - 1)) \times 1] / 1 = 889 \text{ m/z (observed)}$$

$$[741 + (\overset{2}{\cancel{0}} \times 149) + (1 - (3 - 2)) \times 1] / 1 = 1038 \text{ m/z (observed)}$$

$$[741 + (\overset{3}{\cancel{0}} \times 149) + (1 - (3 - 3)) \times 1] / 1 = 1189 \text{ m/z (not observed)}$$

Although the fourth peak predicted above is not observed, a signal is present at m/z 1211 arising from the addition of a Na^+ ion rather than a proton. Experiments are underway in the research group of Dr. Jim Ballantine at Swansea to investigate whether the intensities of ions of the former type may be enhanced (at the expense of the sodium-containing species) by addition of appropriate compounds.

Analogous behaviour is observed for the complexes of the dicationic complexes such as $[\text{Pb.40}]^{2+}$. In fact, in these cases, the most intense signal is almost invariably that corresponding to M^{2+} , appearing at $M/2$. For example, for $[\text{Pb.40}]^{2+}$, the cation mass is 1168 and the strongest signal occurred at 584. Triflate-associated signals predicted using the above analysis were also observed.

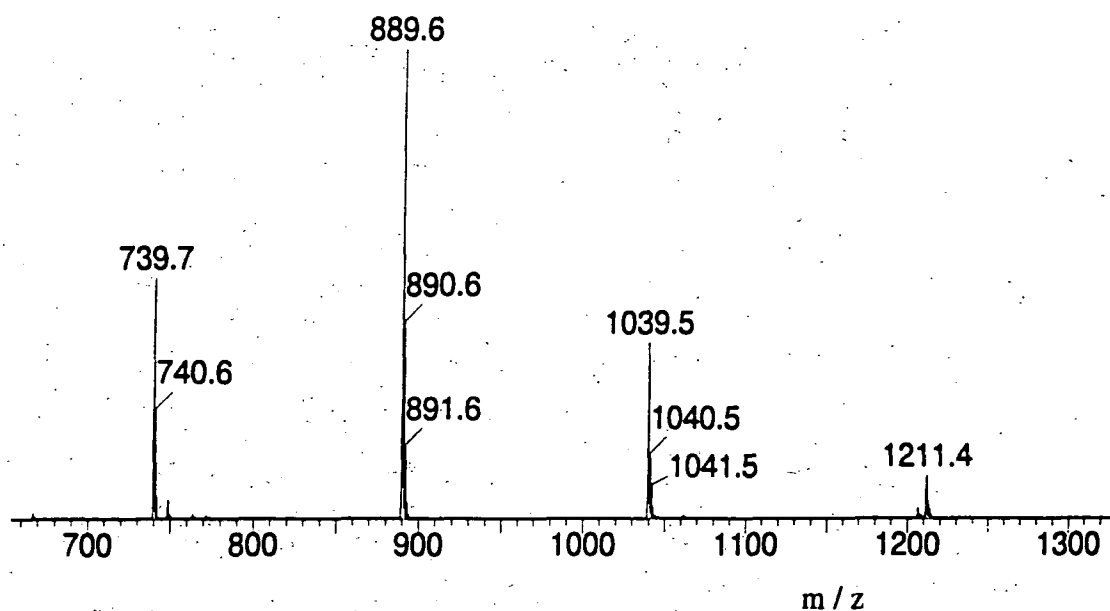


FIGURE 4.15 A portion of the electrospray ionisation mass spectrum (positive ion detection) for $[\text{Tb.39}]^{3+}$, showing the signals arising from the association of triflate anions with the cation.

4.12 Luminescence of the Europium Complexes of 39 - 42

In principle, the naphthyl group may function as an antenna chromophore, sensitising the luminescence of the bound lanthanide ion. For europium, the energy of the emissive excited 5D_0 state lies 47 kJ mol^{-1} below that of the triplet state of free naphthalene. This energy gap is relatively small and might be expected to favour efficient energy transfer from the naphthyl group to the metal, as discussed in section 2.11. The characteristic europium luminescence was indeed observed for the europium complexes of both **39** and **40** upon excitation at 270 nm. The luminescence excitation spectra confirmed that sensitisation through the naphthyl groups was occurring. The emission spectrum of $[\text{Eu.39}]^{3+}$ is shown in Figure 4.16. That of $[\text{Eu.40}]^{3+}$ is very similar, reflecting the similarity of the immediate coordination environments of the metal in the two complexes. Comparison with the spectra in Figure 3.15 (see also Table 3.2) shows that there is a distinct similarity to the spectrum of $[\text{Eu.DOTA}]^-$, with a relatively high $\Delta J = 1 / \Delta J = 2$ ratio and with the shorter wavelength component of the $\Delta J = 2$ band displaying a much higher intensity than its longer wavelength neighbour.

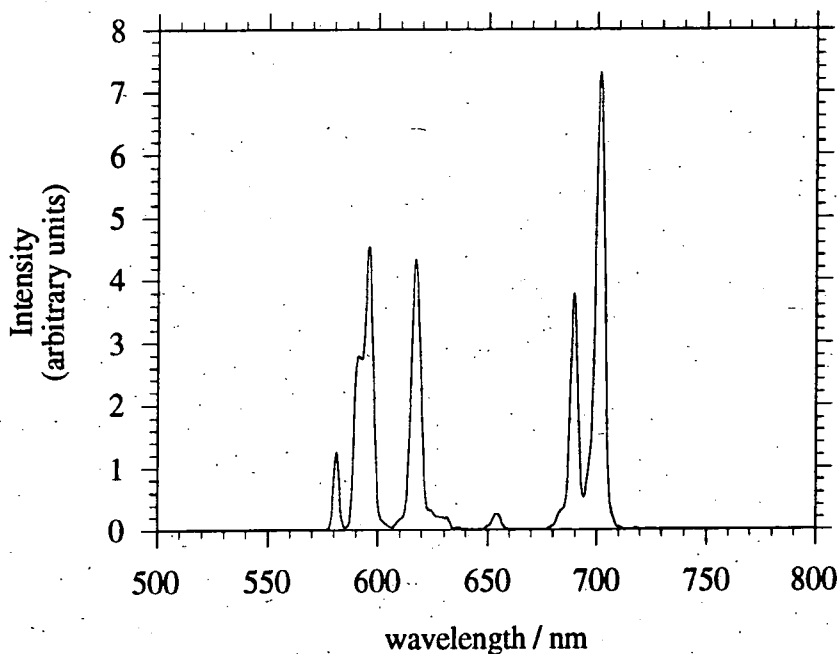


FIGURE 4.16 Metal luminescence emission spectrum of $[\text{Eu.39}]^{3+}$ in D_2O following excitation at 270 nm

Again, the luminescence was weak, with quantum yields of the order of 4×10^{-4} in CD_3OD . One important reason for this is apparent from the *fluorescence* spectrum of the naphthyl group in the europium complexes. Reference to Table 4.4 shows that the fluorescence quantum yield of $[\text{Eu.39}]^{3+}$ is very much lower than that of the terbium complex or the free ligand, both in H_2O and in CH_3CN . This behaviour probably reflects the fact that Eu^{3+} is able to deactivate the naphthyl excited singlet state efficiently, through an electron transfer mechanism involving transient formation of Eu^{2+} . Such a process is favoured by the relative ease of reduction of Eu^{3+} to Eu^{2+} as mentioned earlier. Indeed a study of intermolecular quenching of this type has been carried out³⁴ and a bimolecular quenching rate constant of $7.2 \times 10^9 \text{ M}^{-1}\text{s}^{-1}$ was reported in CH_3CN (briefly alluded to in section 4.9). This high rate constant, coupled with the high local concentration of Eu^{3+} in the vicinity of the naphthyl group, will result in electron transfer quenching which is highly competitive with fluorescence, accounting for the reduced quantum yield. Clearly, triplet formation will suffer for the same reason and hence the naphthyl-sensitised metal emission will be low.

The europium complexes of the bis-naphthyl containing ligands **41** and **42** were also prepared in CH_3CN . Bearing in mind that these compounds emit strongly around 400 nm (the excimer band) and that the free Eu^{3+} ion displays one of its strongest absorption bands at 397 nm ($\epsilon \approx 3 \text{ M}^{-1}\text{s}^{-1}$)³⁵, the overlap integral, J , for energy transfer from the naphthyl excimer to the bound europium ion should be high (this applies to both of the energy transfer mechanisms discussed in section 2.11). On this basis, it was hoped that the europium complexes of these ligands would show more intense metal emission than $[\text{Eu.39}]^{3+}$ and $[\text{Eu.40}]^{3+}$. Unfortunately, this did not prove to be the case. The most likely explanation is that the electron transfer quenching pathway is too fast relative to excimer formation and subsequent energy transfer to the metal. Again, the total fluorescence emission intensity was greatly reduced (Table 4.5).

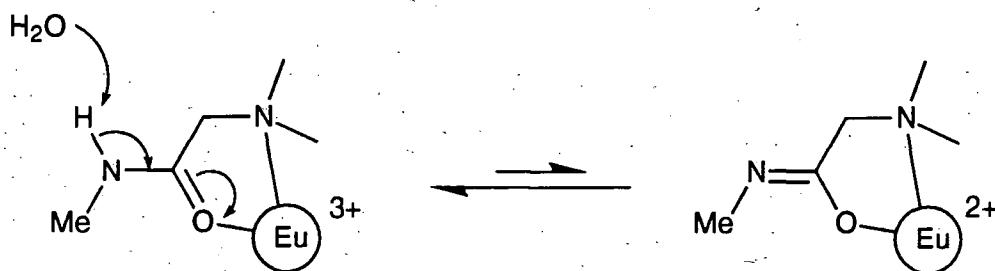
The excited state lifetimes have been measured in protiated and deuteriated solvents. Use of the Horrocks equation (section 1.3.3) gives q values of 1.37 and 1.33 for [Eu.39]²⁺ and [Eu.40]²⁺ respectively. Given that only one water molecule is bound to europium in the related, more hydrophilic complex [Eu.38]³⁺(3), a q value of unity would have been expected. The reason behind this discrepancy became apparent when lifetimes were recorded in acetonitrile. When measurements of lifetimes were compared for dried samples of [Eu.39]³⁺ or [Eu.40]³⁺ in MeCN and in MeCN after H/D exchange of the amide NH hydrogens (i.e. after dissolution in D₂O), it was found that the lifetime after H/D exchange was significantly longer (Table 4.8). Enhanced phosphorescence emission intensities were also noted following H/D exchange. A similar NH/ND exchange occurred rapidly in deuteriomethanol and the lifetimes in the deuteriated solvent were appreciably longer than those found in CH₃OH (Table 4.8). Such behaviour implies that there is an additional deactivation mechanism for the europium ⁵D₀ state through coupling to amide NH vibrational levels as mentioned in Chapter 3. Such a mechanism is much less efficient for amide N-D vibrations, owing to their lower stretching frequencies. An effect of this sort has not been reported before for an amide-bound europium complex although the effect has been noted with a 7-coordinate ligand based on 12N₄ where the single ring secondary amine underwent rapid NH/D exchange and led to a lengthening of the excited state lifetime.³⁶

This NH/ND exchange appeared to occur rapidly only with the europium complex. Monitoring of the ¹H NMR spectrum of the related yttrium complex of **40** showed that amide NH/ND exchange occurred quite slowly (eg. the amide resonance was still apparent in D₂O several hours after dissolution of the complex and the CH₂ protons of the C₁₀H₇CH₂NH unit appeared as a doublet). This may be ascribed to the ease of reduction of the europium complex (Eu^{III} to Eu^{II}) in such a way that the europium acts as a charge sink in the H/D exchange mechanism, promoting amide imidolisation (Scheme 4.6).

TABLE 4.8 Lifetimes of the excited states of [Eu.39]³⁺ and [Eu.40]³⁺ and the effect of N-H / N-D exchange

Complex	Solvent	τ / ms	k / ms ⁻¹
[Eu.39] ³⁺	H ₂ O	0.58	1.72
	D ₂ O	2.40	0.42
	CH ₃ CN ^a	0.85	1.18
	CH ₃ CN ^b	1.90	0.53
	CH ₃ OH	0.67	1.49
	CD ₃ OD	2.07	0.48
[Eu.40] ³⁺	H ₂ O	0.59	1.69
	D ₂ O	2.40	0.42
	CH ₃ CN ^{a,c}	1.02	0.98
	CH ₃ CN ^{b,c}	1.80	0.56
	CH ₃ OH ^c	0.74	1.35
	CD ₃ OD ^c	2.11	0.47

(a) No significant change in τ was found in CD₃CN. (b) After N-H / N-D exchange, following dissolution of the complex in D₂O followed by drying of the complex in vacuo (<10⁻² mmHg, 60°C, 3h). (c) Quantum yields of [Eu.40]³⁺ were as follows: in CH₃OH, 0.12 x 10⁻³; in CD₃OD, 0.38 x 10⁻³; in CH₃CN, 0.19 x 10⁻³; and in CH₃CN after H/D exchange, 0.27 x 10⁻³.



SCHEME 4.6 Possible rôle of europium in promoting N-H / N-D exchange ($R = \text{Me}$ or CH_2Np here)

The rate constant for depopulation of the europium excited state in water may be partitioned as the sum of the different contributions (equation 45) where k_{nat} is the natural luminescence rate constant for emission, k_{nr} the rate constant for non-radiative deactivation, k_{OH} the rate constant for energy transfer to coordinated OH oscillators and k_{NH} the rate constant for energy transfer to proximate NH oscillators.

$$k_{\text{H}_2\text{O}} = k_{\text{nat}} + k_{\text{nr}} + k_{\text{OH}} + k_{\text{NH}} \quad (45)$$

If $k_{\text{D}_2\text{O}} = k_{\text{nat}} + k_{\text{nr}}$, then equation (46) holds.

$$k_{\text{H}_2\text{O}} - k_{\text{D}_2\text{O}} = k_{\text{OH}} + k_{\text{NH}} \quad (46)$$

In the absence of an NH/ND effect and *assuming* that $q = 1$ (as is suggested by the X-ray analysis of a structurally similar compound, [Eu.38]³⁺), then $k_{\text{OH}} = 1/1.05 = 0.95$ (ms)⁻¹ (from equations 5 and 46). From this it follows that for [Eu.39]³⁺ (using equation 46 with values from Table 4.8):

$$1.72 - 0.42 = 0.95 + k_{\text{NH}} \quad \text{giving} \quad k_{\text{NH}} = 0.35 \text{ (ms)}^{-1} = 350 \text{ s}^{-1}$$

A similar analysis for [Eu.40]³⁺ gives $k_{\text{NH}} = 320 \text{ s}^{-1}$. Of course, the use of the Horrocks A_{Eu} parameter to estimate the deactivating contribution of the bound water is perhaps of limited validity, bearing in mind the error quoted by Horrocks discussed in Chapter 3. On the other hand, using the lifetime data for the behaviour of the complex in MeCN prior to and after amide H/D exchange, where the problem of estimating the O-H contribution does not arise, a value of 420 s^{-1} is calculated. The reasonable agreement between these values would suggest that this is probably a fairly reliable estimate of the relative contribution of coupling of the amide NH oscillators ($\nu_{\text{NH}} = 3250 \text{ cm}^{-1}$) to the Eu ⁵D₀ emissive state.

Luminescence lifetimes of the europium complex of **38** have been reported very recently.³ Values of k of 1.93 and 0.46 (ms)⁻¹ were reported in H₂O and D₂O respectively (corresponding to $q = 1.54$). These values are not dissimilar to those in Table 4.8 and are consistent with the theory outlined above. Indeed $k_{\text{H}_2\text{O}}$ is rather larger than the values for [Eu.39]³⁺ and [Eu.40]³⁺ which is fully consistent with this theory as there are, of course, more N-H bonds in the primary amide complex [Eu.38]³⁺. A value of 520 s^{-1} (for 8 N-H oscillators) may be calculated in this case.

There are, of course, two different N-H stretches for a primary amide. These have different energies (literature ν_{\max} values are 3390 and 3210 cm^{-1}) and will therefore have different quenching effects on europium. Thus, one would not expect the deactivating effect for eight oscillators in $[\text{Eu.38}]^{3+}$ to be exactly double that for four of them in $[\text{Eu.39}]^{3+}$ and $[\text{Eu.40}]^{3+}$. The authors of the work in question chose to ignore any significance of a q value of 1.54 and dismissed it as being within the usual quoted error of ± 0.5 .

4.13 Luminescence properties of the terbium complexes of 39 and 40

4.13.1 Introduction

The terbium complexes of 39 and 40 displayed only very weak emission. However, degassing of the solutions resulted in an enormous increase in the intensity of the metal luminescence. It is well-established that dissolved molecular oxygen has little effect on terbium luminescence (Chapter 1). On the other hand, the naphthyl triplet state will be susceptible to rapid quenching by molecular oxygen. Bearing in mind the small energy gap between the emissive Tb $^5\text{D}_4$ state (244 kJ mol^{-1}) and the triplet naphthyl level (255 kJ mol^{-1} is literature value for naphthalene itself, Table 4.1), this behaviour could be tentatively ascribed to a back energy-transfer process from the metal emissive state to the naphthyl triplet, which is subsequently deactivated by molecular oxygen. Such an explanation would not be unprecedented (see sections 1.3.4 and 1.7.1). Since the back energy transfer process would require thermal activation, a marked temperature dependence would be expected.

4.13.2 Characteristics of the terbium emission spectra

The terbium emission spectrum showed bands at the wavelengths expected for the transitions normally observed. However, whilst it was noted in Chapter 3 that the terbium spectra for the amide tris-phosphinates were essentially identical to those of the tetraphosphinates, here there are two very notable differences (Figure 4.17 cf. Figure 2.11). Firstly, the $J = 6$ band shows substantially enhanced intensity relative to the $J = 5$ band when compared to the tetraphosphinate complexes. Actually, it is well-known

that the $J = 6$ band is sensitive to the metal environment³⁷ and so this observation is not altogether surprising. A more interesting point is the difference in the fine structure. Here, the $J = 6$ and $J = 5$ bands do not display any sign of splitting, in complete contrast to the phosphinate complexes. Since fine structure is reduced upon moving to higher symmetry, this observation could be interpreted in terms of higher symmetry in the tetraamide complexes compared to the tetraphosphinates and may reflect the change from a square antiprismatic geometry for the former to the inverted square antiprismatic structure of the latter.

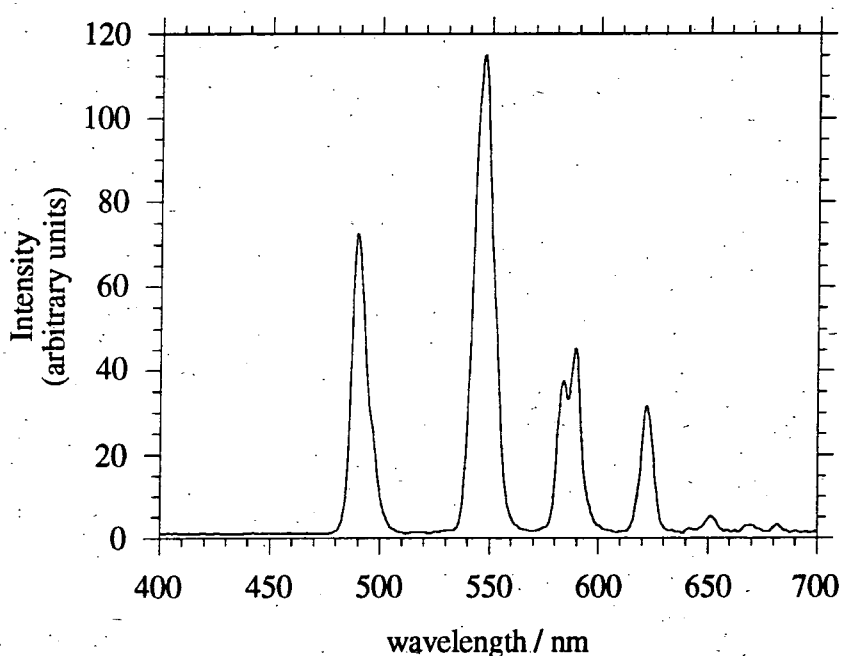


FIGURE 4.17 Metal luminescence emission spectrum of $[Tb.39]^{3+}$ in D_2O (degassed) following excitation at 270 nm (excitation and emission monochromator slit widths of 2.5 nm)

The emissive quantum yield of $[Tb.39]^{3+}$ in degassed ethanol solution at 295K was determined to be 0.11 by means of the fluorimeter (using quinine sulfate as the standard). This compares to emission which was barely detectable using the same instrument under aerated conditions.

4.13.3 A Flash Photolysis Study

With the assistance of Dr. Andrew Beeby of the University of Durham, a nanosecond laser flash photolysis study was undertaken for $[\text{Tb.39}]^{3+}$ in order to investigate, in more detail, the possibility of a thermally-activated back energy transfer process as mentioned above. The experimental details for these experiments are described in Chapter 5. A xenon chloride excimer laser was used to excite the sample at 308 nm. The duration of each laser pulse was 20 ns. During this time, the triplet level of the naphthyl group is populated to a significant extent, owing to the very high intensity of the laser pulse and this allows the absorbance of the triplet state to be monitored (see diagram 5.8). The absorbance at several wavelengths in the range 360 - 430 nm was recorded and the maximum absorbance occurred at 410 nm. This is close to the literature value for $\lambda_{\text{max}}^{\text{T-T}}$ of naphthalene of 415 nm (Table 4.1). Fortunately, ground state naphthalene does not absorb at this wavelength and so the observed absorption is a direct measure of the population of the triplet state. The rate of deactivation of the triplet state can therefore be probed by monitoring the decay of the absorbance at this wavelength, following the excitation pulse. A small modification of the instrumental set-up also allowed the decay of the terbium luminescence to be monitored on a much shorter timescale than that which could be achieved on the fluorimeter.

A degassed solution of $[\text{Tb.39}]^{3+}$ in water (10^{-3} M) at room temperature was examined in this way. The terbium luminescence showed an initial rapid rise over a few microseconds followed by a slow decay over several milliseconds (see Figures 4.19 and 4.20 showing behaviour in ethanol). The profile could be fitted to the sum of two exponentials with good residuals, and acquisition of data on short, intermediate and long timescales (1, 10 and 100 μs per division on the oscilloscope) allowed two rate constants to be extracted. The rate constant, k_1 , for the initial, rapid growth of the emission had a value of about $270\,000\text{ s}^{-1}$ ($\tau = 3.7\ \mu\text{s}$) whilst the rate constant, k_2 , for the slow decay was 1340 s^{-1} ($\tau = 0.75\text{ ms}$).

The naphthyl triplet absorption, on the other hand, displayed a rapid decay over the first few microseconds, with k_1 about $250\,000\text{ s}^{-1}$. The similarity of this value to the rate of growth of the terbium emission is strong evidence in support of an energy transfer process from the triplet state of the naphthyl group to the terbium. Following this initial fast decay, the triplet naphthyl was observed to decay over a much longer timescale with a rate constant, k_2 , of 1500 s^{-1} , which is close to the decay constant of 1340 s^{-1} found for the terbium decay. This observation can be interpreted in terms of formation of triplet naphthalene by energy transfer from the terbium excited state. In other words, an equilibrium is set up between the triplet naphthyl state and the terbium 5D_4 excited state, with the result that both decay at the same rate. The rapid growth of ^3Np through inter-system crossing from the excited singlet state occurred on a timescale which was too fast to monitor using the available instrumentation. The possibility of direct energy transfer from the singlet state to the metal could not be investigated for the same reason.

The effect of oxygen on these four rate constants was examined by studying the behaviour in the presence of a known pressure of oxygen. This was achieved by introducing air into the sample through a vacuum line with an aneroid pressure gauge attached. The voltage across the gauge was directly proportional to the pressure and, assuming that at atmospheric pressure, $[\text{O}_2] = 0.29 \times 10^{-3}\text{ M}$ in water (Table 4.2), this allowed the concentration of dissolved oxygen to be determined at each pressure. Not surprisingly, the rate of the initial fast decay of ^3Np was increased on introduction of oxygen, reflecting the fact that there is now an additional pathway for ^3Np deactivation, namely quenching by oxygen, the significance of which increases as the oxygen concentration increases. In the presence of a quenching species, the observed radiative rate constant, k_f , of an emitting or absorbing state is given by:

$$k_f = k_f^0 + \sum k_i^{\text{nr}} + k_Q[\text{Q}] \quad (47)$$

where the symbols have their usual meanings as in preceding chapters. Thus, a plot of the observed rate constant of deactivation against the concentration of the quencher Q

should yield a straight line of gradient k_Q . The k_1 values for the ^3Np state were plotted against the O_2 concentration and a linear relationship was indeed observed. A value of $1.26 \times 10^9 \text{ M}^{-1}\text{s}^{-1}$ was obtained for the second order rate constant for the quenching process. A similar analysis has been carried out for the rate constants, k_1 , associated with the growth of the terbium emission (Figure 4.18). A k_Q value of $1.4 \times 10^9 \text{ M}^{-1}\text{s}^{-1}$ was determined in this case. The similarity of these values is again consistent with terbium sensitisation by the ^3Np state. The values are similar to the literature k_Q values for oxygen quenching of the triplet state of free naphthalene (Table 4.1). The rate constant for the decay of the terbium emission was also increased on introduction of oxygen, which is further evidence in support of the proposed back energy transfer.

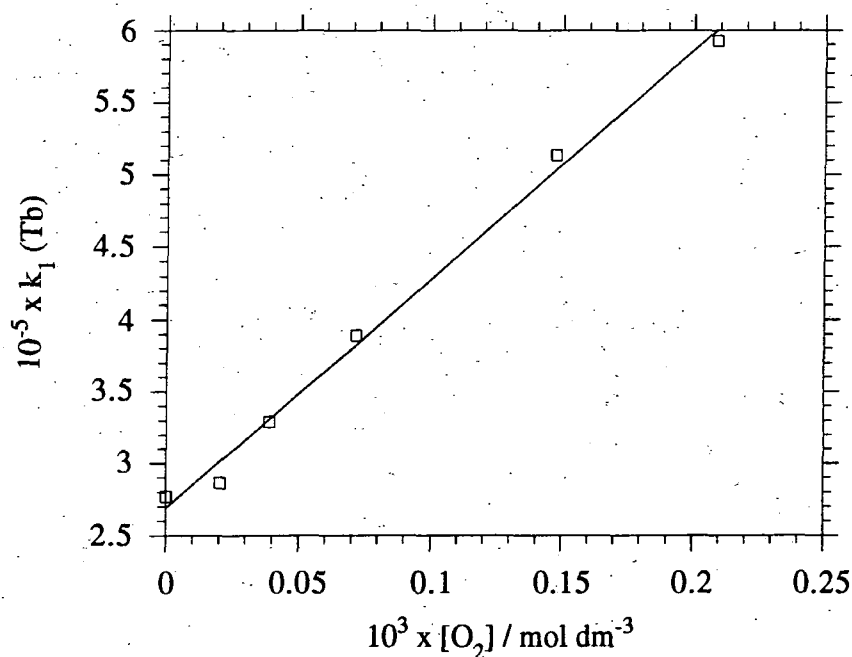


FIGURE 4.18 *The effect of oxygen on the rate constant, k_1 , for the growth of terbium emission, following laser excitation at 308 nm and detection at 490 nm.*

As pointed out earlier, the back energy transfer process is likely to require thermal activation as the triplet state of the naphthyl group is expected to be of slightly higher energy than the $\text{Tb } ^5\text{D}_4$ state. Thus, one would expect the back energy transfer process to be reduced as the temperature is lowered. Of course, at low temperatures, the efficiency of other non-radiative deactivation pathways for both the terbium excited

state and the ^3Np will also be diminished and so a decrease in the rate constants would be expected. A variable temperature study was undertaken making use of an Oxford Instruments cryostat, in which the temperature of the sample is controlled by allowing a flow of liquid nitrogen into the sample chamber which is counterbalanced by the application of an electric current to a heater in the chamber (cf. VT NMR). The temperature was monitored by means of a thermocouple and the current required to maintain the desired temperature was controlled electronically. (Further details in Chapter 5, section 5.2.9). Higher temperatures were obtained through the use of a thermostatted water bath, which rapidly circulated warm water through the sample holder. Ethanol was used as the solvent for this work as it allows a large range of temperatures to be examined in fluid solution. The range 150-330K was investigated.

The growth and decay profiles at 150 and 300 K are shown in Figures 4.19 and 4.20. The rate constant for decay of the terbium luminescence is seen to be reduced from 1250 s^{-1} at 300K to 500 s^{-1} at 150K and the decay of the long-lived ^3Np shows a similar pattern, with a reduction in k_2 from 1500 to 500 s^{-1} . Again, decay profiles which are common to both the metal and the ^3Np are consistent with formation of the latter through back energy transfer from the terbium excited state. A further feature is also apparent from these decay curves. Although the amount of ^3Np initially formed is about the same at both temperatures (initial triplet-triplet absorbance is approximately equal for the two profiles in Figure 4.19), at later times after the flash, there is much less ^3Np at 150K, as evidenced by the smaller triplet absorbance at 150K compared to 300K in Figure 4.20. This indicates that the back energy transfer is indeed a thermally-activated process. Reduction of the temperature from 300K to 150K is seen to reduce substantially its significance. The ratio of the amount of ^3Np at long time intervals (i.e. that which is formed by energy transfer from terbium) to the amount produced initially (by inter-system crossing from the singlet), as measured by the absorbances, is a useful measure of the extent to which the back energy transfer is occurring. This ratio is effectively the equilibrium constant K for the back energy transfer process and was determined at several different temperatures. The variation of K with temperature

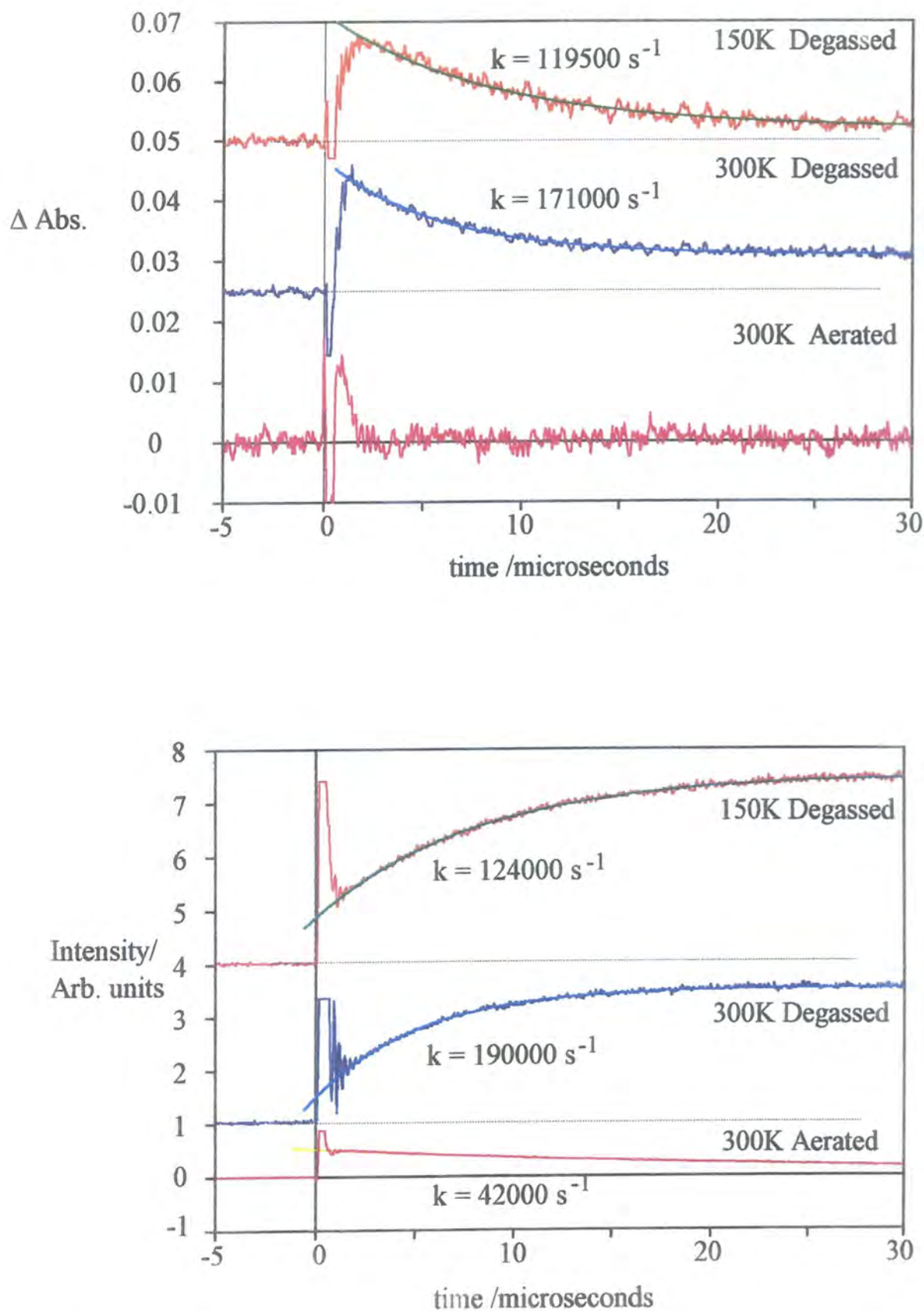


FIGURE 4.19 Growth and initial fast decay of the triplet naphthyl absorbance at 410 nm (upper) and the grow-in of the terbium luminescence at 490 nm (lower) on a microsecond timescale for $[\text{Tb.39}]^{3+}$ in ethanol, following pulsed laser excitation at 308nm.

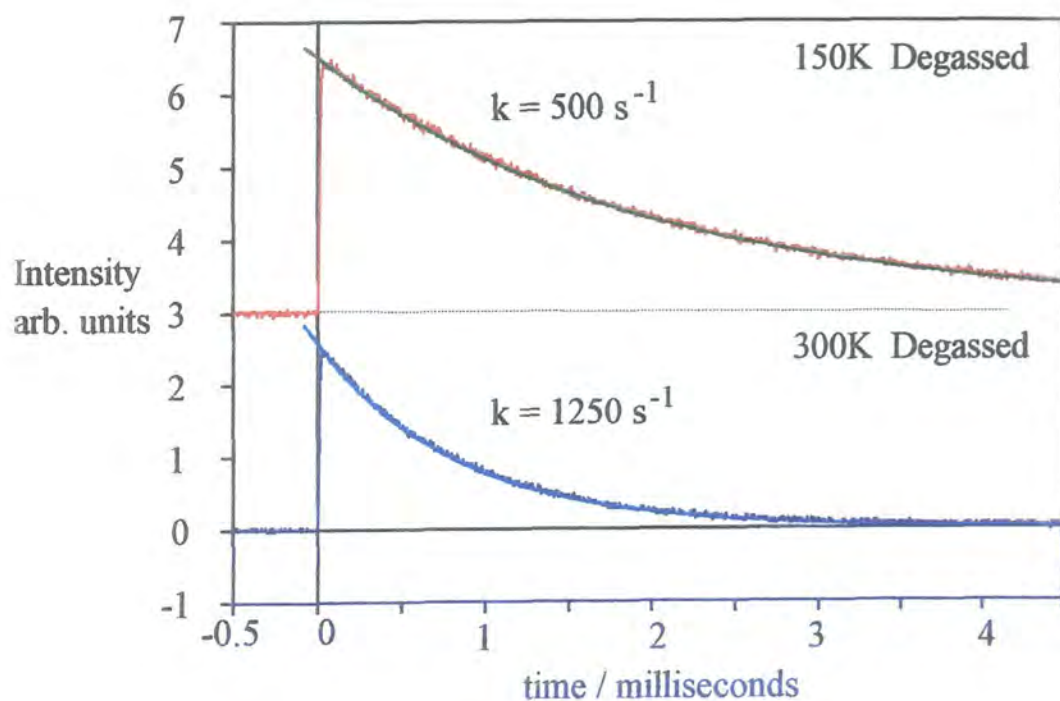
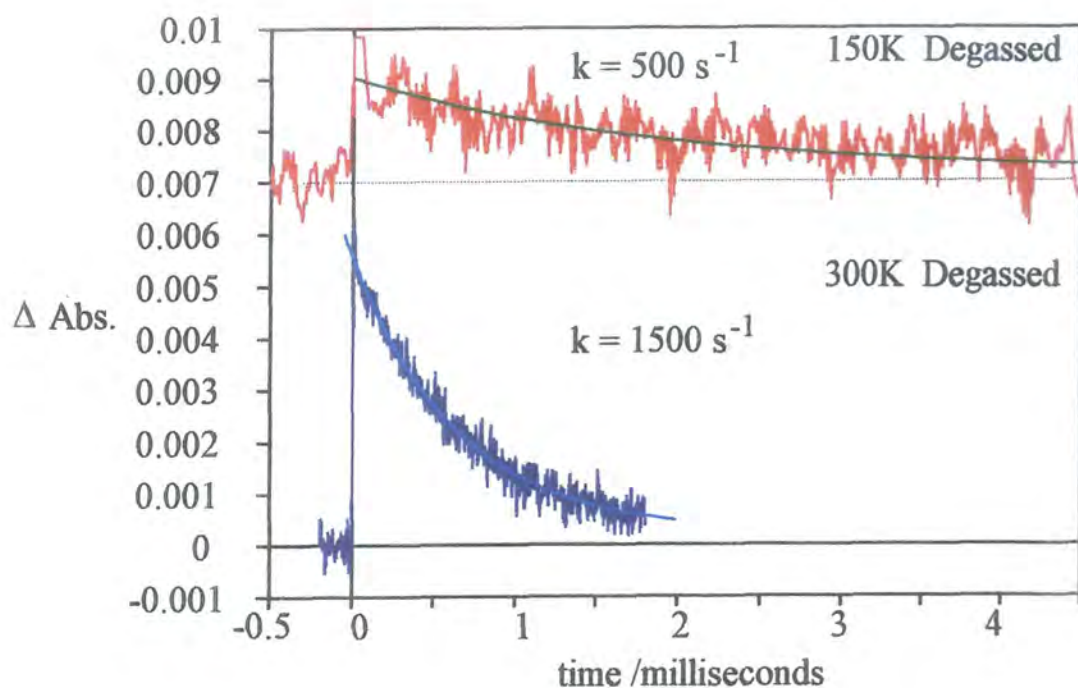


FIGURE 4.20 Decay of the triplet naphthyl absorbance at 410 nm (upper) and of the terbium luminescence at 490 nm (lower) on a millisecond timescale for $[\text{Tb.39}]^{3+}$ in ethanol, following pulsed laser excitation at 308 nm.

should allow the enthalpy change, ΔH^0 , of the energy transfer process to be estimated through application of the van't Hoff isochore (equation 48).

$$\frac{d \ln K}{dT} = \frac{\Delta H^0(T)}{RT^2} \quad (48)$$

Since $(d/dT)(1/T) = -1/T^2$, an alternative form of equation (48) is that given below:

$$\frac{d \ln K}{d(1/T)} = - \frac{\Delta H^0(T)}{R} \quad (49)$$

Thus, the gradient of a plot of $\ln K$ against $1/T$ at a given temperature will provide the value of ΔH^0 at this temperature. Since ΔH^0 is often only weakly temperature-dependent, such a plot may approximate to a straight line. An analysis of this type was carried out on the flash photolysis data and the result is shown in Figure 4.21. The plot does indeed give a reasonable straight line and the enthalpy change ΔH^0 for the back energy transfer process is estimated from the gradient to be 4.5 kJ mol^{-1} . Using literature values for the triplet level of naphthalene and the energy of the excited terbium level, an energy gap of 11 kJ mol^{-1} would be predicted, although it should be noted that this refers to ΔG^0 rather than to ΔH^0 . The value of ΔG^0 at 298K is estimated to be 2.5 kJ mol^{-1} using the $\ln K$ value at this temperature. Of course, one would not expect perfect agreement with the literature estimate as the naphthyl triplet energy in $[\text{Tb.39}]^{3+}(\text{aq})$ will inevitably differ from that of naphthalene itself.

4.13.4 Effect of β -cyclodextrin on terbium luminescence

Reference to Table 4.7 shows that binding of β -cyclodextrin to $[\text{Tb.39}]^{3+}$ (degassed aqueous solution) under the conditions given in the table leads to a significant increase in the fluorescence emission intensity of the naphthyl chromophore. The increase (13%) is of a similar magnitude to that observed for the zinc complex and can be interpreted in terms of reduced non-radiative deactivation of the excited singlet state. Of more interest here is the much larger rise, 44%, in the intensity of the metal emission

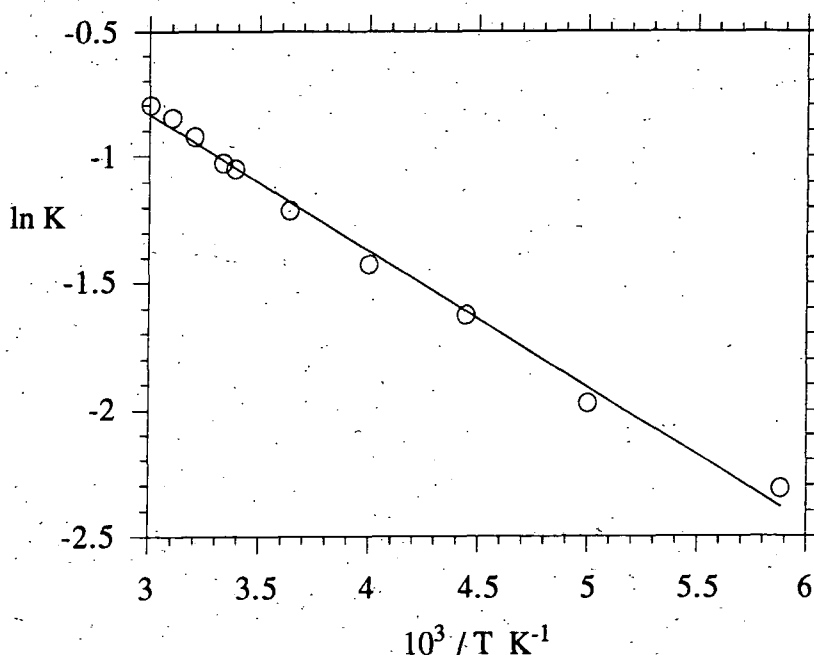


FIGURE 4.21 A plot of $\ln K$ versus $1/T$ where K is the equilibrium constant for the back energy transfer process, as determined from the triplet absorbances at short and long time intervals after the excitation flash.

together with a significant lengthening of the luminescence lifetime (0.67 - 0.85 ms). These observations would appear to indicate that there is a reduction in the efficiency of the back energy transfer deactivation process. It is probably not so much the energy transfer process itself which is affected, but rather the fact that the triplet naphthyl formed as a result of the back energy transfer is subject to a reduced degree of non-radiative deactivation, in a similar manner to the singlet state. Enhanced phosphorescence is commonly observed for aryl groups included inside cyclodextrins.^{32,38} Indeed, the effect on phosphorescence is generally more marked than for fluorescence, partly because triplet-triplet annihilation, a common phosphorescence quenching channel, is greatly suppressed on binding to the cyclodextrin. Thus, the lifetime of the ^3Np will be increased and, since the $\text{Tb } ^5\text{D}_4$ state is in equilibrium with the ^3Np as deduced from the flash photolysis studies above, this increase will also be reflected in a lengthening of the terbium lifetime and an enhancement of the metal luminescence intensity. Indeed, the results of this experiment serve to reinforce the conclusions drawn earlier concerning this equilibrium.

4.14 Other experiments using flash photolysis

As pointed out earlier, the metal emission of the europium complex was weak and the fluorescence of the naphthyl group was much lower than that of the terbium complex. It was suggested that this is probably due to an electron transfer process from the excited naphthyl singlet state to the Eu^{3+} ion, favoured by the relative ease of reduction of Eu^{3+} to Eu^{2+} . Such a process ought to lead to transient formation of a naphthyl radical cation, Np^+ . The triplet-triplet absorption spectrum of such a species is reported to have an absorbance maximum of 685 nm.¹¹ A flash photolysis experiment was carried out on $[\text{Eu.39}]^{3+}$ in CH_3CN and the absorbance at this wavelength was probed. There was no evidence for the formation of a Np^+ transient. Of course, this does not necessarily mean that such a species is not formed, rather that charge recombination occurs on a timescale which is faster than that which could be monitored using the instrumentation available.

The importance of amine-to-aryl photoinduced electron transfer as a deactivation pathway for the naphthyl excited singlet state has been discussed in some detail in preceding sections. The perturbation of the rate of this process accounts for the fluorescence enhancements observed on binding of metals or on protonation. The effect of metal complexation on the *triplet* state of the naphthyl group was examined using the laser flash photolysis apparatus, monitoring the ^3Np T-T absorbance at 410 nm. The ^3Np state of the free ligand **39** in degassed CH_3CN displayed monoexponential decay, with a rate constant, k , of $12\,200\text{ s}^{-1}$ at room temperature. Addition of 5 equivalents of zinc triflate to this solution, followed by degassing, resulted in a reduction of the triplet decay rate constant to 8400 s^{-1} corresponding to an increase in the triplet lifetime from 82 to 120 μs on binding of zinc. This seems to indicate that photoinduced electron transfer from the amine nitrogen atoms may also serve as a deactivation pathway for the triplet state of naphthalene, in a similar manner to the singlet. (This is consistent with the reports of others; for example, Davidson has shown that the triplet excited state of 1-chloronaphthalene is quenched by tertiary amines in polar solvents³⁹). Such a process will again be disfavoured by metal binding,

owing to the increase in the oxidation potential of the amine nitrogens. Of course, the behaviour will be quantitatively different from that observed for the singlet (and the concomitant changes in fluorescence) since the redox properties of the triplet and singlet states will differ.

4.15 Terbium and Europium Complexes of 12N₄ tetraamides incorporating a quinolinone group as sensitiser

As pointed out in Chapter 1, the number of different types of sensitiser which have been investigated in conjunction with highly stable, water soluble complexes of europium and terbium is quite limited. A recent report (September 1994) described the use of a Eu³⁺ complex of a DTPA-based ligand, modified with a 7-amino-4-methyl-2(1H)-quinolinone group as sensitiser (Figure 4.22).⁴⁰ This chromophore has the trivial name carbostyryl 124 and is denoted cs124 in subsequent discussions. The initial report was concerned with the use of this complex as an energy donor in distance measurements based on energy transfer efficiencies (cf. section 2.11). Two subsequent reports have appeared; one on the use of the analogous terbium complex⁴¹ and a second describing the use of the same chromophore linked, as an amide, through one of the carboxylates of TTHA, TETA or DOTA.⁴²

In each of these reports, it was claimed that the emissive quantum yield of the lanthanide ion (as opposed to the quantum yield of the entire complex) is probably almost unity in D₂O. This quantum yield was not actually measured. The authors attempted to justify this rather bold statement on the basis that D₂O is very inefficient at deactivating terbium luminescence, that the carbostyryl sensitiser does not contribute to non-radiative deexcitation and, thirdly, that "polyaminocarboxylate chelates are known to have group frequencies which are unable to deexcite lanthanides." With respect to this third point, the authors cite the early papers by Horrocks on the use of lifetime measurements in D₂O and H₂O for determination of q values. In fact, Horrocks has not claimed that such ligands are unable to deactivate the excited states of the lanthanides.

A further piece of evidence was used to support the assumption of an emissive quantum yield of unity, namely that the energy transfer experiments, making use of Förster theory to calculate R_0 , were in good agreement with the donor-acceptor distances obtained using conventional fluorescence resonance energy transfer experiments and the known lengths of the DNA chains. Actually, the R_0 value is relatively insensitive to the value of the emissive quantum yield of the donor, ϕ_D , owing to the sixth root dependence (equation 50).³⁹

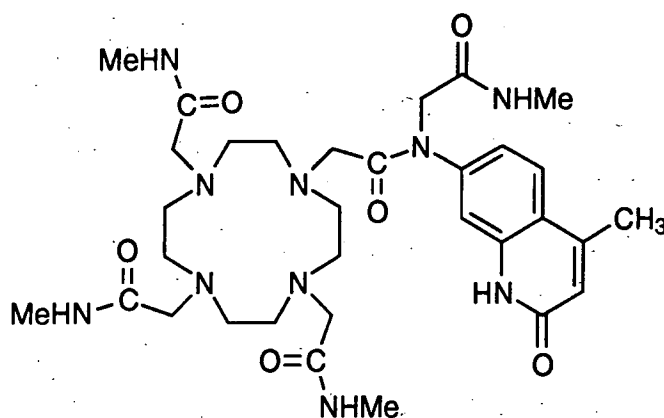
$$R_0^6 = (8.79 \times 10^{-5} J \kappa^2 n^{-4} \phi_D) \text{ \AA} \quad (50)$$

where the symbols have the meanings given in section 2.11. Thus, the authors calculate an R_0 value of 65 Å based on a donor emissive quantum yield of unity. If one assumes a more realistic value of, say, 0.25, then R_0 decreases to 52 Å. Proportionately, this is a relatively small change and could still be roughly consistent with the expected separation of donor and acceptor, especially bearing in mind that there is some uncertainty regarding the exact positions of the dyes due to the flexible six-carbon linkers used for attachment.

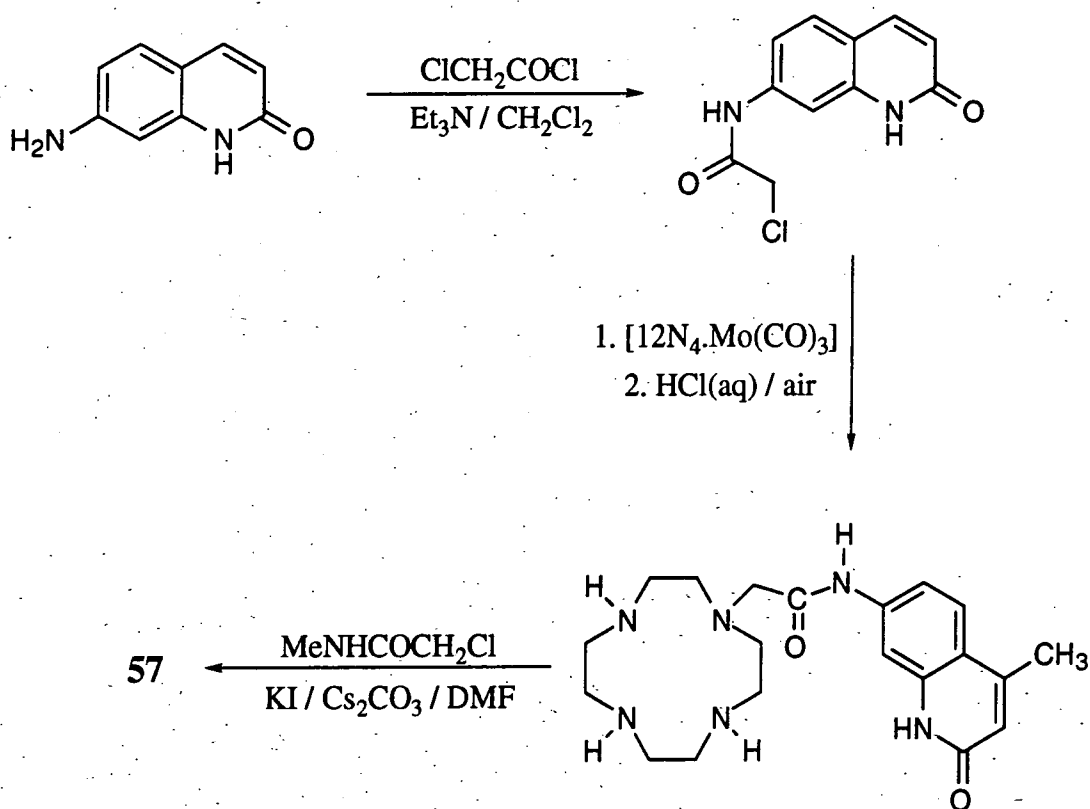
Aside from this assumption of a quantum yield of unity, the work has a more important shortcoming, namely that the overall emissive quantum yields for the complexes, on excitation of the cs124 chromophore, were not measured. In other words, there is no way of concluding from the work published so far whether or not the cs124 group is an *efficient* sensitiser of europium and terbium. The authors maintain that the quantum yield of interest is the probability that the lanthanide re-emits light *after* it has been excited. On this basis, one might just as well use [Tb.DOTA]⁻ or [Eu.DOTA]⁻. The question of the efficiency of the energy transfer from the chromophore to the metal was not addressed.

In connection with the work described in this thesis and the search for efficient sensitisers of europium and terbium, it was of interest to determine the overall quantum

yields attainable through the use of cs124 as sensitiser. This, after all, is the factor which determines the suitability of a given system for the applications in mind and not just the quantum yield of emission. The ligand **57** was therefore prepared using the procedure shown in Scheme 4.7, again making use of the molybdenum tricarbonyl complex of $12N_4$ to allow selective functionalisation of one of the four ring nitrogens. The final product was purified by reverse-phase HPLC and the terbium and europium complexes were subsequently prepared by reaction with the appropriate metal triflate in CH_3CN , as described for the naphthyl compounds **39** and **40**.

**57**

Lifetimes, fluorescence quantum yields of the cs124 group and metal luminescence quantum yields have been determined for the 2 complexes in H_2O and D_2O and the results are shown in Table 4.9, together with the q values determined by the Horrocks equation. The hydration state of the terbium complex is about 1, indicating one bound water molecule, an observation which is entirely consistent with previous results on $12N_4$ -tetraamide complexes as described earlier. The europium complex displays a significantly higher q value of 1.28. This is again consistent with an N-H / N-D exchange process of the type described for the europium complexes of the naphthyl ligands **39** and **40**. It is reassuring to find this behaviour reproduced here, as the 3 structures are very similar.



SCHEME 4.7 The synthetic procedure used in the preparation of ligand 57

The quantum yield of fluorescence for the cs124 moiety is lower in the terbium complex than in the free ligand (Table 4.9). This could be interpreted in terms of energy transfer from the excited singlet state of the chromophore to the bound metal. Bearing in mind that the energy transfer normally occurs from the triplet state (Chapter 1), a rather more likely explanation is that the lanthanide ion, with its high spin-orbit coupling constant, is able to enhance the rate of inter-system crossing. Of rather more interest is the observation that ϕ_{fl} for the europium complex is significantly lower than that of the terbium complex. This could again be due to an electron transfer process from the excited singlet state of the aryl chromophore to the metal, with transient formation of Eu^{2+} and a radical cation.

Such an effect could also account for the relatively low metal luminescence quantum yields observed for the europium complex (H_2O : 0.006; D_2O : 0.014). Sensitisation of terbium is clearly more efficient, with quantum yields an order of magnitude higher.

For both metals, the room temperature metal luminescence excitation spectra (see Figure 4.23) closely resembled the UV absorption spectra, consistent with an energy transfer process from the chromophore. Thus, we can conclude that cs124 does indeed provide reasonably efficient sensitisation of both metals, but is apparently rather more suited to terbium.

The metal excitation spectrum in aqueous solution at 295K resembles that provided by Li and Selvin in their related work. An excitation spectrum was also recorded in ethanol at 150K and is shown in Figure 4.23. Compared to the room temperature spectrum in aqueous solution, a small bathochromic shift is noted and there appear to be some additional bands. These almost certainly reflect a partial resolution of the vibrational fine structure on reducing the temperature.

TABLE 4.9 *Luminescence data for the europium and terbium complexes of ligand 57*

Complex	τ (298K) / ms		ϕ (298K) / ms		q^a	ϕ_{fl}^b
	D ₂ O	H ₂ O	D ₂ O	H ₂ O		
[Eu.57] ³⁺	1.47	0.51	0.014	0.006	1.28	0.018
[Tb.57] ³⁺	1.12	0.88	0.15	0.13	1.02	0.044
[Tb.57] ³⁺	2.09	1.38	0.28	0.25	1.04	0.043

(degassed)

a) q is the hydration state obtained using the Horrocks equation.

b) A fluorescence quantum yield of 0.075 was measured for the ligand 57 in water.

For both europium and terbium, the appearance of the metal luminescence spectra were very similar to those of the corresponding complexes of ligands 39 and 40 (eg. compare figures 4.23 and 4.17). For example, the terbium spectrum again displayed no splitting of the $J = 6$ and $J = 5$ bands but again an enhanced intensity of the former was noted. These observations are consistent with the expected similarity in the structures, all three ligands being N-substituted tetraamides.

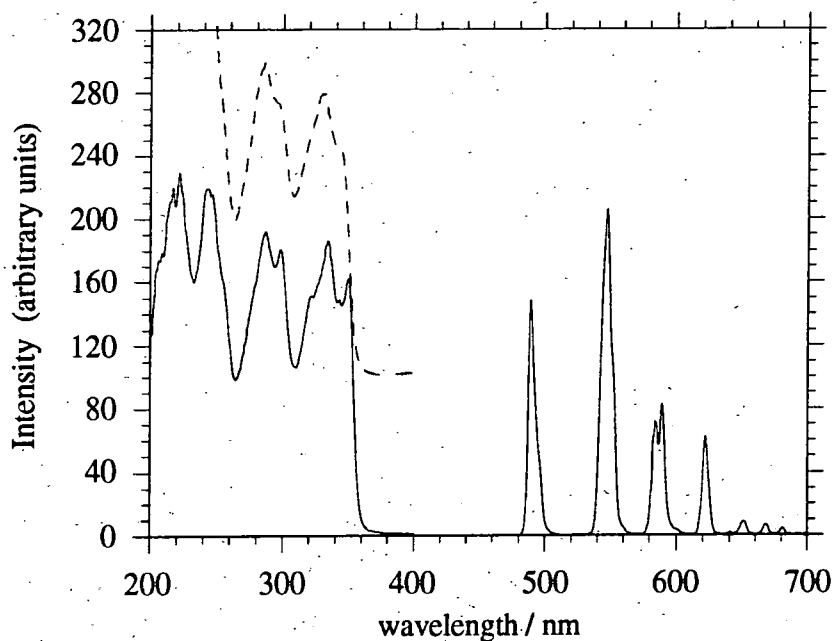


FIGURE 4.23 *Left: Metal luminescence excitation spectra ($\lambda_{em} = 545 \text{ nm}$) of $[\text{Tb.57}]^{3+}$ in water at 298K (dashed line) and in ethanol at 150K (solid line). Right: Corrected emission spectrum ($\lambda_{ex} = 330 \text{ nm}$) of $[\text{Tb.57}]^{3+}$ in solution in ethanol ($20 \mu\text{M}$) at 150K. Excitation and emission monochromator slit widths set to 2.5 nm. in each case.*

A further feature of the terbium complex is also apparent from Table 4.9, namely that a substantial increase in both the quantum yield of metal emission and of the luminescence lifetime is observed upon degassing of the solution. As explained for $[\text{Tb.39}]^{3+}$, since oxygen is known to have little direct effect on lanthanide luminescence, this is most likely to reflect a back energy transfer process from the metal to the triplet state of the chromophore, which may subsequently be deactivated by oxygen. The triplet energy of cs124 is not available but one might expect it to be of the order of $260 - 280 \text{ kJ mol}^{-1}$ by comparison with structurally-related compounds (amounting to an energy gap relative to the $\text{Tb } ^5\text{D}_4$ level of $5 - 30 \text{ kJ mol}^{-1}$). Under such circumstances, significant back energy-transfer at room temperature would not be unreasonable.

Again, such a process will require thermal activation and so a variable temperature study of the lifetimes and intensities of the metal emission was undertaken in order to probe the effect in more detail. The results are shown in Figure 4.24, for an aerated solution of $[\text{Tb.57}]^{3+}$ in ethanol. Clearly, temperature has a very significant effect: the lifetime at 225K is almost 4 times its value at 335K and the intensities are greatly affected. These observations are consistent with the proposed thermally-activated back energy transfer as a deactivation pathway for the excited terbium $^5\text{D}_4$ state. The effects of both temperature and oxygen are not as dramatic as for $[\text{Tb.39}]^{3+}$, where the luminescence was barely detectable under aerated conditions at room temperature. This almost certainly reflects simply a larger energy gap between the Tb $^5\text{D}_4$ level and the triplet state of the chromophore in the present instance.

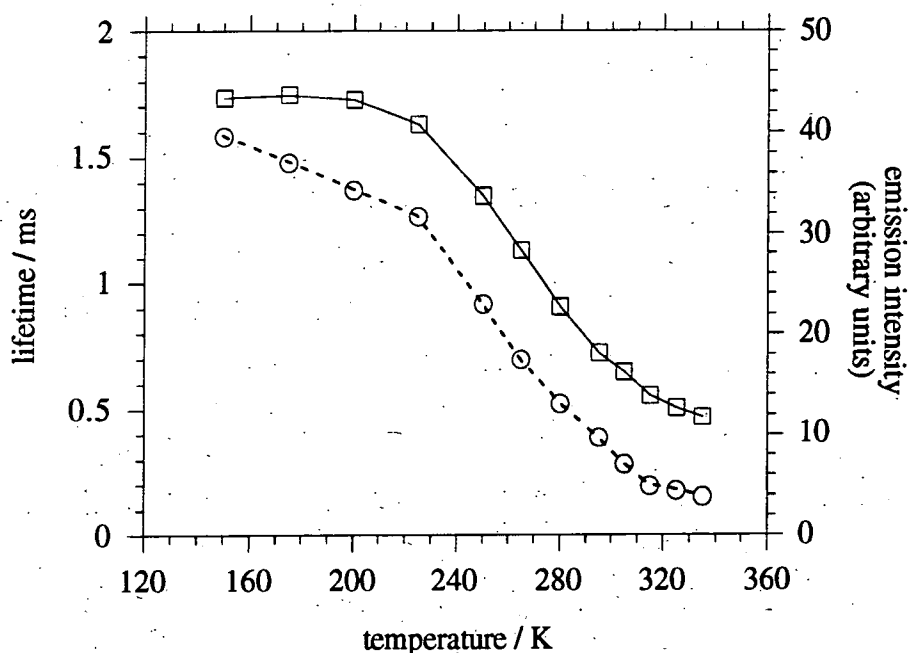


FIGURE 4.24 The effect of temperature on the metal luminescence intensity (circles) and lifetime (squares) for $[\text{Tb.57}]^{3+}$ in solution in ethanol (aerated), following excitation at 320 nm.

Curiously, the previous work on the cs124 systems discussed above found no temperature effect on excited state lifetimes. However, no experimental details concerning this point were provided in any of the publications and it seems likely that only two temperatures were examined, 278 and 295K. The effect over this range would

be quite small and might have been dismissed as being within the experimental error of the measurements. The authors maintain that the similarity of the lifetimes obtained to those of structurally related complexes containing other sensitising groups is good evidence for the lack of a deactivation pathway through the cs124 group, although only two complexes were cited. It is perhaps worth noting in passing that the back energy transfer is not always clear-cut for a given chromophore. For example, it was pointed out in Chapter 1 that back energy transfer to bipyridine is particularly efficient in the terbium complex of cryptand **7**. In contrast, it was subsequently reported that no such effect was observed for [Tb.**9**]³⁺, even though this complex also has three metal-coordinated bipyridine units. This is a rather strange result but would appear to imply that the back energy transfer has a sensitive dependence on the exact structure of the complex. Thus, it is perhaps not completely unreasonable for the cs124 unit to display different behaviour in [Tb.**56**] compared to [Tb.**57**]³⁺, although such a difference would be very difficult to comprehend.

References for Chapter 4

1. R. Katakya, K.E. Matthes, P.E. Nicholson, D. Parker, H.-J. Buschmann, *J. Chem. Soc., Perkin Trans. 2*, 1990, 1425. R. Katakya, D. Parker, A. Teasdale, J.P. Hutchinson and H.-J. Buschmann, *J. Chem. Soc., Perkin Trans. 2*, 1992, 1347.
2. S. Amin, J.R. Morrow, C.H. Lake and M.R. Churchill, *Angew. Chem. Int. Ed. Engl.*, 1994, **33**, 773. J.R. Morrow, S. Amin, C.H. Lake and M.R. Churchill, *Inorg. Chem.*, 1993, **32**, 4566.
3. S. Amin, D.A. Voss, Jr., W. DeW. Horrocks, Jr., C.H. Lake, M.R. Churchill and J.R. Morrow, *Inorg. Chem.*, 1995, **34**, 3294.
4. L. Carlton, R.D. Hancock, H. Maumela and K.P. Wainwright, *J. Chem. Soc., Chem. Commun.*, 1994, 1007.

5. H. Maumela, R.D. Hancock, L. Carlton, J.H. Reibenspies and K.P. Wainwright, *J. Am. Chem. Soc.*, 1995, **117**, 6698.
6. S. Fukuoka, M. Chono and M. Kohno, *J. Chem. Soc., Chem. Commun.*, 1984, 1458. *Idem*, *J. Org. Chem.*, 1984, **49**, 1458.
7. J.F. Desreux, A. Dumont, V. Jacques, P. Qixiu, *Tetrahedron Lett.*, 1994, **35**, 3707.
8. R. Delgado and J.J.R. Frausto da Silva, *Talanta*, 1982, **29**, 815; H. Stetter and W. Frank, *Angew. Chem. Int. Ed. Engl.*, 1976, **15**, 686.
9. D. Rehm and A. Weller, *Isr. J. Chem.*, 1970, **8**, 259.
A. Weller, *Pure Appl. Chem.*, 1968, **16**, 115.
10. F. Scandola, V. Balzani and G.B. Schuster, *J. Am. Chem. Soc.*, 1981, **103**, 2519.
11. S.L. Murov, I. Carmichael and G.L. Hug, 'Handbook of Photochemistry', 2nd edition, Marcel Dekker: New York, 1993.
12. 'CRC Handbook of Organic Photochemistry', Volumes I and II, ed. J.C. Scaiano, CRC Press Inc., Boca Raton, Florida, 1989.
13. T. Förster and K. Kaspar, *Z. Phys. Chem. (Munich)*, 1954, **1**, 275.
14. T. Förster, *Pure Appl. Chem.*, 1962, **4**, 121.
15. F.C. DeSchryver, P. Collart, J. Vandendriessche, R. Goedeweck, A. Swinnen and M. Van der Auweraer, *Acc. Chem. Res.*, 1987, **20**, 159.
16. S.S. Yanari, F.A. Bovey, R. Lumry, *Nature*, 1963, **200**, 242.
17. F. Hirayama, *J. Chem. Phys.*, 1965, **42**, 3163.
18. S. Ito, M. Yamamoto and Y. Nishijima, *Bull. Chem. Soc. Jpn.*, 1981, **54**, 35.
19. M. Goldenberg, J. Emert and H. Morawetz, *J. Am. Chem. Soc.*, 1978, **100**, 7171.
20. J.B. Aladekomo and J.B. Birks, *Proc. R. Soc. London, Ser. A.*, 1965, **284**, 551.
J.B. Birks and T.A. King, *ibid*, 1966, **291**, 244.
21. J.B. Birks, D.J. Dyson and I.H. Munro, *Proc. R. Soc. London, Ser. A.*, 1963, **275**, 575.

22. K.A. Zachariasse, G. Duveneck, G. Kühnle, P. Reynders and G. Striker, *Chem. Phys. Lett.*, 1987, **133**, 390.
23. C. Reichardt, 'Solvents and Solvent Effects in Organic Chemistry', 2nd edn., VCH: Weinheim, 1988, p. 365.
24. P. Tundo and J.H. Fendler, *J. Am. Chem. Soc.*, 1980, **102**, 1760.
25. I. Aoki, H. Kawabata, K. Nakashima and S. Shinkai, *J. Chem. Soc., Chem. Commun.*, 1991, 1771.
26. K. Kumar, M. Magerstädt and O.A. Gansow, *J. Chem. Soc., Chem. Commun.*, 1989, 145.
27. M.-Y. Chae, X.M. Chérian and A.W. Czarnik, *J. Org. Chem.*, 1993, **58**, 5797.
28. L. Fabbrizzi, M. Licchelli, P. Pallavicini, A. Perotti and D. Sacchi, *Angew. Chem. Int. Ed. Engl.*, 1994, **33**, 1975.
29. See, for example, R.Y. Tsien in 'Fluorescent Chemosensors for Ion and Molecule Recognition', Ed: A.W. Czarnik, American Chemical Society: Washington, DC, 1993. Chapter 9.
30. F. Fages, J.-P. Desvergne, H. Bouas-Laurent, J.-M. Lehn, J.P. Konopelski, P. Marsau and Y. Barrans, *J. Chem. Soc., Chem. Commun.*, 1990, 655.
31. R. Ballardini, V. Balzani, A. Credi, M.T. Gandolfi, F. Kotzbyba-Hibert, J.-M. Lehn and L. Prodi, *J. Am. Chem. Soc.*, 1994, **116**, 5741.
32. See, for example: J. Emert, D. Kodali and R. Catena, *J. Chem. Soc., Chem. Commun.*, 1981, 758. N. J. Turro, J.D. Bolt, Y. Kuroda, I. Tabushi, *Photochem. Photobiol.*, 1982, **35**, 69. N. J. Turro, T. Okubo and C. Chung, *J. Am. Chem. Soc.*, 1982, **104**, 1789.
33. Reviews on the history and background to ESMS are provided by: J.B. Fenn, M. Mann, C.K. Meng, S.F. Wong and C.M. Whitehouse, *Science*, 1989, **246**, 64. C.M. Whitehouse, R.N. Dreyer, M. Yamashita and J.B. Fenn., *Anal. Chem.*, 1985, **57**, 675.
34. N. Sabbatini, M.T. Indelli, M.T. Gandolfi and V. Balzani, *J. Phys. Chem.*, 1982, **36**, 3585.

-
35. W.T. Carnall in 'Handbook on the Physics and Chemistry of the Rare Earths', eds. K.A. Gschneider, Jr. and L. Eyring, North Holland Publishing Company, 1979. Chapter 24.
 36. P.L. Anelli, V. Balzani, L. Prodi and F. Uggeri, *Gazz. Chim. Ital.*, 1991, **121**, 359.
 37. J.-C.G. Bünzli in 'Lanthanide Probes in Life, Chemical and Earth Sciences', eds: J.-C.G Bünzli and G.R. Choppin, Elsevier: Amsterdam, 1989. Chapter 7.
 38. R.A. Bissell and A.P. de Silva, *J. Chem. Soc., Chem. Commun.*, 1991, 1148.
 39. R.A. Beecroft, R.S. Davidson, D. Goodwin, J.E. Pratt and X.J. Luo, *J. Chem. Soc., Faraday Trans.*, 1986, **82**, 2393.
 40. P.R. Selvin, T.M. Rana and J.E. Hearst, *J. Am. Chem. Soc.*, 1994, **116**, 6029.
 41. P.R. Selvin and J.E. Hearst, *Proc. Nat. Acad. Sci. USA*, 1994, **91**, 10024.
 42. M. Li and P.R. Selvin, *J. Am. Chem. Soc.*, 1995, **117**, 8132.

Chapter 5

CHAPTER 5

Experimental Procedures

5.1 Synthetic procedures and characterisation

5.1.1 General points

Reaction conditions

Reactions requiring an inert atmosphere or anhydrous conditions were carried out under a dynamic atmosphere of dry, oxygen-free nitrogen or argon using standard Schlenk-line techniques. Solvents were dried from an appropriate drying agent where required and water was purified by the 'Purite_{STILL} plus' system.

Purification procedures

Thin layer chromatography was carried out using neutral aluminium oxide plates (Merck Art 5550) or silica plates (Merck Art 5554), both types being fluorescent on irradiation at 254 nm. Preparative column chromatography was carried out using neutral alumina (Merck Aluminium Oxide 90, activity II-III, 70-230 mesh) pre-treated with ethyl acetate; or using silica (Merck Silica Gel 60, 230-400 mesh). Dichloromethane for chromatography was HPLC or Analar[®] grade; other eluants were distilled prior to use. Analysis by HPLC was performed by means of a Varian 9010/9065 Polychrom system using, unless stated otherwise, a Technical Hypersil 50DS reverse-phase column and a flow-rate of $1.4 \text{ cm}^3 \text{ min}^{-1}$. Preparative HPLC was achieved using a Varian Vista 5500/9050 system.

Characterisation

Infra-red spectra were recorded using a Perkin-Elmer 1600 FT spectrometer with GRAMS Analyst operating software. Solid samples were incorporated into KBr discs; liquids and oils were examined as thin films. The acquisition of solution spectra in methanol was achieved using calcium fluoride solution cells (0.1 cm^3).

The ^1H spectra of the paramagnetic lanthanide complexes (including the two-dimensional COSY spectra) were obtained by workers at the University of Turin using a JEOL EX-90 spectrometer at 90 MHz. The $^{13}\text{C}\{^1\text{H}\}$ spectra of these complexes were acquired using a JEOL EX-400 instrument at 100.6 MHz. In these cases, the proton and carbon chemical shifts were referenced to the resonance of internal *tert*-butanol (one drop; δ_{H} 0, δ_{C} 31.3). Diamagnetic two-dimensional spectra and variable temperature studies were carried out at the University of Durham on a Varian VXR400.

All other NMR spectra were acquired using a Brüker AC250 spectrometer operating at 250.13, 62.9 and 101.1 MHz for ^1H , $^{13}\text{C}\{^1\text{H}\}$ and $^{31}\text{P}\{^1\text{H}\}$ measurements respectively. The ^1H and $^{13}\text{C}\{^1\text{H}\}$ spectra were referenced internally to residual protio-solvent resonances and are reported relative to TMS (δ 0). The $^{31}\text{P}\{^1\text{H}\}$ spectra were referenced externally relative to H_3PO_4 in D_2O . All chemical shifts (δ) are quoted in ppm and coupling constants in Hz. The ^{31}P T_1 relaxation times were measured at the University of Turin using JEOL EX-90, GX-270 and EX-400 spectrometers operating at 36.4, 109.3 and 162 MHz respectively.

Mass spectra (EI, CI and DCI) were recorded with a VG 7070E spectrometer with samples for desorption chemical ionisation being presented as solutions in chloroform using ammonia as the impinging gas. Glycerol was used as the matrix for samples requiring fast-atom-bombardment spectra. Electrospray mass spectra were recorded at the EPSRC Mass Spectrometry Service Centre, University of Wales, Swansea, using a VG Quattro II triple quadrupole spectrometer, or at the University of Durham using a VG platform spectrometer.

5.1.2 Details for Chapter 2

Lanthanide complexes of 1,4,7,10-tetraazacyclododecane-1,4,7,10-tetrayltetra-methylenetetra(benzylphosphinic acid), 27

Ligand **27** was provided by Dr. Kanthi Pulukkody, having been prepared according to the published procedure.¹

[Eu.27]⁻ Europium oxide (530 mg, 0.15 mmol) was added to a solution of ligand **27** (250 mg, 0.30 mmol) in Purite water (20 cm³) at pH 2 and the mixture was heated to reflux for 18 h to give a white suspension. The pH was adjusted to 6.5 (1% KOH solution) and the mixture heated under reflux for a further 2 h. On cooling, it was filtered through a 0.45 μm filter to yield a colourless solution. After concentrating to a volume of 4 cm³, the solution was left to crystallise at 4°C giving a colourless crystalline solid (190 mg, 64%), mp > 250°C. δ_H(D₂O, pD 6, 90MHz): -17.99 (4H, CHHP); -11.41 (4H, CHHP); -7.51 (4H, CHHN ring); -4.50 (4H, CHHN ring); -2.08 (4H, PCHHP); -0.72 (4H, PCHHP); 0.75 (4H, CHHN' ring); 9.47 (4H, para-H, Ar); 10.78 (8H, meta-H, Ar); 14.08 (8H, ortho-H, Ar); 34.40 (4H, CHHN' ring). δ_P{¹H} (D₂O, pD 6): +86.1. m/z (ES⁻): 992 (100, M⁻ for ¹⁵¹Eu); 994 (85, M⁻ for ¹⁵³Eu). IR (KBr): 3064m (Ar-H str), 2971m and 2859m (HC-H), 1495m, 1453m, 1231m, 1165s, 1117s, 1049s, 1031s, 801m, 699s, 602m.

[Tb.27]⁻ Terbium acetate (hydrate, 101 mg, 0.30 mmol) was added to an aqueous solution of ligand **27** (250 mg, 0.30 mmol) and the pH of the resulting solution raised to 6.5 (1% KOH solution). After heating to reflux for 2h, the solution was concentrated to a volume of 4 cm³ and left to crystallise at 4°C to yield a colourless crystalline solid (130 mg, 43%). δ_P{¹H} (D₂O, pD 6): +547. m/z (ES⁻): 999 (100, M⁻). IR (KBr): identical to that of [Eu.27]⁻.

[Dy.27]⁻ This was prepared from the ligand **27** (100 mg, 0.12 mmol) and dysprosium chloride (hexahydrate, 45 mg, 0.12 mmol) by the procedure described above for the terbium complex. $\delta_P\{^1H\}$ (D₂O, pD 6): +467. m/z (ES⁻): 1003 (100, M⁻). IR (KBr): identical to that of [Eu27]⁻.

Other lanthanide complexes of the ligand **27** were prepared on small scales in solution without isolation, using a stoichiometric amount of the oxide or acetate salts, and characterised by ³¹P{¹H} NMR and ESMS spectra (Table 5.1).

TABLE 5.1 ³¹P{¹H} NMR chemical shifts and mass spectral data for the lanthanide complexes of ligand **27**

Complex of ligand 27	³¹ P chemical shift / ppm (D ₂ O, pD 6)	m/z for the complex ^{a,b} (ESMS negative ion detection) calculated mass in parenthesis ^c
Cerium	33.5	980.6 (980.2)
Praseodymium	1.7	981.5 (981.2)
Neodymium	-0.9	982.5 (982.2)
Samarium	54.1	992.7 (992.2)
Europium	86.0	993.3 (993.2)
Terbium	547	998.6 (999.2)
Dysprosium	467	1004.0 (1004.2)
Holmium	223	1005.8 (1005.2)
Ytterbium	-40.4	1014.7 (1014.2)

(a) m/z for the most intense signal is given (100% peak in all cases except Yb³⁺).

(b) the spectra showed good agreement with the natural isotope distributions of the lanthanides. (c) the calculated mass for the most abundant ion expected is given.

5.1.3 Details for Chapter 3

Chloro-N-phenylethanamide.

Triethylamine (2.45 g, 0.024 mol) was added to a solution of aniline (2.0 g, 0.02 mol) in dry diethylether (100 cm³). The mixture was cooled to -60°C and chloroacetylchloride (2.9 g, 0.024 mol) added dropwise. The mixture was allowed to warm to room temperature and washed with dilute hydrochloric acid (2 x 100 cm³) followed by water (2 x 100 cm³). Removal of solvent under reduced pressure gave a white crystalline solid (2.9 g, 85%), mp. 126-127°C. δ_{H} (CDCl₃): 4.19 (2H, s, ClCH₂); 7.20 (1H, t, ³J 7.2, C₆H₅ *para*-H); 7.36 (2H, m, C₆H₅ *meta*-H); 7.54 (2H, d, ³J 7.9, C₆H₅ *ortho*-H); 8.27 (1H, br s, NH). δ_{C} {¹H} (CDCl₃): 42.8 (ClCH₂); 120.1, 125.3, 129.1 (C₆H₅ *ortho*, *meta*, *para* C); 136.6 (C₆H₅ *ipso*-C); 163.8 (C=O). m/z (CI): 187 and 189 (50 and 17, M+NH₄⁺ for ³⁵Cl and ³⁷Cl); 170 and 172 (100 and 33, M⁺ for ³⁵Cl and ³⁷Cl). IR (KBr): 3265m and 3145m (N-H str), 3096m (Ar-H str), 1671s (C=O str), 1602s, 1559s, 1498s, 1443m, 1344m, 1252s, 962m, 750s cm⁻¹. Found: C, 56.0; H, 4.6; N, 7.9. (C₈H₈ClNO requires C, 56.6; H, 4.8; N, 8.3).

1-(Phenylcarbamoylmethyl)-1,4,7,10-tetraazacyclododecane.

1,4,7,10-Tetraazacyclododecane (1.50 g, 8.8 mmol) in dibutyl ether (40 cm³) was heated to 70°C and molybdenum hexacarbonyl (2.30 g, 8.8 mmol) added. The mixture was heated to reflux under argon for 2 h, giving a bright yellow precipitate of the 1,4,7,10-tetraazacyclododecane-molybdenum tricarbonyl complex, which was filtered under argon and dried under vacuum. The yellow complex was suspended in dry, degassed dimethylformamide (40 cm³) in the presence of anhydrous potassium carbonate (1.8g, 13 mmol) and 2-chloro-N-phenylethanamide (1.50 g, 8.8 mmol) was added. The mixture was heated at 80°C under argon for 2h and the solvent then removed under reduced pressure with mild heating. The resulting brown residue was taken up into aqueous hydrochloric acid (1M, 25 cm³) and the mixture stirred open to the air for 18 h. The pH of the solution was raised to 14 with potassium hydroxide pellets with cooling and the dark green molybdenum residues filtered off giving a clear yellow solution. Extraction into dichloromethane followed by removal of solvent

under reduced pressure gave a yellow-brown oil (1.33 g, 50%). δ_{H} (CDCl_3): 2.66 - 2.93 (19H, br m, CH_2CH_2 , NH ring); 3.25 (2H, s, NCH_2CO); 7.06 (1H, t, 3J 7.4, C_6H_5 *para*-H); 7.29 (2H, m, C_6H_5 *meta*-H); 7.69 (2H, d, 3J 8.1, C_6H_5 *ortho*-H); 10.10 (1H, br s, *HNPh*). $\delta_{\text{C}}\{^1\text{H}\}$ (CDCl_3): 45.7, 47.1, 47.9 (CH_2CH_2); 59.6 (NCH_2CO); 119.4, 123.7, 128.8 (C_6H_5 , *ortho*, *meta*, *para* C); 138.4 (C_6H_5 , *ipso*-C); 170.0 (C=O). m/z (DCI) 306 (100, $\text{M}^+ + 1$).

Triethyl 10-(Phenylcarbamoylmethyl)-1,4,7,10-tetraazacyclododecane-1,4,7-triyltrimethylenetri(methylphosphinate).

The monosubstituted cycle (1.33 g, 4.4 mmol) was heated to 80°C in anhydrous tetrahydrofuran under argon and paraformaldehyde (0.60 g, 19.6 mmol) followed by diethoxy(methyl)phosphine (2.67 g, 19.6 mmol) were added. The solution was heated at reflux under argon for 18 h over molecular sieves. The excess paraformaldehyde was filtered off and the solvent removed under vacuum giving a brown oil. The product was purified by alumina column chromatography, (gradient elution from dichloromethane to 2% methanol-dichloromethane; $R_f = 0.4$, 5% methanol-dichloromethane), giving a yellow-brown oil (1.6 g, 55%). δ_{H} (CDCl_3): 1.25 (9H, t, 3J 7.3, OCH_2CH_3); 1.37 (3H, d, 2J 13.5, PCH_3); 1.47 (6H, d, 2J 13.5, PCH_3); 2.69 - 3.2 (24H, br m, CH_2CH_2 , NCH_2P , NCH_2CO); 4.05 (6H, m, OCH_2CH_3); 7.06 (1H, t, 3J 7.3, C_6H_5 *para*-H); 7.30 (2H, m, C_6H_5 , *meta*-H); 7.68 (2H, d, 3J 8.6, C_6H_5 *ortho*-H); 9.93 (1H, br, *HNPh*). $\delta_{\text{P}}\{^1\text{H}\}$ (CDCl_3): 52.2, 51.8, 51.4. $\delta_{\text{C}}\{^1\text{H}\}$ (CDCl_3): 13.9 (d, 1J 90, PCH_3); 16.6 (OCH_2CH_3); 53.5, 53.7, 54.0, 54.4, 54.9, 55.0, 55.2, 55.8 (CH_2N , ring; NCH_2P ; POCH_2CH_3); 60.0 (NCH_2CO); 119.4; 123.6, 128.7 (C_6H_5 , *ortho*, *meta*, *para* C); 138.5 (*ipso*-C); 169.8 (C=O). m/z (DCI): 666 (91, $\text{M}^+ + 1$); 546 (41, $\text{M}^+ - \text{PhNCO}$). IR (KBr): 3247m and 3131m (N-H str), 3085m (Ar-H str), 2979m and 2867m (HC-H str), 1670s (C=O str), 1599s, 1555s, 1498s, 1425s, 1382s, 1291m, 1254s, 1031m, 901m, 752s cm^{-1} .

10-(Phenylcarbamoylmethyl)-1,4,7,10,-tetraazacyclododecane-1,4,7-triyltrimethylenetri(methylphosphinic acid) 32

The monoamide triester was dissolved in a solution of potassium deuteroxide in deuterium oxide and stirred for 12 h at room temperature. The ^1H NMR spectrum of the reaction mixture showed resonances due to ethanol and the required product. The solution was acidified with dilute hydrochloric acid to pH 6, the water removed under reduced pressure and the residue extracted into absolute ethanol giving ligand **32** in quantitative yield. δ_{H} (D_2O , pD 6): 1.02 (9H, d, 2J 13.9, PCH_3); 2.37 - 2.62 (24H, br m, CH_2CH_2 , NCH_2P , NCH_2CO); 6.9 - 7.1 (5H, m, C_6H_5). $\delta_{\text{P}}\{^1\text{H}\}$ (D_2O , pD 6): 41.8, 42.8. $\delta_{\text{C}}\{^1\text{H}\}$ (D_2O , pD 6): 16.4 (d, 1J 88, PCH_3); 51.7, 52.2, 52.7 (CH_2 ring); 55.9 (d, 1J 99, NCH_2P); 57.3 (NCH_2CO); 122.1, 125.6, 129.2 (C_6H_5 , *ortho*, *meta*, *para* C); 137.0 (C_6H_5 , *ipso* C); 173.6 ($\text{C}=\text{O}$). IR (KBr): 3262m and 3143m (N-H str), 3096m (Ar-H str), 2982m and 2873w (HC-H str), 1666s ($\text{C}=\text{O}$ str), 1602s, 1559s, 1498s, 1443m, 1422s, 1390s, 1344m, 1252s, 1144m, 1039m, 886m, 750s cm^{-1} .

Ligands **31**, **33** and **34** were prepared in a similar manner and as reported previously.¹

Lanthanide Complexes of Ligands 31 - 34

[Eu.32] The ligand **32** (200 mg, 0.35 mmol) was dissolved in water (10 cm^3) and the pH adjusted to 2 with dilute hydrochloric acid. Europium oxide (61 mg, 0.18 mmol) was added and the solution heated to reflux for 3 h giving a clear solution. The pH was raised to 6 with aqueous potassium hydroxide and heating continued for a further 3 h. The solution was filtered through a $0.45 \mu\text{m}$ (Millipore) filter and the water was removed under reduced pressure. The product was purified by alumina column chromatography (10% methanol-dichloromethane, $R_f = 0.7$ in 25% methanol-dichloromethane) to give a colourless solid (150 mg, 60%), mp $> 250^\circ\text{C}$. $\delta_{\text{P}}\{^1\text{H}\}$ (D_2O) 67.0, 86.1, 101.1. m/z (FAB) 732 (82, M^++1). IR (KBr): 3396s (br, O-H str of water and N-H amide str), 2977s and 2871s (HC-H str), 1626s ($\text{C}=\text{O}$ str), 1596s, 1571s, 1454m, 1425m, 1327m, 1294s, 1137s, 1070m, 1034s, 891m, 810m, 743m, 526m.

Found: C 33.4; H 5.9; N 8.1. ($C_{22}H_{39}N_5O_7P_3Eu \cdot 3H_2O$ requires C 33.7; H 5.7; N 8.9).

[Tb.32] The ligand **32** (200 mg, 0.35 mmol) was dissolved in water (10 cm³) and the pH adjusted to 6. Terbium acetate (hydrate, 117 mg, 0.35 mmol) was added and the solution refluxed for 18 h. The water was removed under reduced pressure and the product extracted into absolute ethanol. The complex was purified by alumina column chromatography (10% methanol-dichloromethane, $R_f = 0.65$ in 25% methanol-dichloromethane), giving a colourless solid (170 mg, 66%), mp > 250°C. $\delta_P\{^1H\}$ (D_2O): 468.1, 614.9, 634.2. m/z (FAB) 738 (100, M^++1). IR - identical to that of [Eu.32]. Found: C 33.1; H 5.6; N 7.6. ($C_{22}H_{39}N_5O_7P_3Tb \cdot 3H_2O$ requires C 33.4; H 5.7; N 8.8).

[Yb.32]. The ytterbium complex was prepared from the ligand **32** and ytterbium oxide by an identical procedure to that described for [Eu.32]. $\delta_P\{^1H\}$ (D_2O) -60.7, -43.2, -32.0. IR - identical to that of [Eu.32]. m/z (FAB): 753 (100, M^++1). Found: C 30.8; H 5.7; N 7.0. ($C_{22}H_{39}N_5O_7P_3Yb \cdot 6H_2O$ requires C 30.7; H 5.9; N 8.1).

[Gd.32] The gadolinium complex was prepared from the ligand **32** and gadolinium oxide by an identical procedure to that described for [Eu.32]. The extreme line-broadening induced by Gd^{3+} prevents any NMR measurements from being made. IR - identical to that of [Eu.32]. m/z (FAB): 737 (15, M^++1). Found: C 32.9; H 6.5; N 8.4. ($C_{22}H_{39}N_5O_7P_3Gd \cdot 4H_2O$ requires C 32.7; H 5.9; N 8.7).

The complexes of ligands **31**, **33** and **34** were prepared in an analogous manner.

[Eu.33] $\delta_P\{^1H\}$ (D_2O) 80.7, 93.1, 97.1. IR (KBr): 3406s (br, O-H str of water), 2860m (HC-H str), 1625s (C=O str), 1460m, 1426m, 1294m, 1228m, 1144s, 1071m, 1030s, 976m, 892m, 743m, 524m. m/z (FAB) 684 (10, M^++1). Found C 27.3; H 6.5; N 8.3. ($C_{18}H_{39}N_5O_7P_3Eu \cdot 6H_2O$ requires C 27.3; H 6.5; N 8.8).

[Tb.33] $\delta_P\{^1\text{H}\}$ (D_2O) 568.7, 574.0, 578.7. IR - identical to that of [Eu.33]. m/z (FAB) 690 (35, M^++1). Found C 27.3; H 6.3; N 8.5. ($\text{C}_{18}\text{H}_{39}\text{N}_5\text{O}_7\text{P}_3\text{Tb}.6\text{H}_2\text{O}$ requires C 27.1; H 6.4; N 8.8).

[Yb.33] $\delta_P\{^1\text{H}\}$ (D_2O) -50.3, -14.8, -13.7. IR - identical to that of [Eu.33]. m/z (FAB) 705 (11, M^++1). Found C 27.5; H 6.3; N 8.3. ($\text{C}_{18}\text{H}_{39}\text{N}_5\text{O}_7\text{P}_3\text{Yb}.5\text{H}_2\text{O}$ requires C 27.2; H 6.2; N 8.8).

[Eu.34] $\delta_P\{^1\text{H}\}$ (D_2O) 55.6, 76.0, 91.4. IR (KBr): 3406s (br, O-H str of water), 2867m (HC-H str), 1602s (C=O str), 1454m, 1297m, 1228m, 1144s, 1073m, 1030s, 890m, 805m, 741m, 702m, 518m. m/z (FAB) 836 (69, M^++1). Found: C 41.1; H 6.5; N 7.0. ($\text{C}_{30}\text{H}_{47}\text{N}_5\text{O}_7\text{P}_3\text{Eu}.3\text{H}_2\text{O}$ requires C 40.5; H 6.0; N 7.9).

[Tb.34] $\delta_P\{^1\text{H}\}$ (D_2O) 488.5, 694.7, 747.8. IR - identical to that of [Eu.34]. m/z (FAB) 842 (100, M^++1). Found: C 40.8; H 6.3; N 7.0. ($\text{C}_{30}\text{H}_{47}\text{N}_5\text{O}_7\text{P}_3\text{Tb}.3\text{H}_2\text{O}$ requires C 40.2; H 5.9; N 7.8).

[Yb.34] $\delta_P\{^1\text{H}\}$ (D_2O) -41.3, -35.2, -25.0. IR - identical to that of [Eu.34]. m/z (FAB) 857 (100, M^++1). Found: C 39.4; H 6.4; N 7.0. ($\text{C}_{30}\text{H}_{47}\text{N}_5\text{O}_7\text{P}_3\text{Yb}.4\text{H}_2\text{O}$ requires C 38.8; H 5.9; N 7.6).

[Tb.31] $\delta_P\{^1\text{H}\}$ (D_2O): 530.7, 598.5, 602.1. m/z (FAB): 676 (77, M^++1). Found: C 27.42; H 6.50. ($\text{C}_{17}\text{H}_{37}\text{N}_5\text{P}_3\text{O}_7\text{Tb}.4\text{H}_2\text{O}$ requires C 27.4; H 6.0). IR (KBr): 3404s (O-H str of water and N-H amide str), 2974m and 2869m (HC-H str), 1639s (C=O str), 1459m, 1412m, 1296m, 1230m, 1148s, 1070m, 1025s, 891m, 807s, 522s.

[Eu.31] $\delta_P\{^1\text{H}\}$ (D_2O): 73.1, 88.3, 93.2. IR - identical to that of [Tb.31]. m/z (ES -): 668 (100, M^-).

l-Acetyl-1,4,7,10-tetraazacyclododecane

A suspension of the molybdenum tricarbonyl complex of 1,4,7,10-tetraazacyclododecane (840 mg, 2.4 mmol) in dry dimethylformamide (25 cm^3) containing potassium carbonate (500 mg, 3.6 mmol) was cooled to 0°C and acetic anhydride (0.23 cm^3 ; 2.4 mmol) was added dropwise under an atmosphere of argon. The mixture was allowed to warm to room temperature, during which time a yellow

solution formed which was heated to 60°C for 1 h. The solvent was removed under reduced pressure with mild heating leaving a pale brown powder which was taken into HCl(aq) (1M, 20 cm³) and stirred open to the air for 18 h. The pH of the solution was raised to 13 (KOH pellets), the solid molybdenum residues filtered off and the resulting yellow solution extracted with chloroform (4 x 30 cm³). The chloroform solution was dried over anhydrous potassium carbonate, filtered and the solvent removed under reduced pressure giving a colourless oil (400 mg, 78%). δ_{H} (CDCl₃): 2.16 (3H, s, NCOCH₃); 2.66 (8H, br, HNCH₂CH₂NH); 2.79 (8H, br, NCH₂CH₂NCOMe); 3.54 (3H, br, NH). $\delta_{\text{C}}\{^1\text{H}\}$ (CDCl₃): 22.4 (NCOCH₃); 43.8, 45.8, 46.6, 47.3, 47.6, 48.3, 48.4, 50.8 (CH₂ ring); 172.2 (C=O). *m/z* (DCI): 215 (100, M⁺+1). IR (thin film): 2929s and 2835s (HC-H str); 1632s (C=O str); 1469s; 1418s; 1356s; 1285m; 1261m; 1034m; 1023m; 752s; 663m.

1-Phenacyl-1,4,7,10-tetraazacyclododecane

Benzoyl chloride (0.33 cm³, 2.86 mmol) was added dropwise to a stirred suspension of the molybdenum tricarbonyl complex of 1,4,7,10-tetraazacyclododecane (1.00 g, 2.86 mmol) in dry dimethylformamide (25 cm³) in the presence of potassium carbonate (590 mg, 4.28 mmol), under an atmosphere of argon and with cooling to 0°C. The mixture was allowed to warm to room temperature and stirred for a further 2 h, after which the solvent was removed under reduced pressure. The residue was taken into aqueous hydrochloric acid (1M, 20 cm³) and stirred open to the air for 18 h. The pH of the solution was raised to 14 with KOH pellets with cooling and the dark green molybdenum residues filtered off, leaving a yellow solution. The product amine was extracted into dichloromethane, the solution dried over anhydrous potassium carbonate and the solvent removed under reduced pressure giving a yellow oil (490 mg, 62%). δ_{H} (CDCl₃): 2.30 (3H, br, NH); 2.67 (4H, br, CH₂ ring); 2.78 (8H, br, CH₂ ring); 3.61 (4H, br, CH₂ ring adjacent to N-COPh); 7.37 (3H, m, *meta* and *para* Ar-H); 7.47 (2H, m, *ortho* Ar-H). $\delta_{\text{C}}\{^1\text{H}\}$ (CDCl₃): 45.6, 47.3, 47.7 (CH₂ ring); 126.9, 128.1 (*ortho* and *meta* C); 128.8 (*para* C); 136.8 (*ipso*-C); 173.2 (C=O). *m/z* (DCI): 277 (100, M⁺+1). IR (thin film): 3300m and 3237m (Ar-H str), 2924s and 2819s (HC-H

str), 1672s (C=O str), 1625s (Ar C=C conj. to amide C=O), 1445s, 1414s, 1368s, 1353s, 1261m, 1120m, 1069m, 922m, 732s, 706s cm^{-1} .

Triethyl 10-(phenacyl)-1,4,7,10-tetraazacyclododecane-1,4,7-triyltrimethylene-tri(methylphosphinate)

The monosubstituted cycle (450 mg, 1.63 mmol) was heated to 80°C in anhydrous tetrahydrofuran under argon and paraformaldehyde (196 mg, 6.52 mmol) followed by diethoxy(methyl)phosphine (887 mg, 6.52 mmol) were added. The solution was heated to reflux under argon for 18 h over molecular sieves contained in a Soxhlet. The excess paraformaldehyde was filtered off and the solvent removed under reduced pressure giving a brown oil. This was purified by alumina column chromatography (gradient elution from dichloromethane to 2% methanol-dichloromethane; $R_f = 0.4$, 5% methanol-dichloromethane); giving a pale yellow oil (180 mg, 17%). δ_H (CDCl_3): 1.28 (9H, t, 3J 6.9, OCH_2CH_3); 1.50 (9H, d, 2J 13.6, PCH_3); 2.65 - 2.95 (22H, br, CH_2 ring and NCH_2P); 4.03 (6H, m, OCH_2CH_3); 7.35 (5H, br, aromatic H). δ_P (^1H) (CDCl_3): 52.3, 52.5. δ_C (^1H) (CDCl_3): 13.6 (d, 1J 90, PCH_3); 16.6 (OCH_2CH_3); 52.3, 53.1, 54.0, 56.0 (CH_2 ring, NCH_2P , POCH_2CH_3); 60.0 (NCH_2CO); 126.2, 128.3 (*ortho* and *meta* C); 129.1 (*para* C); 136.8 (*ipso* C); 171.8 (C=O). m/z (DCI): 637 (10, M^++1); 397 (100, possibly $\text{M}^+-2[\text{CHP}(\text{Me})\text{O}_2\text{Et}]$). IR (thin film): 3054w (Ar-H str), 2983m and 2846m (HC-H str), 1620s (C=O str), 1446m, 1420m, 1303m, 1187s, 1102m, 1035s, 961s, 792m, 707m cm^{-1} .

1-Cyanomethyl-1,4,7,10-tetraazacyclododecane

Bromoacetonitrile (0.238 cm^3 , 3.42 mmol) was added dropwise to a suspension of the molybdenum-tricarbonyl complex of 1,4,7,10-tetraazacyclododecane (1.20 g, 3.42 mmol) in dry dimethylformamide (30 cm^3) containing potassium carbonate (710 mg, 5.14 mmol) at room temperature and under an atmosphere of argon. A brown solution was formed which was heated at 60°C for 1 h. The solvent was removed under reduced pressure with mild heating giving a brown residue which was taken into $\text{HCl}(\text{aq})$ (1M, 20 cm^3) and stirred open to the air for 18 h. The molybdenum residues were filtered off

and the yellow solution extracted with chloroform (4 x 30 cm³). The chloroform solution was dried over anhydrous potassium carbonate, filtered and the solvent removed under reduced pressure giving a yellow oil (230 mg, 32%). δ_{H} (CDCl₃): 2.59 (4H, br, CH₂ ring); 2.71 (8H, br, CH₂ ring); 2.80 (4H, br, CH₂ ring); 3.65 (NCH₂CN). $\delta_{\text{C}}\{^1\text{H}\}$ (CDCl₃): 42.9, 43.9, 45.7, 46.4 (CH₂ ring); 50.3 (NCH₂CN); 114.8 (NCH₂CN). m/z (DCI): 212 (100, M⁺+1). IR (thin film): 2934s and 2836s (HC-H str), 2231w (C=N str), 1668s, 1459s, 1355m, 1115m, 1058m, 918s, 732m cm⁻¹.

5.1.4 Details for Chapter 4

2-Naphthylmethylamine.

Borane-THF (1.0M, 80 cm³) was added to a solution of 2-cyanonaphthalene (2.5 g, 16 mmol) in THF (5 cm³) and the mixture heated to reflux for 48 h. Excess of borane was destroyed with methanol after which the solvent was removed under reduced pressure and the residue heated to reflux in 6M HCl for 4 h. Removal of water gave a brown residue, to which was added aqueous base (20% KOH, 30 cm³) giving a yellow emulsion. The mixture was extracted with dichloromethane (2 x 40 cm³) and the extracts dried over anhydrous potassium carbonate and evaporated to give a yellow-brown solid (2.1 g, 84%), mp 58-60°C (lit.² 59-60°C). δ_{H} (CDCl₃): 1.63 (2H, br s, NH₂); 4.08 (2H, s, CH₂); 7.46-7.52 and 7.79-7.88 (7H, m, C₁₀H₇). $\delta_{\text{C}}\{^1\text{H}\}$ (CDCl₃): 46.6 (s, CH₂); 125.0, 125.6, 125.9, 126.1, 127.8, 128.2 (singlets, aromatic C); 132.6, 133.6, 140.9 (singlets, quaternary aromatic C). m/z (DCI): 158 (100, M⁺+1). IR (KBr): 3345m (N-H str), 3048m (Ar-H str), 2905m and 2833w (HC-H str), 1560m, 1464m, 1381s, 1310m, 1037m, 829s, 738s cm⁻¹.

Chloro-N-(2-naphthylmethyl)ethanamide 43

Triethylamine (1.56 g, 15 mmol) was added to a solution of 2-naphthylmethylamine (2.0 g, 12.7 mmol) in dry dichloromethane (80 cm³). The solution was cooled to -10°C and chloroacetylchloride (1.7 g, 15 mmol) was added dropwise, the temperature being maintained below 0°C. The mixture was then allowed to warm to room temperature and washed with aqueous HCl (0.1M, 2 x 40 cm³) followed by water (2 x 40 cm³). The

solution was dried over anhydrous potassium carbonate and the solvent removed under reduced pressure giving a pale-brown solid (2.3g, 78%), mp. 98-101°C. δ_{H} (CDCl_3): 4.18 (2H, s, ClCH_2), 4.70 (2H, d, 3J 5, CH_2NH), 7.42-7.55 and 7.78-7.90 (7H, m, C_{10}H_7). $\delta_{\text{C}}\{^1\text{H}\}$ (CDCl_3): 42.7(s) and 44.0 (s) (ClCH_2 and NHCH_2); 125.7(s), 126.1(s), 126.5(s), 127.7(s), 128.7(s), (aromatic C), 132.8(s), 133.3(s), 134.7(s) (quaternary aromatic C). m/z (DCI): 253 (8, $\text{M}+\text{NH}_4^+$ for ^{37}Cl); 251 (24, $\text{M}+\text{NH}_4^+$ for ^{35}Cl); 236 (35, M^++1 for ^{37}Cl); 234 (100, M^++1 for ^{35}Cl). IR (KBr): 3269m (N-H str), 3053m (Ar-H str), 2934w (HC-H str), 1650s (C=O str), 1538s, 1423m, 1261m, 1239m, 1030m, 823s, 752s cm^{-1} .

1,4,7,10-tetrakis(2-naphthylmethylcarbamoylmethyl)-1,4,7,10-tetraazacyclododecane, compound 40

To a solution of 1,4,7,10-tetraazacyclododecane (60 mg, 0.35 mmol) in dry dimethylformamide was added anhydrous caesium carbonate (570 mg, 1.75 mmol) and chloro-N-(2-naphthylmethyl)ethanamide (410 mg, 1.75 mmol). The mixture was stirred at 70°C under argon for 12 h. The solids were separated off by centrifuge and washed with water (5 x 5 cm^3) followed by methanol (3 x 5 cm^3) leaving a white solid (240 mg, 71%), mp. 245°C (dec.). $\delta_{\text{C}}\{^1\text{H}\}$ [CDCl_3 (0.75 cm^3) containing 10 μl of trifluoroacetic acid]: 3.18 (24H, v br, ring CH_2 and NCH_2CO); 4.25 (8H, s, $\text{NHCH}_2\text{C}_{10}\text{H}_7$); 7.26-7.61 (28H, overlapping multiplets, aromatic H); 7.95 (4H, br s, CONH). $\delta_{\text{C}}\{^1\text{H}\}$ [CDCl_3 (0.75 cm^3) containing 10 μl trifluoroacetic acid]: 44.1 (s, $\text{C}_{10}\text{H}_7\text{CH}_2\text{NH}$); 50.8 (br, $\text{NCH}_2\text{CH}_2\text{N}$ ring); 55.8 (s, NCH_2CO); 125.4, 126.1, 126.6, 127.0, 128.2, 129 (singlets, aromatic C); 133.2, 133.7, 134.8 (singlets, quaternary aromatic C); 165.1 (s, C=O). m/z (DCI): 961 (M^++1). IR (KBr): 3267s (N-H str), 3052m (Ar-H str), 2844m (HC-H str), 1674s (C=O str), 1600m, 1530s, 1447m, 1369m, 1238m, 1106s, 827s, 745s, 578m cm^{-1} . Found: C, 73.3; H, 6.9; N, 11.5. ($\text{C}_{60}\text{H}_{64}\text{N}_8\text{O}_4 \cdot \text{H}_2\text{O}$ requires C, 73.6; H, 6.8; N, 11.4).

Chloro-N-methylethanamide.

Dichloromethane (80 cm³) was added to an aqueous solution (40% w/w) of methylamine (15.5 g, 0.2 mol MeNH₂) containing 8 g of sodium hydroxide and the mixture stirred vigorously with cooling to -10°C. Chloroacetyl chloride (25 g, 0.22 mol) was added dropwise such that the temperature did not rise above 0°C. After addition, the mixture was allowed to warm to room temperature and the organic layer was separated, washed with aqueous HCl (1M, 2 x 30 cm³) followed by water (2 x 50 cm³) and dried over potassium carbonate. Removal of solvent under reduced pressure gave a colourless, crystalline solid (7.5 g, 33%). M.p. 44-46°C (lit.³ 45-46°C). δ_{H} (CDCl₃): 2.88 (3H, d, ³J 4.5, NHCH₃); 4.05 (2H, s, ClCH₂); 6.61 (1H, br, CONH). $\delta_{\text{C}}\{^1\text{H}\}$ (CDCl₃): 26.5 (NCH₃); 42.5 (CH₂Cl); 166.8 (C=O). m/z (CI): 127 (32, M+NH₄⁺ for ³⁷Cl); 125 (100, M+NH₄⁺ for ³⁵Cl); 110 (30, M⁺⁺1 for ³⁷Cl); 108 (94, M⁺⁺1 for ³⁵Cl). IR (KBr): 3326m (N-H str); 2955m and 2882m (HC-H str), 1661s (C=O str), 1551s, 1412s, 1265s, 1161m, 929m, 763s, 703m, 565m. Found C, 33.1; H, 5.5; N, 12.6. (C₃H₆ClNO requires C, 33.5; H, 5.6; N, 13.0).

1-(2-Naphthylmethylcarbamoylmethyl)-1,4,7,10-tetraazacyclododecane 44

1,4,7,10-Tetraazacyclododecane (0.88 g, 5.12 mmol) and molybdenum hexacarbonyl (1.34 g, 5.12 mmol) in dibutyl ether (40 cm³) were heated at 160°C under argon for 2 h giving a bright yellow precipitate of the 1,4,7,10-tetraazacyclododecane-molybdenum tricarbonyl complex, which was filtered under argon and dried under vacuum. The yellow complex (1.65 g, 4.7 mmol) and anhydrous potassium carbonate (1g, 7.2 mmol) were taken into dry, degassed dimethylformamide (30 cm³) and chloro-N-(2-naphthylmethyl)ethanamide (1.10 g, 4.7 mmol) was added under argon. The mixture was heated to 75°C under an atmosphere of argon for 3 h. The solvent was distilled off under vacuum and the residue taken up into aqueous HCl (1M, 40 cm³). The resulting brown suspension was stirred open to the air for 15 h. The pH of the solution was raised to 14 with potassium hydroxide pellets, with cooling. The dark green precipitate formed was separated by centrifuge and extracted with dichloromethane (3 x 30 cm³) giving a pale yellow solution. Removal of solvent under reduced pressure gave a pale

yellow oil (0.70 g, 40%). $\delta_{\text{H}}(\text{CDCl}_3)$: 2.42-2.70 (16H, overlapping multiplets, $\text{NCH}_2\text{CH}_2\text{N}$ ring); 3.27 (2H, s, $\text{C}_{10}\text{H}_7\text{CH}_2\text{NH}$); 4.65 (2H, d, 3J 5.8, NCH_2CO); 7.45-7.86 (7H, overlapping multiplets, C_{10}H_7); 8.50 (1H, br, CONH). $\delta_{\text{C}}\{^1\text{H}\}(\text{CDCl}_3)$: 43.1 (s), 45.5 (s), 46.4 (s), 46.9 (s), (singlets, CH_2 in ring); 53.1 (s, $\text{C}_{10}\text{H}_7\text{CH}_2\text{NH}$); 58.9 (s, NCH_2CO); 125.7, 126.0, 126.1, 126.2, 127.4, 127.9, 128.1 (singlets, aromatic C); 132.3, 133.1, 136.0 (singlets, quaternary aromatic C); 171.5 (s, C=O). m/z (DCI): 370 (100, M^++1); 199 (31, $\text{C}_{10}\text{H}_7\text{CH}_2\text{NHCOCH}_3$); 173 (protonated unsubstituted cycle).

1,4,7-Tris(methylcarbamoylmethyl)-10-(2-naphthylmethylcarbamoylmethyl)-1,4,7,10-tetraazacyclododecane 39

The monosubstituted cycle (200 mg, 0.54 mmol) and anhydrous caesium carbonate (620 mg, 1.9 mmol) were taken up into dry dimethylformamide (3 cm^3) and chloro-N-methylethanamide (200 mg, 1.9 mmol) added. The mixture was stirred at 70°C under argon for 24 h. Caesium salts were removed by centrifuge and the solvent removed under vacuum to give a brown oil. The product was purified by alumina column chromatography (gradient elution from dichloromethane to 3% methanol-dichloromethane, $R_f = 0.4$ in 10% methanol-dichloromethane) and was isolated as a colourless glassy solid (135mg, 43%). $\delta_{\text{H}}(\text{CDCl}_3)$: 2.65-2.76 (25H, overlapping multiplets, br, NCH_2CH_2 ring and NHCH_3), 3.08 (4H, s, $\text{NCH}_2\text{CONHMe}$), 3.12 (2H, s, $\text{NCH}_2\text{CONHMe}$), 3.32 (2H, s, $\text{NCH}_2\text{CONHCH}_2\text{C}_{10}\text{H}_7$); 4.63 (2H, d, 3J 4.4, $\text{C}_{10}\text{H}_7\text{CH}_2\text{NH}$); 7.42-7.85 (7H, overlapping multiplets, C_{10}H_7). $\delta_{\text{C}}\{^1\text{H}\}(\text{CDCl}_3)$: 22.4 (s, NHCH_3); 25.9 (s, NHCH_3); 43.3 (s, $\text{C}_{10}\text{H}_7\text{CH}_2\text{NH}$); 52.3 (br, CH_2 in ring); 57.8 (s, NCH_2CO); 58.0 (s, NCH_2CO); 58.2 (s, NCH_2CO); 125.9, 126.0, 126.2, 126.4, 127.6, 127.7, 128.4 (singlets, aromatic C); 132.6, 133.2, 136.0 (singlets, quaternary aromatic C); 170.1, 170.7, 175.9 (singlets, C=O). m/z (DCI): 583 (14, M^++1); 442 (100, $\text{M}^+-2\{\text{CH}_2\text{CONHMe}\}$); 386 (66, $\text{M}^+-\{\text{CH}_2\text{CONHCH}_2\text{C}_{10}\text{H}_7\}$). IR (KBr): 3250m (N-H str), 3073w (Ar-H str), 2960m and 2828m (HC-H str), 1657s (C=O str), 1562s, 1441w, 1358m, 1310m, 1239m, 1159w, 1106m, 995w cm^{-1}

Complex formation for ligand 40

[Eu.40]³⁺ A solution of europium triflate in dry dimethylformamide (1 cm³) was added to a suspension of the tetranaphthyl ligand (26 mg, 26 mmol) in dry dimethylformamide (1 cm³). The mixture was heated at 70°C for 30 min, during which time a yellow solution formed. The solvent was removed under reduced pressure and the residue taken up into acetonitrile. The resulting solution was filtered, concentrated to a volume of 0.2 cm³ and added dropwise to a large excess of diethyl ether in a centrifuge tube, with vigorous shaking between additions. The complex precipitated as an off-white solid, which was separated from the ether by centrifuge and dried under a stream of argon (18 mg, 43%). m/z (ES +): 1412 {22, [M³⁺+2(CF₃SO₃⁻)]⁺}; 1261 {22, [M³⁺+(CF₃SO₃⁻)+e⁻]⁺}; 1112 {10, [M³⁺+2e⁻]⁺}; 632 {36, [M³⁺+(CF₃SO₃⁻)]²⁺}; 556 {50, [M³⁺+e⁻]²⁺}. IR (KBr): 3473m (N-H str), 3111m (Ar-H str), 2935w and 2878w (HC-H str), 1628s (C=O str), 1509m, 1435m, 1388m, 1254s, 1226s, 1165s, 1031s, 822m, 757m, 639s cm⁻¹. Found: C, 48.7; H, 4.6; N, 7.4. [C₆₀H₆₄N₈O₄Eu(CF₃SO₃⁻)₃ requires C, 48.5; H, 4.1; N 7.2].

The terbium, yttrium, cadmium and lead complexes of ligand 40 were prepared by a similar procedure.

[Tb.40]³⁺ m/z (ES +): 1417 {25, [M³⁺+2(CF₃SO₃⁻)]⁺}; 1268 {42, [M³⁺+(CF₃SO₃⁻)+e⁻]⁺}; 1119 {40, [M³⁺+2e⁻]⁺}; 634 {40, [M³⁺+(CF₃SO₃⁻)]²⁺}; 560 {68, [M³⁺+e⁻]²⁺}. IR: identical to that of [Eu.40]³⁺. Found: C, 48.3; H, 4.6; N, 7.2. [C₆₀H₆₄N₈O₄Tb(CF₃SO₃⁻)₃ requires C, 48.3; H, 4.1; N, 7.1].

[Y.40]³⁺ δ_H (CD₃OD, ¹H-¹H COSY, 400 MHz): 2.20 (4H, m, axial CH₂CH₂ ring); 2.30 (4H, d, ²J 14, equatorial CH₂CH₂ ring); 2.57 (4H, d, ²J 14, equatorial CH₂CH₂ ring); 2.64 (4H, d, ²J 17, NCH₂CO); 2.95 (4H, d, ²J 17, NCH₂CO); 3.34 (4H, m, axial CH₂CH₂ ring); 4.58 (8H, d, ³J 3, C₁₀H₇CH₂NH); 7.38 - 7.90 (28H, m, aromatic H). δ_C {¹H} (CD₃OD): 46.1 (s, C₁₀H₇CH₂NH); 56.2, 57.1 (CH₂CH₂); 64.1 (NCH₂CO); 126.8, 128.1, 129.0, 129.3, 130.4 (singlets, aromatic C); 134.6, 135.0, 135.9 (singlets, quaternary aromatic C); 177.3 (C=O). m/z (ES +): 1348 {35, [M³⁺+2(CF₃SO₃⁻)]⁺}; 1198 {12, [M³⁺+(CF₃SO₃⁻)+e⁻]⁺}; 599 {28, [M³⁺+(CF₃SO₃⁻)]²⁺}; 524 {100,

$[M^{3+}+e^{-}]^{2+}$. IR identical to that of $[Eu.40]^{3+}$. Found: C, 48.9; H, 4.5; N, 7.4. $[C_{60}H_{64}N_8O_4Y(CF_3SO_3^-)_3]$ requires C, 50.5; H, 4.3; N, 7.5].

$[Cd.40]^{2+}$ $\delta_C\{^1H\}$ (CD_3OD): 45.0 (s, $C_{10}H_7CH_2NH$); 52.9 (br s, CH_2CH_2 ring); 56.5 (s, NCH_2CO); 127.2, 127.5, 127.8, 128.9, 129.7 (aromatic C), 134.4, 135.0, 137.2 (quaternary aromatic C); 173.8 (C=O). m/z (ES +): 1223 {18, $[M^{2+}+(CF_3SO_3^-)]^+$ }; 537 {100, M^{2+} }. IR (KBr): 3295m (N-H str), 3109w and 3058w (Ar-H str), 2859w (HC-H str), 1645s (C=O str), 1559m, 1281s, 1249s, 1160m, 1029s, 817s, 755m, 637s cm^{-1} . Found: C, 53.3; H, 4.7; N, 7.8. $[C_{60}H_{64}N_8O_4Cd.(CF_3SO_3^-)_2.H_2O]$ requires C, 53.6; H, 4.8; N, 8.1].

$[Pb.40]^{2+}$ $\delta_C\{^1H\}$ (CD_3OD): 44.9 (s, $C_{10}H_7CH_2NH$); 52.0, 54.4 (CH_2CH_2 ring); 58.0 (NCH_2CO); 127.2, 127.6, 129.0, 129.8, (singlets, aromatic C); 134.4, 135.0, 137.1 (singlets, quaternary aromatic C); 173.7 (C=O). m/z (ES +): 1317 {77, $[M^{2+}+(CF_3SO_3^-)]^+$ }; 1168 {38, $[M^{2+}+e^{-}]^+$ }; 584 {100, M^{2+} }. IR (KBr): 3290m (N-H str), 3106w and 3055w (Ar-H str), 2856w (HC-H str), 1640s (C=O str), 1559m, 1279s, 1247s, 1163s, 1089m, 1029s, 815m, 754m, 637s cm^{-1} . Found: C, 49.0; H, 4.3; N, 7.2. $[C_{60}H_{64}N_8O_4Pb.(CF_3SO_3^-)_2.3H_2O]$ requires C, 49.0; H, 4.6; N, 7.4].

Complex formation for ligand 39

$[Eu.39]^{3+}$ A solution of europium triflate (29 mg, 48 μ mol) in dry acetonitrile (1 cm^3) was added to a solution of the mononaphthyl ligand 39 (28 mg, 48 μ mol) also in dry acetonitrile (1 cm^3). The resulting solution was heated for 30 min at 60°C, after which the solvent and volatile material were removed under reduced pressure. The yellow glassy solid obtained was dissolved in the minimum amount of acetonitrile and added dropwise to a large excess (5 cm^3) of diethyl ether in a centrifuge tube, with vigorous shaking between additions (Whirlimix). The complex precipitated as a fine, microcrystalline solid. (29mg, 50%). m/z (ES +): 1032. {60, $[M^{3+}+2(CF_3SO_3^-)]^+$ }; 883 {18, $[M^{3+}+(CF_3SO_3^-)+e^{-}]^+$ }. IR (KBr): 3304s (N-H str), 3135m (Ar-H str),

2953m and 2881m (HC-H str), 1643s (C=O str), 1585m, 1465m, 1417m, 1281s, 1225s, 1165s, 1087m, 1029s, 638s, 517m cm^{-1} .

The terbium and zinc complexes were prepared by a similar procedure.

[Tb.39]³⁺ m/z (ES +): 1211 {5, [M³⁺+3(CF₃SO₃⁻)+Na⁺]⁺}; 1206 {2, [M³⁺+3(CF₃SO₃⁻)+NH₄⁺]⁺}; 1040 {55, [M³⁺+2(CF₃SO₃⁻)]⁺}; 890 {17, [M³⁺+(CF₃SO₃⁻+e⁻)]⁺}; 445 {12, [M³⁺+(CF₃SO₃⁻)]²⁺}. IR (KBr) as for Eu³⁺ complex.

[Zn.39]²⁺ IR (KBr): 3333s (N-H str), 3127m (Ar-H str), 2942w and 2867w (HC-H str), 1665s (C=O str), 1636s, 1575m, 1475m, 1413m, 1256s, 1177s, 1035s, 643s, 519m cm^{-1} . m/z (ES +): 324 {100, M²⁺}.

Preparation of Metal Triflates.

Lead Triflate. Trifluoromethanesulfonic acid (3 cm^3) was carefully added to lead(II) chloride (1.0 g, 3.6 mmol) in a two-necked flask fitted with a nitrogen bubbler. A steady stream of nitrogen was passed through the suspension and the mixture was warmed to 60°C for 30 min. Anhydrous diethyl ether was added with cooling to 0°C and the white solid removed by filtration and washed with more diethyl ether (4 x 20 cm^3). The solid was extracted into acetonitrile, the solution filtered and the solvent removed under reduced pressure giving a white solid (1.5 g, 83%). IR (KBr): 3446s, 1634m, 1263s, 1180s, 1034s, 646s, 582s, 518s cm^{-1} . Found: C, 4.7; H, 0.4; N, 0. (C₂F₆O₆S₂Pb.H₂O requires C, 4.6; H, 0.4; N, 0).

Cadmium triflate. This was prepared in a similar manner from cadmium chloride, but yields were very low.

Terbium triflate. Obtained by a similar procedure using the acetate but, in this case, it was essential to use a minimum volume of diethyl ether as the metal triflate itself has substantial solubility in this solvent. Residual acetic acid was removed by heating the crude solid to 50°C under vacuum (0.01mmHg) for 72 h. Recrystallisation from acetonitrile provided the metal triflate as a white solid.

Europium triflate. Prepared by a procedure similar to that previously described for lanthanum triflate.⁴ Trifluoromethanesulphonic acid (1 cm³) was added to a suspension of Eu₂O₃ in water. Excess oxide was added to bring the pH to 6-7. The undissolved oxide was removed by filtration through a 0.45µm (Millipore) filter and the water removed under reduced pressure. The resulting white solid was dried at 160°C under vacuum (0.01mmHg) (1.6 g, 71%). IR (KBr): 3452s, 1663m, 1640m, 1256s, 1174s, 1029s, 640s, 581s, 523s cm⁻¹. Found: C, 5.6; H, 1.0; N, 0. (C₃F₉O₉S₃Eu.3H₂O requires C, 5.5; H, 0.9; N, 0).

Yttrium triflate. This was prepared similarly from Y₂O₃.

Zinc triflate and *copper(II) triflate* are commercially available and were used as supplied.

N-(2'-naphthylmethyl)-2-naphthylamide 47

A solution of 2-naphthoyl chloride (850 mg, 4.46 mmol) in dichloromethane (20 cm³) was added dropwise to a solution of 2-naphthylmethylamine (700 mg, 4.46 mmol) in dichloromethane (50 cm³) in the presence of triethylamine (1.2 cm³, 9 mmol) with cooling to 0°C. On warming to room temperature, chloroform (250 cm³) was added until a homogeneous solution was obtained. The solution was washed with HCl(aq) (1M, 3 x 100 cm³) followed by water (3 x 100 cm³), dried over anhydrous potassium carbonate and the solvent removed under reduced pressure leaving a white solid (1.14 g, 82%), mp 220 - 223°C. δ_H (CDCl₃): 4.89 (2H, d, ³J 5.7, C₁₀H₇CH₂N); 6.65 (1H, br, CONH); 7.48 - 7.59 and 7.83 - 7.94 (13H, overlapping multiplets, aromatic H); 8.34 (1H, s, H on position 1 of C₁₀H₇CO). δ_C{¹H} (CDCl₃): 45.2 (s, C₁₀H₇CH₂N); 124.3, 126.8, 127.1, 127.4, 127.5, 128.2, 128.4, 129.3, 129.4, 129.6 (singlets, aromatic C). Quaternary aromatic carbons and carbonyl carbon not observed despite > 10 000 scans and 3 s relaxation delay, owing to the poor solubility of the compound. m/z (DCI): 312 (100, M⁺+1); 155 (17, C₁₀H₇C=O⁺). IR (KBr): 3300s (N-H str), 3055m (Ar-H str), 2923w (HC-H str), 1638s (C=O str), 1625s, 1547s, 1417m, 1308s, 1002w, 783m, 479m.

N-(2'-naphthylmethyl)-2-naphthylmethyimine 48

2-Naphthylmethylamine (460 mg, 2.93 mmol) was dissolved in absolute ethanol (50 cm³) and a solution of 2-naphthaldehyde (460 mg, 2.93 mmol) in absolute ethanol (10 cm³) was added. The mixture was heated at reflux for 2h, during which time a pale yellow crystalline solid precipitated. On cooling, the solid was separated, washed with cold ethanol and dried under vacuum (630 mg, 70%), mp 177-178°C. δ_{H} (CDCl₃): 5.16 (2H, s, C₁₀H₇CH₂N); 7.51 - 8.21 (14H, overlapping multiplets, aromatic H); 8.72 (1H, s, C₁₀H₇CH=N-). $\delta_{\text{C}}\{^1\text{H}\}$ (CDCl₃): 65.9 (s, C₁₀H₇CH₂N); 124.6, 126.3, 126.7, 127.2, 127.9, 128.4, 128.6, 128.9, 129.2, 129.3, 130.9 (singlets, aromatic C); 133.5, 134.0, 134.9, 138.0 (singlets, quaternary aromatic C); 162.9 (s, C₁₀H₇CH=N-). m/z (DCI): 296 (100, M⁺+1); 156 (22, C₁₀H₇CH=NH₂⁺). IR (KBr): 3047m (Ar-H str), 2865m and 2806w (HC-H str), 1636s (C=N str), 1507m, 1299s, 866m, 829s, 745s, 477s. Found: C, 89.0; H, 5.8; N, 5.5. (C₂₂H₁₇N requires C, 89.5; H, 5.8; N, 4.8).

N,N-Bis(2-naphthylmethyl)amine 49

The imine (0.58 g, 1.97 mmol) was taken into absolute ethanol (30 cm³) and sodium borohydride (0.16 g, 4.2 mmol) was added to the stirred suspension. The mixture was heated under reflux for 2h, during which time a yellow solution was formed. The solvent was removed under reduced pressure and the residue taken up into dichloromethane (25 cm³) and washed with aqueous base (KOH, 1M, 3 x 15 cm³). The solution was dried over K₂CO₃ and the solvent removed under reduced pressure leaving a pale yellow solid (470 mg, 81%), mp 82 - 83°C. δ_{H} (CDCl₃): 1.91 (1H, br s, NH); 4.11 (4H, s, C₁₀H₇CH₂N); 7.52 - 7.63 (6H, overlapping multiplets, aromatic H); 7.90 - 7.96 (8H, overlapping multiplets, aromatic H). $\delta_{\text{C}}\{^1\text{H}\}$ (CDCl₃): 53.7 (s, C₁₀H₇CH₂N); 126.0, 126.5, 127.0, 127.1, 128.2, 128.5 (singlets, aromatic C); 133.2, 133.9, 138.3 (quaternary aromatic C). m/z (DCI): 298 (100, M⁺+1); 156 (17, C₁₀H₇CH₂NH⁺); 141 (21, C₁₀H₇CH₂⁺). IR (KBr): 3447m (N-H str), 3050m (Ar-H str), 2814m and 2770w (HC-H str), 1507m, 1433m, 1360w, 1095m, 863m, 815s, 746s, 478s.

N,N-Bis(2-naphthylmethyl)ethanamide 46

Triethylamine (0.068 cm³, 0.49 mmol) followed by acetic anhydride (0.046 cm³, 0.49 mmol) were added to a solution of the bis-naphthyl amine (112 mg, 0.38 mmol) in dichloromethane (2 cm³) and the mixture stirred at room temperature under argon for 18 h. More dichloromethane (10 cm³) was added and the solution washed with HCl(aq) (0.1M, 2 x 10 cm³) followed by water (3 x 10 cm³). After drying over anhydrous potassium carbonate, the solvent was removed under reduced pressure leaving a brown oil. Purification was achieved by means of silica column chromatography, (gradient elution from hexane to 20% ethyl acetate / 80% hexane, R_f = 0.55 in 20% EtOAc / 80% hexane) giving a pale yellow oil (30 mg, 24%). δ_H(CDCl₃): 2.34 (3H, s, CH₃); 4.66 (2H, s, C₁₀H₇CH₂N); 4.88 (2H, s, C₁₀H₇CH₂N); 7.50 - 7.92 (14H, overlapping multiplets, aromatic H). δ_C{¹H} (CDCl₃): 21.8 (CH₃); 48.2 (C₁₀H₇CH₂N); 50.8 (C₁₀H₇CH₂N); 124.4, 124.8, 125.9, 126.2, 126.4, 126.6, 127.1, 127.7, 128.5, 128.9 (aromatic C); 132.8, 133.3, 133.5, 133.7, 134.8 (quaternary aromatic C); 171.4 (C=O). m/z (DCI): 340 (100, M⁺+1); 198 (12, C₁₀H₇CH₂NCOMe⁺); 156 (17, C₁₀H₇CH₂NH⁺). IR (KBr): 3053m (Ar-H str), 2950m and 2926m (HC-H str), 1645s (C=O str), 1421s, 1367m, 1238m, 989w, 816s, 752m.

Chloro-N,N-bis(2-naphthylmethyl)ethanamide 45

The bis-naphthyl amine (470mg, 1.58 mmol) was dissolved in dry dichloromethane (20cm³) and triethylamine (350ml, 2.5 mmol) was added. The solution was stirred under argon with cooling to -10°C and chloroacetylchloride (200ml, 2.5 mmol) was added dropwise, the temperature being maintained below 0°C. On warming to room temperature, the solution was washed with HCl(aq) (1M, 3 x 10cm³) followed by water (3 x 10cm³), dried over anhydrous K₂CO₃ and the solvent removed under reduced pressure, leaving a pale brown oil, (530mg, 89%). δ_H (CDCl₃): 4.24 (2H, s, ClCH₂); 4.71 (2H, s, C₁₀H₇CH₂NCO); 4.87 (2H, s, C₁₀H₇CH₂NCO); 7.40 - 7.90 (14H, overlapping multiplets, aromatic H). δ_C{¹H} (CDCl₃): 42.1 (s, ClCH₂); 49.3 (s, C₁₀H₇CH₂NCO); 50.9 (s, C₁₀H₇CH₂NCO); 124.9, 125.6, 126.6, 126.9, 127.2, 127.7, 128.3, 129.2, 129.6 (singlets, aromatic C); 133.4, 133.6, 133.8, 133.9, 134.4 (singlets,

quaternary aromatic C); 167.9 (C=O). m/z (DCI): 376 (9, M^++1 for ^{37}Cl); 374 (26, M^++1 for ^{35}Cl); 340 (100, $[M^+-\text{Cl}+\text{H}]+1$); 141 (18, $\text{C}_{10}\text{H}_7\text{CH}_2^+$). IR (KBr): 3053m (Ar-H str), 2942m and 2868w (HC-H str), 1657s (C=O str), 1453s, 1370s, 1271m, 1209m, 942m, 816s, 753s.

Compound 51

The molybdenum tricarbonyl complex of 1,4,7,10-tetraazacyclododecane (430mg, 1.23 mmol) was taken into dry, degassed dimethylformamide (25 cm^3) with anhydrous potassium carbonate (250mg, 1.8 mmol) and chloro-*N,N*-bis(2-naphthylmethyl)-ethanamide was added under argon. The mixture was heated at 80°C under argon for 3h, during which time a brown solution was obtained. The solvent was removed under reduced pressure and the residue taken up into HCl(aq) (1M, 30 cm^3) and stirred open to air for 18h. The brown solid formed was separated by centrifuge and extracted with dichloromethane. The resulting yellow solution was washed with aqueous base (KOH, 1M, 3 x 25 cm^3), dried over anhydrous potassium carbonate and the solvent removed under reduced pressure leaving a yellow oil, (550mg, 40%). The purity of the product at this stage, as judged by HPLC, was poor. An attempt at purification by reverse-phase HPLC proved unsatisfactory and the compound was therefore used in the next step without further purification. δ_{H} (CDCl_3): 2.67-2.84 (12H, br, overlapping multiplets, CH_2 ring); 3.03 (7H, br, $\text{NCH}_2\text{CH}_2\text{NCO}_2$ and N-H); 4.72 (2H, s, $\text{NCO}_2\text{CH}_2\text{CO}$); 4.92 (2H, s, $\text{C}_{10}\text{H}_7\text{CH}_2\text{N}$); 4.95 (2H, s, $\text{C}_{10}\text{H}_7\text{CH}_2\text{N}$); 7.51 - 7.98 (28H, overlapping multiplets, aromatic H). $\delta_{\text{C}}\{^1\text{H}\}$ (CDCl_3): 43.3 ($\text{NHCH}_2\text{CH}_2\text{NHCH}_2\text{CH}_2\text{NCO}_2$); 43.8 ($\text{NHCH}_2\text{CH}_2\text{NHCH}_2\text{CH}_2\text{NCO}_2$); 45.1 ($\text{NHCH}_2\text{CH}_2\text{CO}_2$); 49.5 ($\text{C}_{10}\text{H}_7\text{CH}_2\text{N}$); 50.4 ($\text{C}_{10}\text{H}_7\text{CH}_2\text{N}$); 51.6 ($\text{NHCH}_2\text{CH}_2\text{CO}_2$); 63.9 (NCO_2CH_2); 124.5, 125.1, 125.8, 126.0, 126.5, 127.1, 127.4, 128.4, 129.7, 130.0, 132.9, 133.5, 133.8, 134.1 (aromatic C); 156.6 (NCO_2); 170.3 (NCOCH_2). m/z (DCI): 414 (20, $M^+-\text{C}_{10}\text{H}_7\text{CH}_2+\text{H}+1$); 356 (45, $M^+ - [(\text{C}_2\text{H}_4\text{N})_4\text{C}=\text{O}]+\text{H}+1$); 340 (100, $M^+ - [(\text{C}_2\text{H}_4\text{N})_4\text{CO}_2]+\text{H}+1$); 199 (33, $(\text{C}_2\text{H}_4\text{N})_4\text{C}=\text{O}^+$); 141 ($\text{C}_{10}\text{H}_7\text{CH}_2^+$). IR (thin film): 3052m (Ar-H str); 2935m,

2846m (HC-H str); 1703m (carbamate C=O str); 1655s (amide C=O str); 1466m; 1370m; 1222w; 817m.

Ligand 41

The monoalkylated derivative **51** (200 mg, 0.36 mmol) was dissolved in anhydrous dimethylformamide (2 cm³) and anhydrous caesium carbonate (472 mg, 1.45 mmol) was added, followed by chloro-N-methylethanamide (156 mg, 1.45 mmol). The mixture was heated at 80°C under argon for 18h. Removal of solvent under reduced pressure gave a brown oil, which was purified by silica column chromatography {gradient elution from CH₂Cl₂ / MeOH / NH₃(aq, 0.88) = 55/45/0 to 50/45/5; R_f = 0.6 (55/45/5)} giving a colourless solid (40 mg, 15%), mp. dec (180°C). $\delta_{\text{H}}(\text{CDCl}_3)$: 2.66 (8H, br s, CH₂CH₂ ring); 2.75 - 2.79 (9H, overlapping doublets, CONHCH₃); 3.05 - 3.07 (4H, NCH₂CH₂NCO₂CH₂ and 2H, NCH₂CONHMe); 3.20 (s, 4H, NCH₂CONHMe); 3.49 (4H, br, NCH₂CH₂NCO₂); 4.56 (2H, s, NCO₂CH₂CON); 4.83 (C₁₀H₇CH₂N); 4.89 (C₁₀H₇CH₂N); 7.29 - 7.95 (14H, overlapping multiplets, aromatic H; and 3H, br, CONHMe overlapping with aromatic H). $\delta_{\text{C}}\{^1\text{H}\}(\text{CDCl}_3)$: 28.6 (CONHCH₃); 47.0 (NCH₂CH₂NCH₂CH₂NCO₂); 48.6 (NCH₂CH₂NCH₂CH₂NCO₂); 54.0 (s, NCH₂CH₂NCO₂); 54.3 (NCH₂CH₂NCO₂); 59.3 (s, NCH₂CONHMe); 62.9 (CO₂CH₂CON); 124.9, 125.0, 126.5, 126.8, 127.1, 127.4, 128.4, 129.4, 129.9 (singlets, aromatic C); 133.3, 133.6, 134.0, 134.4 (singlets, quaternary aromatic C); 157.0 (s, NCO₂CH₂); 168.1 [s, (C₁₀H₇CH₂)₂NCO]; 171.4, 171.5 (singlets, MeNHCO). *m/z* (ES +): 790 {5, [M+Na]⁺}; 768 {100, [M+1]⁺}. IR (KBr): 3319m (N-H str); 3054w (Ar-H str); 2938m, 2817m (HC-H str); 1702s (carbamate C=O str); 1663 (amide I); 1533 (amide II). Found (FAB, NOBA matrix): M⁺ 767.4240 (0.6 ppm). [C₄₂H₅₅N₈O₆ requires *M* 767.4245].

Complexes of the carbamate ligand 41 were prepared in solution in acetonitrile without isolation, using a 10% excess of the appropriate metal triflate salt, and were characterised by electrospray mass spectroscopy (positive ion detection mode):

Cu²⁺ 978 {3, [M²⁺+(CF₃SO₃)⁻]⁺}; 829 {8, [M²⁺+e]⁺}; 415 {100, M²⁺}.

Zn²⁺ 980 {6, [M²⁺+(CF₃SO₃⁻)]⁺}; 416 {100, M²⁺}.

Pb²⁺ 1122 {6, [M²⁺+(CF₃SO₃⁻)]⁺}; 487 {100, M²⁺}.

1,7-Bis(paramethoxybenzenesulphonyl)-1,4,7,10-tetraazacyclododecane 53

A procedure similar to that described previously for the preparation of the paratoluene-sulfonyl analogue (52) was employed.⁵ A solution of 1,4,7,10-tetraazacyclododecane (1.29 g, 7.5 mmol) in dry pyridine (12 cm³) was added dropwise to a solution of 4-methoxybenzenesulfonyl chloride (3.10 g, 15 mmol) in pyridine (30 cm³) over a period of 15 minutes, with cooling to 0°C. The mixture was allowed to warm to room temperature and stirred for a further 2h. The pyridine was removed under reduced pressure and the yellow residue treated with water (30 cm³) and the resulting suspension stirred at room temperature for 1h. The solid was separated by filtration, washed with water (3 x 30 cm³) followed by saturated aqueous potassium carbonate solution (3 x 30 cm³) and finally methanol (3 x 30 cm³). (Yield 3.1 g, 81%). Mp > 250°C. δ_H (CDCl₃): 3.28 (8H, br, HNCH₂CH₂NSO₂Ar); 3.52 (8H, br, NCH₂CH₂NSO₂Ar); 4.00 (s, 6H, OCH₃); 7.15 (4H, d, ³J 8.9, Ar); 7.85 (4H, d, ³J 8.9, Ar). δ_C{¹H} (CDCl₃): 49.2 (s, OCH₃); 52.3 (s, NCH₂CH₂NSO₂Ar); 55.7 (s, NCH₂CH₂NSO₂Ar); 114.4 (s, *meta* C); 128.5 (s, C-OMe); 129.5 (s, *ortho* C); 163.9 (s, C-SO₂). m/z (ESMS, positive ion): 513 (55, M⁺+1); 535 (17, M+Na⁺); 551 (6, M+K⁺). IR (KBr): 3447m (N-H str), 3170w (Ar-H str), 2978m and 2937m (HC-H str), 1597s, 1496s, 1339s, 1258s, 1157s, 1095m, 1016m, 701s, 561s. Found: M⁺ (CI): 513.1850. [C₂₂H₃₃N₄S₂O₆ requires M 513.1842].

1,7-Bis(4-methoxybenzenesulphonyl)-4,10-bis(methylcarbamoylmethyl)-1,4,7,10-tetraazacyclododecane 54

Chloro-N-methylethanamide (580 mg, 5.40 mmol) was added to a suspension of the disulfonamide (1.1 g, 2.15 mmol) in dry dimethylformamide (10 cm³) containing anhydrous caesium carbonate (1.76 g, 5.40 mmol) and potassium iodide (714 mg, 4.30 mmol). The mixture was heated at 75°C under an atmosphere of argon for 48h. [The progress of the reaction was readily monitored by alumina TLC: the R_f values (5%

methanol-dichloromethane) of the starting material and the monoalkylated and dialkylated compounds were 0.4, 0.6 and 0.8 respectively]. The solvent was removed under reduced pressure and the residue taken into dichloromethane and filtered. Removal of solvent from the resulting yellow solution gave a brown residue which was purified by silica column chromatography, (gradient elution from dichloromethane to 3% methanol-dichloromethane, $R_f = 0.4$ in 5% methanol-dichloromethane), giving a colourless solid (1.19 g, 84%), mp 112 - 115°C. δ_H ($CDCl_3$): 2.87 (6H, d, 3J 4.9, $CONHCH_3$); 2.95 (8H, br, NCH_2CH_2N); 3.12 (8H, br, NCH_2CH_2N); 3.25 (4H, s, $NCH_2CONHMe$); 7.00 (4H, d, 3J 8.8, Ar); 7.69 (4H, d, 3J 8.8, Ar). $\delta_C\{^1H\}$ ($CDCl_3$): 26.2 (s, $CONHCH_3$); 50.7 (s, OCH_3); 55.8 and 56.0 (singlets, NCH_2CH_2N); 58.7 (s, $NCH_2CONHMe$); 114.8 (s, *meta* C); 129.2 (s, C-OMe); 129.7 (s, *ortho* C); 163.5 (s, C-SO₂); 171.8 (CONHMe). m/z (ES +): 655 (100, M^++1); 677 (80, $M+Na^+$). IR (KBr): 3395m (N-H str), 3076w (Ar-H str), 2943m and 2841m (HC-H str), 1662s (C=O str), 1596s, 1497m, 1335s, 1261s, 1155s, 1093m, 1023m, 699s, 558s. Found: C, 49.2; H, 6.2; N, 12.2 ($C_{28}H_{42}N_6S_2O_8 \cdot 2H_2O$ requires C, 48.7; H, 6.7; N, 12.2).

1,7-Bis(methylcarbamoylmethyl)-1,4,7,10-tetraazacyclododecane 55

A solution of hydrogen bromide in acetic acid (33%, 30 cm³) was added to **54** (2.0 g, 3.06 mmol) in the presence of phenol (2.88 g, 30.6 mmol) and the mixture was heated at 110°C for 48 h. A further 20 cm³ of HBr/AcOH was then added and heating continued for a further 48 h. The resulting brown solution was added dropwise to a large excess of diethyl ether in a large centrifuge tube. The solid which precipitated was separated by centrifuge, washed with ether, dried under reduced pressure and taken up into water. The pink solution obtained was filtered and passed down an anion exchange column (Amberlite IRA 400 in OH⁻ form). The basic fractions collected were combined and the water removed by freeze-drying giving an oily solid. ¹³C NMR indicated that the required compound was present but contaminated with a significant proportion of monoamide. Separation was achieved by selective precipitation of the diamide from toluene, giving a colourless solid (300mg, 31%). Mp. 95 - 98°C. δ_H ($CDCl_3$): 2.45 (2H, br s, NH amine); 2.65 (16H, br, CH_2CH_2 ring); 2.81 (6H, d, 3J

4.8, CONHCH₃); 3.17 (4H, s, NCH₂CO); 7.51 (2H, br d, ³J 4.8, CONHMe). δ_C{¹H} (CDCl₃): 26.6 (s, CONHCH₃); 46.6 (s, NHCH₂CH₂NCH₂CO); 54.1 (s, NHCH₂CH₂NCH₂CO); 60.3 (s, NCH₂CO); 172.7 (s, CONHMe). m/z (DCI): 315 (100, M⁺+1). IR (KBr): 2941m and 2835m (H-H str), 1654s (C=O str), 1560s, 1465m, 1406m, 1281w, 1068m, 975m, 786w cm⁻¹. Found: M+ (CI): 315.2508. [C₁₄H₃₁N₆O₂ requires M 315.25085].

1,7-Bis[N,N-bis(2-naphthylmethyl)carbamoylmethyl]-4,10-

bis(methylcarbamoylmethyl)-1,4,7,10-tetraazacyclododecane: Ca²⁺ complex

[Ca.42]²⁺(I)₂

A solution of the bis-naphthyl chloroamide **45** (232 mg, 0.62 mmol) in dry dimethylformamide (1 cm³) was added to a solution of the *trans*-diamide **55** (96 mg, 0.31 mmol) in dimethylformamide (1 cm³) in the presence of anhydrous caesium carbonate (250 mg, 0.77 mmol) and potassium iodide (103 mg, 0.62 mmol). The mixture was heated at 75°C under an atmosphere of argon for 48 h. The solvent was removed under reduced pressure and the residue taken into dichloromethane and filtered. Removal of solvent gave a brown oil which was purified by column chromatography on silica (gradient elution from dichloromethane to 2% NH₃(aq) / 18% methanol / 80% dichloromethane, R_f = 0.5 by TLC under these conditions). The product was further purified by precipitation from chloroform-ethanol giving a fine, off-white solid which proved to be the calcium complex of the required ligand as its iodide salt (40 mg, 10%), mp > 250°C. δ_H(d₆-DMSO, 363K, 400 MHz): 2.48 (8H, br, NCH₂CH₂N ring); 2.57 (6H, d, ³J 4.4, CONHCH₃); 2.83 (8H, br, NCH₂CH₂N ring); 3.33 (4H, s, NCH₂CO); 3.73 (4H, s, NCH₂CO); 4.82 (8H, s, C₁₀H₇CH₂N); 7.38 - 7.92 (28H, overlapping multiplets, Ar-H); 8.62 (2H, d, ³J 4.4, CONHMe). δ_C{¹H} (CDCl₃, 298K): 27.0 (CH₃); 49.5 (br, C₁₀H₇CH₂N); 51.1 (NCH₂CH₂N); 53.3 (NCH₂CH₂N); 57.3 (NCH₂CO); 58.0 (NCH₂CO); 124.7, 126.0, 126.4, 127.1, 127.5, 128.4, 128.6, 129.6, 130.0, 132.5, 133.5, 133.7, 133.9 (aromatic C); 174.4 (C=O); 174.6 (C=O). m/z (ES +): 1156 {5, [M²⁺+I]⁺}; 515 {100, M²⁺}. IR(KBr): 3223m (N-H str), 3103m (Ar-H str), 2985m and 2851m (HC-H str), 1643s (C=O str), 1616s,

1309m, 1234m, 1093m, 999m, 817m, 754m. Found: C, 56.6; H, 5.0; N, 8.4; Ca, 3.1; I, 18.7. ($C_{62}H_{68}CaI_2N_8O_4 \cdot H_2O$ requires C, 57.2; H, 5.4; N, 8.6; Ca, 3.1; I, 19.5).

1,7-Bis[N,N-bis(2-naphthylmethyl)carbamoymethyl]-4,10-bis(methylcarbamoymethyl)-1,4,7,10-tetraazacyclododecane 42

Dilute aqueous acid (HCl, 0.01M, 3 cm³) was added to the calcium complex obtained as above (15 mg, 0.012 mmol) followed by methanol (1 cm³). The mixture was stirred at room temperature for 18h and an excess of DOTA was added. The pH was raised slowly to 13 by the dropwise addition of KOH (0.1M aq). Extraction into dichloromethane (3 x 5 cm³) and removal of solvent under reduced pressure gave a colourless residue (4 mg, 35%). $\delta_H(CDCl_3)$: 2.55 (16H, br, CH₂ ring); 2.67 (6H, d, ³J 4.6, CONHCH₃); 3.32 (4H, br s, NCH₂CO); 3.47 (4H, br s, NCH₂CO); 4.64 (4H, br s, C₁₀H₇CH₂N); 4.86 (4H, br s, C₁₀H₇CH₂N); 7.35 - 7.91 (28H, overlapping multiplets, aromatic H). m/z (ES +): 1012 {5, [M+Na⁺]⁺}; 990 {12, [M+H⁺]⁺}; 496 {30, [M+(H⁺)₂]²⁺}. IR (KBr): 3210m (N-H str), 3115m (Ar-H str), 2969m and 2843m (HC-H str), 1643s (C=O str), 1313m, 1085m, 990m, 754m.

Complexes of the bis-naphthyl ligand 42 were prepared in solution in acetonitrile without isolation, using a 10% excess of the appropriate metal triflate, and were characterised by electrospray mass spectroscopy (positive ion detection):

Cu²⁺ 526 {70, M²⁺}

Pb²⁺ 598 {80, M²⁺}

Eu³⁺ 1140 {12, [M³⁺+2e]⁺}

Chloro-N-[7-(4-methyl-2(1H)-quinolinone)]ethanamide

7-Amino-4-methyl-2(1H)-quinolinone (carbostyryl-124, 200 mg, 1.15 mmol) was taken into dry dichloromethane (2 cm³) and triethylamine (0.19 cm³, 1.38 mmol) was added. Chloroacetylchloride (0.11 cm³, 1.38 mmol) was added dropwise to the stirred suspension under argon with cooling to -10°C. The mixture was allowed to warm to room temperature and stirred for a further 2h. The resulting white solid was separated

by centrifuge and washed with HCl(aq) (0.1M, 2 x 4 cm³) followed by water (4 x 4 cm³) and finally methanol (4 x 4 cm³). The solid was dried under vacuum to give the required product (210 mg, 73%), mp > 250°C. δ_{H} (*d*₆-DMSO): 2.38 (3H, s, CH₃); 4.29 (2H, s, ClCH₂); 6.28 (1H, s, C=CH-CO); 7.34 (1H, dd, *J* 2.0 and 8.7, Ar-H position-6); 7.66 (1H, d, *J* 8.7, Ar-H position-5); 7.74 (1H, d, *J* 2.0, Ar-H position-8); 10.57 (1H, s, ClCH₂CONH); 11.61 (1H, s, C=CH-CONH). Compound not sufficiently soluble to obtain ¹³C NMR. *m/z* (CI): 253 (33, M⁺+1 for ³⁷Cl); 251 (100, M⁺+1 for ³⁵Cl); 217 (33, [M⁺-Cl+H]+1). *m/z* (EI): 252 (26, M⁺ for ³⁷Cl); 250 (78, M⁺ for ³⁵Cl); 174 (100, M⁺-ClCHCO). IR (KBr): 3171m (N-H str), 3025m (Ar-H str), 2972m and 2919m (aliphatic C-H str), 1675s (amide I band for open-chain amide), 1647s (amide I band for ring amide), 1613s (C=C conjugated to C=O), 1585m (amide II band for open-chain amide), 1547s, 1459m, 1403s, 1269m, 885m, 856m. Found: C, 53.5; H 4.4; N, 10.4. (C₁₂H₁₁N₂O₂Cl.H₂O requires C, 53.6; H, 4.9; N, 10.4).

1-[[7-(4-methyl-2(1H)-quinolinone)]carbamoylmethyl]-1,4,7,10-tetraazacyclododecane

The molybdenum tricarbonyl complex of 1,4,7,10-tetraazacyclododecane (280 mg, 0.8 mmol), prepared as described above in the synthesis of ligand **32**, was taken up into dry, degassed dimethylformamide (5 cm³) and anhydrous potassium carbonate (166 mg, 1.2 mmol) and potassium bromide (95 mg, 0.8 mmol) were added. The chloroacetylated carbostyryl (200 mg, 0.8 mmol) was added and the mixture stirred at 70°C for 6h under an atmosphere of argon, after which the solvent was removed under reduced pressure with mild heating. The resulting brown residue was taken into HCl(aq) (1M, 10 cm³) and the mixture stirred at room temperature and open to the air for 18 h. The pH of the solution was raised to 14 with KOH pellets with cooling and the dark green molybdenum residues filtered off giving a clear, pale yellow solution. Extraction into dichloromethane (6 x 15 cm³) followed by removal of solvent under reduced pressure gave a pale yellow oil (170 mg, 55%). δ_{H} (CDCl₃): 2.44 (1H, s, CH₃); 2.74 (16H, br, CH₂ ring); 2.88 (3H, br, amine N-H in ring); 3.35 (2H, s, NCH₂CO); 6.35 (1H, s, C=CH-CO); 7.55 (1H, d, *J* 8.8, Ar-H position-5); 7.60 (1H, d

not sufficiently resolved to obtain J value, Ar-H position-8); 7.91 (1H, dd, larger J 8.8, Ar-H position-6); 10.56 (1H, s, ClCH₂CONH). $\delta_{\text{C}}\{^1\text{H}\}$ (CDCl₃): 19.6 (CH₃); 46.2, 46.7, 47.6, 47.7 (CH₂ ring); 60.3 (NCH₂CO); 106.0 (CH₃C=CH); 117.4 (CH₃C=CH); 115.0, 119.3, 125.7 (tertiary aromatic carbons); 139.7, 141.2, 149.2 (aromatic quaternary carbons); 165.0 (CH₃C=CHC=O); 171.5 (NCH₂CO). m/z (ES +): 387 (100, M⁺+1); 409 (M+Na⁺). IR (thin film): 2940m, 2843m (HC-H str); 1674s (amide I band for open-chain amide); 1654s (amide I band for ring amide); 1607m (C=C conj to C=O); 1541s; 1459m; 1405m; 1356m; 1293m; 819w.

1,4,7-Tris(methylcarbamoylmethyl)-10-[N-[7-(4-methyl-2(1H)-quinolinone)]-N-[methylcarbamoylmethyl]carbamoylmethyl]-1,4,7,10-tetraazacyclododecane 57

The monoalkylated macrocycle (150 mg, 0.39 mmol) was dissolved in dry dimethylformamide (2 cm³) and anhydrous caesium carbonate (190 mg, 0.58 mmol) and potassium iodide (65 mg, 0.39 mmol) were added. Chloro-N-methylethanamide (210 mg, 1.95 mmol) was added and the mixture stirred under an atmosphere of argon at 75°C for 48 h. The solvent was removed under reduced pressure and the residue taken into dichloromethane, filtered and the dichloromethane removed from the resulting clear solution leaving a yellow oil. The product was purified by alumina column chromatography (gradient elution from dichloromethane to 3% methanol-dichloromethane; R_f = 0.6, 10% methanol-dichloromethane) giving a yellow oil. The product obtained required further purification which was achieved by means of preparative reverse-phase HPLC, using a Rainin Dynamax 60Å column, gradient elution from 10% A / 90% B at t = 0 to 90% A / 10% B at t = 20, flow rate = 10 cm³ min⁻¹, λ_{obs} = 330 nm, retention time = 10.4 min. (A = CH₃CN containing 0.1% trifluoroacetic acid; B = H₂O containing 0.1% trifluoroacetic acid). Removal of solvent by freeze-drying gave the required compound as a pale yellow solid (45 mg, 13%). δ_{H} (D₂O): 2.13 (3H, s, CH=CCH₃); 2.23 (3H, s, NHCH₃); 2.34 (3H, s, NHCH₃); 2.38 (6H, s, NHCH₃); 3.6 - 2.7 (24H, v br, CH₂ ring + NCH₂CO); 6.20 (1H, s, CH₃C=CH); 6.95 (1H, br s, Ar-H position-8); 7.26 (1H, br d, J 8.5, Ar-H position-6); 7.45 (1H, d, J 8.5, Ar-H position-5). $\delta_{\text{C}}\{^1\text{H}\}$ (D₂O): 18.1 (CH=CCH₃); 25.6, 25.7 (NHCH₃); 48.9,

50.5 (CH₂ ring); 54.8, 55.0, 55.4 (NCH₂CO); 104.6 (CH₃C=CH); 115.6, 117.3, 126.6 (tertiary aromatic C); 118.4 (CH₃C=CH); 138.6, 140.0, 150.4 (quaternary aromatic C); 163.6 (CH₃C=CHCO); 169.6 (NCH₂CO). m/z (ES +): 672 (34, M⁺+1); 356 (100, M+Ca²⁺). IR (KBr): 3303m (N-H str); 3104 m (Ar-H str); 2973m, 2919m (aliphatic C-H str); 1684s, 1677s, 1655s, 1648s (amide I bands); 1585m (amide II band); 1429m, 1397m, 1205s, 1133m, 801m, 722m.

Lanthanide complexes of ligand 57

[Eu.57]³⁺ The ligand **57** (its diprotonated trifluoroacetate salt, 15 mg, 0.0167 mmol) was dissolved in anhydrous acetonitrile (1 cm³) to which was added a solution of europium triflate (10 mg, 0.0167 mmol) in acetonitrile (2 cm³). The mixture was warmed to 50°C for 2h after which the solvent was removed under reduced pressure. The residue was taken up into the minimum volume of acetonitrile and added dropwise to a large volume of anhydrous diethyl ether (5 cm³) in a centrifuge tube, with vigorous shaking between additions (Whirlimix). The complex precipitated as a fine microcrystalline solid (10 mg, 47%). [The complex proved to be too hygroscopic to obtain a reliable microanalysis; sample homogeneity was confirmed by analytical HPLC using the conditions described in the preparation of the ligand **57**, retention time 7.4 min]. m/z (ES +): 1120 {6, [M³⁺+(CF₃SO₃⁻)₂]⁺}; 971 {2, [M³⁺+(CF₃SO₃⁻)+e⁻]⁺}; 822 {3, [M³⁺+2e⁻]⁺}; 486 {78, [M³⁺+(CF₃SO₃⁻)₂]²⁺}; 410 {45, [M³⁺+e⁻]²⁺}. IR (KBr): 3151w (Ar-H str); 2985w, 2927w (aliphatic C-H str); 1639s (amide I band); 1545m (amide II); 1418m, 1279s, 1251s, 1171s, 1031s, 640s.

[Tb.57]³⁺ The terbium complex was prepared in a similar manner to that described above for the europium complex, from the ligand **57** (15 mg, 0.0167 mmol) and terbium triflate (10 mg, 0.0167 mmol). (Yield = 11 mg, 52%). m/z (ES +): 1128 {3, [M³⁺+(CF₃SO₃⁻)₂]⁺}; 829 {12, [M³⁺+2e⁻]⁺}; 489 {48, M³⁺+(CF₃SO₃⁻)²⁺}; 414 {100, [M³⁺+e⁻]²⁺}. IR: identical to that of the europium complex.

5.2 Experimental Details of Luminescence Measurements

5.2.1 Ultra-violet Spectroscopy

Ultra-violet absorbance spectra were obtained using a Unicam UV / Vis Spectrometer UV2-100, controlled through Unicam Vision Software Version 2.11 on a PC. A tungsten lamp was used for wavelengths greater than 325nm; shorter wavelengths were produced by a deuterium lamp. Spectra were acquired with a bandwidth of 2 nm and were measured using a scan speed of 120 nm min⁻¹ and a data interval of 0.5 or 2.0 nm. Samples were contained in quartz cuvettes with a path length of 1 cm. All spectra were run against a reference of pure solvent contained in a matched cell.

Extinction coefficients were calculated using the Beer-Lambert Law:

$$A = \epsilon c l$$

where A is the absorbance $\{= \log_{10}(I_0/I)\}$ where I_0 and I are the measured light intensities in the absence and presence of the sample, respectively}, c the concentration (mol dm⁻³) and l the path length (cm). The absorbance at a number of different solution concentrations was measured and the extinction coefficient obtained from the gradient of a plot of A against c.

5.2.2 Luminescence Spectroscopy: Instrumentation

Fluorescence and phosphorescence spectra were acquired using a Perkin-Elmer LS 50B Luminescence Spectrometer controlled through Perkin-Elmer Fluorescence Data Manager Instrument Control Version 3.00 on a PC. The optical layout and the path of the radiation is shown in Figure 5.1. The excitation source is a xenon flash tube, triggered at a frequency of 50Hz, which produces an intense, short duration pulse of radiation over the spectral range 200 - 800 nm, with a width at half peak intensity of less than 10 μ s. The light is focussed onto the excitation monochromator, where it is diffracted by the grating (controlled by a stepper motor). A narrow wavelength band emerges, the half-peak width of which is determined by the slit widths selected (typically 2.5 - 15 nm). The majority of the excitation beam is focused onto the sample but a small proportion is reflected by a beam splitter onto a reference photomultiplier

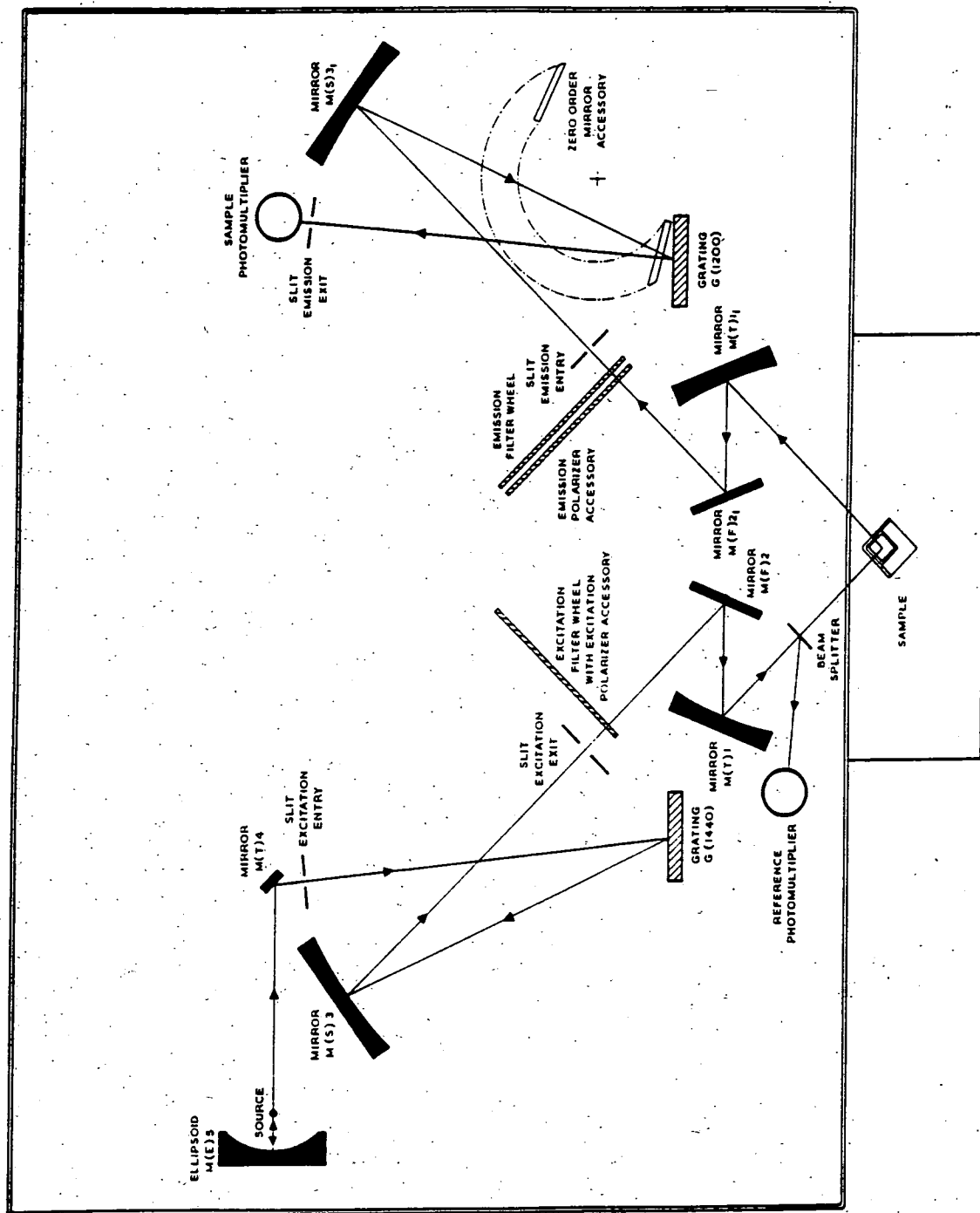


FIGURE 5.1 Optical layout of the Perkin-Elmer LS 50B luminescence spectrometer (reproduced from reference 6).

tube. This allows the signal from the sample to be corrected for fluctuations in the intensity of light from the source. Light emitted by the sample is focused onto the emission monochromator, the resolution again being determined by the slit widths selected, and is subsequently detected by the sample photomultiplier tube.

5.2.3 Acquisition of fluorescence and phosphorescence spectra

In fluorescence mode, at each wavelength interval, the signal is integrated over $80 \mu\text{s}$ to collect all the light emitted by the sample. Phosphorescence occurs over a much longer time interval ($> 80 \mu\text{s}$) and two further parameters must be considered in this case, namely the gate time, over which the integration is performed, and the delay time, which is the interval between excitation of the sample and commencement of the integration (Figure 5.2).

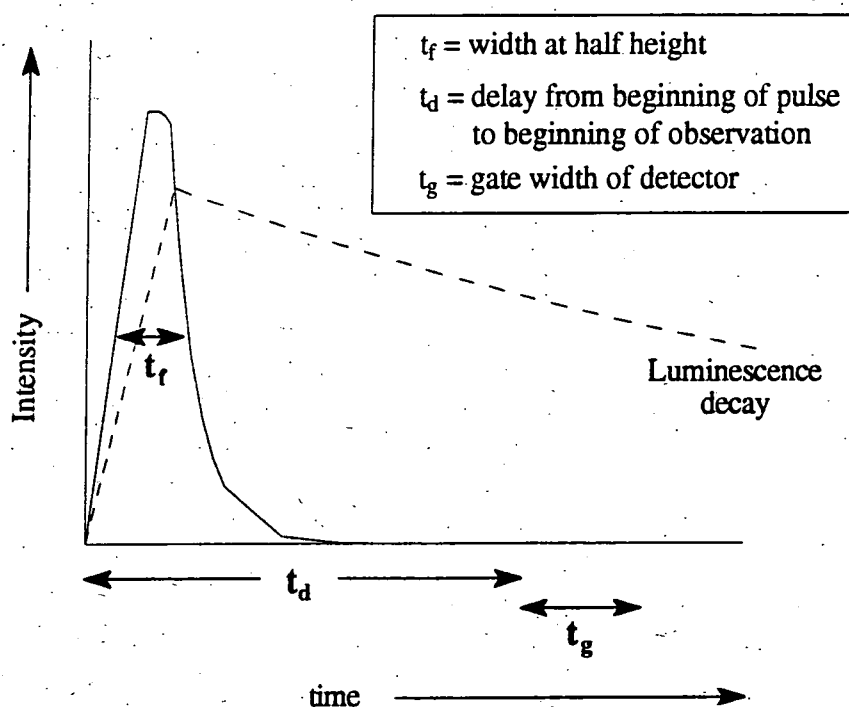


FIGURE 5.2 Diagram illustrating some of the variables in the acquisition of phosphorescence spectra

In acquiring metal luminescence spectra, a delay time of 0.1 ms was normally used, with a gate time of 10 ms . Since the lifetimes of the complexes studied were all of the

order 0.5 - 4.5 ms, these conditions ensured that a large proportion of the emitted light was detected, thereby favouring the signal-to-noise ratio.

Solutions for acquiring fluorescence and phosphorescence spectra were contained in quartz fluorescence cuvettes with a path length of 1 cm. The absorbance at the selected excitation wavelength was 0.5 or less in all cases (< 0.1 for the determination of quantum yields - section 5.2.5). The excitation and emission monochromator slit widths may be varied independently. In all discussions, the slit width value refers to the half-height bandwidth; for example, a "2.5 nm slit width" corresponds to a slit width giving a half-peak width of 2.5 nm. Large slit widths give a higher signal intensity but with a loss of resolution. The most highly resolved emission spectra were obtained with slit widths of 10 nm (excitation) and 2.5 nm (emission).

A Hamamatsu R928 photomultiplier tube was used for detection of the emitted light. This has a higher sensitivity in the red region of the spectrum compared to other commonly-used, commercially available detectors, which is particularly important in the study of the europium complexes. The sensitivity of the tube has a marked dependence on wavelength, however, and spectra must be corrected for this. This was achieved by dividing spectra obtained by a correction curve (Figure 5.3). All of the spectra shown in this thesis have been corrected in this way. The correction curve was generated by running an emission spectrum of the light emitted by a lamp of known spectral profile and ratioing the spectrum so obtained with the known spectrum.

Phosphorescence excitation spectra were acquired by monitoring the emission at 619 nm (for Eu^{III}) and 545 nm (for Tb^{III}). Excitation spectra are automatically corrected by the spectrometer for wavelengths greater than 230 nm, by means of the reference photomultiplier tube.

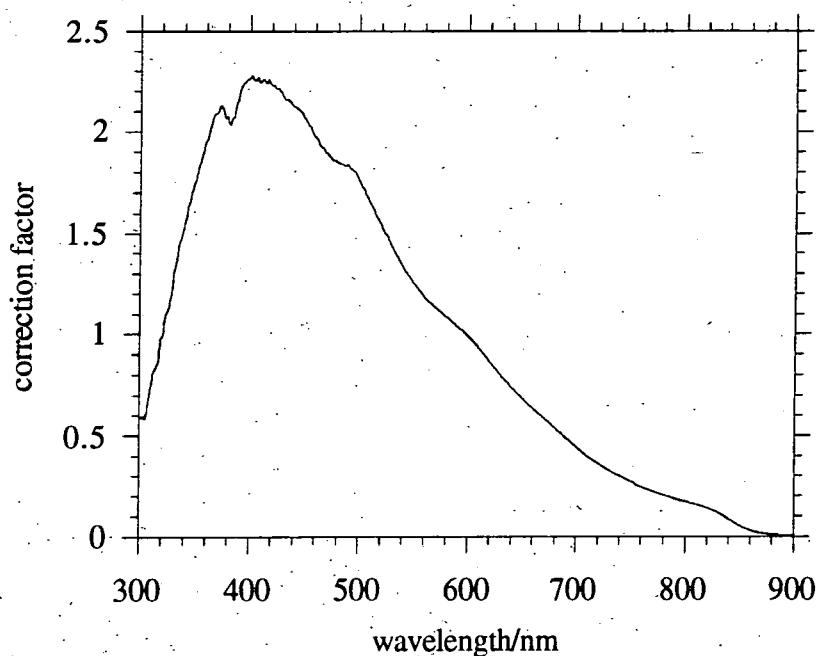


FIGURE 5.3 Correction curve generated for the R928 photomultiplier tube.

5.2.4 Lifetimes

Quoted lifetimes (τ) are the average of at least 5 separate measurements, each of which was obtained by monitoring the emission intensity at 619 nm (for Eu^{III}) or 545 nm (for Tb^{III}) after 20 different delay times spanning a range of at least 2 lifetimes. Slit widths of 15 nm were typically used for the europium complexes; the higher intensities of most of the terbium complexes allowed slit widths of 5 nm or lower to be used. In order for an accurate decay curve to be generated, it is important that the gate time is short compared to the luminescence lifetime: it proved possible to use a gate time of 0.1 ms in most cases whilst maintaining a satisfactory signal-to-noise ratio.

Except where stated otherwise, monoexponential decay of the luminescence was observed: the phosphorescence decay curves were fitted with good residuals to an equation of the form

$$I(t) = I(0) \exp(-t/\tau)$$

using a curve-fitting program (Kaleidagraph software running on an Apple Macintosh or Grafit software on a PC).

{Here $I(t)$ is the intensity at time t after the excitation flash, $I(0)$ the initial intensity at time $t = 0$ and τ is the phosphorescence lifetime}.

Unless stated otherwise, lifetimes were found to be independent of concentration over the range examined (corresponding to an absorbance range of 0.5 to 0.05) and were generally reproducible to within at least ± 0.1 ms.

5.2.5 Quantum yields.

Quantum yields of fluorescence and phosphorescence were measured according to the method of Haas and Stein,⁷ which may be summarised as follows.

$$\phi = \frac{\text{number of photons emitted}}{\text{number of photons absorbed}} \propto \frac{E}{A}$$

where A is the area under the absorbance curve in the excitation band and E is the combined area under the emission bands.

Therefore

$$\frac{\phi_u}{\phi_s} = \frac{E_u/A_u}{E_s/A_s} \quad (49)$$

where s denotes values for a standard and u the values for the sample under investigation. The integrated emission intensities of the standard and the unknown were obtained under the same conditions, using minimum excitation slit widths (to minimise the spread of excitation wavelengths). Spectra were acquired for a number of solutions of different absorbance in the range 0.01 - 0.1 and the emission intensity was plotted against the absorbance. Under these conditions, the luminescence intensity should be directly proportional to the absorbance and a straight line is expected, the gradient of which gives E/A . The ratio of the gradients for sample and standard thus gives the relative quantum yield.

In the case of phosphorescence, only a portion of the total emission is observed, as determined by the gate and delay times. The observed emission (E_{obs}) can be related to the required total emission (E_{total}) through the following expression:⁸

$$\frac{E_{\text{total}}}{E_{\text{obs}}} = \frac{1 - \exp(-c / \tau)}{\exp(-t_d / \tau) - \exp[-(t_d + t_g) / \tau]} \quad (50)$$

where τ is the lifetime, t_d and t_g are the delay and gate times respectively and c is the cycle time (time interval between successive flashes; $c = 20$ ms in this work).

Quinine sulfate [$\phi = 0.546$ in H_2SO_4 (1M)⁹] was used as the standard for the terbium complexes and $[\text{Ru}(\text{bipy})_3]^{2+}$ ($\phi = 0.028$ in aerated water¹⁰) for the europium complexes. In general, the quantum yields were reproducible to within about 10%. There is a larger error in the values for most of the europium complexes, owing to the low intensity of emission. Excitation wavelengths were chosen to correspond to reasonably 'flat' portions of the absorbance spectra, thereby minimising the uncertainty in the absorbance.

5.2.6 Effect of metal ions on fluorescence intensities

The effect of metal ions on fluorescence (Chapter 4) was investigated by addition of a solution of the metal triflate to 3 cm³ of a solution of the ligand in the same solvent. In each case, the concentration of the metal triflate solution was first adjusted such that the volume of solution to be added, containing the required number of equivalents of M^{n+} , was 100 μl . The addition thus results in a constant dilution (of only 3.3%) which is the same for all the metals and which has a negligible effect on the fluorescence intensity.

The rates of metal complexation in the naphthyl systems were studied by monitoring the fluorescence intensity at 337 nm (for monomer emission) or 401 nm (excimer) at intervals of 1 s (for the aqueous solutions) or every 0.2 s (for the solutions in acetonitrile), following addition of the metal salt. The resulting growth or decay curves

were examined using Kaleidagraph software, as exemplified by the effect of Cd^{2+} on the tetranaphthyl ligand **40** (Figure 5.4).

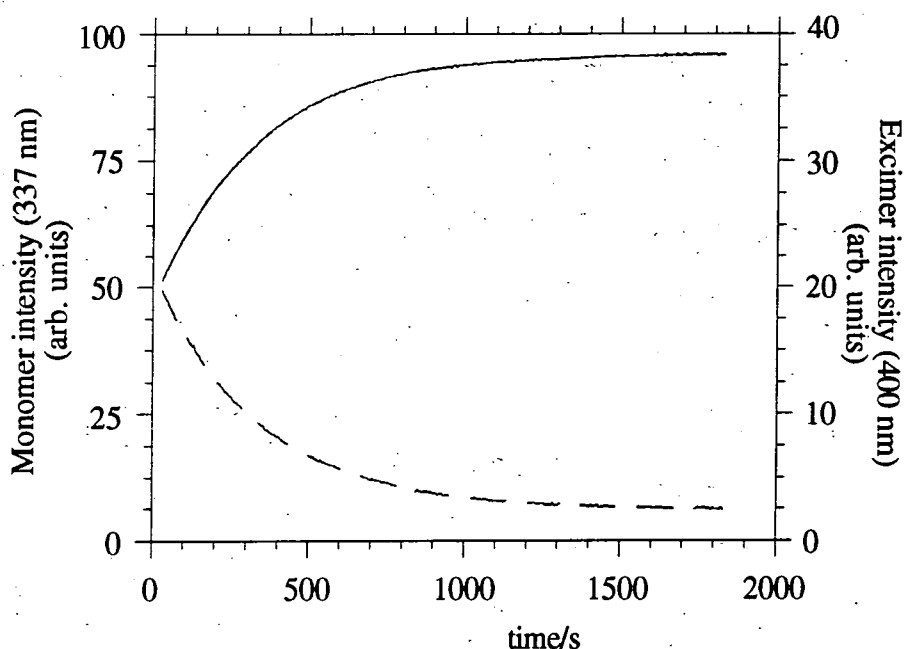


FIGURE 5.4 Increase in monomer emission (solid line) and decay in excimer emission (broken line) for ligand **40** (MeCN, $[\mathbf{40}] = 5 \times 10^{-6} \text{ M}$, $[\text{CF}_3\text{CO}_2\text{H}] = 10^{-4} \text{ M}$) following addition of $\text{Cd}(\text{CF}_3\text{SO}_3)_2$ ($5 \times 10^{-5} \text{ M}$). Under these conditions, pseudo-first-order kinetics are followed and the data were fitted to an equation of the form

$I(t) = c - A \exp(-kt)$ for the increase in monomer emission, giving $k = 3.1 \times 10^{-3} \text{ s}^{-1}$ (correlation coefficient = 0.999 95). Excimer decay was fitted to a curve of the form $I(t) = c + A \exp(-kt)$, giving $k = 2.95 \times 10^{-3} \text{ s}^{-1}$ ($R = 0.999 92$).

5.2.7 Effect of β -cyclodextrin

When monitoring the effect of added β -cyclodextrin (Aldrich) on the complexes of the naphthyl ligands, the following procedure was adopted. A solution of the complex in water was prepared ($3.64 \times 10^{-5} \text{ mol dm}^{-3}$) and a 1.5 cm^3 aliquot was diluted with 1.5 cm^3 water and its fluorescence spectrum was recorded ($\lambda_{\text{ex}} 270 \text{ nm}$, excitation and emission slit widths of 5 nm). A second 1.5 cm^3 sample was added to 1.5 cm^3 of a solution of β -cyclodextrin in water ($1.82 \times 10^{-3} \text{ mol dm}^{-3}$) and the fluorescence spectrum recorded. The difference in emission intensities for the two solutions was

noted and, as a control, the spectrum of the initially prepared sample was recorded again. The enhancements in fluorescence intensity were found to be highly reproducible. The effect was also investigated at other concentrations as detailed in Chapter 4.

5.2.8 Degassing of solutions

Where necessary, solutions were degassed by means of four freeze-pump-thaw cycles in degassing cells of the type shown in Figure 5.5. A vacuum-line equipped with a mercury diffusion pump was used for this purpose, (base pressure $<10^{-3}$ mmHg).

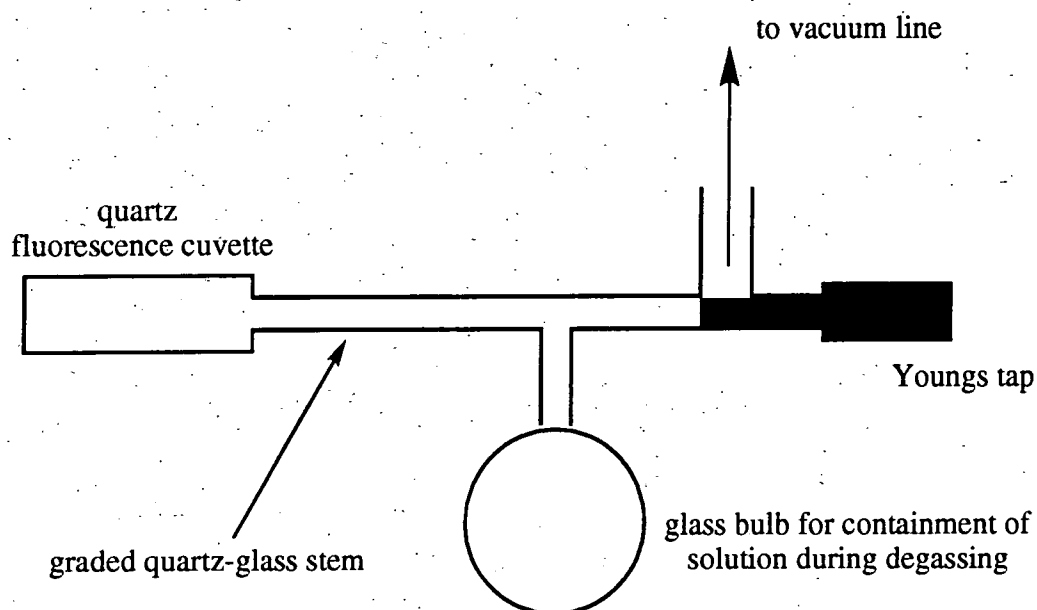


FIGURE 5.5 *Diagram of the cells used for measuring luminescence spectra of degassed solutions*

5.2.9 Variable Temperature Luminescence Spectroscopy

In recording spectra at temperatures exceeding 298K, a Grant thermostatted water bath was used, which rapidly circulated warm water through a channel bored into the sample holder of the spectrometer.

Low temperature spectra were acquired using a variable temperature liquid nitrogen cryostat, Oxford Instruments model DN1704, controlled by an Oxford Instruments ITC 4 temperature controller. A schematic diagram of the cryostat is shown in Figure 5.6. The sample cell is loaded from the top and positioned at the bottom in a chamber which is pump-filled with dry helium prior to use. There are four quartz windows providing optical access to the sample; these are separated from the outer windows by an evacuated chamber, thus excluding water vapour which would otherwise condense on the inner windows on cooling. A liquid nitrogen reservoir, isolated from the surroundings by an outer vacuum chamber, surrounds the central sample access tube. The sample is cooled by allowing a flow of liquid nitrogen from the reservoir to the sample space heat exchanger, through a capillary tube. The flow rate is controlled by the exhaust valve. A platinum resistance thermometer and heater are fitted to the heat exchanger; the temperature controller is used to supply the required amount of heat to balance the cooling power and thus set the required temperature. The fluorimeter was adapted to hold the cryostat in such a way that the sample was positioned in a reproducible position at the intersection of the excitation and emission beam paths of the instrument.

Ethanol was chosen as the solvent for variable temperature studies as its freezing point is sufficiently low for a large range of temperatures to be available in fluid solution (the range 150 - 330K was used). Low temperature spectra of the terbium complex of the carbostyryl ligand (**57**) were obtained in aerated solution. A Hellma Suprasil 101.098 QS low-temperature cuvette was used for this purpose. These cells are manufactured from a single piece of quartz and are less prone to fracture on warming to room temperature than are conventional cells. In the case of the terbium complexes of the naphthyl ligand, it was necessary to de-gas the solutions for low temperature study. This was achieved by modifying the low temperature cells in a similar manner to that shown in Figure 5.5, but with a much longer glass stem (ca. 30 cm), in order to allow the sample to be positioned at the bottom of the cryostat.

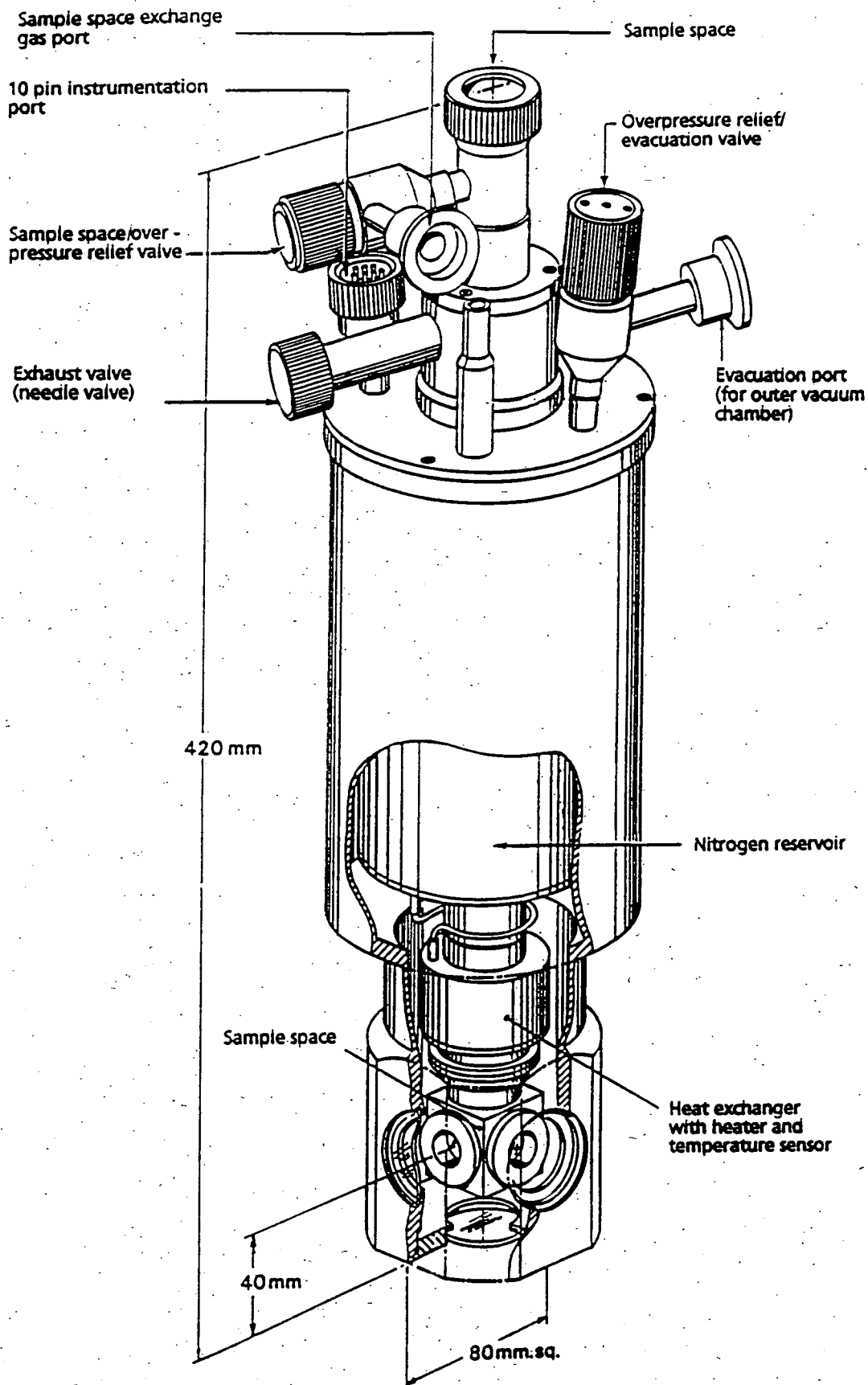


FIGURE 5.6 Schematic diagram of the DNI704 variable temperature liquid nitrogen cryostat used for low temperature luminescence. (Reproduced from reference 11).

5.2.10 Flash Photolysis and Laser Induced Emission Studies

The apparatus used for nanosecond laser flash photolysis is shown in Figure 5.8. The sample was excited by pulses of laser radiation of wavelength 308 nm, produced by a Lambda Physik EMG101 xenon chloride excimer laser. Maximum pulse energy at the sample was of the order of 1 mJ, with a pulse duration of 20 ns.

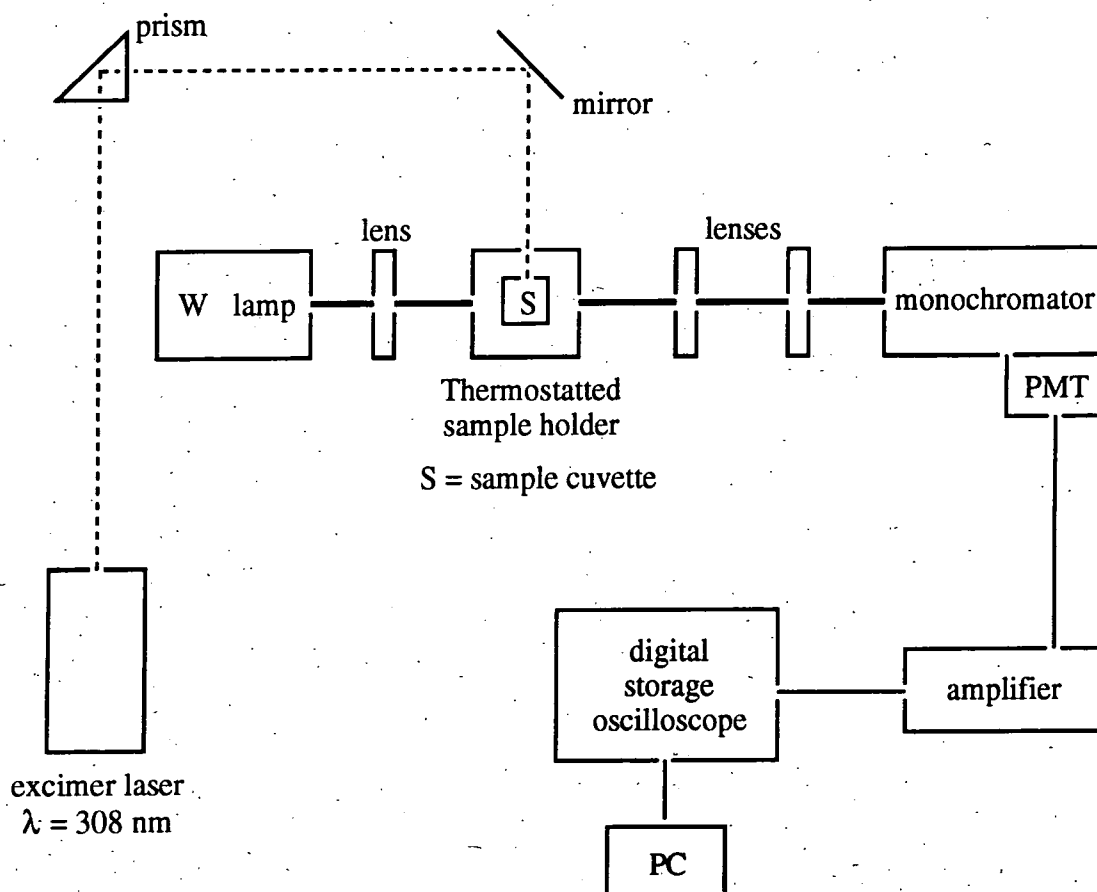


FIGURE 5.8 Schematic diagram of the apparatus for nanosecond laser flash photolysis measurements.

The transient naphthyl triplet produced on laser excitation was observed by absorption spectroscopy (410 nm) at right angles to the exciting pulse. Light from a 100W tungsten filament lamp was focussed onto the sample and the attenuated light emerging was focussed onto a Bentham TM300 monochromator (set at 410 nm) and integrated using a photomultiplier tube (Hamamatsu R928). The output was split into two components by the amplifier, one of which represented the large I_0 value (Figure 5.9).

The other was AC coupled, such that only the rapidly changing component of the signal due to the transient was observed, (I_a) and amplified $\times 10$. The signals were fed into a Tektronix TDS 320 digital storage oscilloscope connected to a PC and were recorded when triggered by a photodiode with the firing of the laser. The transient decay was observed after about 10 consecutive laser pulses, as this increased the signal-to-noise ratio.

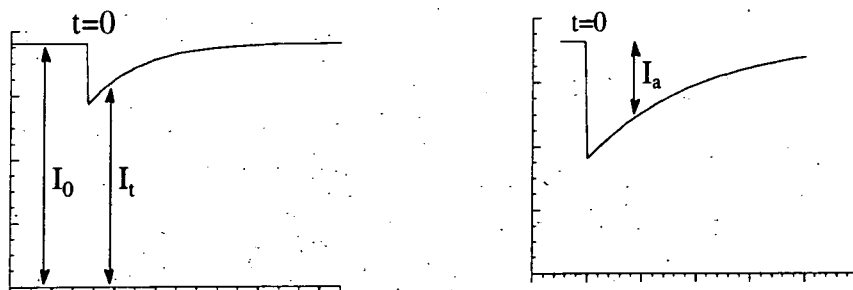


FIGURE 5.9 Illustrating the output signals I_0 and I_a from the amplifier of the flash-photolysis set-up and their relationship to the quantity of interest, I_t .

The absorbance at time t was calculated as follows:

$$A_t = \log_{10} \left(\frac{I_0}{I_t} \right) = \log_{10} \left[\frac{I_0}{I_0 - \left(\frac{I_a(\text{measured})}{10} \right)} \right]$$

The observed signals were thus converted to a plot of absorbance against time. At the wavelength used (410 nm), ground-state naphthalene does not absorb and so the profile obtained represents the decay of the triplet naphthalene with time.

The experimental set-up for observation of the laser-induced metal luminescence was similar except that the lamp was disconnected, the monochromator was set to 490 nm (terbium emits strongly at this wavelength) and the monochromator slit width was increased to allow more light onto the grating.

References for Chapter 5

1. K.P. Pulukkody, T.J. Norman, D. Parker, L. Royle and C.J. Broan, *J. Chem. Soc. Perkin Trans. 2*, 1993, 605.
2. E. Bamberger and O. Boekman, *Ber. Dtsch. Chem. Ges.*, 1887, **20**, 1115.
3. W.A. Jacobs and M. Heidelberger, *J. Biol. Chem.*, 1915, **21**, 147.
4. P.H. Smith and K.N. Raymond, *Inorg. Chem.*, 1985, **24**, 3469.
5. J.F. Desreux, A. Dumont, V. Jacques, P. Qixiu, *Tetrahedron Lett.*, 1994, **35**, 3707.
6. 'LS 50B User's Manual', Perkin-Elmer Ltd: Beaconsfield, 1991.
7. Y. Haas and G. Stein, *J. Phys. Chem.*, 1971, **75**, 3668.
8. A.T. Rhys Williams, S.A. Winfield and J.N. Miller, *Analyst*, 1983, **108**, 1471.
9. S.R. Meech and D. Phillips, *J. Photochem.*, 1983, **23**, 193.
10. K. Nakamaru, *Bull. Chem. Soc. Jpn.*, 1982, **55**, 2697.
11. 'Variable Temperature Liquid Nitrogen Cryostat DN1704 Operator's Handbook', Oxford Instruments (UK) Ltd: Eynsham, 1993.

Appendix

Appendix
Courses Lectures and Seminars Attended

First year courses

Ionic and Molecular Recognition

Organometallics in Synthesis

Polymer Synthesis

Research colloquia, seminars and lectures

-organized by the Department of Chemistry (October 1992- July 1995)

The following were attended:

1992

- October 20th Dr. H. E. Bryndza, Du Pont Central Research.
 Synthesis, Reactions and Thermochemistry of Metal (Alkyl) Cyanide Complexes and their Impact on Olefin Hydrocyanation Catalysis.
- October 22nd Prof. A. Davies, University College London.
The Ingold-Albert Lecture The Behaviour of Hydrogen as a Pseudometal.
- November 5th Dr. C. J. Ludman, University of Durham.
 Explosions, A Demonstration Lecture.
- November 11th Prof. D. Robins, Glasgow University.
 Pyrrolizidine Alkaloids : Biological Activity, Biosynthesis and Benefits.
- November 12th Prof. M. R. Truter, University College, London.
 Luck and Logic in Host - Guest Chemistry.
- December 2nd Prof. A. F. Hegarty, University College, Dublin.
 Highly Reactive Enols Stabilised by Steric Protection.
- December 9th Dr. R. A. Aitken, University of St. Andrews.
 The Versatile Cycloaddition Chemistry of $\text{Bu}_3\text{P} \cdot \text{CS}_2$.

1993

- January 21st Prof. L. Hall, Cambridge.
NMR - Window to the Human Body.
- January 27th Dr. W. Kerr, University of Strathclyde.
Development of the Pauson-Khand Annulation Reaction :
Organocobalt Mediated Synthesis of Natural and Unnatural Products.
- February 11th Prof. S. Knox, Bristol University.
The Tilden Lecture Organic Chemistry at Polynuclear Metal Centres.
- February 17th Dr. R. W. Kemmitt, University of Leicester.
Oxatrimethylenemethane Metal Complexes.
- March 10th Dr. P. K. Baker, University College of North Wales, Bangor.
'Chemistry of Highly Versatile 7-Coordinate Complexes'.
- March 24th Prof. I. O. Sutherland, University of Liverpool.
Chromogenic Reagents for Cations.
- June 16th Prof. A. K. Covington, University of Newcastle.
Use of Ion Selective Electrodes as Detectors in Ion Chromatography.
- October 21st Prof. R. Adams, University of South Carolina, USA.
Chemistry of Metal Carbonyl Cluster Complexes : Development of
Cluster Based Alkyne Hydrogenation Catalysts.
- November 17th Dr. A. Parker, Rutherford Appleton Laboratory, Didcot.
Applications of Time Resolved Resonance Raman Spectroscopy to
Chemical and Biochemical Problems.
- November 24th Dr. P.G. Bruce, University of St. Andrews.
Structure and Properties of Inorganic Solids and Polymers.
- November 25th Dr. R.P. Wayne, University of Oxford.
The Origin and Evolution of the Atmosphere.

- December 1st Prof. M.A. McKervery, Queen's University, Belfast.
Synthesis and Applications of Chemically Modified Calixarenes.
- 1994
- January 26th Prof. J. Evans, University of Southampton.
Shining Light on Catalysts.
- February 9th Prof. D. Young, University of Sussex.
Chemical and Biological Studies on the Coenzyme Tetrahydrofolic Acid.
- February 16th Prof. K.H. Theopold, University of Delaware, USA.
Paramagnetic Chromium Alkyls : Synthesis and Reactivity.
- February 23rd Prof. P.M. Maitlis, University of Sheffield.
Across the Border : From Homogeneous to Heterogeneous Catalysis.
- March 2nd Dr. C. Hunter, University of Sheffield.
Noncovalent Interactions between Aromatic Molecules.
- March 9th Prof. F. Wilkinson, Loughborough University of Technology.
Nanosecond and Picosecond Laser Flash Photolysis.
- March 10th Prof. S.V. Ley, University of Cambridge.
New Methods for Organic Synthesis.
- March 25th Dr. J. Dilworth, University of Essex.
Technetium and Rhenium Compounds with Applications as Imaging Agents.
- November 16th Prof. M. Page, University of Huddersfield.
Four Membered Rings and β -Lactamase.
- November 23rd Dr J. M. J. Williams, University of Loughborough.
New Approaches to Asymmetric Catalysis.

1995

- January 11th Prof. P. Parsons, University of Reading.
Applications of Tandem Reactions in Organic Synthesis.
- January 18th Dr G. Rumbles, Imperial College, London.
Real or Imaginary 3rd Order non-Linear Optical Materials.
- February 8th Dr D. O'Hare, Oxford University.
Synthesis and Solid State Properties of Poly-, Oligo- and Multidecker
Metallocenes.
- February 22nd Prof. E Schaumann, University of Clausthal.
Silicon and Sulphur Mediated Ring-opening Reactions of Epoxide.
- March 1st Dr M. Rosseinsky, Oxford University.
Fullerene Intercalation Chemistry.
- April 26th Dr M. Schröder, University of Edinburgh.
Redox Active Macrocyclic Complexes : Rings, Stacks and Liquid
Crystals.
- May 4th Prof. A. J. Kresge, University of Toronto.
The Ingold Lecture Reactive Intermediates : Carboxylic Acid Enols
and Other Unstable Species.

Graduate Colloquia, comprising talks by third-year graduate students, have been attended each year.

Conferences Attended

- | | |
|---|--------------------------------|
| XVIIIth International Symposium On Macrocyclic Chemistry,*
University Of Twente, Enschede, The Netherlands | June 27th - July 2nd
1993 |
| Stereochemistry at Sheffield,
University of Sheffield | December 15 th 1993 |

R.S.C. U.K. Macrocycles Group,*
University of Warwick

January 5-6th 1994

R.S.C. U.K. Macrocycles Group,
University of Newcastle upon Tyne

January 4-5th 1995

* indicates poster presented

Publications

M. Murru, D. Parker, G. Williams and A. Beeby, 'Luminescence Behaviour of Stable Europium and Terbium Complexes of Tetraaza Phosphinates: Efficient Through-space Energy Transfer From Phenyl to Terbium', *J. Chem. Soc., Chem. Commun.*, 1993, 1116.

S. Aime, A.S. Batsanov, M. Botta, J.A.K. Howard, D. Parker, K. Senanayake and G. Williams, 'Solution and Solid-State Characterisation of Highly Rigid, Eight-Coordinate Lanthanide(III) Complexes of a Macrocyclic Tetrabenzylphosphinate', *Inorg. Chem.*, 1994, **33**, 4696.

S. Aime, M. Botta, D. Parker and J.A.G. Williams, 'Nuclear Magnetic Resonance Studies of Neutral Lanthanide(III) Complexes with Tetraaza-macrocyclic Ligands containing Three Phosphinate and One Carboxamide Coordinating Arms', *J. Chem. Soc., Dalton Trans.*, 1995, 2259.

D. Parker and J.A.G. Williams, 'Luminescence Behaviour of Cadmium, Lead, Zinc, Copper, Nickel and Lanthanide Complexes of Octadentate Macrocyclic Ligands Bearing Naphthyl Chromophores', *J. Chem. Soc. Perkin Trans. 2*, 1995, 1305.

